Synthesis and characterisation of macrocyclic ligands with hydroxyalkyl and thiol pendant arms tethered on 1,5,9-triazacyclododecane and their complex formation chemistry

by

Jimmy Ephet Yafeti Sumani

A thesis submitted in partial fulfilment of the requirements

for the

degree of Masters of Science

at the

University of Stellenbosch

Supervisor: Dr. R.C. Luckay
Co-supervisor: Prof. H.G. Raubenheimer

April 2010

Declaration

I, Jimmy Ephet Yafeti Sumani, hereby declare that the work presented in this thesis is my own original work except where due reference is made and that I have not previously in its entirety or in part submitted it at any university for a degree.

Signature:.....

Date:.....

Abstract

This investigation comprises the synthesis and characterisation of new macrocyclic ligands with pendant arms appended to the nitrogen donor atoms of 1,5,9-triazacyclododecane (12aneN_3) and their coordination to various transition metal ions. The five macrocyclic ligands, 1,5,9-*tris*[(2*S*)-2-hydroxypropyl]-1,5,9-triazacyclododecane (THPTACD), 1,5,9-*tris*(2-hydroxy-2-methylpropyl)-1,5,9-triazacyclododecane (THMPTACD), 1,5,9-*tris*[(2*S*)-2-hydroxy-2-phenylethyl]-1,5,9-triazacyclododecane (THPETACD), 1,5,9-*tris*[(2S)-2-hydroxybutyl]-1,5,9-triazacyclododecane (THBTACD) and 1,5,9-*tris*(2-mercaptopropyl)-1,5,9-triazacyclododecane (TMPTACD) were prepared by addition of pendant arms that contain alcohol or thiol end groups to a preformed 12aneN_3 macrocycle. The 12aneN_3 was synthesised from simple starting materials using 1,3-propanediol and *bis*(3-aminopropyl)-amine. The macrocycles with oxygen donor atoms on the pendant arms were prepared from the corresponding epoxides whereas for the one that contained sulphur donor atoms, propylene sulphide was used. The reaction progress was followed by ^{13}C and ^{1}H NMR spectroscopy and the final macrocyclic ligands were further analysed by mass spectrometry and in some instances, elemental analysis was also performed.

Protonation constants of the free ligands were determined using potentiometric titrations at 25 ^{o}C and the ionic strength was kept constant at 0.1000 mol dm^{-3} using $NaNO_3$. The log K_1 values were 11.47, 10.96 and 10.47 for THPTACD, THBTACD and THMPTACD, respectively, whereas the corresponding values of 5.81, 6.02 and 5.94 were obtained for log K_2. THPTACD is the most basic mainly due to less steric hindrance whereas THMPTACD is the least basic owing to high steric hindrance to both solvation and formation of strong hydrogen bonds of the protonated species to solvent molecules during the solvation step in a Born Haber-type cycle of the complete process. Protonated THBTACD is the most basic of the three mono-protonated ligands, a result that may be explained in terms of better correlation between inductive and steric effects. The second protonation constant is mostly influenced by inductive effects unlike the first protonation constant which is mostly determined by steric effects. The third protonation constant could not be established because of lack of sensitivity of the glass electrode in very high acidic medium.

The complex stability constants of Co(II), Zn(II), Cd(II) and Pb(II) cations were similarly determined using potentiometric titrations at 25 °C in 0.1000 mol dm^{-3} $NaNO_3$. Log *K* values with THPTACD are 15.45, 21.22, 14.03 and 16.11 for Co(II), Zn(II), Cd(II) and Pb(II), respectively. THBPTACD has corresponding values of 13.93, 20.02, 13.55 and 15.01, whereas for THMPTACD the values of 14.63, 18.08, 12.91 and 14.36 log units were obtained. The Zn(II) 1:1 complexes are the most stable and those of Cd(II) the least stable. A crystal structure determination of $[Zn(THPTACD)]^{2+}$ shows that optimal interaction between the Zn(II) metal ion and the donor atoms with their short Zn(II)-N bond lengths occurs. The short Zn(II)-N distances indicate that the metal ion is situated very close to the macrocyclic hole. On the other hand, each half of the hydrogen-bonded dimeric molecular structure of $[Cd_2(THPTACD)_2]^{4+}$ has long Cd(II)-N bond lengths.

Although metal nitrates, perchlorates and acetates were used in attempted crystal structure determinations, only metal nitrates formed suitable crystals. THPTACD complexes with Co(II), Mn(II), Ni(II), Cu(II), Zn(II) and Cd(II) were subjected to such determinations. Each central metal ion in these complexes is six coordinate to the three N atoms of the parent macrocyclic ring on one plane and the three O atoms of the pendant hydroxypropyl arms forming another plane on the other face of the metal ion. The geometry of all six molecular structures is *pseudo* octahedral with the Cu(II) complexes being the most twisted towards a trigonal prismatic arrangement. The change towards trigonal prismatic can be attributed to packing forces overriding octahedral crystal field stabilisation effects. The overall chirality of the isomorphic complexes of Zn(II), Co(II), Mn(II), Ni(II) and Cu(II) with THPTACD is $[\Lambda((2\lambda''')\delta'''\delta)]$ whereas the overall chirality of each half of the dimeric $[Cd_2(THPTACD)_2]^{4+}$ complex is $[\Lambda(\lambda'''(2\delta''')\delta)]$. The Cu(II) complex with THPETACD has the same overall chirality as the Cu(II) complex with THPTACD but is less twisted towards trigonal prismatic geometry. Both Cu(II) complexes exhibited strong evidence of Jahn-Teller tetragonal distortion in the solid state with tetragonality parameter values of 0.87 and 0.81, respectively. The structure of a new di-μ-chloro bridged binuclear complex of Cd(II)-12aneN_3 was also determined. The molecule contains an inversion centre coinciding with the crystallographic centre of symmetry. Finally, the molecular structure of the protonated 1,5-*bis*[(2*S*)-2-hydroxybutyl]-1,5,9-triazacyclododecane shows that the oxygen donor atoms of the two pendant arms are pre-organised for *meridional* coordination. The hydrogen bond network in this structure emphasises the important role that such weak interactions play in stabilising the

proton even in solution during determination of protonation constants in triazamacrocycles with pendant arms carrying oxygen donor atoms.

In loving memory to late

David William Kawina Sumani

Acknowledgements

Firstly, my deepest appreciation goes to my supervisor, Dr. R. C. Luckay for his patience, guidance and belief. This work is a clear manifestation of his unbelievable supervising ethics, which give students a platform to think beyond Chemistry. I am also very grateful to my co-supervisor Prof. H.G. Raubenheimer for his unlimited financial support and important discussions.

I would also like to thank Christoph Strasser, Dr. Jan Gertenbach and Dr. Catherine Esterhuysen for solving crystal structures. A special thank you should go to Prof. S. Mapolie and his research group members for giving me full access to equipment at their disposal and general friendliness throughout my stay here.

To the entire Sumani's family, in particular to my beloved mother, Maria Goliati Sumani, for always praying for me. I see your prayers in my everyday's life.

Thanks should also go to Elsa Malherbe and Mr. W. Trevor for running my NMR samples and to the technical staff in the department, in particular to, Mr. Eric Ward, Mr. Jonny and Mr. Tommy for technical support.

Special thanks should go to Prof. J.D.K. Saka, Dr. F.F Fabiano and the late Prof. E. Henry, for all the support you offered me before and during my stay in South Africa.

I would also like to thank the following friends for their support: M. Msiska and his family and D. Mazibuko.

Lastly, I would also like to thank NRF, Stellenbosch University, Chemistry Department of Stellenbosch University and University of Malawi, Chancellor College, for financial support.

Poster presentation

Cape Organic Symposium (COS), Breakwater Lodge, Waterfront, Cape Town, October 2008: Synthesis of the novel pendant arm donor macrocycle 1,5,9-*tris*[(2*S*)-2-hydroxypropyl]-1,5,9-triazacyclododecane (THPTACD), and some complex formation chemistry, Sumani J.E.Y., Luckay R.C. and Raubenheimer H.G.

Publication

Strasser C.E., Sumani J.E.Y., Raubenheimer H.G. and Luckay R.C., *Acta. Cryst.*, **2010**, E66, m327.

Abbreviations

Me_3TACN…….……1,4,7-trimethyl-1,4,7-triazacyclononane

EtOH…….……...ethanol

MeOH…….…….……..methanol

3,3,3-tet…….....……*N,N′*-di(3-aminopropyl)propylenediamine

2,3,2-tet…….....……*N,N′*-di(2-aminoethyl)propylenediamine

Cyclam…….....……1,4,8,11-tetraazacyclotetradecane

THPC-14……..……..1,4,8,11-tetrakis(3-hydroxypropyl)-1,4,8,11-tetraazacyclotetradecane

THEC-14…….……...1,4,8,11-tetrakis(2-hydroxyethyl)- 1,4,8,11-tetraazacyclotetradecane

12aneN4…….……1,4,7,10-tetraazacyclododecane

TRIEN…….……..1,4,7,10-tetraazadecane

DIEN…….……1,4,7-triazaheptane

I.U.P.A.C…….……..International Union of Pure and Applied Chemistry

DOTRA…….……1,5,9-triazacyclododecane-1,5,9-triacetic acid

NOTA…….……...1,4,7-triazacyclononane-1,4,7-triacetic acid

DOTA……..……..1,4,7,10-tetraazacyclododecane-1,4,7,10-tetraacetic acid

EMF……...……....Electromotive force

DETA……...…….……1,4,7-triazacyclodecane-1,4,7-triacetic acid

UNTA……...……1,4,8-triazacycloundecane-1,4,8-triacetic acid

EN……...……..ethylenediamine

TETREN……...……tetrakis(aminoethyl)amine

$9aneN_3$……...……1,4,7-triazacyclononane

$10aneN_3$……...……..1,4,7-triazacyclodecane

$11aneN_3$…….....……1,4,8-triazacycloundecane

MS……....….……mass spectrometry

DMF…….....……dimethylformamide

NOTPME…….....……1,4,7-triazacyclononane-1,4,7-*tris*(methylenephosphonatemonoethylester)

NOTP…….……..1,4,7-triazacyclononane-1,4,7-*tris*(methylenephosphonic) acid

DCM……dichloromethane

DMF.....dimethylformamide

12aneN$_4$.....1,4,7,10-tetraazacyclododecane

13aneN$_4$.....1,4,7,10-tetraazacyclotridecane

14aneN$_4$.....1,4,8,11-tetraazacyclotetradecane

15ane-N$_4$.....1,4,8,12-tetraazacyclopentadecane

Å.....angström (1×10^{-10}m)

m/z…….....…….……..mass/charge

MHz…….…….……mega hertz

ESI-MS…….……...electrospray mass spectrometry

ppm……..……..……parts per million

TETA……...……...…….1,4,8,11-tetraazacyclotetradecane-1,4,8,11-tetra acetic acid

THETAC……..……1,4,7-tris(hydroxyethyl)-1,4,7-triazacyclononane

THTD.....……..……...…...1,4,7-*tris*[(2*S*)-2-hydroxypropyl]-1,4,7-triazacyclodecane

THTUD…….....……..1,4,7-*tris*[(2*S*)-2-hydroxypropyl]-1,4,7-triazacycloundecane

[M$^+$]……...…...…….molecular ion

NMR…...……..…...…….nuclear magnetic resonance

^{13}C.....carbon 13

^{1}H.....proton

Calc.....calculated

Anal.....analytical

Table of Contents

List of tables

List of schemes

List of charts

List of figures

Chapter 1

Introduction

1.1 General literature review

The discovery of crown ethers in the late 1960s by Pedersen (Pedersen, 1967) instigated intense research activity in the area of polyethers which lead to the rebirth of macrocyclic chemistry. Pedersen stumbled into dibenzo-18-crown-6 **(1.3)** as a miniature by-product when he was trying to prepare a complexing agent for the catalytic vanadyl ion by linking two catechols (1,2-dihydroxybenzene) through one hydroxyl group on each molecule to form a linear diol **(1.2)**. He protected the catechol with tetrahydropyran **(1.1)** but unknown to him his starting material was contaminated with unprotected catechol (**Scheme 1.1**).

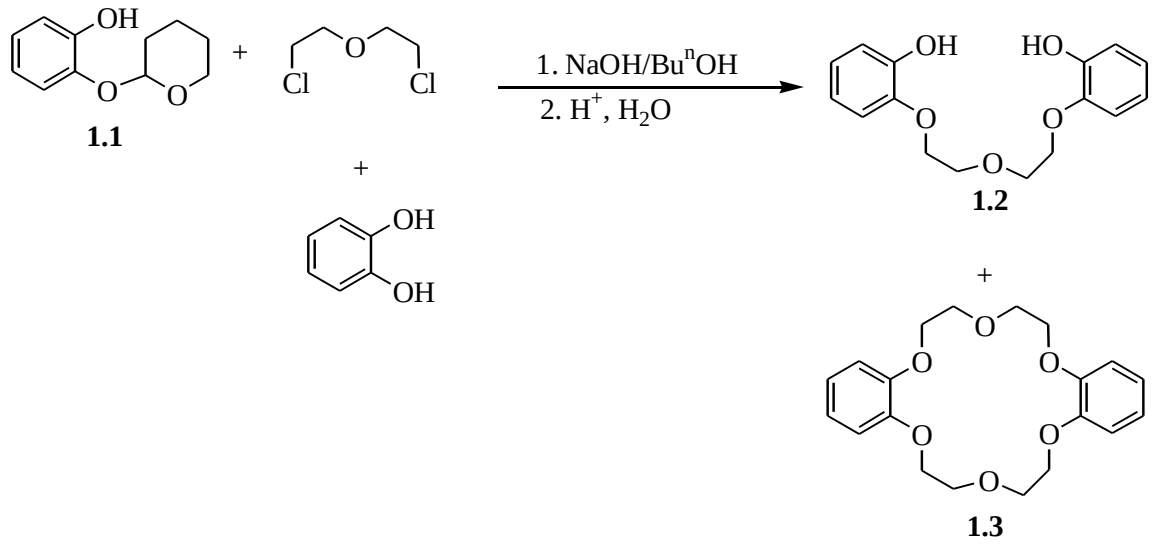

Scheme 1.1: The 'mistaken' original synthesis of dibenzo-18-crown.

Dibenzo-18-crown-6 was recovered as a white fibrous crystalline by-product. Pedersen was amazed by the fact that the crystals were insoluble in butanol but completely and instantaneously dissolved upon addition of sodium salt. This observation led to the discovery of the complexing power of crown ethers and led to the intense research on similar polyethers.

Because of Pedersen's discovery, at first, the interest was constricted to macrocyclic ligands having oxygen donor atoms only but the interest was later expanded to other donor atoms such as sulphur, nitrogen, selenium and mixed donor atoms (Martell and Hancock, 1996). These other donor atoms have different chemical properties to oxygen donor atoms and offered a new dimension in coordination chemistry. For example, unlike oxygen donor atoms which do not allow addition of pendant arms, nitrogen donor atoms allow the possibility of adding pendant arms with or without another donor atom(s) on the *N*-functional group. Macrocyclic molecules with nitrogen donor atoms are readily subjected to systematic modification of their electronic and steric properties by addition of pendant arms. The use of macrocyclic molecules with nitrogen donor atoms has bloomed over the years because of this desirable characteristic. Oxygen is considered as a hard donor atom whereas nitrogen falls in the borderline region in the Hard and Soft Acids and Bases (HSAB) classification (Pedersen, 1963). Macrocycles with oxygen donor atoms are normally known as crown ethers whereas those with nitrogen donor atoms are known as azamacrocycles.

1.2 What are macrocycles?

A macrocycle is defined as a large cyclic molecule which contains three or more potential donor atoms and a ring of at least nine atoms. Macrocyclic ligands can be considered to span two extreme types based on donor atom types. There are those systems which chiefly contain nitrogen, sulphur, phosphorus, and/or selenium donor atoms. These macrocycles tend to show considerable affinity for transition and other heavy metal ions and usually show much less tendency to form stable complexes with ions of the alkali and alkaline earth metals. The second type of macrocyclic ligands consist of a large group of cyclic compounds incorporating ether functions as donor atoms. These polyethers usually show strong complexing ability towards alkali and alkaline earth metal ions but their tendency to coordinate to transition metal ions is less than for the above category (Lindoy, 1989). In general, macrocyclic complexes are usually thermodynamically and kinetically more stable than complexes with related non-cyclic ligands (Constable, 1999). Sulphur, phosphorus and selenium are considered as soft donor atoms whereas oxygen is considered as a hard donor atom in the HSAB classification. In some macrocyclic ligands, a mixture of donor atoms is present either within the same macrocyclic ring or on the peripheral part of the macrocycle. The macrocyclic ligands containing two or more different types of donor atoms offer the

advantage of combining two or more different bonding preferences thereby allowing new types of selectivity in metal ion binding. However, different bonding preferences may lead to reduced stability as opposed to macrocyclic ligands with the same type of donor atoms (Martell and Hancock, 1996). The use of macrocyclic ligands with sulphur donor atoms is limited by the lack of convenient synthetic methods and the use of extremely reactive or toxic intermediates such as $ClCH_2CH_2SCH_2CH_2Cl$ for thiacrowns (Constable, 1999). The nomenclature of macrocyclic ligands is always problematic and although it is possible to devise an I.U.P.A.C name which is usually long, cumbersome and more often does not convey the information in the chemical structure in a useful manner, chemists often use trivial names which emphasise structural features of the macrocycle. For example, 2,3,11,12-dibenzo-1,4,7,10,13,16-hexaoxacyclooctadeca-2,11-diene is commonly named as dibenzo-18-crown-6 which conveys that the macrocycle ring contains eighteen atoms and six oxygen donor atoms. Macrocycle ring sizes vary from a minimum of nine atoms. In general, the ring sizes of cyclic molecules are categorised into four groups namely: small, normal, medium and large (**Table 1.1**) (Constable, 1999).

Table 1.1: The classification of the ring sizes of cyclic molecules

Ring	Size
3,4	Small
5-7	Normal
8-11	Medium
≥12	Large

The size of the macrocyclic ring can be changed by either increasing the number of donor atoms or increasing the carbon bridges. Changing the number of donor atoms is the most effective way of manipulating the size of the macrocycle.

1.3 Steric and inductive effects in chelating ligands

The two most important competing structural factors in chelate formation are steric and inductive effects. In general, the donor strength and the tendency to cause steric hindrance to complex formation increase along the series $NH_3 < NH_2R < NHR_2 < NR_3$ for R = alkyl group, and also as the nature of R changes along the series $CH_3 < CH_3CH_2 < (CH_3)_2CH <$

$(CH_3)_3C$ in ligands such as the RNH_2 series. Either one of these effects can outweigh another depending on the nature of the substituent and the position of substitution. Steric effects normally outweigh inductive effects for *N*-methyl substitution of ethylenediamine. Even though the substituent is directly connected to the donor atom, which enhances positive inductive effect, it denies the donor atom the much required space for proper complexation (**Table 1.2**).

Table 1.2: An example of steric effects outweighing inductive effect for *N*-methyl substitution of ethylenediamine

	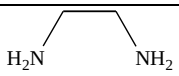	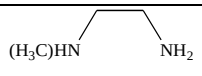	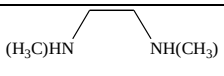	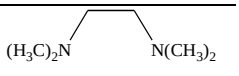
	EN	N-MEEN	N,N′-DIMEEN	N,N,N′,N′-TMEEN
log K_1 Cu(II)	10.48	10.33	10.02	7.20
log K_1 Ni(II)	7.35	7.17	6.89	3.57
log K_1 Cd(II)	5.40	5.47	5.20	3.87

Data from Martell and Hancock, (1996) at 25 °C, in 0.10 mol dm^{-3} KNO_3.

On the other hand, *C*-methyl substitution produces less steric crowding on the donor atoms, and as such, the inductive effect outweighs the steric effect (**Table 1.3**).

Table 1.3: An example of inductive effect outweighing steric effect for *C*-methyl substitution of ethylenediamine

	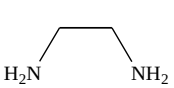	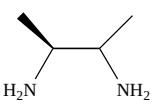	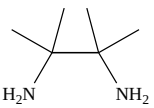	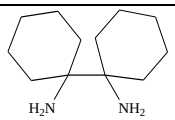
	EN	DMEEN	TMEEN	DICHEN
log K_1 [Cu(II)]	10.48	11.27	11.63	12.20
log β_2 [Ni(II)]	13.54	14.01	14.56	14.90

Data from Lehn, (1978) at 25 °C, in 0.10 mol dm^{-3} $NaNO_3$.

In general, the donor atom basicity increases with increasing alkyl substitution for nitrogen donor atoms along the series zeroth < primary < secondary < tertiary. The trend can be

explained in terms of increase in positive induction effect from zeroth to tertiary nitrogen donor atoms. This has a profound effect on the thermodynamics of complex formation and the electronic spectra of complexes that can be separated from steric effects that often counter the effects of increasing donor atom basicity. Increase in ligand field strength as exemplified by increasing energy of the d-d bands indicate increased overlap in the metal-nitrogen bond (**Table 1.4**) (Martell and Hancock, 1996).

Table 1.4: The enthalpy of complex formation (ΔH) and the energy of the d-d band of ligands with different denticity

	0°	1°	2°	3°
	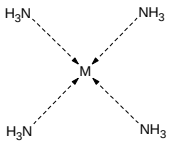	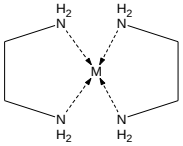	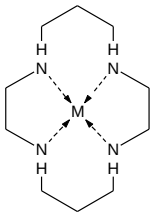	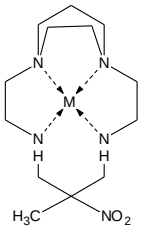
ΔH[Cu(II)](kcalmol^{-1})	-22.0	-25.5	-32.4	a
ν(d-d)(cm^{-1})Cu(II)	17000	18300	19900	21050
ν(d-d)(cm^{-1})Ni(II)	~20000	21600	22470	23900

[a] Data not available.

1.4 Selectivity of macrocyclic ligands for metal ions

The search for factors that control metal ion selectivity has led to several rules for ligand design. Metal ion selectivity is defined as the difference in log K_1 for one metal ion relative to that of another with the same ligand, where log K_1 is the formation constant (Hancock and Martell, 1989). In order to explain the selectivity of macrocyclic ligands for metal ions, the concept of the hole-size relation between the macrocyclic ligand and metal ion is usually invoked. The hole-size of a macrocyclic ligand is a fundamental structural parameter which usually influences the properties of the resultant metal complexes relative to those of the corresponding non-cyclic ligands. The ultimate effect of hole-size match selectivity is that a metal ion will show maximum stability with a macrocyclic ring when the ionic radius of the metal ion matches the cavity of the macrocyclic ring. The hole-size of a cyclic ligand is often determined by the number of atoms and the nature of the donor atoms in the macrocyclic

ring. The most used parameter in determining this relationship is the radius of the cavity which is matched up directly with known metal ion radii in selecting appropriate combinations of metal ion and ligand. The earliest approach was to estimate the radius of the cavity directly by measuring the distance between the nuclei of diametrically opposed donor atoms using molecular or computer generated models, or by taking distances directly from solid state structural determinations of the free ligands or their metal complexes. In this procedure, the radius of a simple macrocycle is measured and consists of the available cavity r(H) plus radius of the donor atom r(D). The hole-size is obtained by subtracting the radii of the donor atom using Pauling covalent radii, though van der Waals radii is also used, from the radius (r). The value of the hole-size is usually reported as a range because macrocycles usually adopt conformations with varying radii (Constable, 1999). The best binding is attained if the guest metal ion fits into the macrocyclic cavity. This refers to the ability to form metal-ligand bonds with the optimal bond lengths and with the distribution of the donor atoms in a favourable geometrical arrangement about the metal ion. Furthermore, the optimal metal-ligand interaction is achieved without the introduction of unfavourable steric interactions within the ligand framework (Constable, 1999). The ligand in its minimum energy metal-binding conformation is optimised for a particular size of metal ion and when other metal ions are bound, the ligand conformational energy increases with a resultant decrease in stability constant. This is considered as the origin of the macrocyclic selectivity of the metal ion. It is important to realise that the hole-size metal ion mismatch does not necessarily mean that no complexation will occur, but rather it means that the stability of the resultant metal complexes is highly decreased. The hole-size metal ion mismatch can happen because of a number of reasons. For example, the metal ion can be too large for the macrocyclic cavity thereby forced to sit above the plane defined by the donor atom set of the ring. In some cases two ligands can sandwich the metal ion. When the metal ion is too small for the hole-size of the macrocyclic ligand, a number of possible things could happen. For example, only some of the donor atoms might be bonded to the metal ion or in the case of a dramatic mismatch in the hole-size and the size of the metal ion, two or more metal ions might be incorporated into the macrocyclic cavity. Another possible consequence is that the macrocyclic ligand may undergo a radical conformational change to adopt some sort of a folded conformation that optimises the metal-donor atom distance. The metal ion electronic configuration preferences can also dictate the macrocyclic ligand to adopt conformational geometries that minimise the strain in the ligand thereby increasing the stability of the resultant metal complexes (Constable, 1999).

Thöm *et al.*, (1984) used molecular mechanics (MM) calculations to show that in its *trans*-conformer 1,4,7,10-tetraazacyclododecane, 12aneN$_4$, has a larger cavity, with best-fit M-N lengths of 2.11 Å, compared with 2.05 Å for 1,4,8,11-tetraazacyclotetradecane, 14aneN$_4$, which explained the paradox that larger metal ions coordinate more strongly to the small macrocycle 12aneN$_4$ than to the large 14aneN$_4$. In addition, the macrocyclic ring of 12aneN$_4$ is more flexible than that of 14aneN$_4$, which allows better response to changes in metal ion size. From the work of these authors it can be concluded that factors which guide hole-size match selectivity for metal complexes are more complicated and cannot necessarily be inferred from the size of the macrocyclic ligand alone. One thing that remains fairly intact though, is that metal ions show maximum stability with macrocyclic ligands when the ionic radius of the metal matches the cavity of the macrocyclic ring in one of its lowest energy conformers regardless of the ring size itself.

There are two ways of increasing the ring size of the macrocycle, firstly by varying the number of donor atoms in the ring and secondly by increasing the size of the carbon bridges between the donor atoms (Martell and Hancock, 1996).

1.5 Metal ion selectivity of nitrogen donor macrocycles

In general, the increase in size of the chelate ring from the five-membered to the six-membered ring increases the selectivity for smaller metal ions relative to large metal ions (Martell and Hancock, 1996). This is one of the most powerful ligand design tools and was used to design a fluorescent ligand that showed immerse selectivity for smaller metal ions such as Zn(II) over larger metal ions such as Cd(II) and Pb(II). The definition of metal-ion size are normally quoted in terms of the ionic radius, r^+, whereby if $r^+ \geq 1.2$ Å then the ion is defined as very large; $1.2 > r^+ > 1.0$ Å large; $1.0 > r^+ > 0.8$ Å medium; $0.8 > r^+ > 0.7$ Å medium-small; $0.7 > r^+ > 0.5$ Å small and very small for $r^+ < 0.5$ Å (Shannon, 1976).

1.5.1 The geometry of the chelate ring and preferred metal ion sizes

The donor atoms in macrocyclic ligands are normally spaced so that on coordination five-, six- and occasionally seven-membered chelate rings are formed with the metal ion. The five-membered chelate rings prefer large metal ions whereas the six-membered chelate rings

prefer small metal ions. This behaviour can be understood by reference to the low-strain form of cyclohexane (**Chart 1.1**) (Martell and Hancock, 1996).

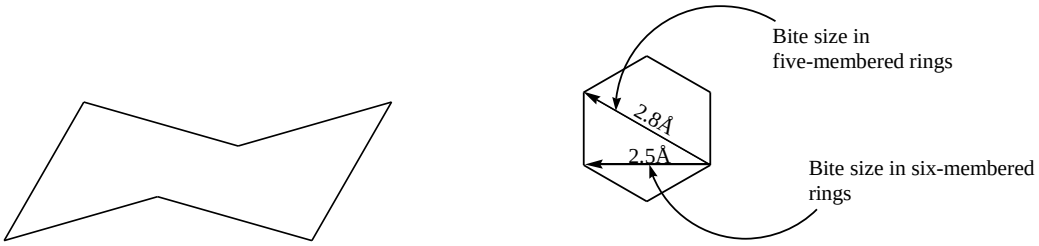

Chart 1.1: Shows a cyclohexane in the chair conformation and the bite size of the five- and six-membered chelate rings.

Considering cyclohexane in the chair conformation, the torsion angles are 60° and the C-C-C bond angles are all ideal at 109.5°. The strain energy is at a minimum in this conformation because all hydrogen atoms are staggered. The six-membered chelate ring of 1,3-diaminopropane involving two nitrogen donor atoms and a metal ion in place of three of the carbon atoms of cyclohexane would also be of very low strain energy as long as the metal ion is about the same size and geometry as an sp^3 hybridised carbon atom. Thus, the 1,3-diaminopropane chelate has the bite size of 2.5 Å, an angle of 109.5° and the distance between the metal ion and the nitrogen atoms of 1.6 Å when complexed to the metal ion in a six-membered chelate ring which is ideal for small metal ions (**Chart 1.2**) (Martell and Hancock, 1996).

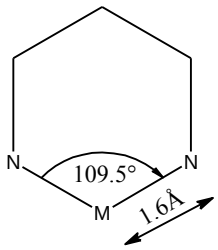

Chart 1.2: The ideal geometry for a six-membered ring with nitrogen donor atoms.

The best size metal ion for the five-membered chelate ring can also be derived by considering the cyclohexane. If a minimum strain ethylenediamine ring is considered, the chelate has the bite size of 2.8 Å, an angle of 69°, and the distance between the metal ion and the nitrogen atoms of 2.5 Å when complexed to the metal ion in a five-membered ring which is ideal for large metal ions (**Chart 1.3**) (Martell and Hancock, 1996).

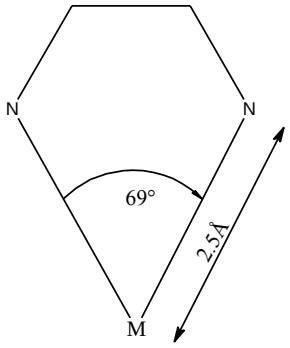

Chart 1.3: The ideal geometry for a five-membered ring with nitrogen donor atoms.

The relationship of complex stability to chelate ring sizes is thus readily understood in terms of the best-fit size of metal ion for complexing with five- and six-membered chelate rings. In particular, smaller metal ions tend to have lower coordination numbers, and so, as the M-N bond lengths become smaller, the N-M-N bond angles increases. Conversely, as the metal ions become larger, the coordination numbers increases, and therefore the N-M-N bond angles become smaller and the M-N bonds become longer (Martell and Hancock, 1996).

When oxygen donor atoms replace nitrogen donor atoms for the five-membered chelate ring, the angle of the chelate becomes 126° whereas the angle with the metal ion changes to 58°. The distance between the oxygen donor atom and the metal ion increases to 3.2 Å (**Chart 1.4**) (Martell and Hancock, 1996).

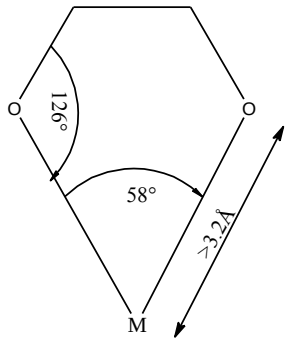

Chart 1.4: The ideal geometry for a five-membered ring with oxygen donor atoms.

When oxygen donor atoms replace nitrogen donor atoms for the six-membered ring, the bite size angle becomes 126° whereas the angle with the metal ion changes to 95°. The distance between the oxygen donor atom and the metal ion becomes 1.9 Å (**Chart 1.5**) (Martell and Hancock, 1996).

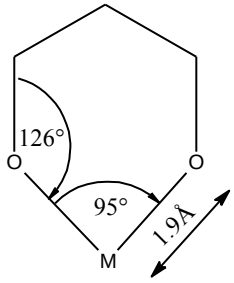

Chart 1.5: The ideal geometry for a six-membered ring with oxygen donor atoms.

There is a big variation in the bond lengths and angles when comparing nitrogen and oxygen donor atoms of a chelate. The difference between the nitrogen and oxygen chelate rings is that for the neutral nitrogen donor atom low strain conformations prefers tetrahedral geometry whereas oxygen donor atom prefers trigonal planar geometry (Martell and Hancock, 1996).

1.5.2 Selectivity for macrocyclic ligands with pendant donor atoms

Macrocyclic ligands with pendant arms usually show different metal ion selectivity to those shown by ligands without pendant arms. Addition of pendant arms more often lead to overcrowding at the *N*-donor atoms which further constricts the macrocyclic hole and brings in steric hindrance within the molecule. The ultimate effect of overcrowding is that the metal ion usually sits above the plane of the macrocyclic donor atoms and the stability of the resultant metal complex is guided by other factors other than the hole-size match selectivity. For example, Huskens and Sherry, (1998) reported several 1,4,7-*tris*(2-hydroxyalkyl)-1,4,7-triazacyclononane and their possible diastereomeric forms that showed large selectivity differences for complexation of Mg(II) and Ca(II). The selectivity, in this case, is related to the twist angle of the plane of coordinating hydroxyl groups relative to the plane of the macrocyclic ring nitrogen donor atoms. The large twist angle makes the cavity for the metal ion small. This means that the stability of the metal complexes of macrocyclic ligands with pendant arms carrying donor atoms is defined by the way the metal ion induce ligand conformation.

1.6 The chelate effect

The observation that macrocyclic ligands in aqueous solution generally form more stable complexes with metal ions than their open chain counterparts with the same number and type

of donor atom groups puzzled the scientific community because they expected the stability of these ligands to be comparable. This unusual stability was termed the macrocyclic effect (Cabbines and Margerum, 1969) or multiple juxtapositional fixedness (Busch *et al.*, 1971) in order to distinguish it from the chelate effect. In macrocyclic effect there is an additional enhancement in stability beyond that expected from the gain in transitional entropy when chelates replace coordinated solvent from metal ions. The result of the chelate effect is that ligands with many donor atoms (multidentate ligands) form thermodynamically more stable complexes than analogous complexes containing unidentate ligands. **Table 1.5** gives the quantitative values of the formation constants of complexes of Ni(II) with n-dentate polyamines as compared to the analogous complexes with ammonia.

Table 1.5: The chelate effect for complexes of Ni(II) (spin, s = 1) with polyamines of the formula $NH_2(CH_2CH_2NH)_{(n-1)}H$[a]

polyamine	EN	DIEN	TRIEN	TETREN	PENTEN[b]
Denticity, n	2	3	4	5	6
Log β_n (NH_3)	5.08	6.85	8.12	8.93	9.08
Log K_1 (polyamine)	7.47	10.7	14.4	17.4	19.1

[a] log *K* data from Martell and Smith, (1974-1989), at 25 °C in 0.5 mol dm^{-3}. [b] Ligand is non-linear, with formula corresponding to $(NH_2CH_2CH_2)_2NCH_2CH_2N(CH_2CH_2NH_2)_2$.

1.7 A case study of $Ni(cyclam)^{2+}$ and $Ni(2,3,2\text{-tet})^{2+}$ by Hinz and Margerum

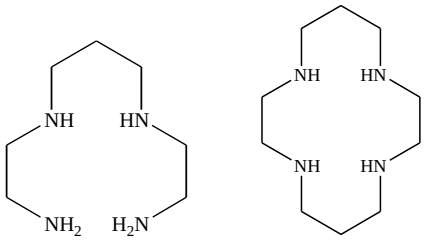

Chart 1.6: The molecular structure of 2,3,2-tet (left) and cyclam (right).

Hinz and Margerum, (1974) reported an unusual stability constant of $Ni(cyclam)^{2+}$ over that of $Ni(2,3,2\text{-tet})^{2+}$ (see **Chart 1.6** for key to ligand abbreviation) that was in orders of over

10^6-fold. Although the stability of a particular complex type increases with increase in the number of chelate rings (the chelate effect), the additional stability of the macrocyclic Ni(II) complex was about an order of magnitude greater than expected solely from the presence of an additional chelate ring. This discrepancy in stability was not assigned to stronger Ni-N bonds because both compounds have exactly the same number of such bonds and although cyclam has more secondary amine donors than 2,3,2-tet, secondary amines, in general, form less stable Ni(II) complexes than primary amines. Furthermore, the difference in the ΔH^o values for the formation of $Ni(2,3,2\text{-tet})^{2+}$ and $Ni(en)_2^{2+}$ is small (Davies *et al.,* 1954; Poulsen and Bjerrum, 1955; Holmes and Williams, 1967; Ciampolina *et al.,* 1960). The puzzle stemmed from the fact that macrocyclic rings cannot force better coordination geometry with the metal ion than their open-chain counterparts because of the rigidity brought about by the cyclic nature of the bonded donor atoms. Neither ligand can be regarded as being very restrictive as there is no reported evidence of unfavourable ring conformations or of unusual nickel-nitrogen geometry in the crystal structure of $Ni(cyclam)^{2+}$. $Ni(cyclam)^{2+}$ complexes exist primarily as the yellow square planar complexes whereas $Ni(2,3,2\text{-tet})^{2+}$ exist as a mixture of the blue octahedral and the yellow square planar complexes in aqueous solution (Bosnich *et al.,* 1965). When a correction is made so that the stability constants are compared for only the square planar complexes in each case then $Ni(cyclam)^{2+}$ has a larger stability constant than $Ni(2,3,2\text{-tet})^{2+}$ by a factor of $10^{6.8}$. Based on these findings, Hinz and Margerum concluded that it is reasonable to assign the macrocyclic effect to differences in configurational entropy because a greater loss in entropy would be expected in the complex formation reaction of the open chain ligands than in the reaction of the macrocyclic ligands.

The equilibrium and calorimetric studies showed that the greater stability of the macrocyclic complex is actually due to a more favourable change in ΔH^o (a difference of -14 kcal/mol) which overcomes a less favourable change in ΔS^o (a difference of -16 cal/(^{o}K mol)) for the reaction. The effect of ligand solvation plays a very crucial role in determining the overall gain in stabilisation energy after the complexation reaction (**Equation 1.1**). The reaction equation where the primary solvation (y) of the ligand L is:

$$Ni(H_2O)_x^{2+} + L(H_2O)_y \rightleftharpoons NiL(H_2O)_z^{2+} + (x+y-z)H_2O \qquad \textbf{(Equation 1.1)}$$

The value of ΔH^o for the reaction increases (be less negative) with increase in the enthalpy of solvation of L and the value of ΔS^o increases with increase in y due to the additional H_2O molecules released in the reaction. This means that ΔH^o is much more negative for the complexation of cyclam because it is less solvated by water than is 2,3,2-tet. Cyclam is not able to accommodate as many hydrogen-bonded water molecules on its nitrogen donor atoms because of steric hindrance. The result is that for cyclam less enthalpic energy is lost in breaking hydrogen bonds with the solvent molecules ($\Delta H^o \approx 7$ kcal/mol) (Arnett *et al.,* 1970; Clague *et al.,* 1969; Kollman and Allen, 1971) and a more favourable ΔH^o change is found for the reaction depicted in **Equation 1.1**. On the other hand, ΔS^o is less positive for the cyclam reaction than for the 2,3,2-tet reaction because the more solvated the ligand is, the more water solvent molecules are released upon desolvation. However, there is greater loss of configurational entropy in the open chain ligand, 2,3,2-tet, than in the cyclam such that the overall reaction is enthalpy driven.

1.8 The Schwarzenbach model: an explanation of the chelate effect

According to this model when a unidentate ligand attaches itself to a metal ion, there is no restriction on the second unidentate ligand and is free to translate anywhere in the system. On the other hand, when the first donor atom of a bidentate ligand is complexed to a metal ion, the second donor atom is confined to move only within the volume as defined by the distance between the two donor atoms. This in effect reduces the entropy of the second donor atom of the bidentate ligand as compared to the entropy of the second unidentate ligand (**Chart 1.7**). This means that the Schwarzenbach model predicts that the chelate effect would prove itself as a more favourable entropy complex formation for the bidentate ligand than would be the case for the analogous unidentate complex formation. This model explains nicely the observation that when the chelate bridge becomes too large, the chelate effect is greatly reduced because of the increase in the number of degrees of freedom for the second donor atom as opposed to the small chelate bridge. There should be an optimal length in the bridge beyond which the entropy is greatly reduced. The model is not in accord with the observation that for chelate sizes less than seven, the dominant factor is an enthalpy effect. The model assumes the entropy effect to be the dominant factor in all ring sizes (Schwarzenbach, 1952).

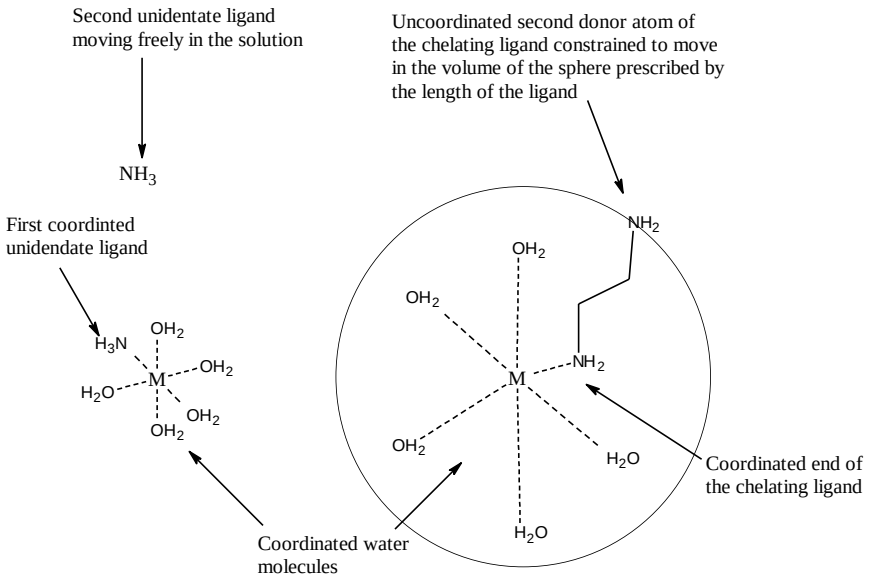

Chart 1.7: The diagram illustrates the Schwarzenbach model of the chelate effect. The second ammonia in unidentate ligand is free to translate in solution, while in ethylenediamine the second donor atom of the chelating ligand is constrained to move in a sphere, the radius of which is prescribed by the length of the bridge connecting the two donor atoms (Martell and Hancock, 1996).

An alternative explanation for the chelate effect was put forward by Adamson, (1954).

1.9 The standard reference state

Adamson noted that the units used for the concentration of the species involved in the formation constants were such that the overall formation constant, β_n, would have the units of 1^n mol^{-n} that was attributed to the asymmetry of the standard reference state. The asymmetry of the standard reference arises from the fact that the solvent is given an activity of unity, whereas the concentrations of all other species in the equilibrium are expressed as mol dm^{-3}. This means that unidentate and chelate ligands with the same number of donor atoms coordinated to the same metal ion have different values of n for β_n with different units which render the comparison done in **Table 1.5** erroneous. The chelate effect in **Table 1.5** is actually reversed when the concentrations are expressed in mol ml^{-1} instead of mol dm^{-3}, with complexes of unidentate ligands appearing to be more stable (Adamson, 1954). To solve this problem, Adamson suggested that the concentrations should be expressed as mole fractions, which makes the formation constant dimensionless thereby enabling the direct comparison between ligands to be made without getting spurious results. The idea behind the Adamson

model is that, at infinite dilution or low concentration, the total number of moles present in the solution is effectively the molarity of pure water which is 55.5 mol dm^{-3} at 25 °C. Thus, the mole fraction of each species in the equilibrium is obtained by dividing its molarity by 55.5. This means that nlog 55.5 must be added to all log β_n values to make them comparable and when this is done the chelate effect largely disappears.

Adamson's proposal leads to **Equation 1.2** for relating the formation constant of an n-dentate chelating ligand to that of the analogous complex containing unidentate ligands (Adamson, 1954):

$$\log K_1 \text{ (polydentate)} = \log \beta_n \text{ (unidentate)} + (n-1)\log 55.5 \qquad \textbf{(Equation 1.2)}$$

This equation gives lower values for polyamine complexes because the primary and secondary nitrogen donor atoms ($pK_a = 10.6$) of the polyamines are more basic than the zero order nitrogen of ammonia ($pK_a = 9.2$). This is corrected by adding the inductive effect factor to **Equation 1.2** of 1.152 (= 10.6/9.2), to give **Equation 1.3** for polyamines (Hancock and Marsicano, 1976):

$$\log K_1 \text{ (polyamine)} = 1.152\log \beta_n \text{ (ammonia)} + (n-1)\log 55.5 \qquad \textbf{(Equation 1.3)}$$

This means that the formation constant of complexes of polyamines can be accounted for in terms of (i) the entropy contribution from the asymmetry of the standard reference, and (ii) an inductive effect contribution from the alkyl bridges connecting the donor atoms of the polyamine ligand. At the heart of Adamson's model is the suggestion that the chelate effect should be primarily an entropy effect from contribution (i), with an enthalpy contribution from the inductive effect coming from contribution (ii).

The explanation on the origin of chelate effect put forward by Adamson, (1954) and Schwarzenbach, (1952) are in agreement in that, in the Schwarzenbach model the translational entropy of the second unidentate ligand is set close to zero by making it move in the restricted volume, whereas in the Adamson model the translational entropy of the second unidentate ligand is set close to zero by making each reactant fill completely the space of the standard reference state once the constants are expressed as mole fractions. However, in

practical terms the Adamson model is simpler to apply because it makes no assumptions about the geometry or the length of the bridge connecting the two or more donor atoms (Martell and Hancock, 1996).

The four factors that play a crucial role in macrocyclic ligands were summed up by Martell and Hancock, (1996) as follows:

(1) Macrocyclic ligands are more pre-organised in comparison to chelate ligands. This means that for the macrocycle the conformation of the ligand does not need to change much in binding to the metal ion whereas in open chain analogues there is a substantial change in conformation. In essence the increase in strain energy on complex formation may be far much less for the macrocycle than for their open chain analogue.

(2) The solvation of the donor atoms of the macrocycle is likely to be less than that of their open chain analogue. The macrocyclic cavity can only accommodate a limited number of solvent molecules and less energy is needed to remove them from the cavity. In an open chain there are far more solvent molecules than in the macrocycle and therefore more energy is needed to remove solvent molecules for the metal ion to complex in the open chain ligands than in macrocyclic ligands.

(3) The intrinsic basicity effects due to the induction effect of the carbon bridges between the donor atoms; the carbon bridges have positive induction effect on the donor atoms, causing the donor atoms to be more basic.

(4) The lone pair-lone pair repulsion is likely to be higher in the macrocycle than their open chain analogue. Electron lone pairs in macrocycles are directed towards one another as opposed to the open chain analogues which can take the conformation which minimises the repulsion. When the metal complex is formed the repulsion between the lone pair of the donor atoms in the cavity of the macrocycle is released resulting in a gain in stabilisation energy.

It is worth noting that there is also a third effect known as the cryptand effect. We will not discuss cryptands (**Chart 1.8**) in this thesis other than noting that cryptands are essentially extensions of the crown ethers that make use of bridgehead nitrogen donor atoms to attach additional functionality thereby giving a bicyclic system. Most of the factors that lead to

macrocycles being more stable than their open chain analogues apply as well to cryptands being more stable than macrocycles because of their superior ability to pre-organise than macrocycles do.

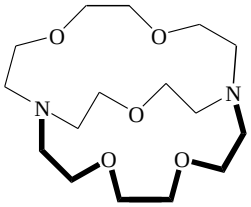

Chart 1.8: The molecular structure of cryptand [2.1.2].

1.10 The effect of mixtures of chelate rings of different sizes on complex stability

The conclusion that, the increase in size of the chelate ring from the five-membered to the six-membered ring increases the selectivity for relatively smaller metal ions is of general use in understanding factors that play a major role in dictating the selectivity of polydentate ligands. For example, if one looks at the series of ligands from 2,2,2-tet through 3,3,3-tet, Cu(II) forms a very stable complex with 2,3,2-tet ligand whereas the stability of the complex with 3,3,3-tet is much lower.

Table 1.6: The macrocyclic effect in complexes of macrocycles containing a mixture of chelate rings

	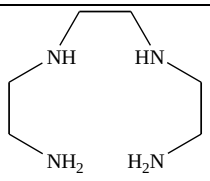	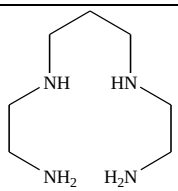	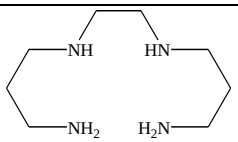	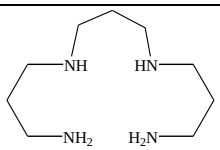
	2,2,2-tet	2,3,2-tet	3,2,3-tet	3,3,3-tet
log K_1Cu(II)	20.1	23.2	21.7	17.1
ΔH[Cu(II)][a]	-21.5	-27.7	-24.8	-19.5

[a] The enthalpy is given in kcal/mol.

The reason for the low stability can be explained in terms of easiness with which chelate rings of different sizes can be joined together. The polyamine complexes having only six-

membered chelate rings cannot be joined together about a square planar or octahedral metal ion without causing a high level of steric strain. In contrast, the fusion of five- and six-membered chelate rings in their minimum strain conformation about a square planar or octahedral metal ion can be carried out with almost no steric strain (Martell and Hancock, 1996). This accounts for the high stability of the 2,3,2-tet complex over the other chelate ring mixtures. In general, ligands which form alternating five- and six-membered chelate rings form more stable complexes than those which form only five-membered chelate rings, or only six-membered chelate rings because of steric strain which is created when fusing the same type of chelate rings (see **Table 1.6** above) (Martell and Hancock, 1996).

1.11 Mixed donor atom macrocycles

Macrocyclic ligands containing two or more different types of donor atoms are widely used. They provide the advantage of combining two or more different bonding preferences thereby allowing a new type of selectivity in metal ion binding. These macrocycles are especially important in maximising the specificity of a ligand for a particular metal ion (Constable, 1999). However, there is a decline in the macrocyclic effect in mixed donor macrocyclic ligands containing oxygen and nitrogen donor atoms as compared to the all nitrogen or all oxygen macrocyclic ligands. The reason for the difference may lie in steric differences between the coordination requirements of the oxygen and nitrogen donors (Martell and Hancock, 1996). The oxygen donor atoms prefer the trigonal planar coordination whereas the nitrogen donor atoms prefer the tetrahedral coordination geometry when coordinated to the metal ion. Thus, the trigonal planar coordination around the oxygen donor atoms produce a very different steric response in *bis*(1,4-aminoethyl)ethylenediol complexes on cyclisation to give the macrocycle 12aneN_2O_2, as compared to the tetrahedral coordination geometry around the coordinated nitrogen donors of the analogous 2,2,2-tet and 12aneN_4 complexes when coordinated to a metal ion (**Table 1.7**) (Martell and Hancock, 1996).

Table 1.7: The macrocyclic effect in macrocyclic complexes of mixed nitrogen and oxygen donor atoms compared to their all-nitrogen donor atom analogues[a]

	all-nitrogen donors			mixed donor analogues		
	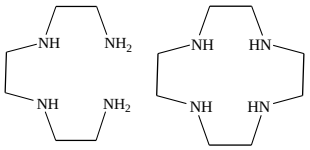			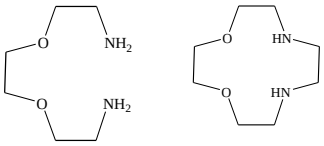		
	log K_1	log K_1	log K(MAC)	log K_1	log K_1	log K(MAC)
Cu(II)	20.1	24.4	+4.3	7.89	8.7	+0.8
Cd(II)	10.6	12.71	+2.1	5.68	b	b
	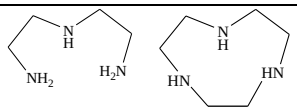			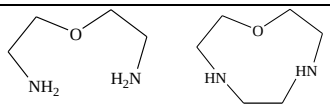		
	log K_1	log K_1	log K(MAC)	log K_1	log K_1	log K(MAC)
Ni(II)	10.5	16.2	+5.7	5.62	8.49	+2.87
Pb(II)	7.5	11.0	+3.5	6.10	5.17	-0.93

[a] Data from (Martell and Hancock, 1996). Log K(MAC) is the thermodynamic macrocyclic effect, and is equal to the log K_1 for the macrocyclic ligand minus log K_1 for the open-chain analogue. [b] Data not available.

1.12 Macrocyclic ligand pre-organisation

The term "pre-organisation" was first used by Cram and co-workers (Cram *et al.,* 1985). The term denotes the observation that the more pre-organised a ligand is, the better the ligand donor atoms are held fixed more nearly to the arrangement required in the final ligand metal complex (**Scheme 1.2**). This offers potential entropic and enthalpic advantage in complex formation. The enthalpic advantages arise because there is less increase in strain energy on complex formation than it would be if the ligand had adopted a rather different conformation of lower energy than that finally adopted in the complex. The enforced proximity of the lone pairs on the donor atoms of the free ligand leads to increasing electrostatic repulsions and the repulsions are relieved upon complex formation. The confined space of a pre-organised ligand allows a limited number of solvent molecules which may require much less energy of

desolvation (Martell and Hancock, 1996). Macrocyclic ligands are generally more pre-organised than their open chain analogues.

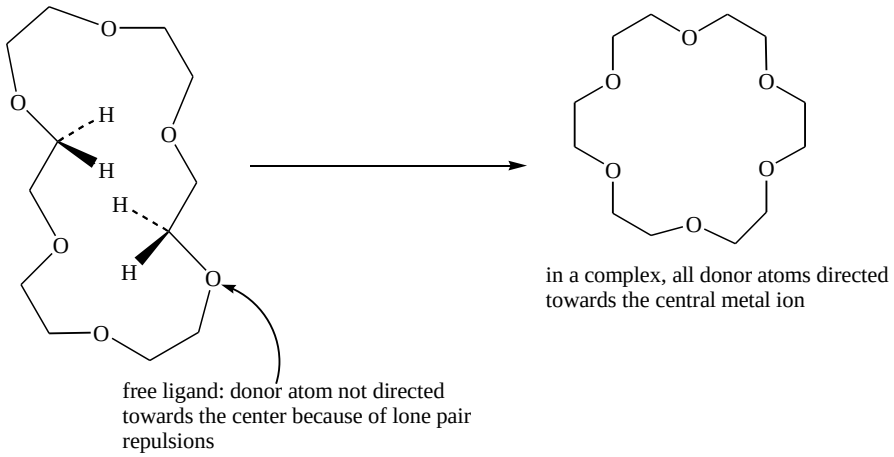

Scheme 1.2: The structure of a free ligand 18-crown-6 (left) and the conformation required in the metal complex (right) from Martell and Hancock, (1996).

1.13 Ligand design principles

The finding of structural factors that can lead to design of ligands that are more selective is of importance in areas ranging from medicine to design of detergents (Martell and Hancock, 1996). Thus, for example, the observation that six-membered chelate rings tend to promote selectivity for small metal ions, while five-membered chelate rings promote selectivity for larger metal ions, is of fairly general application in understanding the size-based selectivity displayed by a wide variety of ligands (Hancock, 1990). This is why efficient design of macrocyclic ligands requires a good knowledge of macrocycle conformational preferences in order to optimise metal-ligand interaction at the same time minimising steric strain in the co-ordinated ligand (De Sousa *et al.*, 1997). During the early days much effort was directed towards designing ligands which would show maximum stability and large selectivity to metal ions for medical applications. The interest moved to designing ligands for various uses such as mimicking metalloenzymes and metalloproteins among others (Haymore *et al.*, 1982). This is an example of how maximising the macrocyclic effect has changed the face of macrocyclic chemistry. Some of the factors which are considered when designing new ligands are (Martell and Hancock, 1996):

(1) The hardness or softness of the metal ion. The individual metal ion preferences for ligands with either more or less electronegative donor atoms form one of the basis for consideration before designing a ligand. These observations were formulated as the A and B type classification by Schwarzenbach, (1952), the a and b type by Ahrland *et al.*, (1958) and the Hard and Soft Acids and Bases principle (HSAB) by Pearson, (1963). Metal ions classified as soft, B, or b type (i.e. Ag(I)), prefer to complex with less electronegative (soft) donor atoms such as iodide, whereas metal ions classified as hard, A, or a type (i.e. In(III)) prefer to complex with more electronegative (hard) donor atoms such as fluoride. Metal ions classified as intermediate (such as Pb(II)) show no strong preferences.

(2) The size of the metal ion (metal ion radius). This is a direct consequence of the observation that the most stable metal complexes are formed when the metal ion fits perfectly in the hole of the macrocyclic ligand.

(3) The coordination number and the geometry of the metal ion e.g. some metal ions prefer square planar geometry as opposed to octahedral geometry because of the electronic demands, for example, gain in ligand field stabilisation energy. In general, such metal ions complex better with ligands containing four donor atoms as opposed to five or six donor atoms.

(4) The size of the macrocyclic ring, the denticity of the donor atoms, the induction effects of the bridges between the donor atoms and the presence of sterically bulky groups on the ligand. This is again a direct consequence of the observation that the most stable metal complexes are formed when the metal ion fits perfectly in the hole of the macrocyclic ligand. The positive induction effect and the influence of the neighbouring groups are very crucial in ligand selectivity.

1.14 The stability of metal complexes

The thermodynamic aspect of the interaction of the metal ions with macrocyclic ligands gives an idea about the stability of the resultant metal complexes. Macrocyclic ligands usually show high thermodynamic stability in aqueous solution which is attributed to either an entropic or enthalpic effect or a combination of the two effects (Hinz and Margerum, 1974;

Kodama and Kimura, 1976; Anachini *et al.*, 1977). Stability constant is a quotient consisting of the activities of the products of the reaction raised to the appropriate power divided by the activities of the reactants also raised to the appropriate power in accordance with **Equations 1.4** and **1.5** (Martell and Motekaitis, 1988).

The quantitative description of the metal complex stability and equilibrium gives an idea of how strongly a ligand will bind to the metal ion and have relevance in a number of fields such as environmental monitoring of toxic metals and in medicinal agents (Raymond and McCormick, 1998).

$$\alpha A + \beta B \rightleftharpoons \gamma C + \delta D \qquad \textbf{(Equation 1.4)}$$

$$K_{eq} = \frac{a_C^{\gamma} a_D^{\delta}}{a_A^{\alpha} a_B^{\beta}} \qquad \textbf{(Equation 1.5)}$$

The determination of the activities of complex ionic species under real conditions and at infinite dilution is a complex and time consuming operation. However, because concentrations closely parallel activities under carefully controlled conditions involving both the temperature and the ionic strength, the equilibrium concentration constants can be used in place of activity constants (**Equation 1.6**).

$$K_c = \frac{[C]^{\gamma}[D]^{\delta}}{[A]^{\alpha}[B]^{\beta}} \qquad \textbf{(Equation 1.6)}$$

The ionic strength is usually controlled by a non-reacting ionic species such as KNO_3 in large excess concentrations over the ionic species involved in the reaction under consideration.

The rate of formation of macrocyclic complexes is most often slower than the rate of complexation for related open chain polydentate ligand systems. The additional steric constraints in the cyclic ligand may restrict the mechanistic pathways available relative to the open chain case and may even alter the location of the rate-determining step (Martell and Hancock, 1996). The kinetic behaviour of the macrocyclic ligands are also determined by the presence of strong donor groups, the relative absence of steric hindrance as well as the flexibility and the favourable relative placement of the donor atoms. For example, the

increase in substitution of both cyclic and linear amines is often reflected by a decrease in the corresponding formation rate constants (Drumhiller *et al.,* 1986). This is a consequence of the reduced flexibility of the substituted ligands since such restrictions tend to hinder the complexation process.

For strongly basic amine ligands, protonation occurs almost spontaneously in water and the resultant electrostatic effects between the positively charged ligand and the metal ion may lead to slow reactions relative to the non-protonated cases (Leugger *et al.,* 1978). The equilibrium constant involving the formation of a metal complex from the aqua metal ion and the most basic form of the ligand is, therefore, a standard measure of the effectiveness of the ligand in coordinating metal ions. For ligands containing an ionisable proton or containing sites which are capable of being protonated, classical potentiometric titrations are widely used. Potentiometric measurements were first used for the measurements of stability constant by Arrhenius, Ostwald and Nernst (Martell and Hancock, 1996). Under this procedure, normally the pK_a values of the ligand involved are first determined independently. Titrations are then performed on a solution containing the ligand and metal ion of interest. The procedure depends on competition between the protons and the metal ions for the ligand binding sites. The pH of the solution is monitored at each titration point after the equilibrium has been established and the stability constant of the metal ion is calculated from known pK_a values of the ligand.

The cyclic nature of macrocyclic ligands is responsible for their characteristic acid-base properties in aqueous solution due to the presence of pH dependent favoured geometries (Yang and Zompa, 1976; Kodama and Kimura, 1976; Zompa, 1978; Geraldes *et al.,* 1985; Geraldes *et al.,* 1991). The most stable conformation is dictated by various interactions, including intramolecular and intermolecular hydrogen bonds and strain energies within the macrocyclic ligand.

1.15 Crystal structures of free macrocycles and macrocyclic complexes

Crystal structure analyses are remarkable for the richness of information that they provide. Structural information derived from crystal structure data has played the key role in the systemisation of structural chemistry since the pioneering work by Pauling (Pauling, 1940). The information from crystal structures yield the geometric structure of a molecule and also characterises the nature and geometry of its interactions with other molecules and ions, and

because of this, crystal structure data are crucially important to a wide range of scientific activities. Examples include: structural and supramolecular chemistry, conformational analysis and the prediction of protein-ligand interactions both of which are vital components of paradigms for rational design and crystal engineering, crystal growth, crystal structure prediction and polymorphism. The above examples are important in drug development and material design and gives invaluable information about the standard molecular dimensions, determining conformational preferences, intermolecular and intramolecular interactions, all of which are crucial in structural chemistry and rational drug design (Allen and Taylor, 2004). Taylor and Kennard, (1982) presented crystal evidence which supported the existence of C-H·····O, C-H·····N and C-H·····Cl hydrogen bonds. The issue of hydrogen bonds of the type proved by Taylor and Kennard created a lot of controversies with some authors supporting of its existence (Sutor, 1963) and others refusing it (Donohue, 1968).

The chemistry of macrocycles more often does not follow the established chemical rules and crystal structure determination has played a big role in understanding the chemical behaviour of macrocyclic ligands. For example, Luckay *et al.,* (1996) provided crystal evidence which helped to explain why THETAC has a high first protonation constant and a very low second protonation constant. These authors showed that the first proton is covalently bonded to one nitrogen donor atom and hydrogen-bonded to the other two nitrogen donor atoms of the parent macrocycle and one oxygen donor atom of the pendant arm. When each pendant arm incorporates the same chiral centre one diastereomer of both the ligand and its metal complexes may be dominantly stable as has been reported for 1,4,7,10-*tetrakis*[(2*R*)-2-hydroxypropyl]- 1,4,7,10-tetraazacyclododecane and 1,4,7,10-*tetrakis*[(2*R*)-2-hydroxy-2-phenylethyl]-1,4,7,10-tetraazacyclododecane and their alkali metal complexes (Whitbread *et al.,* 1998; Dhillon *et al.,* 1997; Dhillon *et al.,* 1998). Such chiral discrimination between diastereomers in a free octadentate ligand and its eight coordinate metal complexes were studied by Weeks *et al.,* (2001). Surprising though, this information can be obtained qualitatively from crystal structures as will be shown in Chapter 5 and can act as a good starting point for further analyses. Crystal structures have also provided crucial evidence regarding mechanism of metal complex catalysed phosphodiester hydrolysis (Hegg *et al.,* 1999).

Pb(II) crystal structure is very important in elucidating the stereochemistry of the lone pair of electrons on Pb(II) metal ion. The lone pair of electrons on Pb(II) can either be

stereochemically active or inactive which has a bearing on how the Pb(II) metal ion behaves in coordination chemistry. The availability of a stereochemically active lone pair of electrons on Pb(II) is evident by availability of the gap in the coordination sphere and the shortening of the Pb(II)-ligand bonds on the side of the Pb(II) opposite to the position of the lone pair. There is also a decrease in the coordination sphere (Hancock *et al.*, 1988). These two effects can readily be detected by crystal structure determination.

1.16 Application of macrocyclic ligands

After the first characterisation of macrocyclic molecules by Pedersen, there was a plethora of research in this field. This was the case because the macrocyclic ligands showed unusual chemical behaviour. The interest in this field is still growing as new macrocyclic ligands are being built specifically for certain functions in industry and medicine. The design and synthesis of these polyazamacrocycles have attracted increasing interest in recent years for the possible relevance as model ligands for metal enzymes and proteins, metal ion selective ligands and for their general coordination chemistry (Norante *et al.,* 1992). Polyazamacrocyclic ligands can either have a pendant arm(s) or not and the pendant arm(s) can either have its own donor atom(s) or not.

Macrocyclic ligands without pendant arms may contain central hydrophilic cavities with electronegative binding atoms and exterior frameworks exhibiting hydrophobic behaviour (Izatt *et al.,* 1985; Izatt *et al.,* 1991; Gerasimchuk *et al.,* 1999; Lindoy, 1989; Kaden *et al.,* 1989; Nation *et al.,* 1996; Amendola *et al.,* 2000). The hydrophobic exteriors may allow the macrocycle to solubilise metal ions in non-aqueous solvents or in membrane media. These properties allow macrocycles to act as models for carrier molecules in the study of active ion transport phenomena as well as sequestering agents for metals of environmental importance, such as Pb(II), Cd(II) or Hg(II) (Arranz *et al.*, 2001). These heavy metals have detrimental physiological effects to both humans and animals. For example, Pb(II) tends to accumulate in the bone tissue, kidneys and liver. The symptom of lead poisoning includes anaemia, headaches, convulsions, damage to the brain and the central nervous system. Cd(II) poisoning occurs even at very low levels and can lead to kidney failure and tumours. The symptoms of Hg(II) poisoning include headaches, tremors and memory loss (Martell and Hancock, 1996).

The coordination chemistry of macrocyclic polyamine ligands bearing flexible pendant donor groups from the cyclic framework has attracted much interest in recent years and has developed to the point where ligands and complexes of this type are now used as starting materials for a variety of secondary scientific investigations and technological applications (Kaden, 1984; Bernhardt and Lawrance, 1990; Wainwright, 1997; Wainwright, 2001; Costamagna *et al.,* 2000). Many syntheses for this class of ligand involve the attachment of pendant arms to a preformed macrocycle through reaction of an appropriate alkylating reagent with one or more secondary amino groups in the macrocycle. This is one of many advantages offered by macrocyclic ligands with nitrogen donor atoms over macrocycles with oxygen donor atoms which do not allow *O*-functionalisation. The donor atoms of the pendant arms can either be the same as the donor atoms of the parent macrocyclic ligand, in this case nitrogen donor atoms, or different, for example oxygen donor atoms, thereby affording macrocyclic ligands with different types of donor atoms. The pendant arms with oxygen donor atoms can be used to bring a chiral centre in the macrocyclic ligand thereby affording macrocyclic ligands with chiral attributes. The combination of different donor atoms may influence the selectivity of the ligands and the stability of the complexes, and may have stereochemical consequences.

1.16.1 Biological and medicinal applications

Macrocyclic ligands and their metal complexes are involved in a number of important biological and medical systems because of their enhanced kinetic and thermodynamic stabilities which is a result of a metal ion being firmly held in the cavity of the macrocycle and are not impaired by competing demetallation reactions. In general, macrocyclic ligands form stable metal complexes than their open chain analogues (macrocyclic effect). This is one of many advantages macrocycles have over their open chain analogues and is intensely exploited in medicine and bioinorganic fields. For example, Zn(II) complexes of 1,5,9-triazacyclododecane are effective models for the active sites in the zinc containing enzymes such as carbonic anhydrase, acid and alkaline phosphatases and alcohol dehydrogenase (Kimura *et al.,* 1994).

The antibiotic nonactin (**Chart 1.9**) is an integral part of Vitamin B_{12} with oxygen donor atoms and binds potassium cation selectively thereby acting as a carrier for this cation across

the cell membranes and artificial lipid barriers. The active transport of the alkali metal ion, potassium cation, is very important in controlling the ionic balance within the cells and the transmission of neutral impulses (Constable, 1999; Lindoy, 1989).

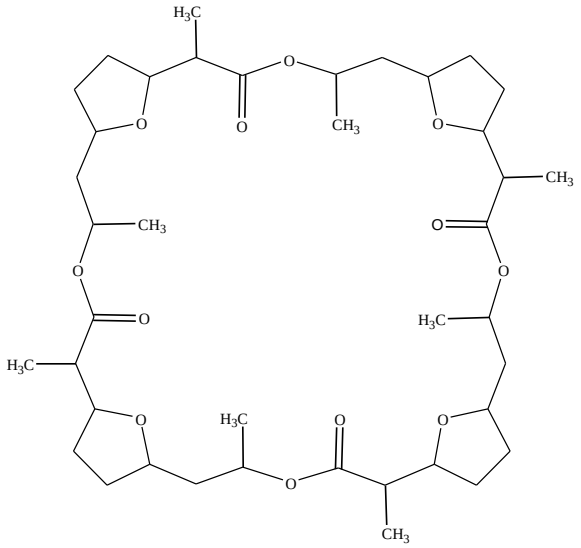

Chart 1.9: The molecular structure of nonactin.

Zn(II) complexes of 1-oxa-4,7,10-triazacyclododecane (12aneN_3O), 1,5,9-triazacyclododecane (12aneN_3), and 1-hydroxyethyl-1,4,7-triazacyclononane (9aneN_3OH) promotes cleavage of the ribonucleic acid (RNA) analogue, 2-hydroxypropyl-4-nitrophenyl phosphate (HpPNP) by promoting transesterification at the phosphate diester to give a 2′,3′-cyclic phosphate diester and concomitant cleavage of the RNA strand (Rossiter *et al.,* 2005).

Liang *et al.,* (2003; 2004) reported that pharmacological tests of the nuclei of [NiL]- and [CuL]-stimulated BEL-7402 (human hepatocellular carcinoma) and HXO-RB44 (retinoblastoma) cells exhibited condensation and break down into chromatin clumps typical of apoptosis and also exhibited perturbation effects to cell cycle which has relevance as an antitumor agent (L = 1,4,7-triazecan-9-ol). 1,4,7-triazecan-9-ol is a rare example of macrocycles with donor atom(s) attached on the carbon backbone of the ring and not directly on the *N*-functional group of the ring (**Chart 1.10**).

The majority of azamacrocyclic ligands are functionalised on the *N*-functional group. The *N*-functionalisation of the azamacrocycles alters their electronic and steric properties and has a

profound effect on the behaviour of the resultant macrocycle. Macrocycles with pendant arms carrying donor atoms of their own represents a new family of synthetic cation binders, characterised by both the parent macrocyclic ligand and the cation-ligating functionalised side-arm. In this class of compounds, the donor group on the flexible sidearm usually provides further coordination site(s) for guest cations trapped within the parent macrocyclic ring or sitting above the plane defined by the ring donor atoms.

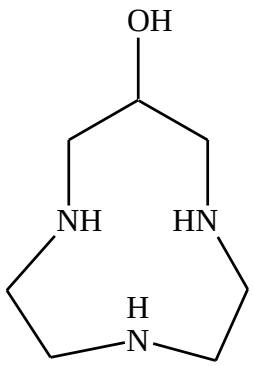

Chart 1.10: The molecular structure of 1,4,7-triazecan-9-ol.

For example, Prata *et al.,* (1999; 2000) reported the *in vivo* behaviour of ^{67}Ga(III) chelates of NOTA, NOTP and NOTPME in Wistar rats. The neutral chelates ^{67}Ga(NOTA) and ^{67}Ga(NOTPME) showed higher depuration efficiency and faster transit time through the kidneys than the negatively charged ^{67}Ga(NOTP)$^{3-}$, a tracer which exhibited slow uptake and long retention by the kidneys. These results demonstrated the importance of ^{67}Ga(NOTA) and ^{67}Ga(NOTPME) in biomedical imaging and bio-distribution owing to their kinetic inertness which make them resistant to decomplexation. The commonly used procedure at the moment involves the injection of ^{67}Ga(III) into the blood stream in the form of gallium citrate, a weak chelate, which results in the Ga(III) ion being transchelated to transferrin and is found in areas of high iron uptake such as bone marrow, liver, spleen, gastrointestinal tract, salivary glands, and in the breast tissue of young adult or lactating females. This is the case because of the slow clearance of the radioisotope from the body (Cox and Rillay, 1995).

The trivalent miniproteins target the CD4-binding sites displayed in the trimeric glycoprotein gp120 complex of HIV-1 was reported by Li *et al.,* (2007). The three CD4M9 miniprotein moieties were tethered on 1,5,9-triazacyclododecane which acted like a threefold symmetric

scaffold (**Chart 1.11**). Antiviral assay of this compound revealed that the synthetic trivalent miniproteins significantly enhanced the anti-HIV activities over the monomeric CD4M9 against both R5- and X4-tropic viruses, indicating the beneficial multivalent effects (three on one versus one on one).

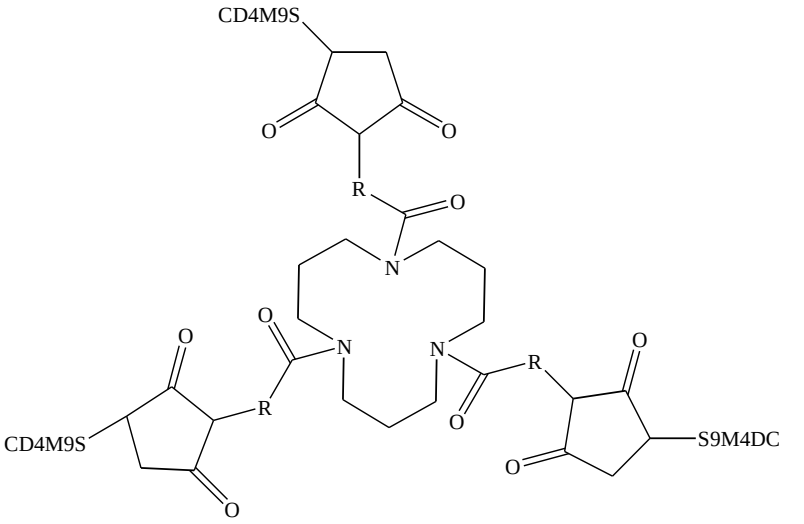

R=$(CH_2)_2$; $(CH_2)_{10}$; $(CH_2)_2CONH(CH_2)_2(OCH_2CH_2)_2$; $(CH_2)_2CONH(CH_2)_2(OCH_2CH_2)_{12}$

Chart 1.11: The CD4M9 miniprotein moieties tethered on a 1,5,9-triazacyclododecane.

Each CD4M9 miniprotein has sulphur linkages (**Chart 1.12**) and is attached to a linker of variable sizes which further increase the lipophilic properties of the protein.

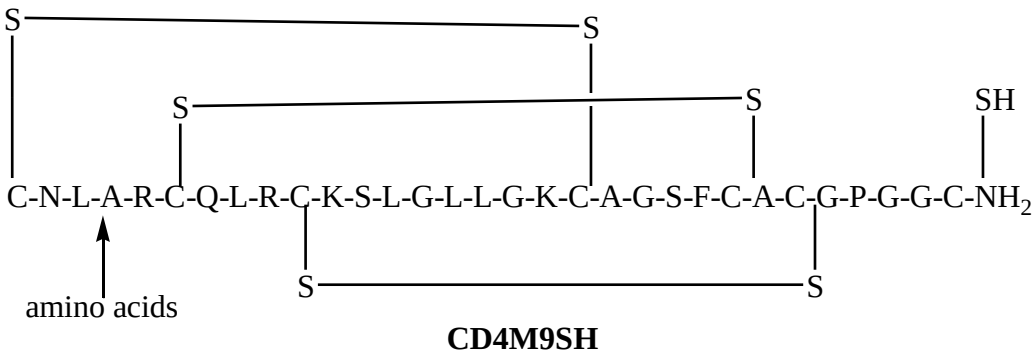

CD4M9SH

Chart 1.12: The thiol linkages in a structure of CD4M9SH.

The parent macrocycle, 1,5,9-triazacyclododecane, substituted with trimesic acid/1,2-diamine cyclooligomers give rise to a new class of two-armed sequence-selective receptors for peptides. The rigidity of 1,5,9-triazacyclododecane provide a conformationally restricted moiety that covalently links and directs two functionalised substrate-binding arms towards

one another to form a binding cleft. Screening of these compounds against a 3375-member library (Boyce *et al.,* 1994) of *N*-acetyl tripeptides revealed novel peptide-binding properties (Iorio and Still, 1996) which has very important application in protein chemistry.

Thöm *et al.,* (1986) reported the synthesis of 1,5,9-*tris*(2,3-dihydroxybenzoyl)-1,5,9-triazacyclododecane to specifically act as a reagent for Fe(II). The design of the structure of 1,5,9-*tris*(2,3-dihydroxybenzoyl)-1,5,9-triazacyclododecane mimics the natural molecule, enterobactin (**Chart 1.13**), used by E. coli to transport Fe(II) through its cell walls. Under strongly alkaline conditions the ligand coordinates to Fe(II) using all six phenolic oxygens to yield an extremely strong complex which is exactly the opposite when the pH is lowered.

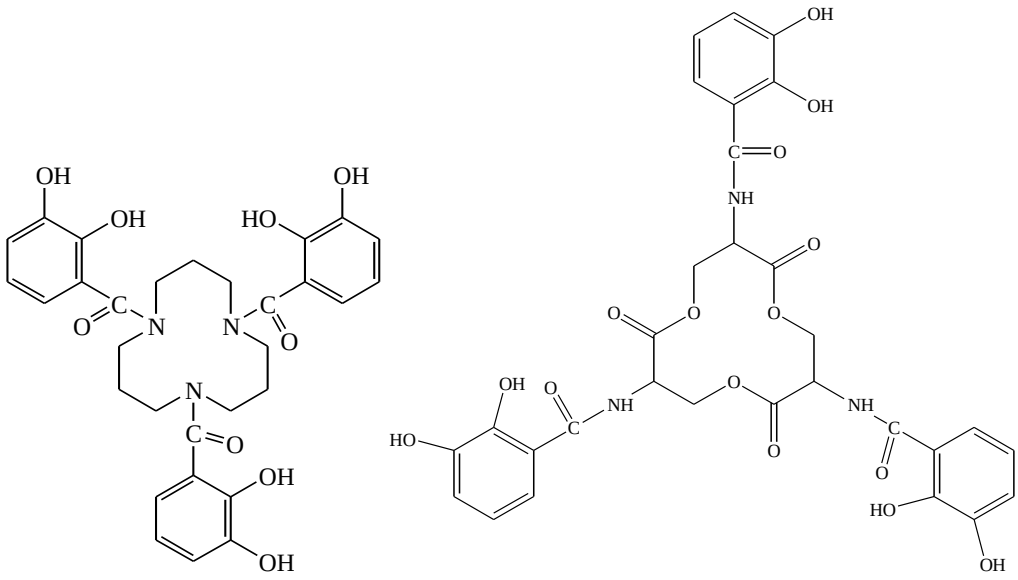

Chart 1.13: The structure of 1,5,9-*tris*(2,3-dihydroxybenzoyl-1,5,9-triazacyclododecane (left) and naturally produced enterobactin (right).

1.16.2 Industrial applications

With the growing industry, the need to replace naturally produced molecules with synthetic molecules is very important to save the environment. Macrocyclic molecules are increasingly finding applications in industry. For example, cyclam and other macrocycles are being employed as the core of surfactants. Larpent *et al.,* (2004) designed and synthesised a surfactant based on cyclam with sugar-based units as pendant arms (**Chart 1.14**). In this way

the versatile surfactants combine the polar properties of the sugar moiety with the cation binding properties of the cyclam macrocycle.

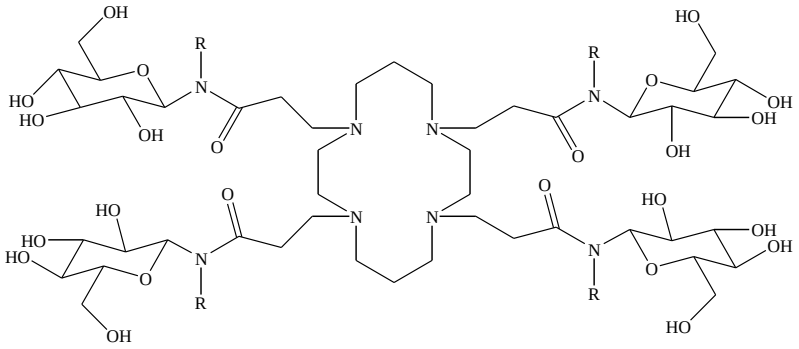

Chart 1.14: Four sugar moieties tethered on cyclam.

The water-gas shift reaction is very important in industry. It is an important route for the production of hydrogen gas from water and the route to increase the hydrogen content of synthetic gas (**Equation 1.7**).

$$H_2O + CO \rightleftharpoons H_2 + CO_2 \qquad \textbf{(Equation 1.7)}$$

Kallinen *et al.,* (1997) reported that reactions of $H_4Ru_4(CO)_{12}$ with cyclic triazaligands resulted in the formation of $[LH]^+[H_3Ru_4(CO)_{12}]^-$ salts, (L = 1,4,7-triazacyclononane, 1,4,7-trimethyl-l,4,7-triaza-cyclononane, 1,5,9-triazacyclododecane and 1,5,9-trimethyl-l,5,9-triazacyclododecane) which showed reactivity towards CO at elevated temperatures, catalytic activity in the water-gas shift reaction (WGSR) and in the carbonylation of methanol.

1.16.3 Catalytic effect of macrocyclic metal complexes

Over the past few years there has been a tremendous increase in the use of macrocyclic ligands as catalysts in most important reactions. For example, the dinuclear manganese complex $[(Me_3TACN)_2Mn^{IV}{}_2(\mu\text{-}O)_3](PF_6)_2$ was reported in a number of publications to catalyse oxygenation of alkanes by peroxyacetic acid or H_2O_2 in the presence of acetic acid to give alkanols, alkanones and alkyl hydroperoxides (Smith and Shul'pin, 1998). Zn(II) complexes of 1,5,9-triazacyclododecane act as catalysts for hydrolysis of esters such as phenyl acetate, *p*-nitrophenyl acetate, *m*-chlorophenyl acetate and *p*-cyanophenyl acetate. The

kinetic data for these hydrolysis reactions is incompatible with the mechanism in which the water and hydroxide ion coordinate to the metal centre and makes a nucleophilic attack at the ester linkage. Instead, the results supported the mechanism in which the ester is first activated by being complexed to the metal centre and then water or hydroxide ion makes a nucleophilic attack at the complexed ester. The data further indicated that the electrostatic interaction between the cationic metal centre and the anionic hydroxide ion facilitated the attack of hydroxide ion at the complexed ester and the C-O bond of the ester is not cleaved significantly in the rate-determining transition state for attack by both water and hydroxide ion (Suh *et al.,* 1998). This saves to showcase the versatility of macrocyclic ligands and their metal complexes.

Chamberlain *et al.,* (1999) reported that the yttrium complexes ligated to the hexadentate ligands, *S*-H_3L^{Me}, *R*-H_3L^{iPr} and H_3L^{Me2} (see **Chart 1.15** for key to ligands abbreviation) catalysed the polymerisation of lactide. The structural differences of the ligands, which are a result of having different hydroxyalkyl pendant arms, influenced the polymerisation rate and the polymer molecular weight.

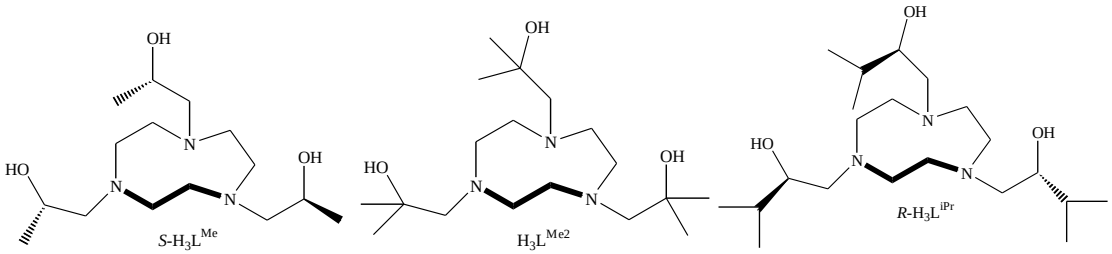

Chart 1.15: The molecular structure of *S*-H_3L^{Me}, H_3L^{Me2} and *R*-H_3L^{iPr} from left to right.

The yttrium complex of *S*-H_3L^{Me} gave modest polymerisation rate with the resultant polymer mostly monodisperse whereas the complex of *R*-H_3L^{iPr} gave high polymerisation rate with the molecular weight of polymers being 2-3 times greater than the polymers obtained using the yttrium complex of *S*-H_3L^{Me}. The yttrium complex of H_3L^{Me2} showed the highest polymerisation rate and greatest molecular weight polymers.

Just recently Feng *et al.,* (2007) reported that the manganese complex of 1,4,7-*tris*(2-hydroxypropyl)-1,4,7-triazacyclononane catalysed the oxidation of sulphide to sulphoxide and sulphone. The results showed that the oxidation of sulphides to sulphone can be achieved stepwise *via* sulphoxide with little to no side reactions. This is very important considering the importance of sulphur chemistry. The most amazing thing is that this ligand (**Chart 1.16**) has

three nitrogen donor atoms on the macrocyclic backbone and oxygen donor atoms on the pendant arms. The design of this macrocyclic ligand is the same as several of the ligands we want to investigate.

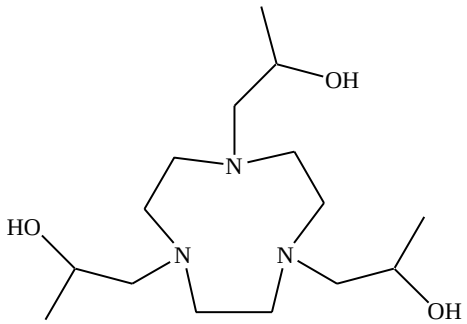

Chart 1.16: Macrocyclic ligand 1,4,7-*tris*(2-hydroxypropyl)-1,4,7-triazacyclononane.

1.16.3.1 Catalytic oxidation of achiral sulphur compounds

The dinuclear manganese complexes $[(Me_3TACN)_2Mn^{IV}{}_2(\mu\text{-}O)_3](PF_6)_2$ and $[(Me_3TACN)_2Mn^{III}{}_2(\mu\text{-}O)(\mu\text{-}O,O'\text{-}O_2CMe)_2](PF_6)_2$ (**Chart 1.17**) have been reported as catalysts for sulphide oxidation with high turnover numbers (TONs) even though the conversion of sulphides is not satisfactory because a large amount of co-catalyst additives are required for the complete oxidation of substrates (Barker and Ren, 2004; Barton *et al.*, 1998). Without the co-catalyst, the dimanganese complexes yield high percentage of disulphides and their respective oxidation products. For example, 42% of disulphide and its oxidation products was reported for the oxidation of 2-chloroethyl phenyl sulphide oxidation with $[(Me_3TACN)_2Mn^{III}{}_2(\mu\text{-}O)(\mu\text{-}O,O'\text{-}O_2CMe)_2](PF_6)_2$. The major problem with the use of co-catalysts is that usually there is over oxidation of the intended sulphoxides to sulphones. For example, Barker and Barton reported that the use of $[(Me_3TACN)_2Mn^{IV}{}_2(\mu\text{-}O)_3](PF_6)_2$, and $[(Me_3TACN)_2Mn^{III}{}_2(\mu\text{-}O)(\mu\text{-}O,O'\text{-}O_2CMe)_2](PF_6)_2$, with co-catalyst resulted in sulphone products only. In spite of successful application as catalysts for sulphide oxidation, there are some disadvantages for manganese complexes of Me_3TACN. In sulphide oxidation with the dimanganese complexes, co-catalyst is used in large quantities (Barker and Ren, 2004; Barton *et al.*, 1998).

Liu *et al.*, (2007) reported that Cu(II) complex of 1,4,7-*tris*(carbamoylethyl)-1,4,7-triazacyclononane (**Chart 1.18**) catalysed the oxygenation of ethyl phenyl sulphide utilising H_2O_2 under ambient conditions. The oxidation of ethyl phenyl sulphide to its corresponding

sulphoxide and sulphone followed a step by step mechanism, which made it possible to control the product.

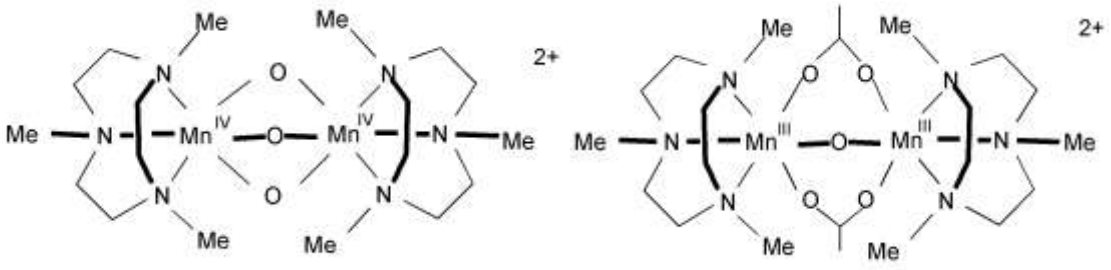

Chart 1.17: The dinuclear manganese complexes $[(Me_3TACN)_2Mn^{IV}{}_2(\mu\text{-}O)_3]^{2+}$ and $[(Me_3TACN)_2Mn^{III}{}_2(\mu\text{-}O)(\mu\text{-}O,O'\text{-}O_2CMe)_2]^{2+}$

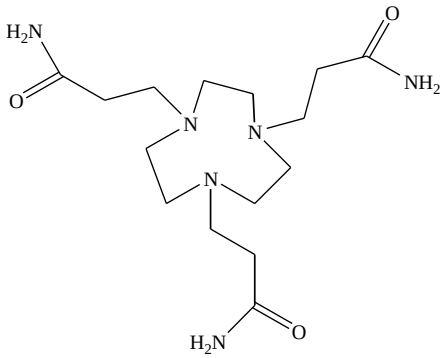

Chart 1.18: Molecular structure of 1,4,7-*tris*(carbamoylethyl)-1,4,7-triazacyclononane.

1.16.3.2 Catalytic oxidation of chiral sulphur compounds

One of the most recently used chiral catalyst, the 1:1 manganese complex of 1,4,7-*tris*(2-hydroxypropyl)-1,4,7-triazacyclononane, [MnL](ClO4)2 (L = 1,4,7-*tris*(2-hydroxypropyl)-1,4,7-triazacyclononane) efficiently catalysed the oxidation of ethyl phenyl sulphide (EPS), butyl sulphide (BBS) and phenyl sulphide (PPS) to their corresponding sulphoxides and sulphones using H_2O_2 as the oxidant. The same authors reported the oxidation of 2-Chloroethyl phenyl sulphide (CEPS) to 2-chloroethyl phenyl sulphone and phenyl vinyl sulphone and presented the UV–Vis and electron paramagnetic resonance (EPR) evidence which showed that the metal centre of the complex was transformed from Mn(II) to Mn(IV) after the addition of H_2O_2 (Feng *et al.*, 2007). By changing the reaction conditions, ethyl phenyl sulphoxide and ethyl phenyl sulphone were produced selectively. In contrast to the sulphide oxidation catalysed by manganese complexes with 'innocent' pendant arms discussed above, no co-catalyst is desired and no disulphides and their oxidation products

were reported in these reactions. Although low turnover numbers were reported for the manganese complex of 1,4,7-*tris*(2-hydroxypropyl)-1,4,7-triazacyclononane than for the dimanganese complexes of Me_3TACN, the former complex offers a lot of advantages as compared to the dimanganese complexes of Me_3TACN. One of the merits is that sulphide conversion is 100% and is oxidised selectively. This is very important because it obviates the need for separation which is normally tedious and leads to loss of products. The other advantage is that disulphides and their oxidation products do not take place in the reactions where the manganese complex of 1,4,7-*tris*(2-hydroxypropyl)-1,4,7-triazacyclononane is used and the complete transformation to oxidised products does not need a co-catalyst. The third advantage is that sulphoxide or sulphone are produced selectively by simply manipulating the reaction conditions (Feng *et al.,* 2007).

1.17 The importance of 12aneN_3 with hydroxyalkyl pendant arms

Kimura *et al.,* (1994) reported the synthesis and characterisation of alcohol pendant 1,5,9-triazacyclododecane ligands (**Chart 1.19**). A complexation study of the Zn(II) complexes of these macrocyclic polyamines revealed that the pendant alcohol of 1-(3-hydroxypropyl)-1,5,9-triazacyclododecane Zn(II) complex deprotonates at an extremely low pK_a value of 7.4 at 25 °C to become an alkoxide anion donor at the fourth coordination site. This illustrates that the serine residue located at the centre of zinc enzymes can be deprotonated at physiological pH.

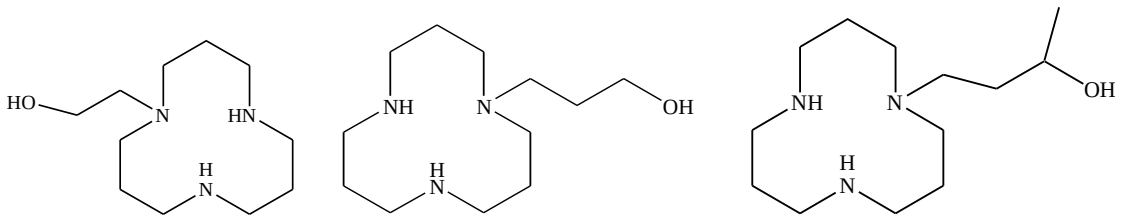

Chart 1.19: Molecular structures of 1-(2-hydroxyethyl)-1,5,9-triazacyclododecane; 1-(3-hydroxypropyl)-1,5,9-triazacyclodode; 1-(3-hydroxybutyl)-1,5,9-triazacyclododecane from left to right.

One of the most important advantages of macrocyclic ligands carrying hydroxyalkyl groups is that they can be easily halogenated thereby acting as a precursor for a series of halogenated

macrocycles. For example, Parker *et al.,* (2005) reported the synthesis of a nitrogen mustard, 1,5,9-*tris*(2-chloroethyl)-1,5,9-triazacyclododecane trihydrochloride, from 1,5,9-*tris*(2-hydroethyl)-1,5,9-triazacyclododecane (**Chart 1.20**) which showed antitumor activity against human chronic myeloid leukemia cell line K562 (Mosmann, 1983). The three hydroxyl groups of 1,5,9-*tris*(2-hydroethyl)-1,5,9-triazacyclododecane provided an opportunity for three alkylating moieties to be tethered on the same molecule.

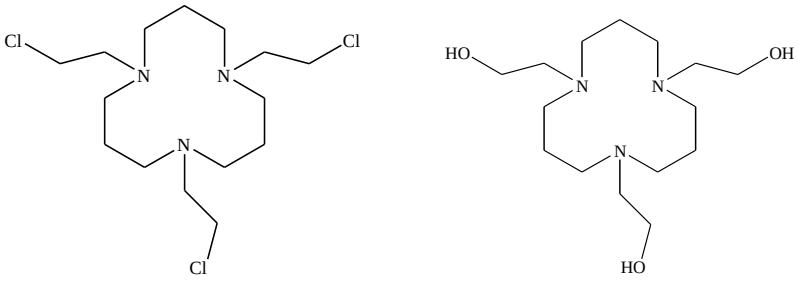

Chart 1.20: The molecular structure of 1,5,9-*tris*(2-chloroethyl)-1,5,9-triazacyclododecane trihydrochloride (left) and 1,5,9-*tris*(2-hydroxyethyl)-1,5,9-triazacyclododecane (right).

By placing a methyl, phenyl, butyl or two methyl substituents on the ethane backbone of the hydroxyethyl units the macrocyclic ligand can be made chiral in the first three cases whereas in the last case it is made more sterically encumbered while retaining its C_3 symmetry in both cases. Addition of the thiol groups on the same parent macrocyclic ligand can make the ligand relatively soft as compared to the ligands with hydroxyalkyl pendant arms.

1.18 Background and justification

The chemistry of macrocycles with pendant donor groups is of great interest because of their potential use in industry and medicine. The hydroxyl pendant arms are particularly interesting because they form complexes in which the OH can remain protonated and act as an alcohol or can be deprotonated and act as an alkoxide. They also present an opportunity to obtain a chiral macrocyclic ligand which forms complexes with single absolute configuration (Belal *et al.,* 1991). In addition, the transition metal complexes with sulphur ligands are of significance because of diverse bonding possibilities and their role as models for biological metal-sulphur interactions (Jain and Jakkal, 1996). In the cases where pendant arms with hydroxyalkyl donor groups are appended on the backbone of azamacrocyclic ligands, the ligand is made

harder by having hard to borderline donor atoms and on the other hand, by replacing the oxygen donor atoms with sulphur donor atoms on the pendant arms, the ligand is made softer by having borderline to soft donor atoms.

The coordination chemistry of 1,4,7-triazacyclononane has been well studied over the last twenty years. There was a widespread belief that among the triazamacrocycles, only $9aneN_3$ and its *N*-alkylated analogues had rich and diverse chelation chemistries owing to the enormous thermodynamic and kinetic stability of the amine-metal fragment regardless of the oxidation state and d^n configuration of the central metal ion (Haines and McAuley, 1981; Zhang and Busch, 1994). More recently, *N*-functionalisation of $9aneN_3$ through incorporation of three pendant arms holding *N*-donor atoms (Sessler *et al.,* 1988; Taylor *et al.,* 1983; Wieghardt *et al.,* 1986; Koikawa *et al.,* 1998; Wieghardt *et al.,* 1990; Stockheim *et al.,* 1996), *O*-donor atom (Wieghardt *et al.,* 1983; van der Merwe *et al.,* 1985; Moore *et al.,* 1989; Matthews *et al.,* 1991; Bossek *et al.,* 1993; Farrugia *et al.,* 1995; Luckay *et al.,* 1996), *S*-donor atom (Moore *et al.,* 1990; Beissel *et al.,* 1993) and *P*-donor atom (Konstantinovskaya *et al.,* 1985) groups afforded a variety of hexadentate ligands which can confer remarkable stability upon metal centres, thereby controlling their coordination geometries and oxidation states. The $9aneN_3$ has been successfully *N*-functionalised with three hydroxyl and thiol pendant arms and have found applications in many fields including catalysis and medicine. Thiol pendant arms form very strong complexes with Ga(III) and In(III) which have vast applications in medicine. Unfortunately very few reports exist on macrocyclic ligands having this pendant arm because of difficulties in its preparation.

However, Gladkikh *et al.,* (2002) reported that larger macrocyclic rings also show interesting properties. The large triazamacrocycle 1,5,9-triazacyclododecane is readily derivatised at the nitrogen atoms to give *N*-functionalised ligands such as 1,5,9-trimethyl-l,5,9-triazacyclododecane (Kallinen, 1997), 1,5,9-*tris*(ethoxycarbonyimetlyl)- 1,5,9-triazacyclododecane, 1,5,9-*tris*(carboxymethyl)-1,5,9-triazacyclododecane, 1,5,9-*tris*(dimethylamidomethyl)-1,5,9-triazacyclododecane (Helps *et al.,* 1989), 1-(2-pyridylmethyl)-1,5,9-triazacyclododecane, 1-(2-pyridyl-2'-ethyl)-1,5,9-triazacyclododecane (Turonek *et al.,* 1995), 1,5,9-*tris*[(2*S*)-2-hydroxybutyric acid]-l,5,9-triazacyclododecane (De Lagrange and Nepveu, 1999).

Although the synthesis of 1,5,9-triazacyclododecane was first reported by van Winkle *et al.*, in 1966, to the best of our knowledge, there has been no report on the synthesis of the novel pendant arm macrocycles with this parent molecule carrying secondary or tertiary alcohol functional group on the pendant arms or thiol pendant arms. This means that a vast body of knowledge on the synthesis, physical and chemical properties of 1,5,9-triazacyclododecane with these pendant arms still needs to be accumulated. It is against this background that we embarked on the synthesis of 1,5,9-*tris*[(2*S*)-hydroxypropyl]-1,5,9-triazacyclododecane (THPTACD), 1,5,9-*tris*(2-hydroxy-2-methylpropyl)-1,5,9-triazacyclododecane (THMPTACD), 1,5,9-*tris*[(2*S*)-2-hydroxy-2-phenylethyl]-1,5,9-triazacyclododecane (THPETACD), 1,5,9-*tris*[(2*S*)-hydroxybutyl)]-1,5,9-triazacyclododecane (THBTACD) and 1,5,9-*tris*(2-mercaptopropyl)-1,5,9-triazacyclododecane (TMPTACD).

1.19 Aim of the research

The main objective of this research project was to synthesise from simple starting materials 12aneN_3 macrocyclic ligand with three hydroxyl and thiol pendant arms, namely THPTACD, THMPTACD, THPETACD, THBTACD and TMPTACD. Previous publications on the synthesis of 12aneN_3 macrocycle reported very low yields (62%) and we also aimed at improving the existing procedures.

Further objectives were to:

-Investigate the protonation constants of the macrocyclic ligands THPTACD, THMPTACD and THBTACD. The protonation constants gives an idea about the acid-base properties of macrocycles and its value is normally used in determining the stability constant of metal ion complexes by using the ESTA-WIN program to calculate the stability constants.

-Investigate the formation constants of THPTACD, THMPTACD and THBTACD with Co(II), Zn(II), Cd(II) and Pb(II). Pb(II) is the largest and Co(II) is the smallest ion of the metal ions used in this study. In a typical metal ion recognition investigation, the determination of the stability constants for the respective 1: l metal-ligand complexes are very important in understanding metal ion preferences.

-Grow crystals of various metal ions with THPTACD, THMPTACD, THPETACD, THBTACD and TMPTACD and to determine the crystal and molecular structures by single crystal X-ray diffraction. Crystal structures give valuable information about bond angles and lengths and thus an idea about bonding preferences of different metal ions. Such an investigation also provides information about the coordination numbers and geometry around the central metal ion. In metal ion recognition investigation, X-ray diffraction structure determination, usually supplement stability constants when studying the selectivity of a particular ligand for metal ions.

Chapter 2

The preparation and characterization of macrocyclic ligands with hydroxyl and thiol pendant arms

2.1 Introduction

In recent years there has been growing interest in preparation of macrocycles with pendant arms mainly because they offer chemists an opportunity to design molecules tailored for specific functions. Among the pendant arms being employed, hydroxyl and thiol pendant arms are of immense interest. Particularly, 9aneN_3 and its derivatives has been extensively studied with hydroxyl pendant arms while the thiol pendant arms have not been fully explored because of difficulties in synthesis which more often leads to polymerisation (Lewin, 2002). On the other hand and to the best of our knowledge, 1,5,9-triazacyclododecane (12aneN_3) with either three thiol pendant arms or three pendant arms carrying oxygen donor atoms attached to the secondary or tertiary carbon atom of the pendant arms has not been explored.

Various methods for the preparation of cyclic amines of medium-large ring size have been reported in the literature (Sabatini and Fabbrizzi, 1979; Richman and Atkins, 1974; Stetter and Meyer, 1961; Collman and Schneider, 1966; Koyama and Yoshino, 1972; Briellmann *et al.,* 1987, Smith *et al.,* 1978; Krakowiak *et al.,* 1989). Each synthetic method offers some advantages, but cannot be used in every case because of low reaction yields, availability and the cost of starting materials in the preparation process and, in many cases, the difficulty of removing protecting groups. Some methods are also limited by the availability of other functional groups which need to be protected to avoid side reactions (Krakowiak and Bradshaw, 2000; Krakowiak *et al.,* 1993). In the past, the cyclisation to medium or large rings was commonly believed to require high dilution in the absence of template effects (Pedersen and Frensdorff, 1972; Green, 1972; Curtis, 1968). However, Richman and Atkins, (1974) reported a procedure that required no rigid structures, high dilution or metal template yet afforded high yields and minimal polymerisation. The procedure reported by these authors revolutionised the manner in which the medium-large ring macrocycles are synthesised.

2.2 Methods of synthesis and pathways

Preparation of macrocyclic ligands poses a very big challenge because of the high probability of obtaining multiple stable products the most likely of which are the open chain polymers. There are several known methods of preparing macrocycles. The most commonly used methods are template synthesis, direct synthesis and synthesis at high dilution (Martell and Hancock, 1996).

2.2.1 Template synthesis

One of the major challenges with the synthesis of macrocycles is the conformational control in bringing the two reactive ends of a chain together in the final cyclisation step (**Scheme 2.1**). Template synthesis is used to circumvent this problem. The method involves the incorporation of a metal ion which coordinates the donor atoms to give the reacting ends of the molecule the required spatial arrangement for the cyclisation reaction. This is the case because the metal ion coordination to the donor atoms pre-organises the intermediate in the conformation required to give the desired cyclic product.

2.2.1.1 Types of template effect

There are two types of template effects, namely:

(1) *The kinetic template effect*. In this case, the function of the metal ion is to control the stereochemistry in the intermediates such that cyclisation is the favoured pathway. The macrocyclic ligand of interest is not formed from the same reactants in the absence of the templating metal ion.

(2) *The thermodynamic template effect*. In this type of template reaction, the macrocyclic product is formed along with other species and in the absence of the templating metal ion. The function of the metal ion is to coordinate to the macrocycle and to remove it from the equilibrium mixture (Constable, 1999).

Template reactions may involve any number of reactants, although [1+1] or [2+2] cyclisation reactions are the most common. It is very often found that the metal ion remains coordinated to the macrocycle **Scheme 2.1**; (Constable, 1999).

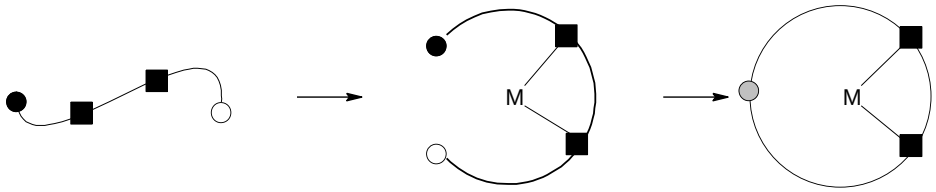

Scheme 2.1: A schematic view of the cyclisation step involved in a template macrocycle synthesis. The circles represent the mutually reactive functional groups and the squares are the additional donor atoms. The binding of the metal to the donor atoms pre-organise the ligand into the required conformation for cyclisation. Some donor atoms have been excluded from the diagram.

In most cases template reactions are used when it is practically impossible to perform the reaction in the absence of a metal ion. For example, in an attempt to obtain **1.1** from the reaction of biacetyl (MeCOCOMe) with $H_2NCH_2CH_2SH$ results in the formation of polymers and the cyclic species **1.2**. However, if the biacetyl is reacted with the Ni(II) complex of $H_2NCH_2CH_2SH$, the Ni(II) complex of **1.1** is obtained.

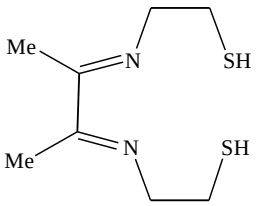

1.1

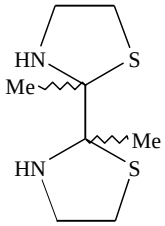

1.2

The metal ion stabilises the acyclic intermediate **1.1**. As a free ligand, **1.1** possesses nucleophilic thiol and electrophilic imine groups and cyclisation arises by attack of the thiol upon the carbon of the imine to give **1.2**. When **1.1** is coordinated to the Ni(II), the nucleophilicity of the thiolate is reduced because it is bonded to an electropositive centre, the thiolate is constrained so that it cannot approach the imine, and the imine is made less electrophilic by the back-donation of d-electron density into the π^* orbitals. The metal also pre-organises the two thiolate groups so that they are correctly oriented for the final cyclisation reaction (**Scheme 2.2**).

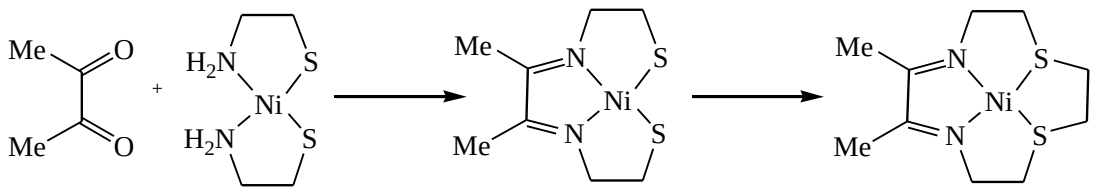

1.3

Scheme 2.2: The Ni(II) template synthesis of a mixed donor macrocycle (Constable, 1999).

2.2.1.2 Generation of free macrocycles from their metal complexes

In many cases, the metal ion remains coordinated to the macrocycle and a metal complex is obtained directly. When there is no need to isolate a free ligand, the exchange of one metal ion with another is used to obtain a new complex. This exchange of one metal ion with another is usually guided by the Irving-Williams stability series (Irving and Williams, 1953). In some cases it is important to remove the macrocycle from its coordinated metal ion. This is a frequent procedure in the macrocycle ligand synthesis due to the fact that the macrocycles are usually employed in other studies such as potentiometry. More often forcing conditions are used to remove the metal ion from the complex because of the high kinetic and thermodynamic stability of the macrocyclic complexes. For example:

(1) The addition of excess acid may lead to demetallation of the complex of an amine-containing macrocycle. For chemically labile systems, the acid protonates the amine functions as they dissociate from the metal ion and thus scavenge the macrocycle and its *N*-protonated form.

(2) Demetallation may be induced by addition of a strongly competing ligand to a solution of the macrocyclic complex, the cyanide ion or the ethylenediaminetetraacetate are frequently used. In some cases, the metal may be removed as an insoluble precipitate leaving the metal-free ligand in the supernatant liquid. This approach is limited to the ligands which are stable and also those which do not undergo subsequent reactions under the demetallation conditions.

(3) When the template ion is weakly coordinated, demetallation can be induced by simply dissolution of the complex in a coordination solvent in which the macrocycle has poor solubility.

(4) For some systems it is necessary to perform a reduction-oxidation reaction (usually a reduction) on the metal complex before it may be removed from the macrocycle. This is often the case when the metal ion in its original oxidation state is kinetically inert. On reduction, the lability of such metal ion is usually increased and then one of the three methods listed in 1, 2 or 3 above can be used to remove the ion from its macrocyclic complex.

The advantages of template reactions include good yields, obtaining metal complexes directly and mild conditions are usually employed during synthesis.
The disadvantages include:

(1) Not all metal ions can act as a template for a desired reaction and it is often a rather imprecise art in finding the correct metal ion. This presents a problem when one is interested in a different metal complex from the templated metal ion and also other factors such as hole-size match selectivity come into play on top of the known factors such as steric and electronic effects.

(2) The conditions required to remove metal ions from the macrocyclic complexes may often lead to fragmentation of the fragile macrocyclic ligand systems and it is not always possible to convert template products to free ligands.

2.2.2 Non-template synthesis

This method is also known as the direct method. The pre-requisite of this approach is that the macrocyclic ligand must be stable and isolable under the reaction conditions. The first step in much contemporary coordination chemistry normally involves time-consuming precursor protection and the final reaction step involves the cyclisation process in which the two ends of a chain, bearing mutually reactive functionalities, come together to create a ring forming bond.
When using the direct method no metal ions are needed to form or to keep any of the precursors in place (**Scheme 2.3**). The use of protection groups make it much easier and the conditions are not extreme to perform these reactions.

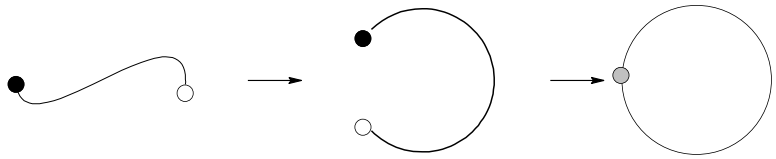

Scheme 2.3: Schematic view of a cyclisation step involved in a non-template macrocyclic ligand synthesis. The circles represent the mutually reactive functional groups. In the first step the appropriate conformation must be adopted so that the reactive functional groups are close to one another and in the correct orientation for reaction. Secondly the new bond is formed and this will complete the macrocycle. Some donor atoms have been excluded from the diagram.

The problem which is illustrated in **Scheme 2.3** is that before the cyclisation reaction can take place, the two reactive groups must be brought close to one another. Unless there are special secondary interactions within the molecule, or highly pre-organised or rigid systems are involved, the extended conformation pathway is more likely than the cyclisation reaction. This is the case because it is relatively unlikely that a reactive group will meet the reaction partner at the other end of its own molecule but rather it is far more likely that it will meet a reactive functionality of a second molecule. The result of this entropic constraint is that the formation of polymeric species is a significant alternative pathway to the desired macrocyclisation reaction that has to be taken care of to maximise the macrocyclic products (Constable, 1999).

2.2.3 High dilution technique

This is one example of non-templated synthesis but it is normally treated on its own. The principle behind this technique is that once the one end of the reacting species has reacted, the probability of the other reactive end of a molecule meeting a second molecule is much less when the concentration of the reacting species is very low. In this technique, very small quantities of one reactant are dispensed into the reaction solvent at a very slow rate such that at any given time, the concentration of the reacted reagents in the solution is extremely small. The reacting species are not pre-organised in any form and cyclisation is favoured as opposed to polymerisation purely based on odds. This means that the more dilute the solution, the better the ratio of macrocycle to polymer.

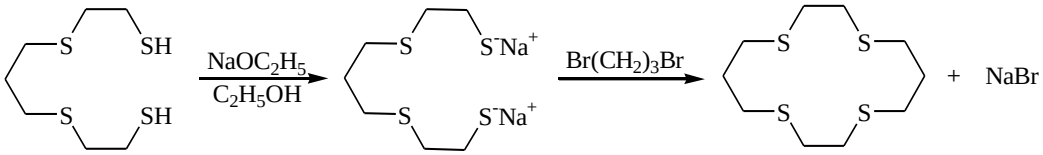

Scheme 2.4: High dilution synthesis of 14-thiacrown-4.

For example, the yield of 14-thiacrown-4 (14aneS_4) (**Scheme 2.4**) is dependent on the degree of dilution under which the condensation reaction is performed. Rosen and Busch, (1969) reported a yield of 7.5%, which was subsequently increased to 55% by performing the reaction at high dilution (Travis and Busch, 1974). The 2:2 condensation products containing eight sulphur donor atoms in the ring are very high when the condensation reaction is not performed at conditions other than high dilution (Travis and Busch, 1974).

In some cases, it is not necessary to use high dilution reactions for the synthesis of macrocyclic ligands. If rigid subunits are incorporated, the various acyclic intermediates are pre-organised by secondary interactions such as intramolecular hydrogen bonds within the precursor that bring about the correct conformation for cyclisation. There are several reported examples where the intrinsic intramolecular or intermolecular interactions give the reacting species the required conformation and proximity that allows a nucleophile-electrophile reaction, which leads to cyclic products as opposed to open-chain polymers (Constable, 1999).

Richman and Atkins, (1974) were the first to report the use of preformed *bis*-sulphonamide sodium salts and sulphonate ester leaving groups in a dipolar aprotic solvent which effectively obviated the high dilution technique. These authors argued that neither steric nor electronic considerations suggested that the immediate precursor to the tosylated macrocyclic ligand coordinated the sodium cation. They proved this by replacing the sodium cations of *bis*-sulphonamide disodium salt with tetramethylammonium cations that still afforded greater than 50% yield of 12aneN_4. These results ruled out a template effect as a dominant factor. Over the last few years the procedure by Richman and Atkins has undergone modification with the aim of improving the yield and purity of the resultant macrocyclic ligands. For example, Sabatini and Fabbrizzi, (1979) reported an improved method with better results.

In this research, a modified procedure by Sabatini and Fabbrizzi, (1979) was used for the preparation of 12aneN_3. The addition of hydroxypropyl, hydroxy-2-methylpropyl and

hydroxybutyl pendant arms were done by using a method reported by Robb and Peacock, (1986), whereas the hydroxy-2-phenylethyl pendant arms was done by using a modified procedure by Weeks *et al.,* (2001) and mercaptopropyl pendant arms by using the procedure reported by Moore *et al.,* (1990).

The procedure by Sabatini and Fabbrizzi was modified in an effort to increase the yield of various steps leading to the final product. The reaction was followed by ^{1}H and ^{13}C NMR and the final product was characterized by ^{1}H and ^{13}C NMR and MS. In some cases crystal structures were determined by X-ray diffraction and proved the existence of the ligands.

2.3 Materials and methods

2.3.1 Chemicals and Reagents

The following chemicals and reagents were used: toluene-4-sulphonyl chloride (tosyl chloride) and 1,3-propanediol, *N*,*N*-dimethylformamide were purchased from Fluka. (*S*)-propylene oxide, 1,2-epoxy-2-methylpropane, (*S*)-(-)-1,2-epoxybutane, (*S*)-(-)-styrene oxide, propylene sulphide, *bis*(3-aminopropyl)-amine, absolute ethanol and 95% ethanol, were purchased from Sigma-Aldrich. Dichloromethane, diethyl ether and chloroform were purchased from Merck. Triethylamine was purchased from SAARCHEM.

2.3.2 Instrumentation

Nuclear magnetic resonance (NMR) spectroscopy, Elemental analysis and Electron impact mass spectrometry were the main techniques used for the characterisation of the ligands and intermediate product. NMR spectra were recorded by the use of Varian 300 MHz and Varian 600 MHz spectrophotometer operating at 300 and 600 MHz, respectively. Chemical shifts (δ) are given in ppm relative to residual solvent signal. The electron impact mass spectrometry was done on an AMD 604 High Resolution Mass Spectrometer and Elemental analysis was done at the University of Cape Town.

2.3.3 Synthesis of the parent macrocyclic ligand, 12aneN$_3$

12aneN$_3$ was synthesised from simple starting materials using a method which can best be described as a sandwich between metal template and high dilution procedure.

2.3.3.1 Tosylation of the 1,3-propanediol

Three different procedures were used:

(1) Tosyl chloride (76.641 g, 0.402 mol) was added in small portions to an open-air stirred solution of 1,3-propanediol (15.296 g, 0.201 mol) in triethylamine (200.00 mL) cooled in an ice bath. The stirring was continued for 1 hour after complete mixing of the reagents. Distilled water (200.00 mL) was then added and further stirred for 3 hours. The white precipitate was filtered and repeatedly washed with distilled water until the filtrate no longer changed the phenolphthalein indicator to a pink colour. The white precipitate was filtered and first recrystallised from a mixture of absolute ethanol/ether (4:1, 200.00 mL) and then from absolute ethanol (200.00 mL) and a yield of 58% (48.220 g, 0.117 mol) was obtained. NMR results are given in **Table 2.1** and spectra are presented in **Appendices 1a-b**.

(2) Tosyl chloride (76.641 g, 0.402 mol) was dissolved in diethyl ether (650.00 mL) and added in one portion to an open-air stirred solution of 1,3-propanediol (15.296 g, 0.201 mol) in triethylamine (200.00 mL) in a 2 L beaker. The solution was further stirred for 14 hours. Distilled water (200.00 mL) was then added and further stirred for 4 hours. The white precipitate was filtered and repeatedly washed with distilled water until the filtrate no longer changed the phenolphthalein indicator to a pink colour. The white precipitate was then first recrystallised from a mixture of absolute ethanol/ether (4:1, 200.00 mL) and then from absolute ethanol (200.00 mL) and a yield of 92% (71.096 g, 0.185 mol) was obtained. Refer to **Table 2.1** for NMR results and **Appendices 1a-b** for the spectra.

(3) Tosyl chloride solid (76.641 g, 0.402 mol) was added in small portions over a period of three minutes to an open-air stirred solution of 1,3-propanediol (15.296 g, 0.201 mol) in triethylamine (200.00 mL) and diethyl ether (200.00 mL) and was left to stir for 14 hours after complete addition of the reagents. Distilled water (200.00 mL) was then added and further stirred for 3 hours. The white precipitate was filtered and repeatedly washed with distilled water until the filtrate no longer changed the phenolphthalein indicator to a pink colour. The white precipitate was filtered and first recrystallised from a mixture of absolute

ethanol/ether (4:1, 200.00 mL) and then from absolute ethanol (200.00 mL) and a yield of 93% (71.869 g, 0.187 mol) was obtained. NMR results are listed in **Table 2.1** and the spectra are shown in **Appendices 1a-b**.

2.3.3.2 Tosylation of the *bis*(3-aminopropyl)-amine

A solution of toluene-4-sulfonyl chloride (115.153 g, 0.604 mol) in diethyl ether (600 mL) was added dropwise to a vigorously stirred solution containing *bis*(3-aminopropyl)-amine (26.620 g, 0.201 mol) and NaOH (24.158 g, 0.604 mol) in distilled water (200.00 mL) at room temperature in a 1 L three-neck round bottomed flask using a mechanical stirrer. After complete addition of toluene-4-sulfonyl chloride solution, the mixture was further stirred overnight. The following morning distilled water (200.00 mL) was added and left stirring for a further 4 hours. The thick white solid was filtered and first recrystallised from a mixture of absolute ethanol/ether (4:1, 200.00 mL) and then from absolute ethanol (200.00 mL) and a yield of 93% (110.997 g, 0.187 mol) was obtained. The NMR results are given in **Table 2.2** and the spectra are presented in **Appendices 2a-b**.

2.3.3.3 Preparation of the tosylated triamine disodium salt (*bis*-sulphonamide sodium salt)

This part was carried out in a 2 L three-neck round bottom flask fitted with a $CaCl_2$ drying tube. The flask was flushed with nitrogen before addition of freshly distilled absolute ethanol. The absolute ethanol was distilled under nitrogen and magnesium metal. Na (4.598 g, 0.200 mol) was transferred to the 2 L three-neck round bottom flask containing absolute ethanol (1.00 L) and after complete reaction, the tosylated triamine (59.379 g, 0.100 mol) was slowly added to the stirred solution. After complete addition of the tosylated triamine, the mixture was left to stir overnight. The *bis*-sulphonamide disodium salt was filtered, washed with absolute ethanol and used immediately in the cyclisation reaction.

The same procedure on a small scale, Na (0.460 g, 0.0200 mol) and tosylated triamine (5.938 g, 0.0100 mol) was used to approximate the percentage yield of the *bis*-sulphonamide sodium salt. Distilled water (1.50 L) was added to the filtrate and the white precipitate formed was dried from which the yield of *bis*-sulphonamide disodium salt was calculated by subtracting

the initial number of moles to the number of moles in the filtrate and a yield of 78% (4.974 g, 0.00780 mol) was obtained.

2.3.3.4 Synthesis of the tosylated 1,5,9-triazacyclododecane

The tosylated triamine disodium salt was immediately dissolved in dimethylformamide (900.00 mL) in a 2 L beaker and heated on a heater equipped with a magnetic stirrer at 120 °C. The tosylated 1,3-propanediol (38.447 g, 0.100 mol) dissolved in DMF (450.00 mL) was added dropwise to a vigorously stirred solution of tosylated triamine disodium salt (63.775 g, 0.100 mol). The solution was further stirred for 2 hours after complete addition of the tosylated 1,3-propanediol. The hot clear yellow solution was then transferred into ice water (2.50 L) in a 5 L jug and left overnight. The precipitate was filtered and repeatedly washed with distilled water (5.00 L). The product was then recrystallised from absolute ethanol and a yield of 76% (48.173 g, 0.0760 mol) was obtained. The NMR results are listed in **Table 2.3** and the spectra are given in **Appendices 3a-b**.

2.3.3.5 Detosylation and formation of the HBr salt of the macrocycle

The tosylated macrocycle (48.173 g, 0.0760 mol) was dissolved in a mixture of 48% hydrobromic acid (1.10 L) and glacial acetic acid (0.60 L) and refluxed for three days after which the hot mixture was filtered using a glass wool mounted in a sintered funnel without a sinter itself. The filtered solution was concentrated to 200.00 mL using vacuum distillation and was then transferred while hot into a solution of ethanol (1.10 L) and ether (400.00 mL) in a 4 L beaker. The white precipitate of amine trihydrobromide was repeatedly washed with diethyl ether (400.00 mL) and was then recrystallised from a mixture of absolute ethanol and ether (4:1, 200.00 mL). A yield of 69% (21.536 g, 0.0524 mol) was obtained. The NMR results are presented in **Table 2.4** and the spectra are shown in **Appendices 4a-b**.

2.3.3.6 Formation of the HCl crystals of the parent 12aneN_3 macrocycle

The HBr salt of the macrocycle (17.045 g, 0.0415 mol) was dissolved in hot HCl (75.00 mL, 3.000 mol dm^{-3}) in a 250 mL beaker and evaporated to 50.00 mL. The hot solution was left to stand from which white crystals were obtained the following day in 60% yield (6.972 g,

0.0249 mol). More crystals were obtained after a week. The NMR results are given in **Table 2.5** and the spectra are presented in **Appendices 5a-b**.

2.3.4 Synthesis of macrocycles with hydroxyalkyl and thiol pendant arms

All five macrocyclic ligands were prepared by addition of alkyl epoxides and propylene sulphide to a deprotonated 12aneN_3.

2.3.4.1 Synthesis of the 1,5,9-*tris*[(2*S*)-hydroxypropyl]-1,5,9-triazacyclododecane ligand

Na (0.4138 g, 0.0180 mol) was dissolved in absolute ethanol (100.00 mL). The macrocyclic-HCl crystals (1.684 g, 0.00600 mol) was then added to the sodium ethoxide solution and stirred for 3 hours. A white precipitate of NaCl salt formed and was filtered. The volume of the solution was then reduced by rotary evaporation at 45 °C and the white salt of NaCl was filtered. The parent macrocycle was repeatedly washed with dichloromethane and the resulting NaCl salt was filtered each time. The dichloromethane was evaporated on a rotary evaporator at 35 °C and further dried under vacuum for 5 hours. The NMR results are given in **Table 2.6** and the spectra are shown in **Appendices 6a-b**. (*S*)-(-)-propylene oxide (1.244 g, 0.0180 mol) was added to the solution of the macrocycle in absolute ethanol (100.00 mL) in a 250 mL round bottom flask and the flask was sealed with a stopper and parafilm. The solution was left to stir at room temperature for 3 days. The new ligand, 1,5,9-*tris*[(2*S*)-hydroxypropyl]-1,5,9-triazacyclododecane, was dried on a rotary evaporator at 45 °C and further dried under vacuum at room temperature to obtain 90% yield (1.866 g, 0.00540 mol). MS (ESI): m/z 346 [M^+]. Anal. Calc % for $C_{18}H_{39}N_3O_3.1.5H_2O$; C, 58.04; N, 11.28; H, 11.36: ratio of C:N = 5:1. Found: C, 58.17; N, 11.17; H, 10.67; ratio of C:N = 5:1. The NMR results are given in **Table 2.7** and the spectra are presented in **Appendices 8a-b**.

2.3.4.2 Synthesis of 1,5,9-*tris*(2-mercaptopropyl)-1,5,9-triazacyclododecane ligand

Deprotonated 1,5,9-triazacyclodocane (1.028 g, 0.00600 mol) was transferred into a 100 mL, two-neck, round-bottom flask, fitted with a reflux condenser and a serum stopper, in chloroform (50.00 mL). The solution was flushed with dry nitrogen gas and propylene sulphide (1.335 g, 0.0180 mol) was added using a syringe. The mixture was stirred for 3

hours after which the solvent was quickly removed on a rotary evaporator giving a pale-yellow oil in 69% yield (1.630 g, 0.00414 mol). The NMR results are listed in **Table 2.8** and the spectra are shown in **Appendices 9a-b**. MS (ESI): m/z 395 [M^+].

2.3.4.3 Synthesis of 1,5,9-*tris*(2-hydroxy-2-methylpropyl)-1,5,9-triazacyclododecane ligand

1,2-epoxy-2-methylpropane (1.299 g, 0.0180 moles) was added to the solution of the free 1,5,9-triazacyclodocane ligand (1.028 g, 0.00600 mol) in absolute ethanol (100.00 mL) in a 250 mL round bottom flask and the flask was sealed with a stopper and parafilm. The solution was left to stir at room temperature for 7 days. The new ligand, 1,5,9-*tris*(2-hydroxy-2-methylpropyl)-1,5,9-triazacyclododecane was obtained upon evaporation of the solvent on a rotary evaporator at 45 °C and the ligand was further dried under vacuum for 48 hours at room temperature in 78% yield (1.814 g, 0.00468 mol). MS (ESI): m/z 388 [M^+]. Anal. Calc % for $C_{21}H_{45}N_3O_3.H_2O$; C, 62.18; N, 10.36; H, 11.68: ratio of C:N = 6:1. Found: C, 55.92; N, 9.31; H, 10.28; ratio of C:N = 6:1.The NMR results are given in **Table 2.9** and the spectra are shown in **Appendices 10a-b**.

2.3.4.4 Synthesis of 1,5,9-*tris*(2*S*)-hydroxybutyl)-1,5,9-triazacyclododecane ligand

(*S*)-(-)-1,2-epoxybutane (1.302 g, 0.0180 moles) was added to the solution of the deprotonated 1,5,9-triazacyclodocane ligand (1.028 g, 0.00600 mol) in absolute ethanol (100.00 mL) in a 250 mL round bottom flask and the flask was sealed with a stopper and parafilm. The solution was kept stirring at room temperature for 5 days. The new ligand, 1,5,9-*tris*[(2*S*)-hydroxybutyl]-1,5,9-triazacyclododecane was obtained upon evaporation of the solvent on a rotary evaporator at 45 °C and the ligand was further dried under vacuum for 48 hours at room temperature in 83% yield (1.930 g, 0.00498 mol). MS (ESI): m/z 388 [M^+]. Anal. Calc % for $C_{21}H_{45}N_3O_3.H_2O$; C, 62.18; N, 10.36; H, 11.68: ratio of C:N = 6:1. Found: C, 57.29; N, 9.54; H, 10.63; ratio of C:N = 6:1. The NMR results are summarised and presented in **Table 2.10** and the spectra are given in **Appendices 11a-b**.

2.3.4.5 Synthesis of 1,5,9-*tris*[(2*S*)-2-hydroxy-2-phenylethyl]-1,5,9-triazacyclododecane ligand

(*S*)-styrene oxide (2.165 g, 0.0180 moles) was added to the solution of the deprotonated 1,5,9-triazacyclodocane ligand (1.028 g, 0.00600 mol) in DMF (79.00 mL) and refluxed for three days at 85 °C. The solution was concentrated by vacuum distillation and was then transferred into cold distilled water (600.00 mL). The off white precipitate was then washed four times with distilled water and left to dry at room temperature in 81% yield (2.584 g, 0.00486 mol). MS (ESI): m/z 532 [M^+]. Anal. Calc % for $C_{33}H_{45}N_3O_3$; C, 74.54; N, 7.90; H, 8.53: ratio of C:N = 9:1. Found: C, 72.65; N, 7.81; H, 8.36; ratio of C:N = 9:1. The NMR results are listed in **Table 2.11** and the spectra are shown in **Appendices 12a-b**.

2.4 Results and Discussion

Preparation of macrocyclic ligands is more often hindered by alternative reaction pathways which normally give by-products that are difficult to separate. Stetter and Roos, (1954) reported a moderate cyclisation yield in condensation of terminal dihalides with *bis*-sulphonamide sodium salts under high dilution because the halide is a poor leaving group as compared to the sulphonate ester. Koyama and Yoshino, (1972) proposed the introduction of protecting groups in macrocyclic ligand synthesis, a procedure that was subsequently improved by Richman and Atkins, (1974). Richman and Atkins reported the synthesis of azamacrocycles in a dipolar aprotic solvent which greatly increased the overall purity and yield of the product. The reaction surprisingly does not require high dilution conditions even though rigid substrates are not involved. Exactly why these reactions proceed under normal concentration conditions is not fully clear, but it is likely that the bulky tosylate groups play some role in pre-organising the open chain precursors and there is also a possibility of Na template effects though not the main driving force (Constable, 1999). The procedure reported by Richman and Atkins has undergone several modifications with the aim of maximizing the macrocyclic polyamine yield while minimising the open chain polymeric products. In this research, 1,5,9-triazacyclododecane was synthesised by using a modified procedure reported by Sabatini and Fabbrizzi, (1979) (**Scheme 2.5**). In this procedure the triamine and diol are protected by *p*-toluenesulphonyl chloride.

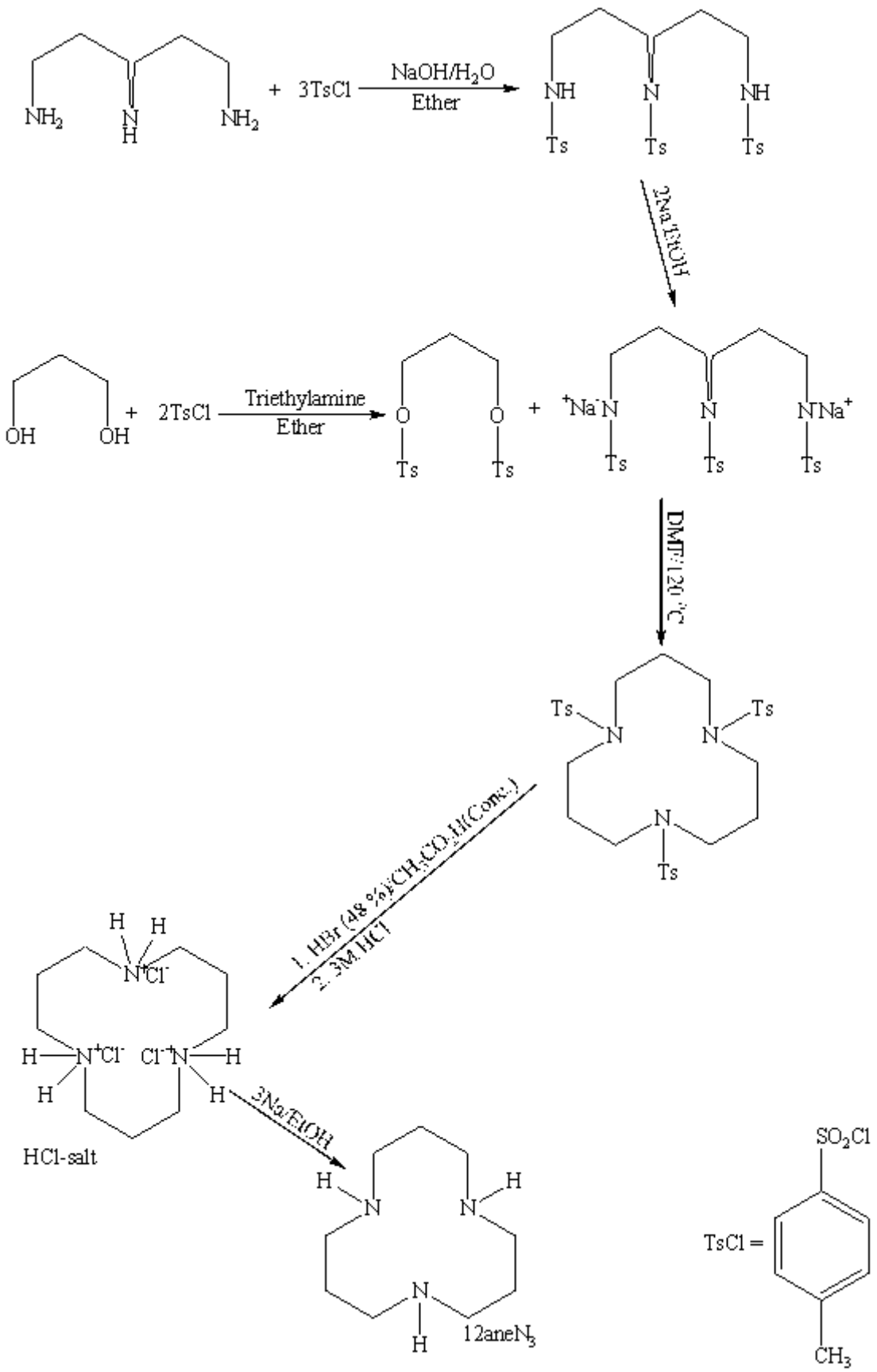

Scheme 2.5: Schematic representation of the synthesis of 12aneN$_3$

The *p*-toluenesulphonate group protecting the diol also functions as a good leaving group and activates the carbon close to the *p*-toluenesulphonate group for nucleophilic attack thereby leading to increasingly better yields. The *p*-toluenesulphonate group also activates the terminal NH groups of the triamine such that deprotonation is possible under moderate conditions. The two terminal NH groups are acidic as a result of the ability of the electron withdrawing tosyl group to delocalize the negative charge of the anion (Constable, 1999).

Three different procedures were tested in the preparation of the tosylated 1,3-propanediol. Sabatini and Fabbrizzi, (1979) had previously reported very low yield (60%) for such a single step (1:2) reaction. When the exact procedure as reported by these authors was used, there was overheating of the reaction at some point regardless of how slow the tosyl chloride was added. In procedure one, the same reaction as reported by these authors was employed but ice was used to cool the reaction and small amounts of the *p*-toluenesulphonyl chloride was added in portions. The reaction still heated up at some point before completion of the reaction and the low yield was attributed to the overheating of the reaction mixture which presumably resulted in the melting of the *p*-toluenesulphonyl chloride before all of it had reacted with the diol. Distilled water was then added to the beaker in order to bring into solution the unreacted substances and excess triethylamine and also to mop up the HCl which comes off to form a quaternary solid salt with triethylamine which is highly soluble in water whereas the tosylated diol is not soluble in water. Upon filtration, the precipitate was further repeatedly washed with distilled water until the triethylamine was washed off (tested with phenolphthalein). The protected diol was crystallised from diethyl ether and ethanol.

In procedure two, *p*-toluenesulphonyl chloride was dissolved in diethyl ether and was added to the beaker containing 1,3-propanediol in triethylamine. At first, the *p*-toluenesulphonyl chloride solution was added dropwise but the reaction was extremely slow, as opposed to when *p*-toluenesulphonyl chloride was added directly in the reaction mixture, such that the solution was added at once. The reaction was left to stir for a further 14 hours and there was no overheating of the reaction mixture at any point. The protected diol was washed with distilled water and recrystallised from diethyl ether and ethanol.

In order to find out if the reaction was not too exothermic because *p*-toluenesulphonyl chloride was pre-dissolved in diethyl ether before mixing the reagent, as opposed to procedure one where solid *p*-toluenesulphonyl chloride was used, a third procedure was used. In this procedure solid tosyl chloride was added in small portions over a period of three minutes to an open-air stirred solution of 1,3-propanediol in triethylamine and diethyl ether and was left to stir for 14 hours after complete addition of the reagents. Just like in procedure two, there was no overheating of the reaction mixture at any point and the percentage yield for procedure two and three were 92% and 93%, respectively. The protected diol was washed with distilled water and recrystallised from diethyl ether and ethanol. This method gave a comparative yield to procedure two and the minor difference in percentage yield can be attributed to normal differences when recrystallisation is involved and method three was adopted for further synthesis of tosylated propanediol.

Table 2.1: ^{1}H and ^{13}C NMR results of the tosylated 1,3-propanediol

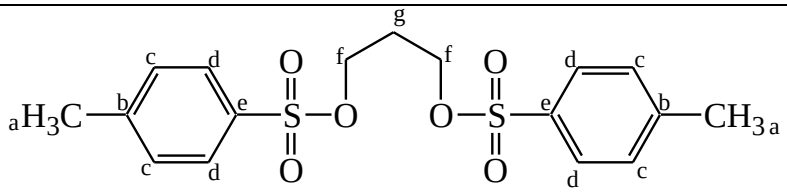

Assignment	δ
^{1}H	
H^{d}	7.75
H^{c}	7.36
H^{f}	4.07
H^{a}	2.46
H^{g}	2.00
^{13}C	
C^{b}	145.24
C^{e}	132.78
C^{c}	130.14
C^{d}	128.05
C^{f}	66.03
C^{g}	28.86
C^{a}	21.83

In all three reactions, *p*-toluenesulphonyl chloride was used in slight excess to make sure that all the diol was tosylated to avoid side reactions.

The tosylated *bis*(3-aminopropyl)-amine was synthesised by addition of diethyl ether solution of tosyl chloride to *bis*(3-aminopropyl)-amine in aqueous sodium hydroxide. The tosylated *bis*(3-aminopropyl)-amine was recrystallised from a mixture of ethanol/diethyl ether to bring in solution unreacted tosyl chloride that was used in slight excess to make sure that all the *bis*(3-aminopropyl)-amine was protected.

The NH proton appears as a triplet at 5.26 ppm and integrates for two protons indicating that the triamine was fully tosylated (**Fig. 2.1**).

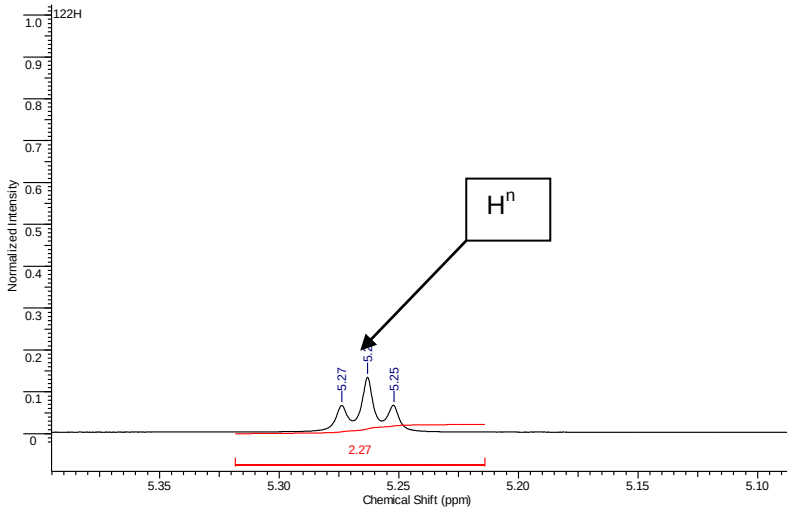

Fig 2.1: The proton spectrum zoomed in to highlight a triplet for the NH protons of the tosylated *bis*(3-aminopropyl)-amine.

This was further confirmed by the quartet and triplet for f and h protons at 2.96 and 3.10 ppm, respectively. The quartet is indicative of the fact that the f protons are near to the NH protons which did not exchange with the deuterated chloroform (**Fig. 2.2**).

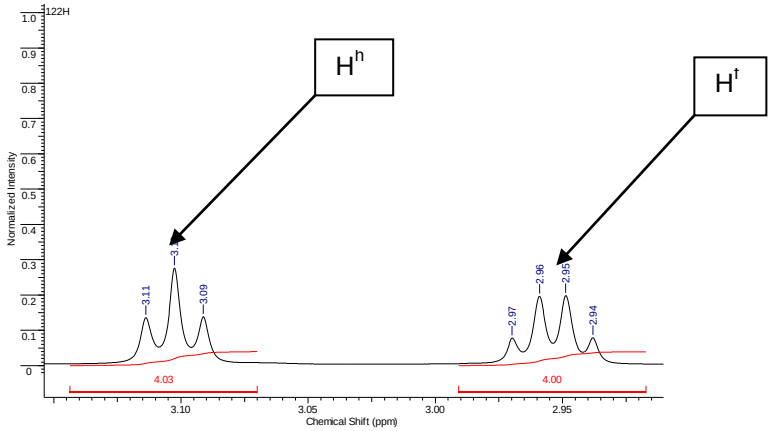

Fig 2.2: The proton spectrum zoomed in to highlight a quartet and triplet for the f and h protons of the tosylated *bis*(3-aminopropyl)-amine.

Two superimposed doublets for the H^k and H^c of the benzene ring are in a similar environment unlike the upper protons (H^d and H^j) which are in a very different environment. The difference emanates from the fact that the middle tosyl group is attached to the secondary nitrogen while the other two are attached to the primary nitrogen atoms (**Fig. 2.3**).

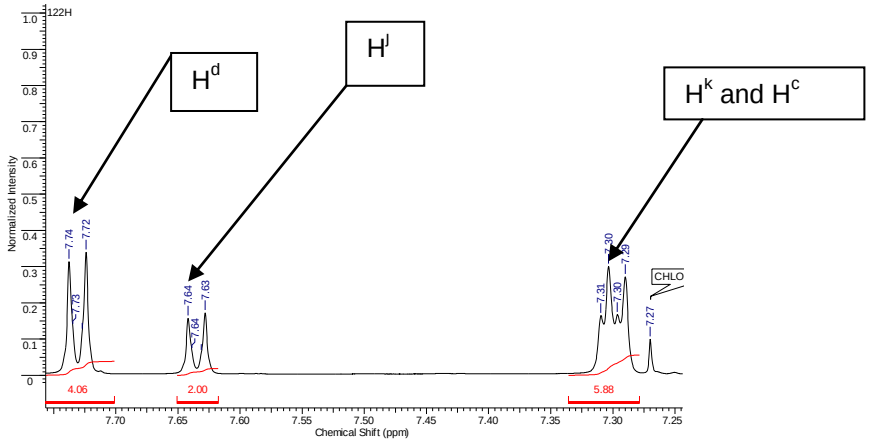

Fig. 2.3: The proton spectrum zoomed in showing the superimposed doublet of phenyl protons of the tosylated *bis*(3-aminopropyl)-amine.

The signal at 2.42 ppm is for the methyl protons of the tosyl group and appears as a superimposed singlet because the methyl protons of the middle tosyl group (H^m) are in a slightly different environment to the other six protons (H^a). The molecule is symmetrical with the centre of symmetry passing through the central tosyl group. This was further confirmed by the carbon-13 spectrum which showed twelve different signals. The procedure for the

preparation of the tosylated *bis*(3-aminopropyl)-amine was not modified because Sabatini and Fabbrizzi, (1979) had reported a yield of 85% and we obtained even a better yield (93%).

The *bis*-sulphonamide disodium salt was prepared from Na metal in freshly prepared absolute ethanol and was used immediately after filtration to minimise reverse reaction. If the *bis*-sulphonamide sodium salt is exposed to the atmosphere, the salt is reprotonated by picking up a proton. The sodium salt can be dried *in vacuo*. To approximate the yield of disodium salt, the same procedure at a small scale was used in which water was added to the filtrate and the precipitates were dried and weighed. As long as the tosylated 1,3-propanediol is added sufficiently slow, it does not present problems when it is used in excess otherwise it may lead to polymerisation.

The cyclisation reaction was done in DMF at 120 °C. Even though this reaction does not qualify strictly as a template reaction, the positive charged sodium metal ion still influences the cyclisation reaction albeit to a small extend. Richman and Atkins, (1974) reported that replacing *bis*-sulphonamide sodium salt with tetramethylammonium cations afforded good yields which ruled out a metal template effect as a major driving force in the cyclisation reaction. The tosylated propanediol was added dropwise to minimise polymerisation. It is very crucial that the tosylated propanediol is added sufficiently slowly to allow full reaction of the reactants and to avoid building up of the tosylated diol which may lead to polymerisation. Even though Richman and Atkins, (1974) reported that this procedure obviates the need for high dilution, better 1:1 stoichiometry products are achieved when less concentrated *bis*-sulphonamide sodium salt is used i.e. when *bis*-sulphonamide sodium salt is dissolved in more dimethylformamide. Richman and Atkins, (1974) also reported that incorporating hydrocarbon segments longer than three methylene units markedly decreases the yield of 1:1 stoichiometry cyclisation products. In such cases significant amounts of 2:2 stoichiometry products are observed. For the 2:2 reaction to dominate, the *bis*-sulphonamide disodium salt upon reaction with tosylated propanediol at one reacting end, the other end of the *bis*-sulphonamide disodium salt should favour reaction with another tosylated propanediol which should then be involved in a cyclisation reaction with a second molecule of *bis*-sulphonamide disodium salt (**Scheme 2.6**).

Table 2.2: ^{1}H and ^{13}C NMR results of the tosylated *bis*(2-aminopropyl)-amine

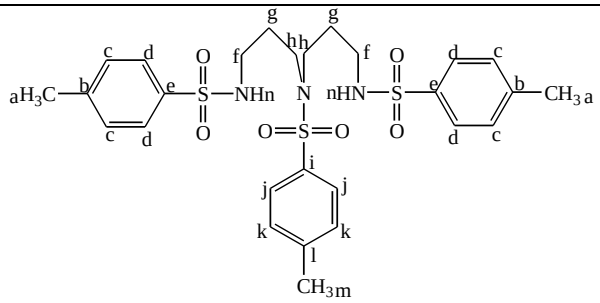

Assignment	δ
^{1}H	
H^{d}	7.73
H^{j}	7.64
$H^{c,k}$	7.30
H^{n}	5.26
H^{h}	3.10
H^{f}	2.95
$H^{a,m}$	2.42
H^{g}	1.71
^{13}C	
C^{l}	143.96
C^{b}	143.59
C^{i}	137.06
C^{e}	135.61
C^{k}	130.10
C^{c}	129.93
C^{j}	127.28
C^{d}	127.20
C^{h}	47.02
C^{f}	40.24
C^{g}	29.48
$C^{a,m}$	21.69

The NMR spectra and elemental analysis cannot distinguish the two products because the number of signals for both ^{1}H and ^{13}C are exactly the same for both products. MS

spectroscopy can distinguish between the two products and the formation of 12aneN_3 was confirmed by crystal structure determination (see later **Section 5.3.9**, **Chapter 5**).

The hot DMF solution was then transferred into ice water (3.00 L). The more the ice water used to quench the reaction the better the resulting tosylated macrocycle. The tosylated macrocycle was filtered and thoroughly washed with distilled water (4.00 L) until the precipitate stopped foaming. It is very essential to remove as much DMF as possible otherwise there is a considerable loss of product during recrystallisation. The disappearance of the NH signal at 5.26 ppm indicated that there was no end –NH–$SO_2C_6H_4CH_3$ group and the disappearance of the middle doublet in the benzene region at 7.64 ppm indicated that the reaction was complete and no polymerisation occurred (**Fig. 2.4**).

The tosylated macrocycle was detosylated using a mixture of hydrobromic acid (HBr)/glacial acetic acid in the ratio of 1.8:1.0. The mixture was refluxed for 3 days to ensure complete detosylation and was filtered using glass wool mounted on a funnel. The filtrate was then concentrated to 200.00 mL by vacuum distillation. The hot concentrated mixture was transferred in small amounts into a mixture of ethanol/diethyl ether (3:1). Portion-wise addition of the hot detosylated HBr solution into the ethanol/diethyl ether appears to increase the purity of the macrocycle and the precipitated macrocycle is relatively easy to wash with diethyl ether. This is the case presumably because the portion wise addition allows the hot macrocycle to crash out of the HBr/glacial acetic acid mixture upon coming into contact with the ethanol/ether mixture. The proton NMR clearly showed no signals in the region typical of phenyl hydrogens and the carbon NMR showed no signals in the region typical of phenyl carbons indicating that there was complete detosylation of the macrocycle. The macrocycle was further purified by recrystallisation from 3 M HCl acid. The HCl salt of the macrocycle was added to the freshly made sodium ethoxide solution and stirred for 3 hours. The resulting NaCl salt was filtered and the solution was concentrated on a rotary evaporator at 49 °C from which more NaCl was precipitated out and was filtered.

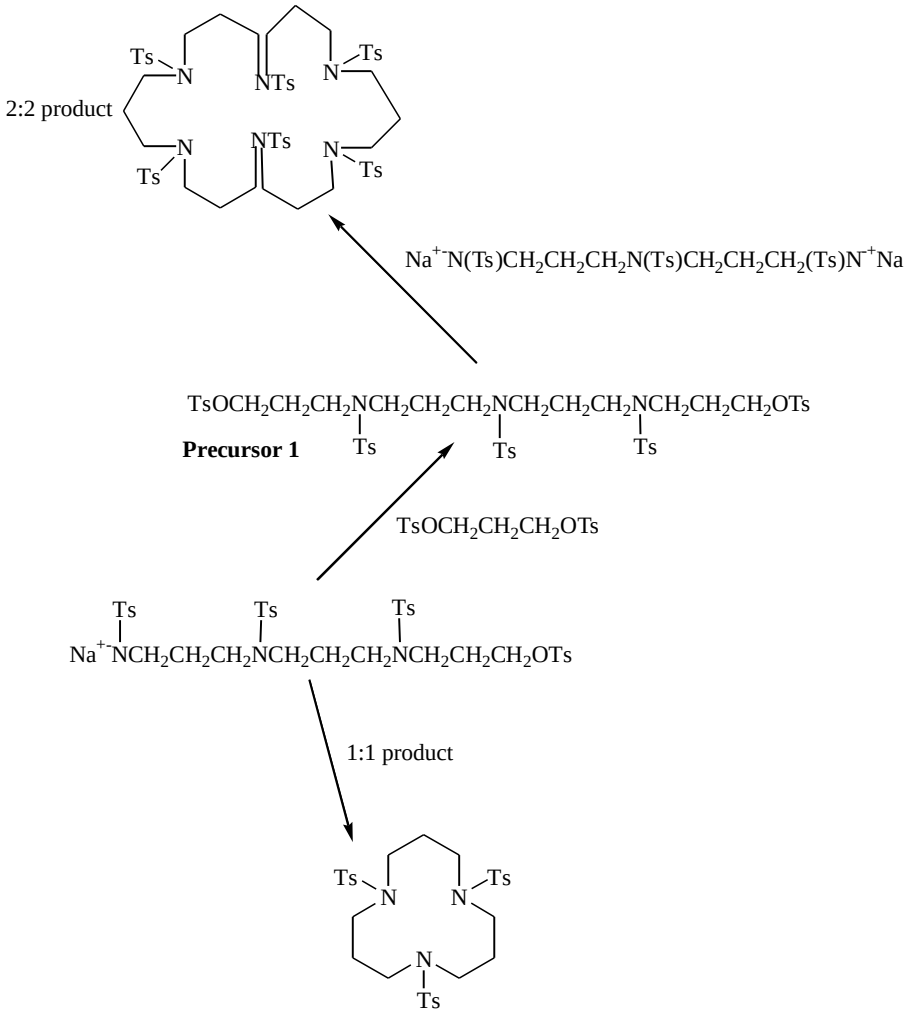

Scheme 2.6: Two possible cyclisation pathways for the formation of the tosylated 1,5,9-triazacyclododecane (1:1 product) and tosylated 1,5,9,13,17,21-hexaazacyclotetracosane (2:2 product). There is also a possibility of an open chain polymer.

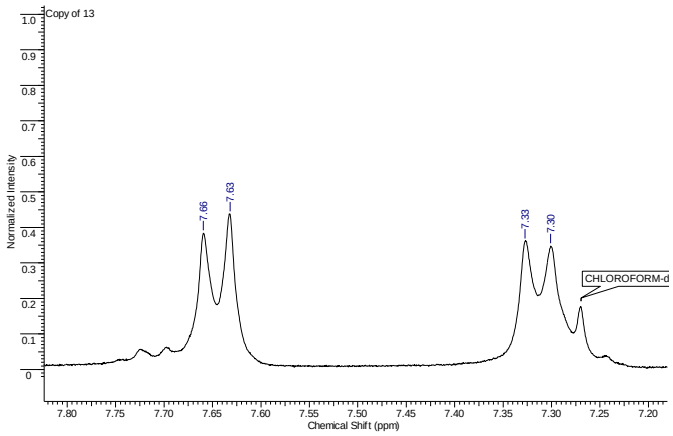

Fig 2.4: The proton spectrum zoomed in to highlight two doublets of the tosylated macrocycle.

Table 2.3: ^{1}H and ^{13}C NMR results of the tosylated 1,5,9-triazacyclododecane macrocycle

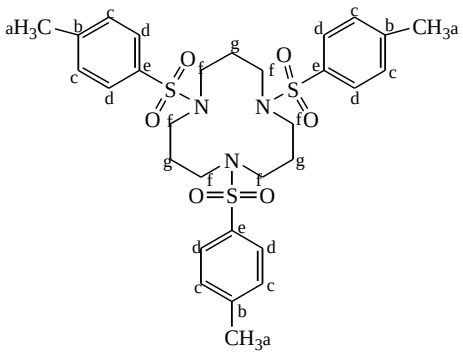

Assignment	δ
^{1}H	
H^{d}	7.65
H^{c}	7.32
H^{f}	3.21
H^{a}	2.43
H^{g}	1.91
^{13}C	
C^{b}	143.91
C^{e}	135.36
C^{c}	130.11
C^{d}	127.56
C^{f}	45.76
C^{g}	26.58
C^{a}	21.81

Dichloromethane was added to the concentrated solution of the mixture upon which more NaCl was precipitated out. This is the case because NaCl is more soluble in ethanol as opposed to DCM in which it is insoluble. The solution was evaporated at 36 °C and this procedure was repeated until all the NaCl was removed.

Table 2.4: ^{1}H and ^{13}C NMR results of the 1,5,9-triazacyclododecane HBr salt

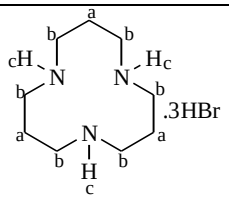

Assignment	δ
^{1}H	
H^{b}	3.68-3.03
H^{a}	2.35-1.99
^{13}C	
C^{b}	47.27
C^{a}	24.91

H^{c} hydrogens exchanged with D_2O.

Table 2.5: ^{1}H and ^{13}C NMR results of the 1,5,9-triazacyclododecane HCl salt

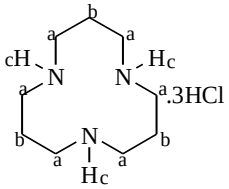

Assignment	δ
^{1}H	
H^{a}	3.35
H^{b}	2.22
^{13}C	
C^{a}	41.30
C^{b}	19.46

Evaporation of ethanol at temperatures above 60 °C and dichloromethane beyond 50 °C leads to decomposition of the macrocycle, probably to form open chain amine compounds.

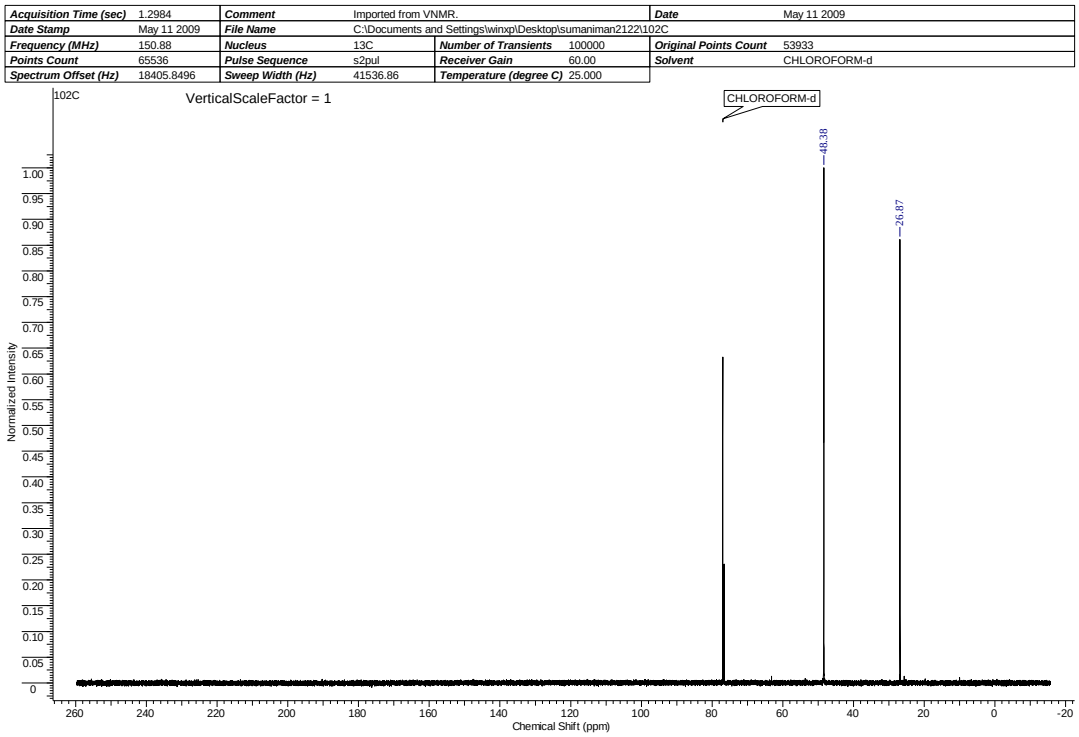

Fig. 2.5: The carbon spectrum of the deprotonated 1,5,9-triazacyclododecane.

The product was further dried on a vacuum pump for 5 hours after which relevant pendant arms were added. The spectrum supported the complete deprotonation of the parent macrocyclic ligand salt and the sample was run in $CDCl_3$ showing a neat triplet and a quintet (**Fig. 2.6**).

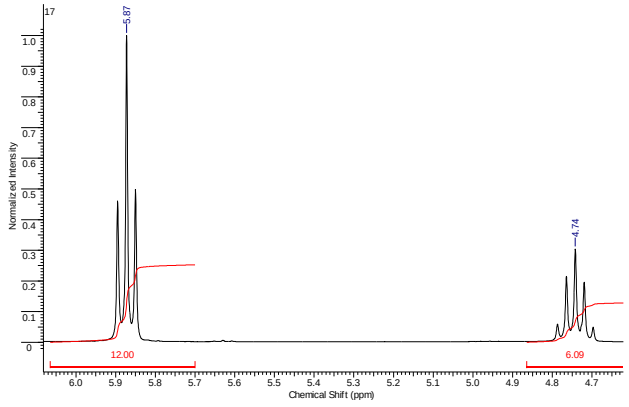

Fig 2.6: The proton spectrum zoomed in to highlight a triplet and quintet for the (a) and (b) protons of the deprotonated macrocycle.

Table 2.6: ^{1}H and ^{13}C NMR results of the deprotonated 1,5,9-triazacyclododecane

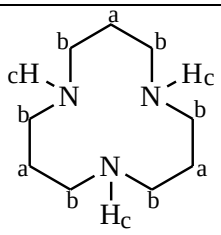

Assignment	δ(ppm)
^{1}H	
H^{b}	5.87
H^{a}	4.74
^{13}C	
C^{b}	48.38
C^{a}	26.87

In some cases deprotonation of the HCl salt of the macrocyclic ligand did not give the required deprotonated macrocyclic ligand as shown by NMR spectrum. In such cases the ^{13}C NMR spectrum showed eight signals (compare **Fig. 2.7** and **Fig. 2.5**).

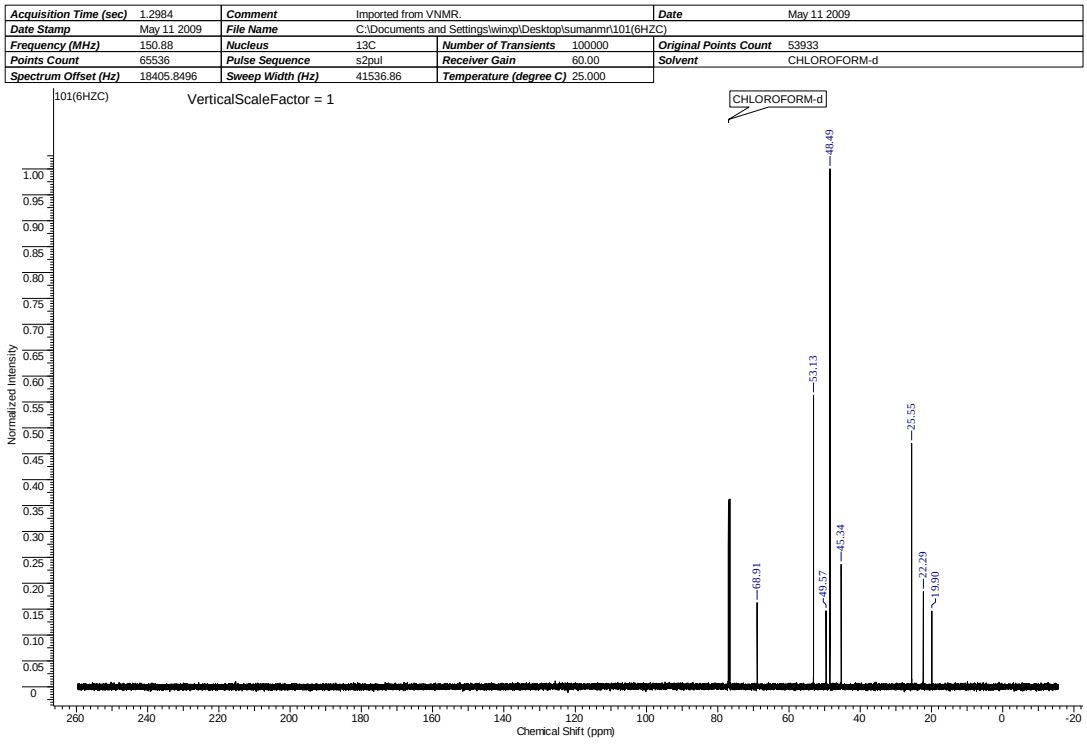

Fig. 2.7: The carbon spectrum of the deprotonated 1,5,9-triazacyclododecane with eight signals.

At first we thought that the imine formed which in principle can react intramolecularly to give product **A** or react with another imine to give product **B** (**Scheme 2.7**). Imines are electrophilic and the empty π* orbitals have a greater coefficient at carbon which is the favoured site of attack (Constable, 1999). **B** was ruled out on the basis that it did not fully explain the ^{13}C NMR as it is expected to give six different signals. Also, as much as **B** has intramolecular hydrogen bonding, the molecule should be very unstable because of the ring strain. No such reaction of $12aneN_3$ has ever been reported. Despite the fact that **A** fully explains the eight signals on the ^{13}C NMR spectrum, reprotonation of the macrocycle, $12aneN_3$, gave two signals in its ^{13}C NMR spectrum just like before deprotonation which ruled out the possibility of **A** formation (**Fig. 2.8**).

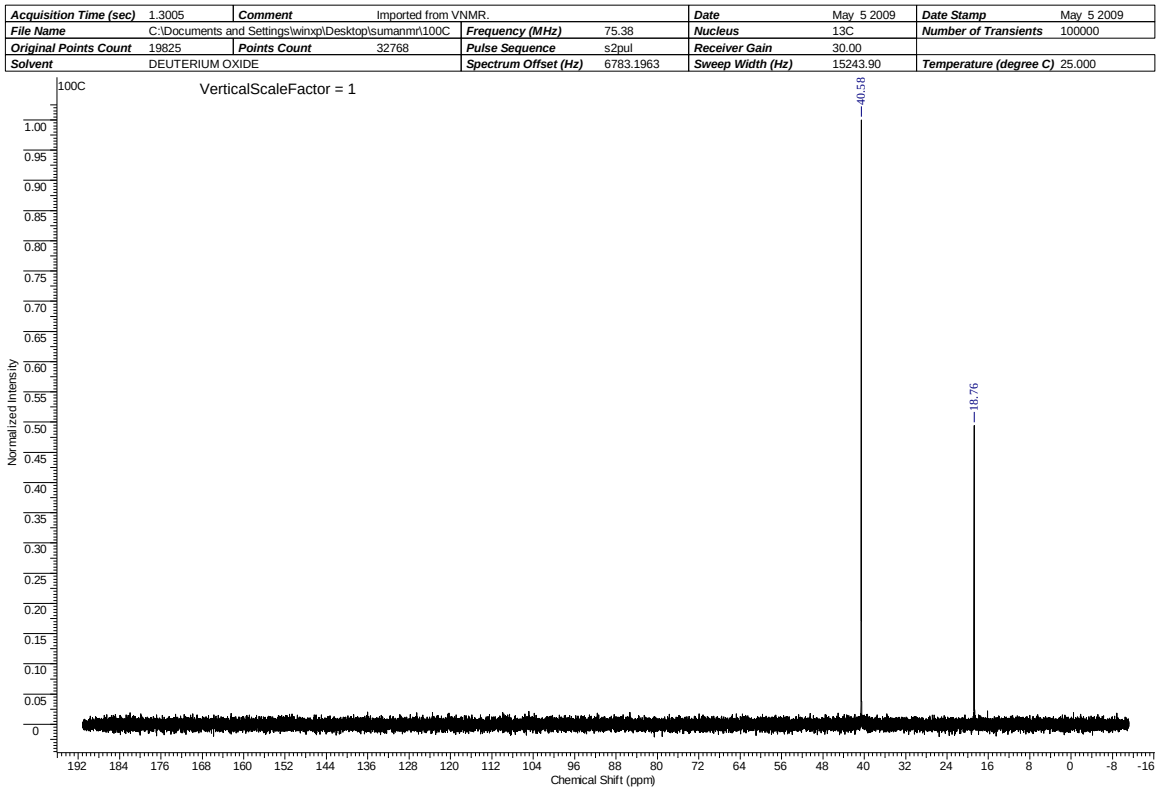

Fig. 2.8: The carbon spectrum of the reprotonated 1,5,9-triazacyclododecane HCl salt.

A cannot be expected to reform the initial macrocyclic ligand on protonation and also to form the imine a much stronger base like NaH is required rather than the sodium ethoxide that was used. The results were very puzzling at first but we finally established that the eight signals resulted from the presence of different deprotonated macrocyclic ligands. A mixture of singly, doubly and triply deprotonated macrocycles formed as confirmed by the crystal structure of free 1,5-*bis*[(2*S*)-hydroxybutyl]-1,5,9-triazacyclododecane (see later **Section**

5.3.8, **Chapter 5**). In this case the macrocyclic ligand which had only two protons removed was isolated.

The above result suggests that less than 3 mole equivalents of sodium ethoxide were used for deprotonation of the parent macrocycle which was not the case. In the preparation of fresh sodium ethoxide, 9% excess Na metal was used to compensate for the errors in the preparation (for example, oxidation of Na metal and extra weight due to paraffin). Normally, one would expect to have the first proton removed before the second one, such that only two and three deprotonated species, in case of insufficient sodium ethoxide, were expected. Complete deprotonation was only achieved when 32% excess sodium metal was used in the preparation of the sodium ethoxide.

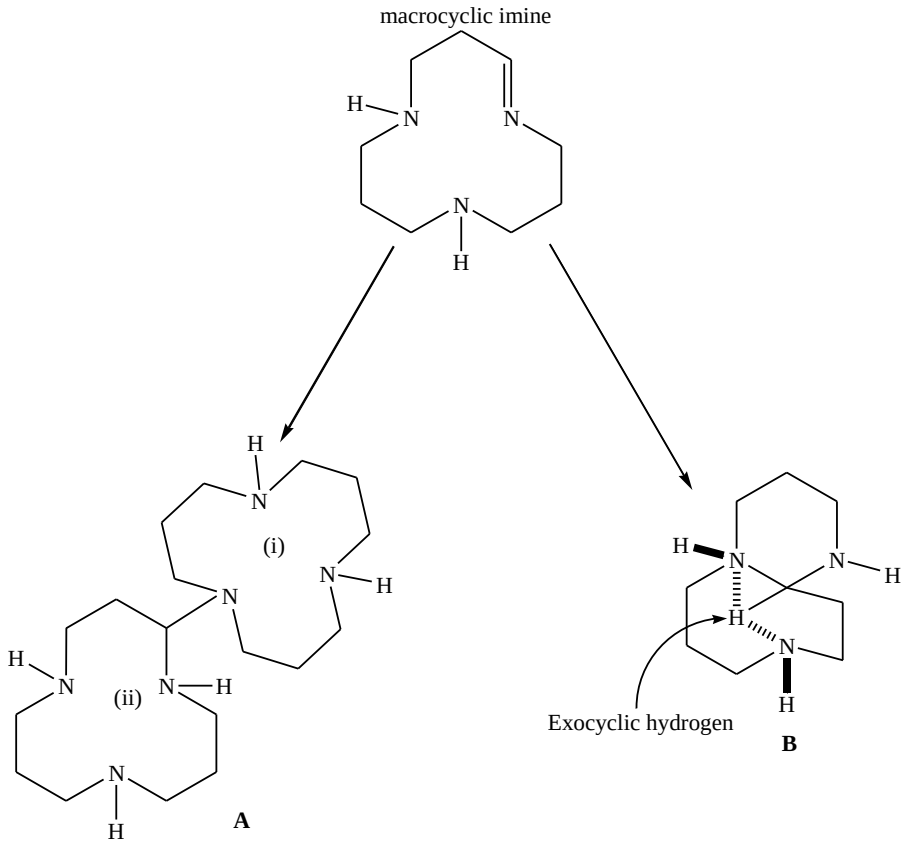

Scheme 2.7: Two possible reaction routes for macrocyclic imine.

Studies are still ongoing to determine why such a large excess Na metal is required for deprotonation. Initial results from Thermo Gravimetric Analysis (TGA) showed that there is no HCl embedded in the matrices of the crystals (**Appendix 7**). The HBr macrocyclic salt

required only 8% excess Na metal but we did not use the ligand prepared from HBr macrocyclic salt for protonation and stability constant experiments because it is less pure than the HCl macrocyclic salt of the parent macrocycle (compare spectra in **Appendices 5a-6b**).

Koyama and Yoshino, (1972) reported the synthesis of 1,4,7-triazacyclonone (TACN), 1,4,7-triazacyclodecane (TACD), 1,4,8-triazacycloundecane (TACUD) and 1,5,9-triazacyclododecane (TACDD) with yields of 88, 82, 79 and 62%, respectively. These results clearly show that as the number of carbons in the bridge increases from ethylene to propylene the yield of the resultant macrocycle decreases. This is not very unusual because the inductive effect should be more pronounced for the propylene bridge as opposed to ethylene bridge thereby destabilising the nucleophile. This effect cannot be a major driving force because of the strong negative induction effect of the tosyl group. The major factor is that once the one end of the *bis*-sulphonamide disodium salt reacts with the tosylated propanediol the propylene bridge of the disodium salt allows more conformations in the transition state leading to a cyclisation reaction with no particular one having the required conformation and electronic properties to enhance cyclization, as opposed to the situation when a small ethylene bridge is used.

The ligand, 1,5,9-*tris*[(2*S*)-hydroxypropyl]-1,5,9-triazacyclododecane, was prepared by treating (*S*)-propylene oxide with a solution of free 12aneN_3 (**Scheme 2.8**) and left to stir for three days in a well sealed flask to avoid evaporation of the volatile epoxide (Robb and Peacock, 1986). The nitrogen atoms of 12aneN_3 could, in principle, attack either the CH_2 or CH(Me) carbons of the propylene oxide. The attack however, was only at the less hindered carbon atom of the epoxide which is also more electrophilic than the other ring carbon owing to the positive inductive effect of the methyl group and thus the absolute configuration at the CH(Me) unit is conserved. The attack was 100% regiospecific and the chirality, *S*, of the ligand was confirmed by metal complex crystal structures.

Table 2.7: ^{1}H and ^{13}C NMR results of the THPTACD

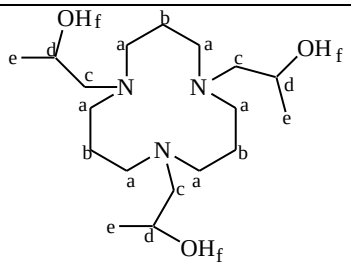

Assignment	δ
^{1}H	
H^{d}	4.06-3.70
$H^{a,c}$	2.93-2.01
H^{b}	1.84-1.52
H^{e}	1.28-0.96
^{13}C	
C^{d}	69.75
C^{c}	65.80
C^{a}	51.74
C^{b}	46.69
C^{e}	28.52

The ligand was dried on the rotary evaporator at 35 °C and then under vacuum at room temperature. Drying at high temperature of more than 45 °C resulted in decomposition of the ligand. The NMR results are summarised and listed in **Table 2.7** and the mass spectrum is shown in **Appendix 8c**. Integration of the proton signals correspond to the number of hydrogen atoms in the same environment.

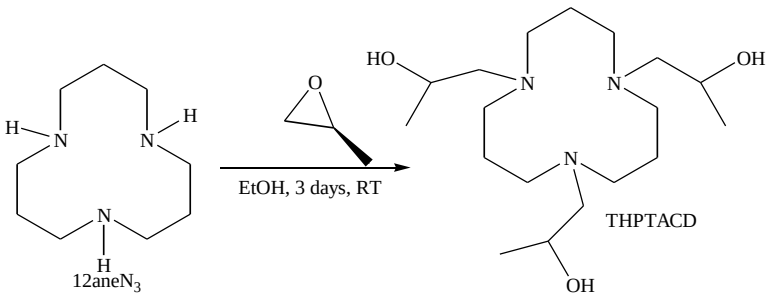

Scheme 2.8: The final step involving the addition of hydroxyl pendant arms to 12aneN$_3$ to give 1,5,9-*tris*[(2*S*)-hydroxypropyl]-1,5,9-triazacyclododecane.

The ligand, 1,5,9-*tris*[2-mercaptopropyl]-1,5,9-triazacyclododecane, was prepared by treating propylene sulphide with a solution of the free ligand, 12aneN$_3$, (**Scheme 2.9**) in a two-neck round-bottom flask fitted with a reflux condenser and a serum stopper in $CHCl_3$ at 50 °C under a blanket of nitrogen. The mixture was stirred for 2.5 hours and the solvent was removed by rotary evaporation. Oligomerisation *via* reaction of thiol with remaining propylene sulphide was minimal as long as extended reaction time and slow evaporation of $CHCl_3$ was avoided. The thiol quickly polymerised when exposed to air as shown by the difference of the NMR spectrum which was done almost immediately and the mass spectrum which was done after 4 hours.

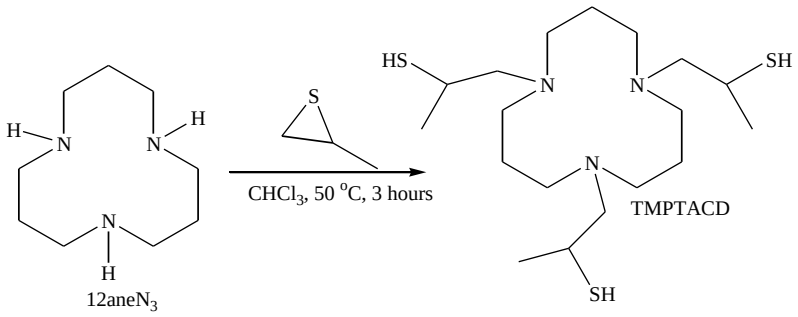

Scheme 2.9: The final step involving the addition of thiol pendant arms to 12aneN$_3$ to give 1,5,9-*tris*[2-mercaptopropyl]-1,5,9-triazacyclododecane.

The NMR spectra did not show any sign of extensive polymerisation whereas the mass spectrum showed extensive polymerisation (**Appendices 9a-c**).

The ligand, 1,5,9-*tris*(2-hydroxy-2-methylpropyl)-1,5,9-triazacyclododecane (THMPTACD), was prepared by treating a solution of free 12aneN$_3$ with 1,2-epoxy-2-methylpropane (**Scheme 2.10**) and stirring the mixture for five days in a well sealed flask to avoid evaporation of the volatile epoxide (Robb and Peacock, 1986). The attack is at the less hindered carbon atom of the epoxide which is also more electrophilic than the other ring carbon owing to the positive inductive effect of the two methyl groups. The epoxide needed 7 days to react completely with the free parent macrocycle. 1,2-epoxy-2-methylpropane is much more sterically encumbered than (*S*)-(-)-1,2-epoxybutane and (*S*)-(-)-propylene oxide and the gain in positive inductive effect is much less than steric hindrance brought about by the two methyl groups on the same carbon.

Table 2.8: ^{1}H and ^{13}C NMR results of the TMPTACD

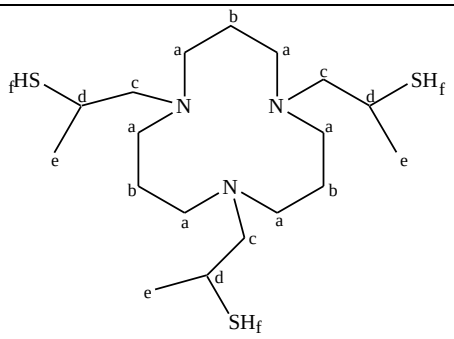

Assignment	δ
^{1}H	
$H^{a,c,d}$	3.43-2.05
$H^{b,e}$	1.96-1.15
^{13}C	
C^{c}	62.98
C^{a}	57.28
C^{d}	50.40
C^{b}	22.78
C^{e}	17.81, 19.50

The solvent was removed on the rotary evaporator at 35 °C and the ligand was further dried under vacuum pump at room temperature for 48 hours. The NMR results are summarised and presented in **Table 2.9** and the mass spectrum is given in **Appendix 10c**.

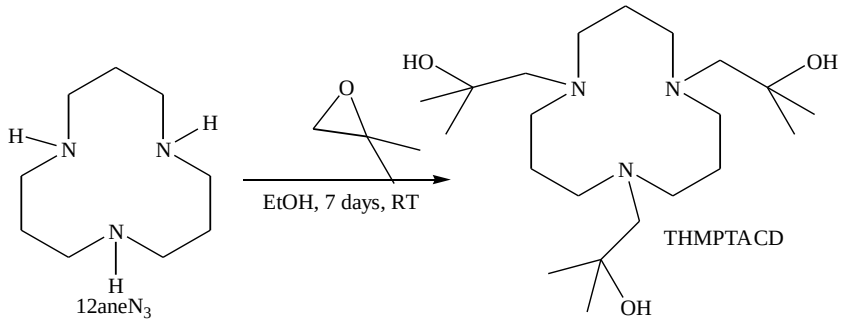

Scheme 2.10: The final step involving the addition of hydroxyl pendant arms to 12aneN$_3$ to give 1,5,9-*tris*(2-hydroxy-2-methylpropyl)-1,5,9-triazacyclododecane.

Table 2.9: ^{1}H and ^{13}C NMR results of the THMPTACD

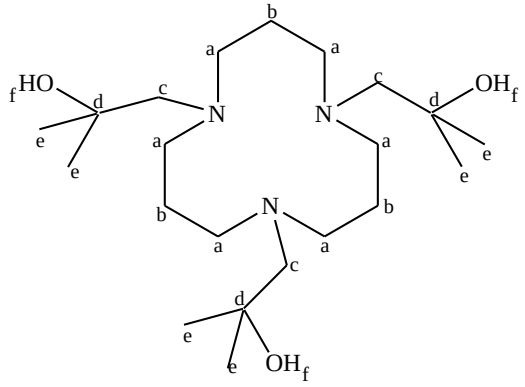

Assignment	δ(ppm)
^{1}H	
H^{c}	2.74-2.50
H^{a}	2.40-2.15
H^{b}	1.73-1.50
H^{e}	1.10
^{13}C	
C^{c}	87.12
C^{d}	74.64
C^{a}	72.62
C^{b}	47.08
C^{e}	43.52

The ligand, 1,5,9-*tris*[(2*S*)-hydroxybutyl]-1,5,9-triazacyclododecane(THBTACD), was prepared by treating (*S*)-(-)-1,2-epoxybutane with a solution of free 12aneN_3 (**Scheme 2.11**). The mixture was left to stir for three days in a well sealed flask to avoid evaporation of the volatile epoxide. The attack is at the less hindered carbon atom of the epoxide which is also more electrophilic than the other ring carbon owing to the positive inductive effect of the methyl group and so that the absolute configuration at the *C*-propylene is conserved. The attack is 100% regiospecific and the chirality, *S*, is maintained like in the case of THPTACD. The solvent was removed on the rotary evaporator at 35 °C and the ligand was further dried under vacuum at room temperature. The NMR results are listed in **Table 2.10** and the mass spectra are presented in **Appendix 11c**.

Table 2.10: ^{1}H and ^{13}C NMR results of the THBTACD

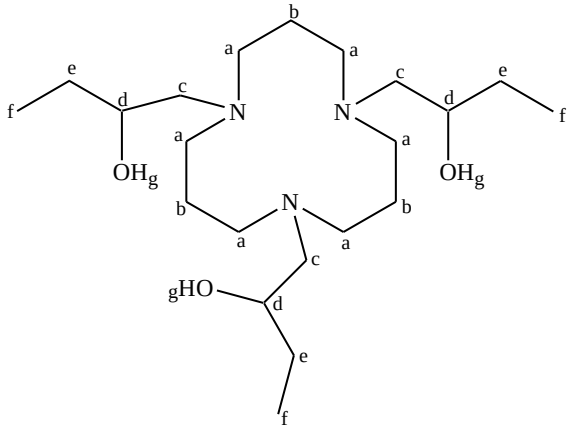

Assignment	δ(ppm)
^{1}H	
H^{d}	3.78-3.91
$H^{a,c}$	3.00-2.50
$H^{b,e}$	2.46-1.61
H^{f}	1.52-0.82
^{13}C	
C^{d}	67.05
C^{c}	64.06
C^{a}	51.64
C^{b}	24.08
C^{e}	20.50
C^{f}	15.52

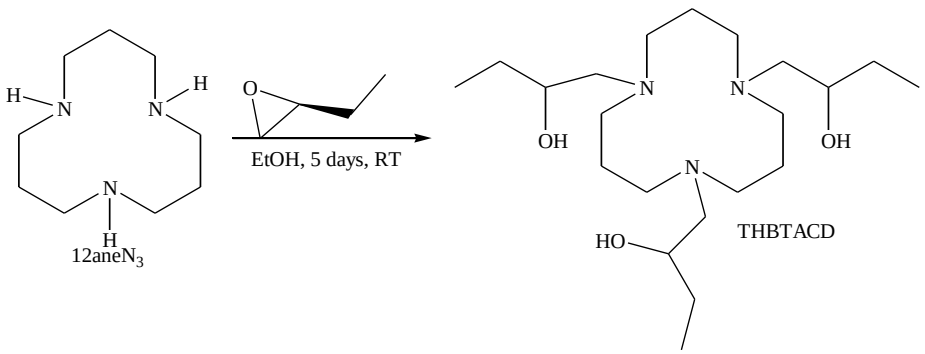

Scheme 2.11: The final step involving the addition of hydroxyl pendant arms to 12aneN$_3$ to give 1,5,9-*tris*(2*S*)-hydroxybutyl)-1,5,9-triazacyclododecane.

The ligand, 1,5,9-*tris*[(2*S*)-2-hydroxy-2-phenylethyl]-1,5,9-triazacyclododecane (THPETACD), was prepared by treating (*S*)-styrene oxide with a solution of free 12aneN$_3$ in DMF and refluxed for three days at 85 °C (**Scheme 2.12**). Achieving a reaction between 12aneN$_3$ and styrene oxide required more energetic conditions than the other four reactions. The solution was concentrated by vacuum distillation and was then transferred into cold distilled water. The off white precipitate was then washed four times with distilled water and left to dry at room temperature. At first, a mixture of water and methanol in a ratio of 1:1 (Weeks *et al.,* 2001) was used but the resultant slurry could not be filtered as it broke the pores of sintered glass funnel and filter papers. The mixture was re-evaporated under vacuum distillation and transferred into cold water. The off white precipitate was filtered and air dried. The NMR results are listed in **Table 2.11** and the mass spectrum is shown in **Appendix 12c**.

The attack is at the less hindered carbon atom of the epoxide which is also more electrophilic than the other ring carbon owing to the positive inductive effect of the phenyl group and so that the absolute configuration at the *C*-phenyl is conserved. The hydroxy-2-phenylethyl pendant arms are more rigid, and as such, the movement in the arms are more restricted than the movement in hydroxypropyl, hydroxybutyl, mercaptopropyl and the hydroxy-2-methylpropyl pendant arms. The carbon spectrum of THPETACD showed eight signals and each signal corresponds to carbon atoms in different environment.

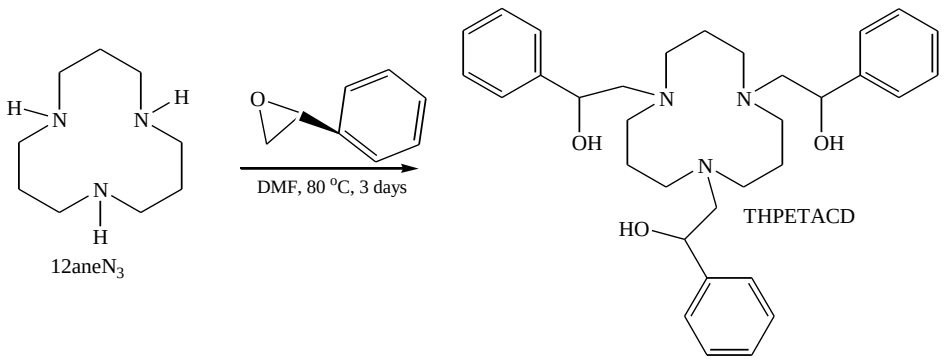

Scheme 2.12: The final step involving the addition of hydroxyl pendant arms to 12aneN$_3$ to give 1,5,9-*tris*[(2*S*)-2-hydroxy-2-phenylethyl]-1,5,9-triazacyclododecane (THPETACD).

Table 2.11: ^{1}H and ^{13}C NMR results of the THPETACD

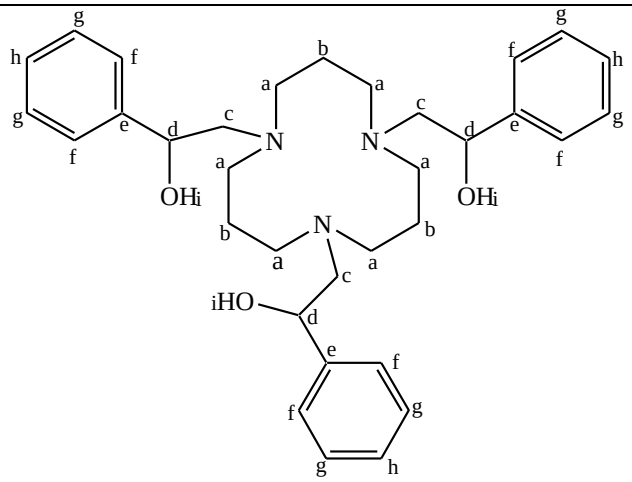

Assignment	δ
^{1}H	
$H^{f,g,h}$	9.51-8.81
H^{d}	7.02-6.49
$H^{a,c}$	5.62-3.97
H^{b}	3.97-2.80
^{13}C	
C^{e}	143.44
C^{g}	128.76
C^{h}	127.79
C^{f}	126.40
C^{d}	70.63
C^{c}	64.31
C^{a}	51.60
C^{b}	24.22

2.5 Conclusion

One of the most daring challenges in macrocycle chemistry is the synthesis of sufficiently pure macrocyclic ligands because the procedures used to get rid of impurities are difficult and cumbersome. The existing separation and purification methods usually involve the use of proteins or chromatography and if we can obviate the need for purification by synthesising sufficiently pure ligands then less time and resources will be required for macrocycle synthesis. This was achieved by purifying the intermediate products leading to the parent

macrocyclic ligand. For example, the purity of the tosylated macrocyclic ligand was improved by portion-wise addition of the hot DMF solution into a large amount of ice-water. The same procedure was employed for the detosylated HBr solution which was added portion-wise to a sufficiently large amount of ethanol-diethyl ether solution. In both cases it seems the ligand crashes out of solution on contact with the solvent which makes portion wise addition very important to keep the solvent at low temperature. The HBr macrocyclic salt of the parent macrocyclic ligand was recrystallised from hydrochloric acid and very pure white HCl macrocyclic salt was obtained.

In this investigation we have managed to optimise, to a greater extent, the procedure developed by Sabatini and Fabbrizzi. The overall yield was greatly improved by improving the tosylation of the diol and portion-wise addition of the hot tosylated macrocyclic ligand solution into a huge amount of ice-water. The purity of the parent macrocycle was sufficiently improved by portion-wise addition of the detosylated HBr macrocyclic salt solution into a mixture of ethanol/diethyl ether and the HBr macrocyclic salt was further purified by growing crystals from three molar hydrochloric acid solution. We report for first time the synthesis of 1,5,9-*tris*[(2*S*)-hydroxypropyl]-1,5,9-triazacyclododecane, 1,5,9-*tris*(2-mercaptopropyl)-1,5,9-triazacyclododecane, 1,5,9-*tris*(2-hydroxy-2-methylpropyl)-1,5,9-triazacyclododecane, 1,5,9-*tris*[(2*S*)-2-hydroxy-2-phenylethyl]-1,5,9-triazacyclododecane and 1,5,9-*tris*[(2*S*)-hydroxybutyl]-1,5,9-triazacyclododecane which were confirmed by conventional characterisation techniques as well as crystal structures.

Chapter 3

Protonation constants of THPTACD, THBTACD and THMPTACD

3.1 Introduction

The acid/base chemistry of macrocyclic ligands is very important in understanding the application of these ligands in medicine, industry and environmental monitoring. There is however limited study of protonation behaviour of triazamacrocyclic ligands in the literature. For example, the chemistry of 1,4,7-*tris*(2-hydroxypropyl)-1,4,7-triazacyclononane has been studied extensively with over fifteen crystal structures published in papers and reviews and over thirty publications on its chemistry but, to the best of our knowledge, no single report exists about its protonation constants. Such oversight has led to difficulties in comparative studies with related ligands. The protonation constants give an idea about the ability of the ligand to associate or dissociate with a proton under acidic or basic conditions. There are several methods of studying protonation constants but the most commonly used are polarography, NMR, potentiometric and spectrophotometric titrations. In this investigation, potentiometric titration was used to determine protonation constants of THPTACD, THBTACD and THMPTACD. Consider the following general chemical reaction:

$$\alpha A + \beta B \rightleftharpoons \sigma S + \tau T \qquad \textbf{(Equation 3.1)}$$

Equation 3.1 is directly associated with the contribution of the activities of individual species participating in an equilibria. Normally the system is investigated under constant temperature and ionic strength such that the activity coefficient of each species remains constant and the equilibrium equation is given as in **Equation 3.2**:

$$K_c = \frac{[S]^{\sigma}[T]^{\tau}}{[A]^{\alpha}[B]^{\beta}} \qquad \textbf{(Equation 3.2)}$$

In general, the stepwise protonation constants for all three ligands, THMPTACD, THBTACD and THPTACD, are defined as in **Equations 3.3-3.8**:

$$H^+ + L \rightleftharpoons HL^+ \qquad \textbf{(Equation 3.3)}$$

$$K_1 = \frac{[HL^+]}{[H^+][L]} \qquad \textbf{(Equation 3.4)}$$

$$H^+ + HL^+ \rightleftharpoons H_2L^{2+} \qquad \textbf{(Equation 3.5)}$$

$$K_2 = \frac{[H_2L^{2+}]}{[H^+][HL^+]} \qquad \textbf{(Equation 3.6)}$$

$$H^+ + H_2L^{2+} \rightleftharpoons H_3L^{3+} \qquad \textbf{(Equation 3.7)}$$

$$K_3 = \frac{[H_3L^{3+}]}{[H^+][H_2L^{2+}]} \qquad \textbf{(Equation 3.8)}$$

L can either be THPTACD, THBTACD or THMPTACD and the constant K_i gives the particular stepwise protonation constant.

The protonation constants in this investigation were obtained by manipulation of the conductivity potential values using the ESTA-WIN computer program (May *et al.*, 1988). This program calculates the overall protonation constants, log β_i, and the stepwise protonation constants, log K_i, are obtained by subtraction. The overall protonation constant, β_i, is a summation of series stepwise protonation constants as shown in **Equations 3.9-3.14**:

$$3H^+ + L \rightleftharpoons H_3L^{3+} \qquad \textbf{(Equation 3.9)}$$

$$\beta_3 = K_3 \text{ x } K_2 \text{ x } K_1 = \frac{[H_3L^{3+}]}{[H^+]^3[L]} \qquad \textbf{(Equation 3.10)}$$

$$2H^+ + L \rightleftharpoons H_2L^{2+} \qquad \textbf{(Equation 3.11)}$$

$$\beta_2 = K_2 \text{ x } K_1 = \frac{[H_2L^{2+}]}{[H^+]^2[L]} \qquad \textbf{(Equation 3.12)}$$

$$H^+ + L \rightleftharpoons HL^+ \qquad \textbf{(Equation 3.13)}$$

$$\beta_1 = K_1 = \frac{[HL^+]}{[H^+][L]} \qquad \textbf{(Equation 3.14)}$$

Protonation constants in non-aqueous solvents are not widely reported because the determination of pH in a non-aqueous, solvent referenced to that solvent, is difficult due to the lack of a way to relate the electrode EMF readings to absolute ${}^{s}_{s}\mathrm{pH}$ (Gibson *et al.*, 2006). Bates *et al.*, (1963) and Grunwald and Berkowitz, (1951) independently determined a correction constant which is used to relate the electrode junction potential to pH in non-aqueous solutions, but the procedure of calculating the correction factor is normally complicated. The expression ${}^{w}_{w}\mathrm{pH}$ is used if pH of an aqueous solution is measured after calibrating the measuring glass electrode with aqueous buffers whereas ${}^{s}_{w}\mathrm{pH}$ is used if the electrode is calibrated in water and the pH of non-aqueous buffered solution is measured. The representation ${}^{s}_{s}\mathrm{pH}$ is used when both calibration and pH determination are done in non-aqueous solutions.

3.2 Materials and methods

3.2.1 Chemicals and reagents

The ligands THPTACD, THBTACD and THMPTACD were synthesised according to the procedures described in **Sections 2.6.1, 2.6.3, 2.6.4** of **Chapter 2**. NaOH volucon (0.1000 mol dm^{-3}), HNO_3 volucon (0.1000 mol dm^{-3}), oxalic acid, $NaNO_3$, methyl orange and phenolphthalein indicators were obtained from Merck.

3.2.2 Instrumentation

A Thermo Orion 420+ pH meter and a 725 Dosimat automatic titrator equipped with a 649 Metrohm magnetic stirrer were used for all titrations (**Fig. 3.1**). Measurements were made with the solutions in a water-jacketed cell (**Fig. 3.2**) connected to a Haake G thermostated

water bath. Atmospheric CO_2 was excluded from the cell during the titration by passing purified N_2 gas across the top of the experimental solution. The standard base was added through a capillary tip at the surface of the solution by a Metrohm Dosimat 725 burette.

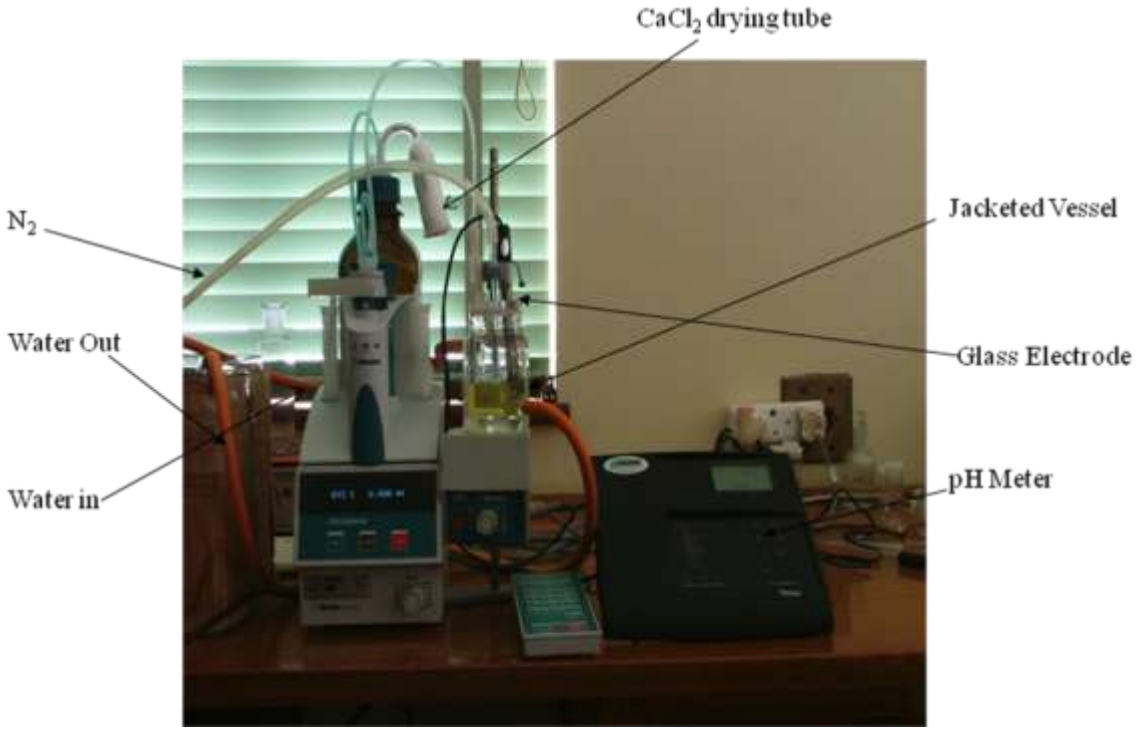

Fig. 3.1: A Thermo Orion 420+ pH meter and a Dosimat 725 automatic titrator.

3.2.3 Preparation of the solutions

A NaOH (0.09922 mol dm^{-3}) volucon was quantitatively transferred into a 1 L volumetric flask and made up to the mark using distilled water. This solution was standardised using oxalic acid.

A HNO_3 (0.1008 mol dm^{-3}) volucon was quantitatively transferred into a 1 L volumetric flask and made up to the mark using distilled water. This solution was standardised using a standard NaOH solution.

THPTACD (0.1728 g, 0.5001 mmol) and $NaNO_3$ (0.8499 g, 0.01000 mol) were quantitatively transferred into a 100 mL volumetric flask and made up to the mark with deionised water. The solutions of THBTACD (0.1942 g, 0.5010 mmol) and THMPTACD (0.1741 g, 0.5008 mmol) were prepared in the same manner.

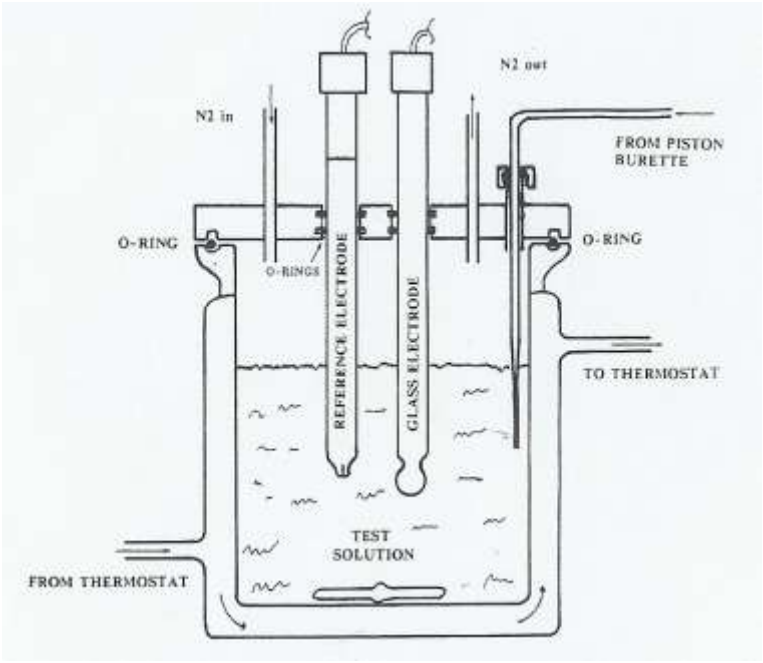

Fig. 3.2: Jacketed cell, electrode, nitrogen entry and exit and stirrer paddle. Redrawn after Luckay (1997).

3.2.4 Potentiometric titration of THPTACD, THBTACD and THMPTACD

A thermo Orion 420+ pH meter was calibrated using two standard buffer solutions at pH 4.01 and 10.01. The first part of the experiment involved the titration of HNO_3 against the NaOH for determination of E° and k (see **Equation 3.15**). HNO_3 (0.1008 mol dm^{-3}, 20.00 mL) was added to a jacketed glass vessel and NaOH (0.09922 mol dm^{-3}) solution was then added in increments of 1.000 mL using a Dosimat 725 automatic titrator equipped with a 649 Metrohm magnetic stirrer under nitrogen atmosphere at 25.0 ± 0.1 °C. The solution was constantly stirred with a 649 Metrohm magnetic stirrer during the course of the titration and points were taken on each side of the end point and recorded in millivolts (mV).

The second part involved the determination of the protonation constants of the three ligands. THPTACD (0.005001 mol dm^{-3}, 10.00 mL) was added to a clean jacketed glass vessel followed by HNO_3 (0.1008 mol dm^{-3}, 20.00 mL). The mixture was titrated with NaOH (0.09922 mol dm^{-3}) solution at the increments of 0.2000 mL up to the basic region using a Dosimat 725 automatic titrator under nitrogen atmosphere at 25.0 ± 0.1°C. The solution was

constantly stirred with a 649 Metrohm magnetic stirrer during the course of the titration and the potential was recorded in mV.

The same titration procedure was repeated with THBTACD (0.005010 mol dm^{-3}, 10.00 mL) and THMPTACD (0.005008 mol dm^{-3}, 10.00 mL) in place of THPTACD.

3.3 Results and discussion

The protonation constants of THPETACD and TMPTACD were not determined because the former is insoluble in water whereas the latter quickly polymerised to form insoluble polymers as soon as it was added to water. The protonation constant of 1,4,7-*tris*[(2*S*)-2-hydroxy-2-phenylethyl]-1,4,7-triazacyclononane, which has a very similar structure to THPETACD, in DMF was reported by Weeks *et al.,* (2001). THMPTACD, THBTACD and THPTACD studied in this work were synthesised according to the procedures outlined in **Chapter 2**. THMPTACD and THBTACD unlike THPTACD do not readily dissolve in water at room temperature. They form spherical balls before dissolving in over 5 hours but dissolve in less than an hour at 35 °C and do not form insoluble balls after cooling to room temperature. The reactions were carried out under a stream of purified N_2 gas to exclude CO_2 which could have interfered with the reaction by forming HCO^{3-} and H_2CO_3. Excess acid was added to the mixture before the start of each titration which means that the ligands were initially fully protonated. All the three ligands studied in this investigation have three neutral nitrogen donor atoms in the parent macrocyclic ring and therefore they have a charge of 3+ when fully protonated.

Prior to each potentiometric titration the glass electrode was calibrated in terms of the $[H^+]$ by titrating solutions of nitric acid and sodium hydroxide of known concentrations and correlating the mV readings with calculated values of $[H^+]$. Points were collected on both the acidic and basic sides of the end point. The $[H^+]$-dependent junction potentials are negligible under the condition of the experiments (Delgado and Frausto da Silva, 1982). The correlation between measured electromotive force and calculated $[H^+]$ is therefore represented by the following equation:

$$E_{cell} = E^o + k \log [H^+] \qquad \textbf{(Equation 3.15)}$$

E^o is the standard cell potential and k is the response slope of the electrode which has approximately the Nernstian value of (2.303 x RT/F), where R is the gas constant, T is the temperature in Kelvin and F the Faraday constant. This relationship is valid for both acidic and basic regions. The values of E^o and k were calculated from a linear plot of E_{cell} versus log $[H^+]$ using a least squares fit on the data. The value for the dissociation of water under the condition of the titrations done in this study and employed in the computations was as given in **Equation 3.16** (Schwarzenbach and Flaschka, 1969; Martell and Motekaitis, 1992):

$$K_w = [H^+][OH^-] = 10^{-13.78} \qquad \textbf{(Equation 3.16)}$$

No report is available on the stability constant of 1,4,7-*tris*(2-hydroxypropyl)-1,4,7-triazacyclononane (THPTACN) (**Chart 3.1**) or its chiral diastereomer analogues. However, the stability constant of 1,4,7-*tris*(2-hydroxyethyl)-1,4,7-triazacyclononane (THETAC) (**Chart 3.1**) was reported by Sayer *et al.*, (1983) and will be used to compare the results we obtained in this investigation.

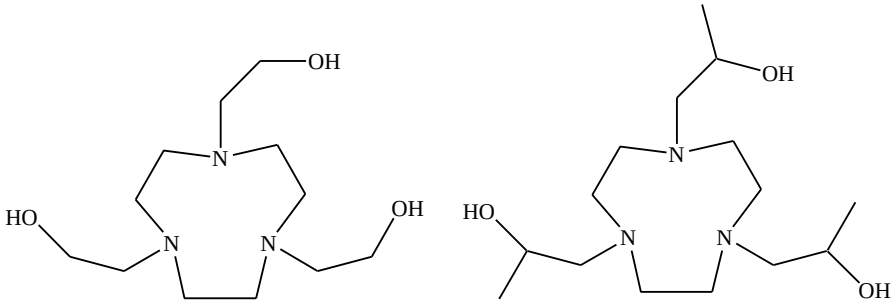

Chart 3.1: The structures of THETAC (left) and THPTACN (right).

The protonation constants of the macrocyclic ligands with similar donor atoms tethered on the same parent ring or with similar donor atoms of the pendant arms appended to the same parent macrocycle, do not differ much in their stability (**Table 3.1**). **Table 3.1** shows the protonation constants of $12aneN_4$, THEC-12 and THP-$12aneN_4$, where the last two ligands have hydroxyethyl and hydroxypropyl pendant arms, respectively (**Chart 3.2**).

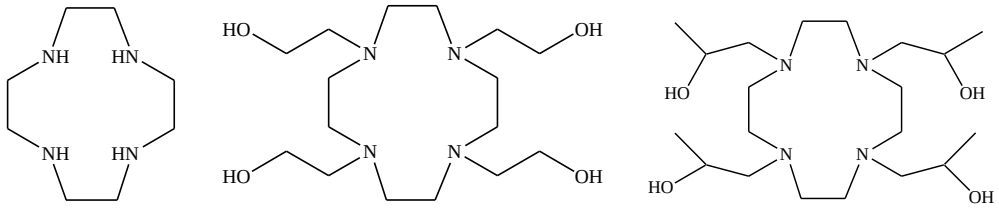

Chart 3.2: The structures of 12aneN$_4$, THEC-12 and THP-12aneN$_4$ from left to right.

Tetraazamacrocycles have more conformational freedom than triazamacrocycles but data in **Table 3.1** shows that the use of THETAC, which has hydroxyethyl pendant arms instead of THPTACN for comparison with the protonation constants reported in this investigation, is justifiable.

Table 3.1: Protonation constants of 12aneN$_4$, THEC-12 and THP-12aneN$_4$ at 25 °C, in 0.10 mol dm^{-3} $NaNO_3$

reaction		12aneN$_4$[a]	THEC-12[b]	THP-12aneN$_4$[a]
$H_2L^{2+} + H^+ \rightleftharpoons H_3L^{3+}$	log K_3	strong	2.3	strong
$HL^+ + H^+ \rightleftharpoons H_2L^{2+}$	log K_2	9.72	8.01	8.26
$L + H^+ \rightleftharpoons HL^+$	log K_1	11.32	9.78	9.98

[a] Data from Hancock *et al.*, (1988). [b] Data from Turonek *et al.*, (1995).

3.3.1 The protonation of THPTACD

The stepwise protonation constants of THPTACD with standard deviations, R-factor and the number of points are reported in **Table 3.2**.

The value of the first protonation constant of THPTACD is 11.47 log units whereas the value of the first protonation constant of the parent macrocycle, 12aneN$_3$, is 12.60 log units (Zompa, 1978). The protonation constant of 12aneN$_3$ dropped by 1.13 log units on addition of the hydroxypropyl pendant arms thereby making THPTACD less basic than 12aneN$_3$. At first glance this may look unusual because THPTACD has three tertiary nitrogen donor atoms compared to secondary nitrogen donor atoms of 12aneN$_3$. The tertiary nitrogen donor atoms in THPTACD should benefit more from the positive inductive effect of the hydroxypropyl groups and the propylene bridges of the parent macrocyclic ring compared to 12aneN$_3$. The general rule is that tertiary nitrogen atoms are more basic than secondary nitrogen atoms which in turn are more basic than primary nitrogen atoms because of the positive inductive

effect of the alkyl groups attached to the nitrogen donor atoms. However, this rule does not hold in polar solvents that are able to form hydrogen bonds of the form N-H·····OH_2 (where H is the hydrogen atom of the primary or secondary amine) with the parent molecule. The hydrogen bonds (between the hydrogen atom on the protonated 1° or 2° nitrogen atom and solvent molecules) help in diffusing the positive charge in primary and secondary nitrogen donor atoms unlike in tertiary nitrogen donor atoms that are unable to form such hydrogen bonds (Hancock, 1989). The pendant arms have oxygen donor atoms attached to them, which means that the inductive effect is not as pronounced as it would be if the arms were purely alkyl groups. Oxygen donor atoms are more electronegative than nitrogen donor atoms, and as such, the most pronounced inductive effect the nitrogen donor atoms experience is from the propylene bridges of the parent macrocyclic ring. This means that the nitrogen donor atoms of the parent macrocyclic ring does not benefit much from having tertiary nitrogen donor atoms because of the electron withdrawing ability of the oxygen donor atoms of the pendant arms.

Table 3.2: Protonation constants, log *K*, of the THPTACD at 25.0 °C, in 0.1000 mol dm^{-3} $NaNO_3$

	log K_1	log K_2
Values	11.47	5.81
Standard deviation	±0.02	±0.02
R-factor	0.015	
Number of titrations	2	
Number of points	228	

Zompa, (1978) reported that on protonating 12aneN_3, the first proton is datively bonded to one nitrogen donor atom and hydrogen-bonded to the remaining two unprotonated nitrogen donor atoms of the ring. Ribeiro-Claro *et al.,* (1996) used molecular mechanics to show that the two hydrogen bonds of the protonated 12aneN_3 are symmetrical. One would expect THPTACD to form hydrogen bonds involving the oxygen donor atoms of the pendant arms in addition to the N-H·····N (where H is the added proton) hydrogen bonds thereby affording a caged structure. The caged structure in the protonated THPTACD should hold the proton

very tightly thereby increasing the basicity of THPTACD with respect to 12aneN$_3$ which cannot adopt a caged structure because of unavailability of pendant arms.

Hydrogen bonds play a very important role in diffusing the positive charge on the macrocyclic nitrogen donor atoms upon protonation. The nitrogen donor atoms of the THPTACD are very close to one another because of the cyclic nature of the parent ring. For example, Luckay *et al.,* (1996) confirmed that the first protonation constant of THETAC (**Chart 3.1**) is very high and presented crystal structure evidence which showed that the first proton is datively bonded to one nitrogen donor atom and hydrogen-bonded to the other two unprotonated nitrogen donor atoms and one oxygen atom of the pendant arm. The first protonation constant of THETAC is 11.52 log units and was first reported by Sayer and co-workers (Sayer *et al.,* 1983). THETAC has similar donor atom sets to THPTACD with hydroxyethyl pendant arms instead of hydroxypropyl pendant arms. The first protonation constant of 9aneN$_3$ is 10.44 log units (Yang and Zompa, 1976). In this case, there is an increase of 1.08 log units in protonation constant on addition of hydroxyethyl pendant arms and therefore, THETAC is more basic than the parent macrocyclic ligand, 9aneN$_3$. The increase in protonation constant on addition of hydroxyethyl pendant arms to 9aneN$_3$ suggests that the hydrogen bonds formed by the oxygen donor atoms are able to compensate for the loss of the N-H$\cdots$OH$_2$ hydrogen bonds (where H is the hydrogen atom of the parent macrocycle) and the small inductive effect of the hydroxyethyl group. The oxygen donor atoms of the pendant arms withdraw electrons of the ethyl group (Sayer *et al.,* 1983).

Based on the similarities in structure between THETAC and THPTACD one would expect the same increase in basicity on addition of hydroxypropyl arms to 12aneN$_3$ but the results show the opposite. The difference can be due to the differences in the nature of the hydrogen bonds and steric effects in the two ligands. The hydroxyethyl pendant arms are appended on a small parent macrocyclic ring, 9aneN$_3$, whereas the hydroxypropyl pendant arms are tethered on a twelve-membered macrocyclic ring, 12aneN$_3$. The tertiary nitrogen donor atoms in THPTACD benefit more from the inductive effect of the hydroxypropyl pendant arms because of the methyl groups which are directly attached to the carbons holding oxygen donor atoms. The methyl groups compensate for the negative inductive effect of the oxygen donor atoms better than the hydrogen atoms in THETAC. The compensation of the negative inductive effect of the oxygen atom by the methyl group importantly comes at the expense of

steric hindrance. THPTACD is more sterically hindered than THETAC. Comparisons of the first protonation constants of the two ligands suggest that THETAC forms stronger hydrogen bonds and the protonated species are more solvated than in THPTACD. The oxygen donor atoms in THPTACD are sterically hindered to such an extent that they cannot approach the proton in the same way as the oxygen donor atoms of the THETAC. This means that any gain in inductive effect is overridden by the increase in steric hindrance. The protonated species of THETAC are more solvated than the protonated species of THPTACD because of stronger steric hindrance to solvation imposed by the hydroxypropyl pendant arms in THPTACD compared to hydroxyethyl pendant arms in THETAC.

This suggestion is supported by the first protonation constant of DOTRA (see **Chart 3.3** for key to ligand abbreviations) which is slightly higher than the first protonation constant of its parent macrocyclic ligand, 12aneN_3. The first protonation constant of DOTRA is 12.80 log units (Geraldes *et al.,* 1991), thus there is an increase of 0.20 log units on addition of acetate pendant arms to 12aneN_3. The nitrogen donor atoms in DOTRA suffer more from negative inductive effect than the nitrogen donor atoms in both THETAC and THPTACD. The acetate groups of the pendant arms in DOTRA are strongly electron withdrawing due to the presence of two oxygen atoms. However, unlike the hydroxypropyl groups in THPTACD, the acetate groups form very strong hydrogen bonds with the proton on the nitrogen donor atom and are more solvated by the solvent molecules. DOTRA is, therefore, able to diffuse the positive charges on the protonated nitrogen atom of the macrocyclic ring better than the oxygen donor atoms of THPTACD.

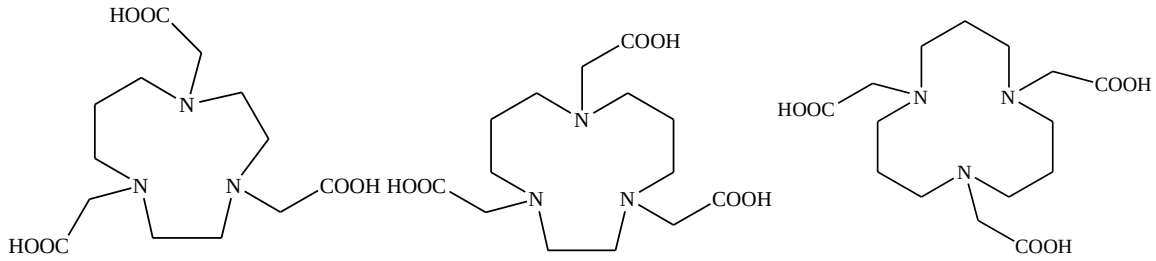

Chart 3.3: The molecular structure of DETA, UNTA and DOTRA from left to right, respectively.

The first protonation constant of 1,4,7-*tris*[(2*S*)-2-hydroxypropyl]-1,4,7-triazacyclodecane is 9.18 log units (Barnard, 2008) which is well below the first protonation constant of its parent

macrocyclic ligand, 10aneN_3, which is 10.44 (Zompa 1978). The same author reported that the first protonation constant of 1,4,8-*tris*[(2*S*)-2-hydroxypropyl]-1,4,8-triazacycloundecane is 11.32 log units (Barnard, 2008) which is again below the protonation constant of its parent macrocyclic ligand, 11aneN_3, which is 12.00 log units (Zompa, 1978). This seems to further support the idea that the hydroxypropyl pendant arms impose more steric demand on the ligand to both protonation and solvation of the protonated species than the hydroxyethyl pendant arms (solvation of the protonated species is an exothermic process). In protonated THPTACD, the new hydrogen bonds do not fully compensate for the loss of N-H·····OH_2 (where H is the hydrogen atom of the parent macrocycle carrying the proton) hydrogen bonds in the protonated parent macrocycle by forming relatively weak hydrogen bonds because of steric hindrance whereas in the case of protonated THETAC and DOTRA the new hydrogen bonds outweigh the negative inductive effect and the loss of N-H·····OH_2 hydrogen bonds of the protonated parent macrocycle. There is also less steric hindrance to solvation in THETAC and DOTRA compared to THPTACD.

It is not easy to predict the individual contributions of entropy effects (mostly due to solvation and desolvation) and enthalpy effects (mostly due to formation of dative and hydrogen bonds) towards the overall Gibbs free energy of the protonation. If the parent macrocyclic rings only is considered, one would expect the macrocycle, 12aneN_3, which has secondary nitrogen donor atoms, to be more solvated than the parent macrocyclic ring of THPTACD, which has tertiary nitrogen donor atoms. The unprotonated tertiary nitrogen donor atoms do not have N-H bonds hence are less solvated than secondary nitrogen atoms which in turn are less solvated than primary nitrogen donor atoms (Arranz *et al.*, 2001). More energy is, therefore, required to desolvate the macrocyclic ring of 12aneN_3 than the ring of THPTACD (desolvation of the macrocyclic hole is an endothermic process). However, the entropy contribution upon desolvation is more favourable for 12aneN_3 than THPTACD. This should be the situation because much as the protonated species are resolvated, not all the solvent molecules are allowed back to occupy the macrocyclic hole which is taken up by the proton. The number of solvation spheres within the macrocyclic hole should, therefore, be less than it was before protonation. The extent to which the hydroxyl groups are solvated and desolvated is difficult to predict but in general nitrogen donor atoms are more solvated than oxygen donor atoms (Hancock and Thöm, 1982). Oxygen donor atoms of the pendant arms are only involved in hydrogen bonding which should not require full desolvation. In general,

the parent macrocyclic ligand is more solvated than THPTACD which means that 12aneN_3 has more favourable entropy contribution than THPTACD upon desolvation.

The second protonation constant of THPTACD is 5.81 log units, which is lower than the first protonation constant by a value of 5.66 log units. The difference between the first and second protonation constants can be attributed to lack of additional hydrogen bond stabilisation that is available to the proton only on first protonation and increase in electrostatic repulsions within the macrocycle. Another important factor which may lead to a low second protonation constant is the mode of entry of the second proton onto the macrocycle. The second proton cannot approach the macrocycle from the top holding the oxygen donor atoms because it would face high electrostatic repulsions from the first proton. Similarly, the proton cannot approach the ring from below the plane of the nitrogen donor atoms because that would mean that the lone pairs of electron of the nitrogen donor atoms would twist at an angle sp^3 hybrid orbitals allow bonding which may not be energetically favourable. This leaves the near-side as the only approachable route for the second protonation.

The second proton is equally stabilised by the hydrogen bond with one oxygen donor atom of the pendant arm. The crystal structure of the protonated 1,5-*bis*[(2*S*)-hydroxybutyl]-1,5,9-triazacyclododecane (see later **Fig. 5.29** of **Section 5.3.8**, **Chapter 5**) gives an idea about the importance of hydrogen bonds in determining the protonation constant of triazamacrocycles with pendant arms carrying oxygen donor atoms. The molecular structure has two pendant arms and two protons in the macrocyclic ring. Both protons are hydrogen-bonded to the nearest oxygen donor atom and unprotonated nitrogen donor atom of the parent macrocycle. The results seem to support the idea that the second proton would be hydrogen-bonded to an oxygen donor atom of the pendant arm attached to the same nitrogen donor atom. The first proton is hydrogen-bonded to the two unprotonated nitrogen donor atoms which mean that before the second proton is datively bonded to one of the two remaining nitrogen donor atoms, hydrogen bonds must first be broken. If the cage structure (where all six donor atoms are involved in hydrogen bonding to the first proton) is assumed, then it means that two hydrogen bonds will be broken (N·····H and O·····H) and replaced by one hydrogen bond between the second proton and the oxygen donor atom of the pendant arm and a dative N-H bond. On the other hand if only one oxygen donor atom is involved in hydrogen bonding as

shown by Luckay *et al.,* (1996) then only one hydrogen bond (N·····H, where N is the nitrogen donor atom to which the second proton is datively bonded) will be broken and replaced by one O·····H hydrogen bond and a dative N-H bond. This means that the replacement of bonds (hydrogen bond with hydrogen bonds or dative bonds) does not play a key role in destabilising the second proton. Such processes are thermodynamically allowed as long as the overall change in Gibbs free energy is negative. This seems to suggest that lack of strong hydrogen bonds stabilisation as influenced by the route of entry onto the macrocyclic ring is responsible for the low second protonation constant.

The second protonation constant of $12aneN_3$ is 7.54 log units (Zompa, 1978), which means that the second protonation constant dropped by 1.73 log units because of the influence of the pendant arms in THPTACD. After the first protonation, $12aneN_3H^+$ remained a better base than $THPTACDH^+$. If the assertion that the second proton bonds to the nitrogen donor atom on the near-side is held, then steric hindrance should not be of much importance in determining the stability of the second protonation. This seems to be the case because the second protonation constant of THMPTACD, which is more sterically encumbered than THPTACD, is higher than the second protonation of THPTACD. Ribeiro-Claro *et al.,* (1996) showed that the most stable conformation, after the second protonation of $12aneN_3$, has each of the two protons (the first and the second proton) hydrogen-bonded to the third nitrogen donor atom with the hydrogen bond length of 2.08 Å and 1.93 Å. The two hydrogen bonds are of comparable strength but there is still an increase in electrostatic repulsion. In THPTACD, however, the second proton cannot form comparable hydrogen bonds to the third nitrogen donor atom of the ring because it is added on the rear-side of the macrocyclic hole. This suggestion is supported by DOTRA which has a higher first protonation constant but a lower second protonation constant than $12aneN_3$. The second protonation constant of DOTRA is 7.55 log units (Geraldes *et al.,* 1991), which is higher than the second protonation constant of THPTACD and can be attributed to strong hydrogen bonds in DOTRA relative to THPTACD.

For the second proton of THPTACD to form a comparable strong hydrogen bond as formed by the first proton, like in the case of $12aneN_3$, the pendant arms have to twist in such a way as to allow a *meridional* hydrogen bonding. The molecular structure of 1,5-*bis*[(2*S*)-

hydroxybutyl]-1,5,9-triazacyclododecane (see later **Fig. 5.29** of **Section 5.3.8**, **Chapter 5**) allowed such hydrogen bonding because only two pendant arms are appended to the parent macrocyclic ring and hence less steric hindrance. The value for log β_2 for THPTACD is 17.28 log units. The log β_2 value for 12aneN_3 is 20.17 log units (Zompa, 1978) thus giving a difference of 2.89 log units, which is mostly due to better stabilisation of the second proton in 12aneN_3 than THPTACD. DOTRA, which is able to stabilise the second proton better than THPTACD, has the log β_2 value of 20.35 (Geraldes *et al.*, 1991).

A third protonation constant is certainly possible for THPTACD because of the three nitrogen donor atoms in the parent macrocyclic ring. In this study, we were unable to determine a constant for such a reaction because of the limitations in the potentiometric titration procedure that was employed. There is a non-linear response of the glass electrodes in very acidic solutions which precludes the usual data analysis (Zompa, 1978). The third protonation can, however, readily be determined by polarography, NMR and UV-VIS spectrophotometry.

3.3.2 The protonation of THBTACD

The stepwise protonation constants for THBTACD with standard deviations, R-factor and the number of points used are shown in **Table 3.3**.

Table 3.3: Protonation constants, log *K*, of the THBTACD at 25.0 °C in 0.1000 mol dm^{-3} $NaNO_3$

	log K_1	log K_2
Values	10.96	6.02
Standard deviation	±0.04	±0.05
R-factor	0.035	
Number of titrations	2	
Number of points	152	

The value of the first protonation constant of THBTACD is 10.96 log units whereas the parent macrocycle, 12aneN_3, has a value of 12.60 log units (Zompa, 1978) which can be

attributed to the same factors explained above for THPTACD. There is a drop in stability constant by 1.64 log units on addition of hydroxybutyl pendant arms to 12aneN$_3$. The molecular structure of THBTACD is similar to the structure of THPTACD (**Chart 3.4**) in having hydroxybutyl and hydroxypropyl pendant arms, respectively, appended to 12aneN$_3$ parent macrocyclic ring. Both molecules have the same donor atom sets.

The tertiary nitrogen donor atoms of the parent ring in THBTACD are not solvated to the same extent like the secondary donor atoms of the 12aneN$_3$. More energy is therefore used to desolvate the parent macrocycle, 12aneN$_3$ but on desolvation more solvent molecules are released such that 12aneN$_3$ has a better entropy term than THBTACD. The hydroxybutyl pendant arms impose steric hindrance to both solvation and formation of strong hydrogen bonds between the proton and the other nitrogen donor atoms of the parent macrocyclic ring as compared to 12aneN$_3$. There are also no hydrogen bonds of the form N-H·····OH$_2$ (where H is the hydrogen atom of the ring and not the first proton) in THBTACD which seems to tip enthalpy in favour of protonation of 12aneN$_3$ as compared to THBTACD. The N-H·····OH$_2$ hydrogen bonds in protonated 12aneN$_3$ help in diffusing the positive charge within the macrocycle.

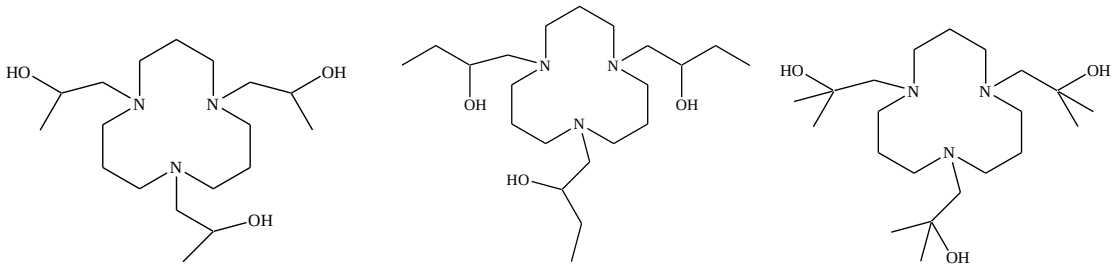

Chart 3.4: The structures of THPTACD, THBTACD and THMPTACD from left to right, respectively.

In general, the first protonation of 12aneN$_3$ is favoured by both entropy and enthalpy contributions. On the other hand, the first protonation constant of THBTACD is hindered by the steric crowding from the pendant arms which seem to affect both solvation and hydrogen bond formation and has relatively less enthalpy and entropy terms than 12aneN$_3$.

The second protonation constant of THBTACD is 6.02 log units whereas 12aneN$_3$ has a value of 7.54 log units (Zompa, 1978). The second protonation constant is lower than the first protonation constant in both instances because of the increase in electrostatic repulsions within the macrocycle and the incoming proton is less stabilised by hydrogen bonds than the first proton. The difference between first and second protonation constant for THBTACD is 4.94 log units. The log β_2 value for THBTACD is 16.98 log units whereas the log β_2 of 12aneN$_3$ is 20.17. The difference of 3.19 log units is again mostly due to better stabilisation of the second proton in 12aneN$_3$ than THBTACD.

The third protonation constant was not determined due to lack of sensitivity of glass electrodes in high acidic medium.

3.3.3 The protonation of THMPTACD

The stepwise protonation constants of THMPTACD with standard deviations, R-factor and the number of points are shown in **Table 3.4**.

Table 3.4: Protonation constant, log *K*, of the THMPTACD at 25.0 °C, in 0.1000 mol dm^{-3} NaNO$_3$

	log K_1	log K_2
Values	10.47	5.94
Standard deviation	±0.02	±0.02
R-factor	0.016	
Number of titrations used	2	
Number of points used	272	

The value of the first protonation constant of THMPTACD is 10.47 log units whereas the value of the first protonation constant of the parent macrocycle, 12aneN$_3$, is 12.50 log units. There is a drop in stability constant by 2.03 log units on addition of hydroxy-2-methylpropyl pendant arms to 12aneN$_3$.

The structure of THMPTACD is similar to the structures of THPTACD and THBTACD (**Chart 3.4**) in having three hydroxyalkyl pendant arms appended on the same parent macrocyclic ligand, 12aneN$_3$, with the same donor atom set, N_3O_3. THMPTACD is less

solvated than 12aneN$_3$, which means that more energy is used to desolvate the parent macrocycle, 12aneN$_3$, but on desolvation more solvent molecules are released such that 12aneN$_3$ has a better entropy term than THMPTACD. The steric hindrance to both solvation and formation of strong hydrogen bonds between the proton and the unprotonated nitrogen donor atoms of the parent macrocyclic ring is more pronounced in THMPTACD as compared to 12aneN$_3$. There are also no hydrogen bonds of the form N-H·····OH$_2$ (where H is the hydrogen atom of the ring and not the first proton) in THMPTACD. In general, the first protonation of 12aneN$_3$ is favoured by both entropy and enthalpy contributions. On the other hand, the first protonation constant of THMPTACD is hindered by the steric crowding from the pendant arms which seem to affect both solvation and hydrogen bond formation and has relatively less enthalpy and entropy term than 12aneN$_3$.

The second protonation constant of THMPTACD is 5.94 log units whereas 12aneN$_3$ has a value of 7.54 log units. In both macrocycles, there is a drop in protonation constant upon addition of a second proton because of the increase in electrostatic repulsions and the incoming proton is less stabilised by hydrogen bonds than the first proton. The difference between the first and the second protonation constants for THMPTACD is 4.53 log units. The log β_2 value for THMPTACD is 16.41 log units whereas the log β_2 of 12aneN$_3$ 20.17.

The third protonation of THMPTACD was not determined because of insensitivity of the glass electrode in very acidic medium.

3.3.4 Comparative study of THPTACD, THBTACD and THMPTACD

The three macrocyclic ligands THPTACD, THBTACD and THMPTACD have the same parent macrocyclic ring but different pendant arms. THPTACD and THBTACD have secondary alcohol pendant arms whereas THMPTACD has tertiary alcohol pendant arms thereby making it more sterically demanding than the first two. **Table 3.5** shows that the first protonation constant increases as the hydroxyalkyl groups become less bulky.

The first protonation constant of THPTACD, THBTACD and THMPTACD are 11.47, 10.96 and 10.47 log units. This means that the basicity of the three macrocyclic ligands increases in the following order:

THMPTACD < THBTACD < THPTACD

Table 3.5: The protonation constants of THPTACD, THBTACD and THMPTACD

reaction		THPTACD	THBTACD	THMPTACD
$H_2L^{2+} + H^+ \rightleftharpoons H_3L^{3+}$	$\log K_3$	strong	strong	strong
$HL^+ + H^+ \rightleftharpoons H_2L^{2+}$	$\log K_2$	5.81	6.02	5.94
$L + H^+ \rightleftharpoons HL^+$	$\log K_1$	11.47	10.96	10.47

All titrations were done at 25 °C, in 0.1000 mol dm^{-3} $NaNO_3$.

THMPTACD has two methyl groups directly attached to the carbon carrying the oxygen donor atom whereas THBTACD and THPTACD have one ethyl group and one methyl group, respectively. This means that hydroxy-2-methylpropyl group should block the solvent molecules more efficiently than both the hydroxybutyl and hydroxypropyl groups and hence THMPTACD is less solvated than THBTACD which in turn is less solvated than THPTACD. The order of increase in solvation due to steric effects of the pendant arms on the macrocyclic ring is as follows:

THMPTACD < THBTACD < THPTACD

Upon desolvation more solvent molecules are released by THPTACD than the other two and hence benefit most from entropy effect. The benefit in entropy comes at a price with more energy being required to desolvate THPTACD as compared to the other two macrocyclic ligands. One would therefore expect THBTACD and THMPTACD to have more favourable enthalpy terms compared to THPTACD because less energy is used to desolvate their macrocyclic ring for protonation. However, the results suggest that THPTACD does not suffer much from using a lot of energy to desolvate the parent macrocyclic ring. This can be explained in terms of less steric hindrance in THPTACD and hence is able to form strong hydrogen bonds and the protonated species are more solvated than in both THBTACD and THMPTACD. The oxygen donor atoms of the pendant arms are able to approach the proton

which is datively bonded to one of the three nitrogen donor atoms of the parent ring. On the other hand, THMPTACD is the most sterically demanding ligand and therefore, it does not form as strong hydrogen bonds as THPTACD and also the protonated species are less solvated by the solvent molecules. The oxygen donor atoms of the pendant arms cannot approach the proton close enough to form strong hydrogen bonds. THBTACD is in between these two extremes and forms stronger hydrogen bonds as compared to THMPTACD but weaker hydrogen bonds as compared to THPTACD. These results suggest that the first protonation of THPTACD, THBTACD and THMPTACD are sterically driven.

The second protonation constant of the three ligands does not seem to follow any trend at first glance. A good starting point would be to compare the second protonation constant of THPTACD and THMPTACD. THMPTACD, as explained above, has two methyl groups attached to the carbon carrying the oxygen donor atom whereas in THPTACD there is only one such methyl group. This means that THMPTACD is more sterically hindered than THPTACD but it has a better positive inductive effect because the two methyl groups are able to compensate the negative inductive effect of oxygen donor atoms better than one methyl group in THPTACD. The second protonation constants of THMPTACD and THPTACD are 5.94 and 5.81 log units, respectively. The results show that the second protonation constant increases with increasing steric hindrance which is in contrast to the first protonation constant and highlights the importance of inductive effects.

The second protonation constant of THETAC is 3.42 log units (Sayer *et al.*, 1983) which is even lower than the ones reported here. The difference between the first and second protonation constant in this case is 8.10 log units. THETAC has hydroxyethyl pendant arms, and even though is less sterically demanding than the corresponding macrocyclic ligands with hydroxypropyl pendant arms, it has a weak positive inductive effect. The hydroxyethyl groups of the pendant arms are strongly electron withdrawing such that the highest contribution of inductive effect the nitrogen donor atoms of the parent ring experiences, are from the ethylene bridge. These results seem to agree with the suggestion that inductive effects play a bigger role in second protonation constant of macrocyclic ligands with pendant arms holding oxygen donor atoms. The second protonation constant of $9aneN_3$ is 6.82 log units (Yang and Zompa, 1976) which is way higher than the second protonation constant of

THETAC. This excludes the small charge separation in THETAC as the reason behind the drop in protonation constant relative to THPTACD, THBTACD and THMPTACD. The difference between the second protonation constant of 12aneN_3 and 9aneN_3 is 0.75 log units. On the other hand, the negative inductive effects of the secondary and tertiary oxygen donor atoms in THPTACD, THBTACD and THMPTACD are compensated by the methyl, ethyl and two methyl groups respectively, which are directly attached to the carbon atoms carrying the oxygen donor atoms. THPTACD, THBTACD and THMPTACD are able to support the positive charge on the second nitrogen better than THETAC.

The second protonation constant of THBTACD is 6.02 log units which is higher than the second protonation constant of both THPTACD and THMPTACD. THBTACD has a strong inductive effect compared to THPTACD and is expected to stabilise the second proton better than THPTACD. The higher second protonation constant of THBTACD than THMPTACD suggest that in THBTACD, the inductive and steric effects are supporting one another better than in THMPTACD. THBTACD with hydroxybutyl groups benefit more from positive inductive effects while the steric effects are not as critical as in THMPTACD. This is supported because even though the second protonation constant of THBTACD is higher than the second protonation constant of THMPTACD, the drop in protonation constant, $\Delta\log K$, is higher for THBTACD than THMPTACD (**Table 3.6**).

Table 3.6: $\Delta\log K$ for THPTACD, THBTACD and THMPTACD

Ligand	THPTACD	THBTACD	THMPTACD
$\log K_1$	11.47	10.96	10.47
$\log K_2$	5.81	6.02	5.94
$\Delta\log K$	**5.66**	**4.94**	**4.53**

With these results we can conclude that the first protonation is mostly sterically driven whereas the second protonation is inductively driven. The first proton has to force its way into the middle of the ligand where it is covalently bonded to one nitrogen atom and hydrogen-bonded to the other two unprotonated nitrogen donor atoms of the parent ring and

oxygen atoms of the pendant arms. This proton is strongly stabilised by the cage nature of the hydrogen bonds. On the other hand, the second proton is more likely to add from the near-side of the cavity and hence faces less opposition from the pendant arms. The values for log β_2 for THPTACD, THBTACD and THMPTACD are 17.28, 16.98 and 16.41 log units, respectively. The value for third protonation is usually very small and has little impact on the trend in basicity. The decrease in basicity is therefore as follows:
THPTACD > THBTACD > THMPTACD

The trend in overall basicity can be explained in terms of steric effects outweighing inductive effects. The overall protonation of the three ligands is therefore sterically driven.

3.3.5 Comparative study of the protonation constants of THTD, THTUD and THPTACD

The triprotonated cyclic amines are strongly acidic, which can be explained on the basis of positive charge localisation. The protonated amine functions are forced into close proximity in cyclic amine than in their open chain analogues and loss of proton is facilitated. The series of 9- to 12-triazamacrocyclic ligands were studied by Zompa, (1978) (**Chart 3.5**).

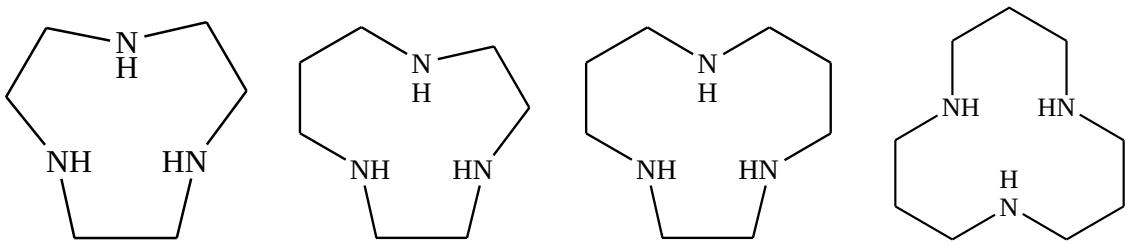

Chart 3.5: The molecular structures of 9aneN_3, 10aneN_3, 11aneN_3 and 12aneN_3 from left to right, respectively.

The series showed interesting properties afforded by the chelate rings as the five-membered chelate rings are progressively replaced by the six-membered chelate rings. The general trend is that the basicity of the triazamacrocycles increases as the five-membered chelate rings are progressively replaced by the six-membered chelate rings (**Table 3.7**). The observed enhancement in basicity of the ring nitrogen donor atoms as the ring sizes increase from nine

to twelve membered triazamacrocycles can, in part, be explained by decrease in electrostatic repulsion in larger rings. However, for the $10aneN_3$ and $11aneN_3$ the acidity is reversed due to involvement of different tautomeric forms (Zompa, 1978). The conformational effect and the involvement of several microscopic processes involving protonated intermediates of different tautometric forms are more pronounced in the second protonation constant (Zompa, 1978). In macrocyclic ligands with oxygen donor atoms on the pendant arms, protonation occurs at the ring nitrogen donor atoms and no report exists where protonation occurred on the oxygen donor atom of the pendant arms.

Table 3.7: The protonation constants of the $9aneN_3$, $10aneN_3$, $11aneN_3$ and $12aneN_3$ triazamacrocycles

reaction		$9aneN_3$[b]	$10aneN_3$[a]	$11aneN_3$[a]	$12aneN_3$[a]
$H_2L^{2+} + H^+ \rightleftharpoons H_3L^{3+}$	$\log K_3$	Strong[c]	strong	strong	2.41
$HL^+ + H^+ \rightleftharpoons H_2L^{2+}$	$\log K_2$	6.82	6.59	7.61	7.57
$L + H^+ \rightleftharpoons HL^+$	$\log K_1$	10.42	12.02	11.96	12.60

[a] From Zompa, (1978). [b] Data from Yang and Zompa, (1976). [c] Strong for potentiometric titration but Geraldes *et al.*, (1991) reported a value of 0.70 log units using NMR titration. Data reported at 25 °C, in 0.1 mol dm^{-3} KNO_3.

The ligands THTD, THTUD and THPTACD have the same pendant arms but tethered on different parent macrocyclic rings. The number of propylene bridges increase from one in THTD to three in THPTACD (**Chart 3.6**).

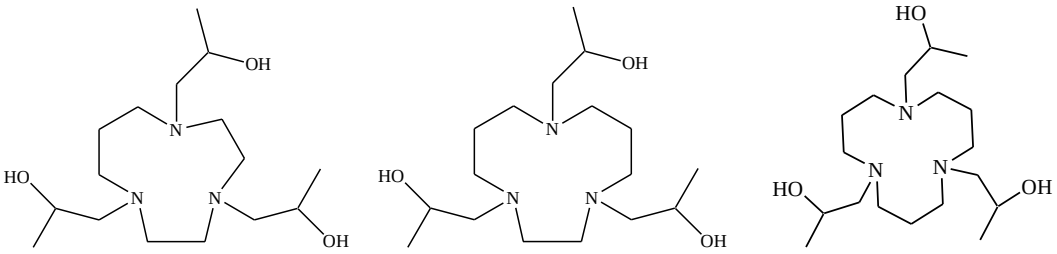

Chart 3.6: The molecular structure of THTD, THTUD and THPTACD from left to right, respectively.

In general, there is a decrease in protonation constant on addition of hydroxypropyl pendant arms (**Table 3.8**). The decrease in protonation constant can be attributed to either lack of strong hydrogen bonds involving the solvent molecules in the tertiary amines or steric effects due to repulsions in the pendant arms (Arranz *et al.*, 2001). THTD, THTUD and THPTACD have exactly the same pendant arms appended to the three nitrogen donor atoms, which means that the difference in their basicity comes from the differences in the number of propylene bridges. THPTACD has several advantages over both THTD and THTUD. Firstly, the propylene bridges between the nitrogen donor atoms offer longer distances between the protonated amines such that electrostatic forces are less felt in THPTACD than in THTUD and THTD. The propylene bridges also offer a much better positive inductive effect than the ethylene bridges and as such stabilise the positive charge on the amine better than the ethylene bridges resulting in better interaction between the proton and the amines.

Table 3.8: The protonation constants of the THTD, THTUD and THPTACD triazamacrocycles

reaction		THTD[a]	THTUD[a]	THPTACD[b]
$H_2L^{2+} + H^+ \rightleftharpoons H_3L^{3+}$	$\log K_3$	strong	strong	strong
$HL^+ + H^+ \rightleftharpoons H_2L^{2+}$	$\log K_2$	4.20	5.87	5.81
$L + H^+ \rightleftharpoons HL^+$	$\log K_1$	9.18	11.32	11.47

[a] Data from Barnard, (2008). [b] This work. Data reported at 25 °C, in 0.1000 mol dm^{-3} $NaNO_3$.

The singly protonated $12aneN_3$ has more conformational freedom than both singly protonated $11aneN_3$ and $10aneN_3$ (Ribeiro-Claro *et al.*, 1996). This means that even though the conformational freedom is greatly reduced in THPTACD, THTD and THTUD because of the pendant arms, the decrease should roughly be the same and overall, THPTACD has the greatest conformational freedom. THPTACD, therefore, has a better entropy term (more positive) than both THTD and THTUD and hence better overall Gibbs free energy. The more negative the Gibbs free energy is, the more stable the compound. Gibbs free energy is defined as:

$$\Delta G = \Delta H - T\Delta S \qquad \textbf{(Equation 3.17)}$$

The conformational freedom in protonated species is in contrast to conformational freedom in metal complexes where the six-membered chelate rings have far much less degrees of conformational freedom than the five-membered chelate rings because of unwillingness of the six-membered chelate rings to adopt conformations other than the chair form (Martell and Hancock, 1996). The proton is very small such that it does not force the ligand to adopt chair conformations in all its stable conformations as shown by molecular mechanical studies (Ribeiro-Claro *et al.*, 1996).

The increase in second protonation constant with the ring size in both the parent macrocycles and their corresponding triazamacrocycles with hydroxypropyl pendant arms are non-monotonic which may reflect pH dependent conformational effects. In these cases, both electrostatic interactions as well as hydrogen bond formation play a profound role in determining the overall proton stabilisation.

Table 3.9: The protonation constants of DETA, UNTA and DOTRA

reaction		DETA	UNTA	DOTRA
$H_2L^{2+} + H^+ \rightleftharpoons H_3L^{3+}$	$\log K_3$	3.69	3.40	3.65
$HL^+ + H^+ \rightleftharpoons H_2L^{2+}$	$\log K_2$	6.12	7.20	7.55
$L + H^+ \rightleftharpoons HL^+$	$\log K_1$	13.50	13.90	12.80

Data from Geraldes *et al.*, (1991) and reported at 25 °C, in 0.1 mol dm^{-3} KNO_3.

The *N*-functionalisation on each nitrogen donor atom of the parent macrocycle with acetate groups sharply increases the first protonation constant (**Table 3.9**). In this series, protonation first occurs at one of the ring nitrogen donor atoms whose basicity is increased by the negative charge of the neighbouring ionised carboxylate group (Geraldes *et al.*, 1991). The first two protonation constants correspond to protonation of the ring nitrogen donor atoms and the third protonation occurs at the acetate group (Geraldes *et al.*, 1991).

The increase in second protonation with the increase in propylene bridges is monotonic reflecting the important role played by the strong hydrogen bonds in minimising the pH dependent conformational effects which are dominant in both the parent macrocycles and the macrocycles with hydroxypropyl pendant arms.

The values for log β_2 for THPTACD, THTUD and THTD are 17.28, 17.19 and 13.38 log units, respectively. The decrease in basicity is as follows:
THPTACD > THTUD > THTD

The trend in basicity can be explained in terms of increase in inductive effect and charge separation as ethylene bridges are progressively replaced by propylene bridges.

3.4 Conclusion

The protonation constants were successfully determined by potentiometric titration. The protonation constants of the three ligands cannot be attributed to one factor. The most pronounced factors include: the hydrogen bonds, availability of different pH dependent conformations, inductive and steric effects. The first protonation constant decreases with increasing steric hindrance in the following order: THPTACD > THBTACD > THMPTACD. The first protonation constants of all three ligands are less than the protonation constant of the parent macrocyclic ligand 12aneN_3. The decrease in basicity on addition of the hydroxyalkyl pendant arms is due to loss of hydrogen bonds involving the solvent molecules, the replacement of strong symmetrical hydrogen bonds and the increase in steric effects. The increase in steric effects overrides the gain in inductive effect for the first protonation because the proton has to find its way into the middle of the macrocyclic ring. The first protonation constant is mostly sterically driven. The second protonation constant, in general, increases with increase in inductive effects. The second proton does not enjoy the same hydrogen stabilisation as the first proton and is therefore mostly inductively driven.

Chapter 4

Determination of the stability constants of THMPTACD, THBTACD and THPTACD

4.1 Introduction

Macrocyclic polyamines are versatile ligands which form well-defined complexes with a wide range of metal ions. The selectivity and stability of metal complex formation is a sensitive function of a number of nitrogen binding sites, their relative disposition and the conformation of the macrocyclic ligand. For example, $12aneN_3$ forms three mutually-adjacent six-membered chelate rings on complexation with the central metal ion whereas $9aneN_3$ forms three mutually adjacent five-membered chelate rings. The addition of pendant arms, with or without donor atoms, can enhance the selectivity of the azamacrocycle for a metal cation or inorganic anion depending on the cavity size and the nature of the substituents (Skerlj *et al.,* 2002). The stability constant of a given ligand is an important parameter which gives a good measure of selectivity of a ligand for one metal over another.

The study of stability constants for the formation of metal ion complexes in aqueous solution is spurred on by the importance of such data to biochemistry, medicine, industry and the environment. For example, synthetic macrocyclic chelators are used on a large scale in plant nutrition to form soluble metal complexes whereby the nutrients are made bio-available to plants. Stability constant data are employed to determine the efficacy and efficiency of these artificial carriers (Martell and Motekaitis, 1988). Functionalised macrocycles have been successfully employed in the synthesis of metal-chelating agents for medical applications owing to the kinetic inertness of the complexes which make them resistant to decomplexation (Morphy *et al.,* 1998). For example, ^{153}Sm and ^{166}Ho complexes with tetraazamacrocycles linked to different biomolecules such as monoclonal antibodies or peptides, are considered excellent candidates for therapy and are under intensive investigation (Shin *et al.,* 2001; Ferro-Flores *et al.,* 2004; Fani *et al.,* 2002; Hu *et al.,* 2002; Li *et al.,* 2003). For therapeutic purposes in nuclear medicine, the radiotherapeutic agent should be stable *in vivo* in order to prevent its dissociation in blood and the formation of species resulting from binding to blood components (Marques *et al.,* 2004).

Structural factors such as the rigidity, the cavity size, the nature and number of donor atoms of the macrocyclic bi-functional chelators play a significant role in the chemical and biological behaviour of their complexes (Thöm *et al.,* 1984; Izatt *et al.,* 1995; Chang *et al.,* 2001). The stabilities of complexes formed by multidentate and macrocyclic ligands forming six coordinate first row d-block transition metal divalent cations generally follow the Irving-Williams sequence (Turonek *et al.,* 1995). The Irving-Williams series gives an idea about the affinity of a particular ligand with a metal ion and is given as follows (Irving and Williams, 1953):

$$Mn(II) < Fe(II) < Co(II) < Ni(II) < Cu(II) > Zn(II)$$

A distinct pattern in the behaviour of stability constants with regard to particular groups of donor atoms led to the classification of metal ions by Ahrland *et al.,* (1958) into a- and b-types. Pearson, (1963) reclassified Lewis acids (metal ions) and bases (ligands) into Hard and Soft Acids and Bases (HSAB) based on their preferential bonding. Hard acids prefer to bind to hard bases and soft acids prefer to bind to soft bases.

It is generally accepted that complexation of a metal ion by a multidentate ligand in aqueous solution occurs in several steps, as shown in **Equation 4.1** (all charges omitted for simplicity) (Eigen, 1961):

$$M(H_2O)_6 + L \xleftrightarrow{K_{os}} M(H_2O)_6.L \rightleftharpoons ML1(H_2O)_5 + H_2O \rightleftharpoons \cdots \rightleftharpoons ML_x(H_2O)_{6-x} + xH_2O \quad (\textbf{Equation 4.1})$$

The arrow (↔) is used to represent essentially instantaneous, kinetically unobservable equilibrium and the double arrow (⇌) is used for slow equilibrium in which the product formation can, at least theoretically, be followed experimentally. With the assumption of octahedral coordination, $ML_x(H_2O)_{6-x}$ represents the complex with the multidentate ligand occupying x sites while $(6 - x)$ coordinated water molecules are left in the octahedral complex.

The first step in such complexation formation involves the outer-sphere interaction of the aquated metal ion, $M(H_2O)_6$, with the ligand L, to form an outer-sphere complex, $M(H_2O)_6.L$. This reaction is fast and is quantitatively defined by the outer sphere stability constant, K_{OS} (McCann *et al.,* 2007).

The second step is a ligand exchange reaction where one coordinated water molecule is replaced by the first coordinating Lewis base site of the ligand. This step is rate-determining and is controlled by the water exchange rate of the hexaqua complex. The subsequent steps, which involve the replacement of more coordinated water molecules by additional ligand sites, are much faster and, consequently, they are usually not observable (Hegg *et al.,* 1999).

It is important to note that all steps in reaction **Equation 4.1** are reversible reactions. In the case of macrocyclic ligands, the stability constants of the resultant complexes are very high and therefore the complex formation at sufficiently high pH can be regarded as irreversible even though in most cases double equilibrium arrows are still used. Omitting the water molecules still coordinated to the complex (correctly, ML below should be written as $ML_x(H_2O)_{6-x}$), and due to the difficulty of detecting the secondary water-ligand exchange reactions, the observable reaction reduces to (charges and aquated water molecules are omitted for clarity):

$$M + L \rightleftharpoons ML \qquad \textbf{(Equation 4.2)}$$

$$K = \frac{[ML]}{[M][L]} \qquad \textbf{(Equation 4.3)}$$

In aqueous solution this system of reaction steps is tremendously complicated by the ligand solvation, the presence of protonation equilibria and different conformations of the ligands which may favour some reactions at the expense of others. The aquated metal ion can sometimes also undergo hydrolysis, and most ligands are weak Brønsted bases and thus will be involved in pH dependent protonation equilibria (Hegg *et al.,* 1999) before a metal complexation reaction takes place.

4.2 Materials and methods

4.2.1 Chemicals and Reagents

The ligands THPTACD, THBTACD and THMPTACD were synthesised according to the procedures described in **Chapter 2**, **Sections 2.6.1, 2.6.3, 2.6.4**. NaOH volucon (0.1000 mol dm^{-3}), HNO_3 volucon (0.1000 mol dm^{-3}), oxalic acid, $NaNO_3$, methyl orange and phenolphthalein indicators, $Pb(NO_3)_2$, $Co(NO_3)_2.6H_2O$, $Zn(NO_3)_2.6H_2O$ were purchased from Merck. $Cd(NO_3)_2.4H_2O$ was purchased from Fluka.

4.2.2 Instrumentation

A Thermo Orion 420+ pH meter and a 725 Dosimat automatic titrator equipped with 649 Metrohm magnetic stirrer were used for all titrations. The set up is shown in **Chapter 3**, **Section 3.2.2**.

4.2.3 Preparation of the solutions

A NaOH (0.1000 mol dm^{-3}) volucon was quantitatively transferred into a 1 L volumetric flask and made up to the mark using distilled water. This solution was standardised from the standard oxalic acid.

A HNO_3 (0.1000 mol dm^{-3}) volucon was quantitatively transferred into a 1 L volumetric flask and made up to the mark using distilled water, and standardised with standard NaOH.

THPTACD (0.1728 g, 0.5001 mmol) and $NaNO_3$ (0.8499 g, 0.01000 mol) were quantitatively transferred into a 100 mL volumetric flask and made up to the mark with deionised water.

The solutions of THBTACD (0.1942 g, 0.5010 mmol) and THMPTACD (0.1741 g, 0.5008 mmol) were prepared in the same manner.

$Pb(NO_3)_2$ (1.1029 g, 0.003330 mol) was quantitatively transferred into a 100 mL volumetric flask and made up to the mark using distilled water.

The same procedure was used to prepare the stock solutions of $Co(NO_3)_2.6H_2O$ (0.9692 g, 0.003330 mol), $Cd(NO_3)_2$.4H2O (1.0272 g, 0.003330 mol) and $Zn(NO_3)_2.6H_2O$ (0.9906 g, 0.003330 mol).

4.2.4 Cell calibration titration

A thermo Orion 420+ pH meter was calibrated by two buffer solutions at pH 4.01 and 10.01. The first part of the experiment involved the titration of NaOH against HNO_3 for determination of E° in which HNO_3 (20.00 mL, 0.1008 mol dm^{-3}) (the value of the volume written as given by the thermo titrator) was added to a jacketed glass vessel and allowed to equilibrate, after which, it was titrated with NaOH (0.09922 mol dm^{-3}) solution in increments of 1.000 mL using a Dosimat 725 automatic titrator under nitrogen atmosphere at 25.0 ± 0.1 °C. The solution was constantly stirred with a 649 Metrohm magnetic stirrer during the course of the titration and points were taken at each side of the end point and recorded in millivolts (mV). This procedure was repeated each day of titration or whenever the pH meter was switched on after a recess in the titration. The data was then analysed in an EXCEL spread sheet to determine the E° value.

4.2.5 Potentiometric titration of THPTACD with Zn(II), Cd(II), Co(II) and Pb(II) cations

HNO_3 (15.00 mL, 0.1008 mol dm^{-3}) was added to a jacketed glass vessel followed by Zn(II) (0.8850 mL, 0.03330 mol dm^{-3}) and THPTACD (7.000 mL, 0.005001 mol dm^{-3}). The solution was allowed to equilibriate at 25.0 ± 0.1 °C under a stream of nitrogen gas. The equilibrated solution was then titrated with NaOH (0.09922 mol dm^{-3}). The solution was constantly stirred with a 649 Metrohm magnetic stirrer during the course of the titration and the change in volume of the base was recorded against cell potential in mV. The same titration procedure was repeated with the following mixture: HNO_3 (15.00 mL, 0.1008 mol dm^{-3}), Zn(II) (0.7100 mL, 0.03330 mol dm^{-3}) and THPTACD (7.000 mL, 0.005001mol dm^{-3}).

The same procedure was repeated with Zn(II) metal solution replaced by: Cd(II) (0.8850 mL, 0.03330 mol dm^{-3}), Cd(II) (0.7100 mL, 0.03330 mol dm^{-3}); Co(II) (0.8850 mL, 0.03330 mol dm^{-3}), Co(II) (0.7100 mL, 0.03330 mol dm^{-3}); Pb(II) (0.8850 mL, 0.03330 mol dm^{-3}), Pb(II) (0.7100 mL, 0.03330 mol dm^{-3}).

4.2.6 Potentiometric titration of THBTACD with Co(II), Zn(II), Cd(II) and Pb(II) cations

HNO_3 (15.00 mL, 0.1008 mol dm^{-3}) was added to a jacketed glass vessel followed by Zn(II) (0.8850 mL, 0.03330 mol dm^{-3}) and THBTACD (7.000 mL, 0.005010 mol dm^{-3}). The solution was allowed to equilibriate at 25.0 ± 0.1 °C under a stream of nitrogen gas. The equilibrated solution was then titrated with NaOH (0.09922 mol dm^{-3}). The solution was constantly stirred with a 649 Metrohm magnetic stirrer during the course of the titration and the change in volume of the base was recorded against cell potential in mV. The same titration procedure was repeated with the following mixture: HNO_3 (15.00 mL, 0.1008 mol dm^{-3}), Zn(II) (0.7100 mL, 0.03330 mol dm^{-3}) and THBTACD (7.000 mL, 0.005010 mol dm^{-3}).

The same procedure was repeated with the following metal ion systems: Cd(II) (0.8850 mL, 0.03330 mol dm^{-3}), Cd(II) (0.7100 mL, 0.03330 mol dm^{-3}); Co(II) (0.8850 mL, 0.03330 mol dm^{-3}), Co(II) (0.7100 mL, 0.03330 mol dm^{-3}); Pb(II) (0.8850 mL, 0.03330 mol dm^{-3}), Pb(II) (0.7100 mL, 0.03330 mol dm^{-3}).

4.2.7 Potentiometric titration of THMPTACD with Zn(II), Cd(II), Co(II) and Pb(II) cations

HNO_3 (15.00 mL, 0.1008 mol dm^{-3}) was added to a jacketed glass vessel followed by Zn(II) (0.8850 mL, 0.03330 mol dm^{-3}) and THMPTACD (7.000 mL, 0.005008 mol dm^{-3}). The solution was allowed to equilibriate at 25.0 ± 0.1 °C under a stream of nitrogen gas. The equilibrated solution was then titrated with NaOH (0.09922 mol dm^{-3}). The solution was constantly stirred with a 649 Metrohm magnetic stirrer during the course of the titration and the change in volume of the base was recorded against cell potential in mV. The same titration procedure was repeated with the following mixture: HNO_3 (15.00 mL, 0.1008 mol dm^{-3}), Zn(II) (0.7100 mL, 0.03330 mol dm^{-3}) and THMPTACD (7.000 mL, 0.005008 mol dm^{-3}).

The following metal systems were also determined in the same manner: Cd(II) (0.8850 mL, 0.03330 mol dm^{-3}), Cd(II) (0.7100 mL, 0.03330 mol dm^{-3}); Co(II) (0.8850 mL, 0.03330 mol

dm^{-3}), Co(II) (0.7100 mL, 0.03330 mol dm^{-3}); Pb(II) (0.8850 mL, 0.03330 mol dm^{-3}), Pb(II) (0.7100 mL, 0.03330 mol dm^{-3}).

The stability constants of the metal complexes were obtained by manipulating the conductivity potential values using ESTA-WIN computer program (May *et al.*, 1988). This program calculates the overall stability constants, log β_i. In this case the stepwise stability constant, log *K*, is the same as the overall stability constant, log β, because all three ligands are hexadentate and only 1:1 complexes were formed.

4.3 Results and discussion

Potentiometric titration methods are relatively simple and reliable not only for the determination of protonation constants, but also for stability constants of metal complexes. In favourable cases, the speciation of mixtures of metal-ion-containing complexes in solution can be proposed on the basis of the results (Martell and Motekaitis, 1988). The stability constant of THPETACD and TMPTACD were not determined because of their insolubility and fast polymerisation in water, respectively. The complexes of THPTACD, THBTACD and THMPTACD with Cu(II) and Ni(II) were too inert to allow the determination of the formation constants in a reasonable amount of time using direct potentiometric titrations. Therefore only the complexes of Zn(II), Cd(II), Co(II) and Pb(II) were studied. Zompa, (1978) reported the stability constant of the Ni(II) metal ion with $12aneN_3$ and $9aneN_3$ using an out of cell method where the data were collected over a period of 4 months, but the solutions were monitored over a period of 1 year. This behaviour is in accord with the generally lower rate of substitution processes occurring at Ni(II) due to its high ligand field stabilisation (Davies *et al.*, 1996).

The stability constants determination of Pb(II), Cd(II), Zn(II) and Co(II) with THPTACD, THBTACD and THMPTACD were done by potentiometric titrations of the ligand aqueous solution at 25 °C in 0.1000 mol dm^{-3} $NaNO_3$ under constant flow of purified nitrogen gas. The nitrogen gas eliminates CO_2 gas from the reaction mixture. Formation of precipitates is indicated by a sudden discontinuity in pH readings, which can be detected before visual observation of the presence of the insoluble material. Such readings were not used in the equilibrium calculations.

The glass electrode was calibrated, at the start of each titration, in terms of the $[H^+]$ by titrating solutions of nitric acid and sodium hydroxide of known concentrations and correlating the mV readings with calculated values of $[H^+]$. The $[H^+]$-dependent junction potentials are negligible under the conditions of the experiment (Delgado and Frausto da Silva, 1982). The E° and k values were calculated in the same way as for the protonation constant (see **Equation 3.15**, **Chapter 3**).

4.3.1 The stability constant of THPTACD with Zn(II), Cd(II), Co(II) and Pb(II)

The stability constants, standard deviations and R-factors of the reaction between THPTACD and Zn(II), Cd(II), Co(II) and Pb(II) are given in **Table 4.1**.

Table 4.1: The stability constants of THPTACD with Zn(II), Cd(II), Co(II) and Pb(II) at 25 °C in 0.1000 mol dm^{-3} $NaNO_3$

Metal ion	log *K*	Standard deviation	R-factor
Zn(II)	21.22	±0.12	0.08
Cd(II)	14.03	±0.14	0.05
Co(II)	15.45	±0.17	0.09
Pb(II)	16.11	±0.03	0.03

4.3.1.1 Complexation with Zn(II)

Zn(II) is regarded as a borderline acid in the SHAB classification and is expected to form strong metal complexes with borderline donor atoms such as N. The stability constant of Zn(II) with THPTACD is 21.22 log units whereas the stability constant for the parent macrocyclic ligand, 12aneN_3, is 8.75 log units (Zompa, 1978). The significant increase of 12.47 log units in stability can be ascribed to the influence of the pendant arms that are tethered on the nitrogen donor atoms of the parent macrocycle carrying oxygen donor atoms.

Zn(II), with ionic radius of 0.74 Å (Shannon, 1976), is regarded as a small metal ion but evidence from crystal and molecular structure determination shows that it does not fit into the cavity of the parent macrocyclic ligand, 12aneN_3 (Schaber *et al.*, 1988; Notni *et al.*, 2006).

The metal ion sits above the plane defined by the nitrogen donor atoms. In such examples, factors that determine the stability of the resultant metal complexes are different from those that dictate the stability of such complexes when the given ion fits exactly into the hole of the macrocyclic ligand, i.e., hole-size match selectivity. The stability of the metal complexes is no longer defined by the cavity size, and the subsequent hole-size match, but by the optimal bond distances and angles between the central metal ion and both sets of the donor atoms of the macrocycle. Strong interaction occurs between the central metal ion and the nitrogen donor atoms when they meet at an optimal angle with an appropriate bond length. This means that the bonding orbitals of both the metal ion and the ligand have to adjust so that they meet at an optimal angle that may effect distortion of the resultant bond angles. Unlike $9aneN_3$, which is able to form sandwich complexes with small metal ions, two $12aneN_3$ units cannot sandwich Zn(II) because of strong electrostatic repulsion (Zompa and Margulis, 1978) and there is no report or evidence of such bonding without the use of bridged atoms. It can be concluded that the rather small stability of Zn(II) complexes with $12aneN_3$ is, in part a result of poor interactions between the nitrogen donor atoms of the ligand with the central metal ion.

Similarly, Zn(II) does not fit into the cavity of THPTACD as shown by crystal structure determination (see later **Fig. 5.2** of **Section 5.3.1**, **Chapter 5**). However, unlike in the case of $12aneN_3$, the pendant arms of THPTACD envelops the metal ion giving a cage like structure with nitrogen donor atoms in one plane below the central metal ion and oxygen donor atoms above the plane of the central metal ion. The nitrogen donor atoms of the parent macrocyclic ring form six-membered chelate rings, with the central metal ion, which favour small metal ions over big metal ions. The oxygen donor atoms of the pendant arms and the corresponding nitrogen donor atoms on which the pendant arms are appended form five-membered chelate rings, which favour big metal ions over small metal ions (Martell and Hancock, 1996). Six-membered chelate rings are able, with very small metal ions, to have all their hydrogen atoms in the energetically more favourable staggered position (Hancock, 1986). The five-membered chelate rings have more conformational freedom than six-membered chelate rings because of the unwillingness of the six-membered chelate rings to adopt conformations other than the chair-form. This is different from the protonation situation where the six-membered chelate rings do not adopt a chair conformation owing to the small size of the proton. The conformation freedom is then defined in terms of the ability of the ligand to diffuse the

electrostatic repulsions by twisting its bonds. Ribeiro-Claro *et al.,* (1996) reported that 12aneN$_3$, which forms six-membered chelate rings on protonation, has more conformational freedom than 9aneN$_3$, which forms five-membered chelate rings. Since nitrogen donor atoms are more basic than oxygen donor atoms, and form the basis of the macrocyclic ring, they make the greatest contribution towards the stability of the resultant metal complex (Cortes *et al.,* 1990). Pendant arms have also far more degrees of freedom than the parent macrocycle which means that the donor atoms on the pendant arms need to move far more to have the desired conformation to allow complexation with the metal ion than the donor atoms on the parent ring. This, however, does not affect the overall stability of the complexes because, in most instances, the donor atoms on the pendant arms are pre-organised for coordination (Martell and Hancock, 1996).

The parent macrocycle, 12aneN$_3$, has three secondary nitrogen donor atoms whereas THPTACD has three tertiary amines. Generally, tertiary amines are less solvated compared to secondary amines due to lack of N-H···O hydrogen bonds in the latter case and as such the nitrogen donor atoms of THPTACD are less solvated than those of 12aneN$_3$. It is actually the hydrogen bonds with the protonation form (enthalpy effect) which make secondary amines more basic than tertiary amines in aqueous solvents whereas in gaseous phase the positive inductive effect plays a more significant role and the basicity is reversed (Meyerstein, 1999; Hancock and Martell, 1989). The pendant arms in THPTACD also constrict the macrocyclic hole thereby reducing the number of solvent coordination spheres the hole can hold hence less solvent molecules are accommodated than in 12aneN$_3$. The oxygen donor atoms are generally less solvated than nitrogen donor atoms (Hancock and Thöm, 1982). The above two effects together with the actual steric hindrance provided by the pendant arms result in THPTACD accommodating much less solvent molecules in its macrocyclic hole and therefore much less energy is needed to desolvate the cavity for complexation as compared to 12aneN$_3$. This means that 12aneN$_3$ has a more favourable entropy term than THPTACD because more solvent molecules are released upon desolvation of 12aneN$_3$ than THPTACD. On the other hand, THPTACD has a more negative enthalpy term because less energy is used to desolvate the cavity of the macrocycle. In both instances the entropy term is positive but it is more positive for 12aneN$_3$ than for THPTACD. This means that the overall Gibbs free energy is much more negative for THPTACD than it is for 12aneN$_3$ because of the decisive enthalpy term.

In most macrocyclic ligands, heat of desolvation plays a fundamental role in determining the overall stability of the resultant metal complex (Hinz and Margerum, 1974) which is different from protonation equilibria where the solvent interaction with the protonated form of the ligand is equally more important. In addition to having a favourable heat of solvation, THPTACD has six donor atoms and hence it is a hexadentate ligand whereas 12aneN$_3$ is a tridentate ligand; and the general rule of denticity states that the greater the denticity the more stable the resultant metal complex (Song *et al.*, 1994). The central metal ion is further stabilised by a network of hydrogen bonds involving the hydrogens of the hydroxypropyl group of the pendant arms and the donor atoms of the solvent molecules thereby increasing the overall enthalpy of formation of the complexes.

The stability constant of Zn(II) complex with THETAC is 12.07 log units (Sayer *et al.*, 1983) whereas the stability constant of the parent macrocyclic ligand, 9aneN$_3$, is 11.62 log units (Zompa, 1975). In this case, there is a small increase of 0.45 log units in stability on addition of hydroxyethyl pendant arms to 9aneN$_3$. This is in contrast to the large increase in stability constant on addition of hydroxypropyl pendant arms to 12aneN$_3$. THETAC, unlike THPTACD which has hydroxypropyl pendant arms and six-membered chelate rings, has hydroxyethyl pendant arms and three five-membered rings (**Chart 3.1** of **Section 3.3**, **Chapter 3**). Hydroxyethyl groups are less bulky and therefore expected to impose a diminished steric hindrance on solvation. This means that neutral THETAC is more solvated than its analogues with hydroxypropyl pendant arms. More energy is, therefore, needed to remove the solvent molecules in THETAC than in corresponding macrocycles with hydroxypropyl pendant arms. Simultaneously THETAC has a more favourable entropy term in the first step of the reaction. However, the enthalpy term is smaller compared to its analogues with hydroxypropyl pendant arms. Unlike THPTACD which has six-membered chelate rings, THETAC has three five-membered chelate rings which are known to favour large metal ions and therefore it is not surprising that THPTACD forms more stable Zn(II) complexes than THETAC.

4.3.1.2 Complexation with Cd(II)

Cd(II) is regarded as a soft acid in the SHAB classification and is expected to form strong metal complexes with soft donor atoms such as sulphur (Martell and Hancock, 1996). The

stability constant of Cd(II) with THPTACD is 14.03 log units compared to a value of 7.01 for the parent macrocycle, 12aneN$_3$ (Zompa, 1975) - a significant increase of 7.02 log units on addition of hydroxypropyl pendant arms to 12aneN$_3$. This means that THPTACD forms very stable complexes with Cd(II) because of the influence of the pendant arms. It is unusual that there is such a huge jump in stability constant on addition of pendant arms because oxygen donor atoms are regarded as hard in the SHAB classification, unlike Cd(II) which is regarded as a soft acid. Cd(II) is a medium to large metal ion with a radius of about 0.95 Å (Shannon, 1976) and is expected to form stable complexes with ligands having five-membered chelate rings.

The crystal structures of Cd(II) with both THPTACD and 12aneN$_3$ clearly show that the metal ion sits above the plane of the nitrogen donor atoms (compare later **Fig. 5.18** and **5.35** of **Section 5.3.6** and **5.3.9**, **Chapter 5**). The factors that determine the stability of the resultant metal complexes are based on how well the central metal ion interacts with the donor atoms of the ligand. Optimal interactions between the orbitals of the donor atoms and the central metal ion results in strong bonds and the resulting complexes are more stable than they would be if no such interactions are possible. The interactions are optimal if the Cd(II) metal ion and the nitrogen donor atoms meet at an optimal angle with appropriate bond length.

The Cd(II)-N bond lengths of the 12aneN$_3$ and THPTACD complexes are around 2.3 Å (compare later **Table 5.12**, **5.14** and **5.19** of **Section 5.3.6** and **5.3.9**, **Chapter 5**). This means that THPTACD does not suffer much strain as a result of having hydroxypropyl pendant arms tethered on nitrogen donor atoms relative to 12aneN$_3$. However, unlike the situation in 12aneN$_3$, the oxygen donor atoms of the pendant arms together with the nitrogen donor atoms of the parent macrocyclic ring in THPTACD envelop the central metal ion such that the resulting metal ion complex is much stronger by being held in a cage like structure. The central metal ion is further stabilised by a network of hydrogen bonds involving the hydrogens of the hydroxypropyl group of the pendant arms and the donor atoms of the solvent molecules thereby increasing the overall enthalpy of formation of the complex. In 12aneN$_3$ on the other hand, the available coordination sites are occupied by either unidentate solvent molecules or counter ions (see later **Fig. 5.33** of **Section 5.3.9**, **Chapter 5**) such that Cd(II) complex in 12aneN$_3$ does not benefit much from the chelate effect.

The nitrogen donor atoms of the parent macrocyclic ring form six-membered chelate rings with the central metal ion, which favour small metal ions over large metal ions. On the other hand, the oxygen donor atoms of the pendant arms and the corresponding nitrogen donor atoms of the parent macrocyclic ring on which they are appended form five-membered chelate rings which favour big metal ions over small metal ions. This means that THPTACD has both five- and six-membered chelate rings. McDougall *et al.,* (1978) reported that alternating five- and six-membered chelate rings in some cases lead to strain release relative to systems containing five- or six-membered chelate rings only.

Just like in the case of Zn(II), the parent macrocyclic ring, 12aneN_3, is heavily solvated as compared to THPTACD and the heat of desolvation is much more for 12aneN_3 than it is for THPTACD. 12aneN_3 has, therefore, a more positive entropy term than THPTACD which exhibits more favourable enthalpy term in turn. As discussed in detail for Zn(II) in **Section 4.3.1.1**, the Gibbs free energy for THPTACD complexation with Cd(II) metal ion turns out to be more negative than for 12aneN_3 metal complexation.

The stability constant of Cd(II) with THETAC is 10.60 log units (Luckay *et al.,* 1996) whereas the stability constant of the parent macrocyclic ligand, 9aneN_3, is 9.33 log units (Zompa, 1978) . In this case, there is a small increase of 1.27 log units in stability on addition of hydroxyethyl pendant arms to 9aneN_3. This increase is small but still larger than the increase in stability constant for Zn(II) probably because of the fact that THETAC has only five-membered chelate rings, which favour large metal ions over small metal ions. The increase in stability constant for THETAC is smaller than for THPTACD compared to their parent macrocycles. This is probably due to smaller heat of desolvation in the case of THPTACD and better stabilisation of the metal positive charge since hydroxypropyl pendant arms are better electron donors than hydroxyethyl arms. THETAC is very small compared to 12aneN_3, which is known to favour large metal ions because of higher conformational freedom, such that the six five-membered chelate rings in THETAC may lead to higher ring strain. THPTACD on the other hand form three six-membered chelate rings involving the nitrogen donor atoms of the parent macrocyclic ring and three five-membered chelate rings involving oxygen donor atoms of the pendant arms and the corresponding nitrogen donor atoms on which they are appended, which may relieve some of the steric strain.

4.3.1.3 Complexation with Co(II)

Co(II) is regarded as a borderline acid in the HSAB classification. Unlike Cd(II) and Zn(II) which are d^{10} metal ions, Co(II) is a d^7 metal ion. The geometry of the metal complexes plays a more crucial role in determining the stability of the resultant metal complexes in Co(II) than in Zn(II) or Cd(II). Even within a specific geometry, Co(II) can exist as either a high spin metal ion, where electrons prefers to occupy individual orbitals of higher energy than pairing with another electron in lower energy orbitals, or a low spin metal ion where electrons prefer pairing in low energy orbitals. For example, in weak field ligands with octahedral geometry, less energy is needed to excite electrons to high energy orbitals (the e_g) as opposed to pairing in the low lying t_{2g} orbitals and as such Co(II) has an electron configuration of $t^5_{2g}e^2_g$. In this configuration Co(II) has three unpaired electrons thereby forming high spin complexes with a CFSE (crystal field stabilisation energy) of 0.8 Δ_o. On the other hand, in strong field ligands with octahedral geometry, less energy is needed to pair electrons in low energy orbitals (the t_{2g}) as opposed to exciting the electrons to the high energy orbitals (the e_g) giving Co(II) an electron configuration of $t^6_{2g}e^1_g$. In this configuration Co(II) metal ion has one unpaired electron thereby forming low spin complexes with CFSE of 1.8 Δ_o. Generally, the factors that determine the stability of Co(II) metal complexes are much more complicated than those that determine Cd(II) and Zn(II) metal complexes.

The stability constant of Co(II) with THPTACD is 15.45 log units. Co(II) is the smallest metal ion of the four metal ions studied in this research with ionic radius of 0.65 Å (Shannon, 1976). The pendant arms constrict the macrocyclic hole of 12aneN_3 parent macrocycle and therefore Co(II) should experience less steric strain than the other metal ions. However, the results showed that THPTACD forms more stable metal complexes with Zn(II) and even relatively stable Pb(II) complexes than with Co(II). The molecular structure of Co(II) with THPTACD (**Fig. 5.10** of **Section 5.3.2**, **Chapter 5**), shows that the metal ion, though small, does not fit into the cavity of the macrocyclic ligand and sits above the plane defined by the nitrogen donor atoms. This means that Co(II) must tolerate the deformations in its orbitals for effective overlap with the orbitals of nitrogen donor atoms compared to a situation when the Co(II) and the donor atoms are in the same plane.

There is no data available for the stability constant of Co(II) with the parent macrocyclic ligand, 12aneN_3, which makes it difficult to compare the effect of the addition of pendant arms to 12aneN_3. However, Co(II) should probably form more stable complexes with THPTACD than with 12aneN_3. THPTACD is a hexadentate ligand whereas 12aneN_3 is a tridentate ligand. The pendant arms envelop the metal ion from the opposite side of the plane defined by the nitrogen donor atoms thereby giving rise to a cage structure with the metal ion occupying nearly the central position defined by both nitrogen and oxygen donor atoms. The stability constant value suggests that the two sets of chelate rings are not complimenting one another as effectively as they do in the Zn(II) complex.

4.3.1.4 Complexation with Pb(II)

Pb(II) is regarded as a borderline Lewis acid metal in the HSAB classification and is expected to form strong metal complexes with borderline donor atoms. Pb(II) is the biggest metal ion of the four metal ions studied in this investigation with ionic radius of 1.19 Å (Shannon, 1976). The Pb(II) metal complexes with THPTACD should be the least stable of the four metal complexes studied if the six-membered chelate rings formed by the nitrogen donor atoms of the parent macrocycle play a major role in determining the stability of the metal complexes. If, on the other hand, the five-membered chelate rings, formed by the oxygen donor atoms of the pendant arms and the corresponding nitrogen donor atoms on which the arms are attached, play a major role in determining the stability of the resulting metal complexes, then the Pb(II) complex should have reasonable stability. However, Pb(II) should form relatively stable metal complexes compared to Cd(II) independent of which effect is dominant since hard-soft consideration should benefit Pb(II) (borderline) compared to Cd(II) (soft).

The stability constant of Pb(II) with THPTACD is 16.11 log units. There is no data available for the stability constant of Pb(II) with the parent macrocyclic ligand, 12aneN_3. Pb(II), as the biggest metal ion of the four used in this study, would certainly not fit into the macrocyclic cavity of either 12aneN_3 or THPTACD and therefore it should sit above the plane defined by the nitrogen donor atoms of the parent macrocycle.

THPTACD is a hexadentate ligand with three nitrogen and three oxygen donor atoms whereas 12aneN_3 is a tridentate ligand with three nitrogen donor atoms only. In THPTACD,

the oxygen donor atoms of the pendant arms are expected to envelop the Pb(II) metal ion from the opposite side of the plane defined by the nitrogen donor atoms to give rise of a cage structure with the metal ion occupying the central position.

The stability constant of Pb(II) with THETAC is 11.98 log units (Luckay *et al.*, 1996) whereas the stability constant of its parent macrocyclic ligand, $9aneN_3$, is 11.10 log units (Zompa, 1978). In this case, there is a small increase of 0.88 log units in stability on addition of hydroxyethyl pendant arms to $9aneN_3$. This is unexpected considering the fact that THETAC forms six five-membered chelate rings (three between nitrogen donor atoms of $9aneN_3$ and the other three from the oxygen donor atoms of the pendant arms and the nitrogen donor atom on which they are attached). The increase in stability constant for Cd(II) and Zn(II) with THETAC is 1.27 and 0.45 log units, respectively. The increase in stability constant for Pb(II) with THETAC is larger than that of Zn(II) but smaller than the Cd(II) which means that other factors other than chelate ring size play a major role in determining the stability of THETAC with Pb(II) metal ion.

4.3.1.5 The use of molecular structures determined by X-ray diffraction in explaining the trends in stability constant for the formation of THPTACD metal complexes

The order of increasing stability of THPTACD with the four metal ions is as follows:

Cd(II) < Co(II) < Pb(II) < Zn(II)

The stability constants show that the hardness and softness of the Lewis acid metal ion is certainly playing a part in determining the overall stability of the metal complexes. This is why Cd(II) forms the least stable complexes with THPTACD which has hard and borderline donor atoms. Co(II) with ionic radius of 0.65 Å is the smallest metal ion followed by Zn(II) with ionic radius of 0.74 Å and should, therefore, form the most stable metal complexes with THPTACD based on ion-size match selectivity. However, the bond lengths and angles of the Co(II) and Zn(II) molecular structures with THPTACD presented in **Table 4.2** (taken from Chapter 5) show that Zn(II) is actually acting like a small metal ion compared to Co(II). The

other way to look at this scenario is that Co(II), as a small metal ion, is drawn away from the parent macrocyclic ring towards the oxygen donor atoms of the pendant arms because of steric crowding. Such interpretation, though plausible, would however contradict the crystal structure results reported by Feng *et al.,* (2007) and presented in **Table 4.4**. As will be shown later, the trend in M(II)-N bond lengths from Mn(II) to Cd(II) shows that the interaction of the central metal ion with the nitrogen donor atoms of the ligands peaks at Zn(II). The M(II)-N bond lengths are 2.266, 2.178, 2.161 and 2.325 Å for Mn(II), Co(II), Zn(II) and Cd(II), respectively. The lengthening in Co(II)-N bond lengths relative to Zn(II)-N bond lengths is not simply the difference in two M(II)-N separations between the two metal complexes because of the differences in ionic radius of the two metal ions. This means that the lengthening of Co(II)-N bond length relative to Zn(II)-N bond distance is greater than 0.017 Å. The M(II)-O bond lengths are 2.131 and 2.168 Å for Co(II) and Zn(II), respectively, which simply shows that the Zn(II) metal ion is closer to the parent macrocyclic ring forming six-membered chelate rings whereas Co(II) is closer to the pendant arms forming five-membered chelate rings. These results suggest that the pendant arms of the THPTACD are able to open up for the Zn(II) metal ion allowing better interaction between the metal ion and the nitrogen donor atoms of the parent macrocyclic ring. Such interactions should lead to strong σ-donation and hence a favourable enthalpy term. Thöm *et al.,* (1985) used molecular mechanics to show that the optimal bond length for Zn(II)-N is 2.1 Å, which is not significantly different from the Zn(II)-N bond length reported here. Various reports exist where the structural features of the metal complexes in crystalline state are used to interpret the structural features in aqueous solution (Haidar *et al.,* 1997; Kimura *et al.,* 1990a; Turonek *et al.,* 1995; De Sousa *et al.,* 1997; Hegg *et al.,* 1999). Hegg *et al.,* (1999) reported that the bond lengths in crystal structures should not vary significantly with the values in solution as the ligand occupies exactly the same volume.

The high stability of the Pb(II) complex over that of Co(II) can be explained in two ways:
(1) Small metal ions involve more covalent interactions and have stricter stereochemical demands for specific geometries. The adjustment of the pre-organised ligand to the small metal ion is, therefore, too difficult and usually results in a larger bond distance than expected. One would expect such distortions to be taken up by bond angle deformation but in Co(II) complexes the increase in bond lengths are not fully compensated by the bond angles of the six-membered chelate rings which are all less than bond angles in Zn(II) complexes. However, the bond angles in Co(II) complexes are larger than bond angles in Cd(II)

complexes as shown in **Table 4.2**. On the other hand, the larger metal ion, Pb(II), has less stereochemical requirements for specific coordination geometries than is the case with the transition metal ions and therefore allows more favourable adjustment of the ligand to the metal ion (Delgado *et al.,* 1993). This assertion holds as larger metal ions are more polarisable than smaller metal ions. The polarisability of Pb(II) complexes leads to more favourable heats of reaction for the complex formation at the expense, though, of configurational entropy changes (Delgado *et al.,* 1989).

(2) Pb(II) lone pair electrons can either be stereochemically active or inactive which greatly affect its electronic environment (Hancock *et al.,* 1988). When the ratio of N:O donor atoms increases, in favour of N donor atoms, the stereochemically inactive lone pair of electrons changes to stereochemically active. Below the transition point, the Pb(II) ion behaves as a large metal ion with rather ionic-like metal-ligand bonds (Hancock *et al.,* 1988). On the other hand, when the lone pair of electrons is stereochemically active, Pb(II) behaves as a smaller, more covalent ion. The lone pair of electrons is regarded as stereochemically inactive when it resides in the spherically symmetric 6s orbital and stereochemically active when it resides in hybrid sp^n or sp^nd^m orbitals in accordance with the Gillespie-Nyholm or Sidgwick-Powell valence shell electron-pair repulsion (VSEPR) model (Gillespie and Nyholm, 1957; Sidgwick and Powell, 1940).

When the lone pair is stereochemically active, it is localised in the gap between the coordination spheres. This leads to the shortening of the Pb(II)-N bonds opposite the lone pair of electrons (Wieghardt *et al.,* 1986). When the lone pair is stereochemically inactive there is no gap in the coordination sphere and the Pb(II)-N bonds are long. The extent of localisation of this lone pair has a marked effect on the complex stability and the selectivity behaviour of the Pb(II) ion (Hancock *et al.,* 1988). The importance of such a change in size, based on the stereochemistry of the lone pair of electrons, is that it changes the response of the Pb(II) metal ion in terms of the rules for selectivity of ligands for metal ions based on metal ion size. If the Pb(II) lone pair remains inactive then the metal ion behaves as a large metal ion with ionic radius of about 1.19 Å. However, once the lone pair of electrons changes from stereochemically inactive to active, the metal ion responds more like a metal ion with ionic radius of about 0.75 Å (Hancock and Martell, 1989). Zn(II) has an ionic radius of 0.74 Å which means that the Pb(II) ion with stereochemically active lone pair of electrons will behave like Zn(II) when complexed to ligands. Thus the high complex stability for Pb(II)

metal complexes over that of Co(II) can be attributed to a Pb(II) metal ion having a stereochemically active lone pair of electrons hence chemically behaving like a Zn(II) metal ion.

We are still attempting to crystallise a Pb(II) metal complex with THPTACD to determine which one of the two factors discussed above plays the more important role in determining the stability of the Pb(II) metal complexes. Such a result can be achieved by comparing the bond lengths of the Pb(II)-N bonds on the basis of guidelines put forward by Hancock and Martell, (1989).

Table 4.2: The bond lengths and angles for $[Mn(C_{18}H_{39}N_3O_3)]^{2+}$, $[Co(C_{18}H_{39}N_3O_3)]^{2+}$, $[Zn(C_{18}H_{39}N_3O_3)]^{2+}$ and $[Cd_2(C_{18}H_{39}N_3O_3)_2]^{4+}$ molecular structures

	M(II)-N	SMCRA-N,N	FMCRA-N,O	M(II)-O
Mn(II)	2.226	96.8	75.7	2.193
Co(II)	2.178	98.7	77.4	2.131
Zn(II)	2.161	100.1	77.3	2.168
Cd(II)	2.325	96.7	74.4	2.309

Where M(II)-N and M(II)-O are bond lengths in Å. SMCRA-N,N are bond angles (°) in six-membered chelate rings involving nitrogen donor atoms. FMCRA-N,O are bond angles (°) in five-membered chelate rings involving nitrogen and oxygen donor atoms.

4.3.2 The stability constant of THBTACD with Cd(II), Zn(II), Co(II) and Pb(II)

The stability constants, standard deviations and R-factors of THBTACD with Cd(II), Zn(II), Co(II) and Pb(II) are summarised in **Table 4.3**.

4.3.2.1 Complexation with Cd(II)

The stability constant of Cd(II) with THBTACD is 13.55 log units compared to a constant for the parent macrocyclic ligand, 12aneN_3, of 7.01 log units. There is an increase of 6.54 log units in stability on addition of hydroxybutyl pendant arms to 12aneN_3. THBTACD, like THPTACD, has three nitrogen donor atoms on the parent macrocyclic ring and three oxygen donor atoms on the pendant arms affording a hexadentate ligand. The six donor atoms are expected to fold around the Cd(II) metal ion thereby forming a caged metal complex structure

with the Cd(II) metal ion sitting in between the oxygen and the nitrogen donor atom sets. De Vos and Bein, (1996) reported the Mn(II) crystal structure of 1,4,7-*tris*(2-hydroxybutyl)-l,4,7-triazacyclononane, which has the same pendant arms as THBTACD but appended on $9aneN_3$, in which the metal centre is six coordinate. THBTACD should have the same advantages as THPTACD over the parent macrocyclic ligand, $12aneN_3$, as outlined in **Section 4.3.1.2**.

Table 4.3: The stability constant of THBTACD with Co(II), Zn(II), Cd(II) and Pb(II) at 25 °C, in 0.1000 mol dm^{-3} $NaNO_3$

Metal cation	log *K*	Standard deviation	R-factor
Cd(II)	13.55	±0.11	0.07
Zn(II)	20.02	±0.09	0.04
Co(II)	13.93	±0.12	0.05
Pb(II)	15.01	±0.03	0.03

The stability constant of Cd(II) with THETAC is 10.60 log units (Luckay *et al.*, 1996) whereas the stability constant of the parent macrocyclic ligand, $9aneN_3$, is 9.33 log units (Zompa *et al.*, 1995). In this case, there is a small increase of 1.27 log units in stability on addition of hydroxyethyl pendant arms to $9aneN_3$. This is in contrast with the large increase in stability constant on addition of hydroxybutyl pendant arms to $12aneN_3$. It is important to note that unlike THBTACD which has hydroxybutyl pendant arms THETAC has hydroxyethyl pendant arms which are less bulky groups and therefore expected to impose a diminished steric hindrance to solvation. This means that the parent macrocyclic ring in THETAC is more solvated than its analogue with hydroxybutyl pendant arms and therefore more energy is needed to desolvate THETAC than THBTACD. THETAC should have more favourable entropy term than THBTACD. However, THBTACD should benefit more from the enthalpy effect than THETAC because less energy is used for desolvation. The difference in stability between THETAC and THBTACD metal complexes is 2.95 log units.

4.3.2.2 Complexation with Zn(II)

The stability constant of Zn(II) with THBTACD is 20.02 log units whereas the stability constant of the parent macrocyclic ligand, $12aneN_3$, is 8.75 log units (Zompa, 1978). There is

an increase of 11.27 log units in stability on addition of hydroxybutyl pendant arms to 12aneN$_3$. The six donor atoms are expected to fold around the Zn(II) metal ion thereby forming a caged metal complex with the Zn(II) metal ion sitting in between the oxygen and nitrogen donor atom sets. THBTACD has the same advantage over its parent macrocyclic ligand that THPTACD has over 12aneN$_3$. This result in THBTACD forming more stable metal complexes with Zn(II) than with the parent macrocycle, 12aneN$_3$.

The stability constant of Zn(II) with THETAC is 12.07 log units (Sayer *et al.*, 1983) whereas the stability constant of the parent macrocyclic ligand, 9aneN$_3$, is 11.62 log units (Zompa, 1978). In this case, there is a small increase of 0.45 log units in stability on addition of the hydroxyethyl pendant arms to 9aneN$_3$. Two important points have to be noted here:

(1) Zn(II) is a small metal ion compared to Cd(II) and if the theory about chelate ring sizes holds in its simple terms then both 9aneN$_3$ and THETAC should form more stable complexes with Cd(II) than Zn(II). This should be the situation because both the nitrogen donor atoms of the parent macrocyclic ring and the ring formed by the oxygen donor atoms of the pendant arms with the nitrogen donor atoms of the parent macrocyclic ring on which they are appended, form five-membered chelate rings which are known to favour large metal ions over the small metal ions. The stability constants of both Zn(II) and Cd(II) with THETAC and 9aneN$_3$ suggest that this is not a dominant factor hence both THETAC and 9aneN$_3$ form relatively stable complexes with Zn(II) than Cd(II) (Luckay *et al.*, 1996).

(2) A bigger jump in stability of the Cd(II) metal complexes ($\Delta\log K$ = 1.27) occurs on addition of hydroxyethyl pendant arms to 9aneN$_3$ than for the Zn(II) metal complexes. The difference in stability, $\Delta\log K$, for Zn(II) between THETAC and 9aneN$_3$ is 0.45 log units. This just shows that steric strain is not playing a big role in determining the overall stability constant between these two metal ions otherwise Cd(II), being the larger metal of the two, should have exhibited the smallest increase in stability constant on addition of pendant arms. Cd(II) may have benefited more from the addition of pendant arms because it is a large metal ion and hence much able to adjust its electronic environment to suite the demands brought about by the arms much better than Zn(II). In the case of THPTACD, Zn(II) has the highest jump and crystal structures showed that Zn(II) is able to force its way closer to the parent macrocyclic ring compared to both Co(II) and Cd(II), which may be the case with

THBTACD as well. However, the situation may be more complicated than the simplified explanation given here.

4.3.2.3 Complexation with Co(II)

The stability constant of Co(II) with THBTACD is 13.93 log units. There is no data available for the stability constant of Co(II) with the parent macrocyclic ligand which makes it difficult to compare the effect of the addition of pendant arms to 12aneN_3. However, Co(II) should form more stable complexes with THBTACD than with 12aneN_3 because THBTACD is a hexadentate ligand whereas 12aneN_3 is a tridentate ligand.

There is also no data available for the stability constant of THETAC with Co(II) metal ion and no conclusion can be made based on the results of stability constant of THETAC with Pb(II), Cd(II) and Zn(II). However, based on crystallographic data for the Co(II) and Zn(II) metal complexes with 1,4,7-*tris*[(2*S*)-2-hydroxypropyl]-1,4,7-triazacyclononane (THPTACN) (see **Chart 3.1** of **Section 3.3**, **Chapter 3**) for molecular structure) reported by Feng *et al.*, (2007), Co(II) complexes should be more stable than Zn(II) complexes of THPTACN as shown in **Table 4.4**. The Co(II)-N bond lengths, in this case, shows that Co(II) is closer to the parent macrocyclic ring than Zn(II). These results are in contrast with the crystal data we reported for THPTACD as presented in **Table 4.2**. Unlike in THPTACD, there is no reversal in the way the metal ions are behaving based on size in the case of THPTACN.

Table 4.4: The bond lengths and angles for $[Co(THPTACN)]^{2+}$ and $[Zn(THPTACN)]^{2+}$ crystal structures

Metal cation	M(II)-N	FMCRA-N,N	FMCRA-N,O	M(II)-O
Co(II)	2.117	83.4	79.8	2.087
Zn(II)	2.143	82.5	80.2	2.109

Data from Feng *et al.*, (2007). M(II)-N and M(II)-O are bond lengths in Å. FMCRA-N,N and FMCRA-N,O are bond angles (°) in five-membered chelate rings with nitrogen and mixed nitrogen and oxygen donor atoms, respectively.

4.3.2.4 Complexation with Pb(II)

The stability constant of Pb(II) with THBTACD is 15.01 log units. There is no data available for the stability constant of Pb(II) with the parent macrocyclic ligand, 12aneN_3, but one would expect Pb(II) to form more stable complexes with a hexadentate ligand, THBTACD, than a tridentate ligand, 12aneN_3. The five-membered chelate rings favour large metal ions which mean that the Pb(II) complexes with THBTACD have extra stability from the five-membered chelate rings.

The stability constant of Pb(II) with THETAC is 11.98 log units (Luckay *et al.*, 1996) whereas the stability constant of its parent macrocyclic ligand, 9aneN_3, is 11.10 log units (Zompa, 1978). In this case, there is a small increase of 0.88 log units in stability on addition of hydroxyethyl pendant arms to 9aneN_3.

4.3.3 The stability constant of THMPTACD with Cd(II), Zn(II), Co(II) and Pb(II)

The stability constants, standard deviations and R-factors of THMPTACD with Zn(II), Cd(II), Co(II) and Pb(II) are given in **Table 4.5**.

4.3.3.1 Complexation with Cd(II)

The stability constant of Cd(II) with THMPTACD is 12.91 log units whereas the stability constant of the parent macrocyclic ligand, 12aneN_3, is 7.01 log units (Zompa, 1978). There is an increase of 5.90 log units in stability on addition of hydroxy-2-methylpropyl pendant arms to 12aneN_3. THMPTACD, like THPTACD, has three nitrogen donor atoms on the parent macrocyclic ring and three oxygen donor atoms on the pendant arms affording a hexadentate ligand. The six donor atoms are expected to fold around the Cd(II) metal ion, thereby forming a caged metal complex structure with the Cd(II) metal ion sitting in between the oxygen and the nitrogen donor atom sets. Chamberlain *et al.*, (1999) reported the crystal structure of yttrium metal complex with 1,4,7-*tris*(2-hydroxy-2-methylpropyl)-l,4,7-triazacyclononane, which has the same pendant arms as THMPTACD, but appended to 9aneN_3. The two sets of the donor atoms enveloped the yttrium metal ion to form a caged structure. The additional five-membered chelate rings formed by the oxygen donor atoms of the pendant arms and the corresponding nitrogen donor atoms of the ring on which they are appended should provide an enhanced stability in THMPTACD than the parent macrocycle, 12aneN_3. In general,

THMPTACD should enjoy the same advantages that both THPTACD and THBTACD have over the parent macrocyclic ligand, 12aneN_3.

Table 4.5: The stability constant of THMPTACD with Co(II), Zn(II), Cd(II) and Pb(II) at 25 °C, in 0.1000 mol dm^{-3} $NaNO_3$

Meta ions	log *K*	Standard deviation	R-factor
Cd(II)	12.91	±0.12	0.03
Zn(II)	18.08	±0.08	0.03
Co(II)	14.63	±0.08	0.07
Pb(II)	14.36	±0.03	0.03

The stability constant of Cd(II) with THETAC is 10.60 log units (Luckay *et al.,* 1996) whereas the stability constant of the parent macrocyclic ligand, 9aneN_3, is 9.33 log units (Zompa *et al.,* 1995). There is a small increase of 1.27 log units in stability on addition of hydroxyethyl pendant arms to 9aneN_3. This is in contrast to the large increase in stability constant on addition of hydroxy-2-methylpropyl pendant arms to 12aneN_3. THETAC has hydroxyethyl pendant arms which are less bulky than the hydroxy-2-methylpropyl and therefore expected to impose weak steric hindrance to solvation. This means that the parent macrocyclic ring in THETAC is more solvated than its analogue with hydroxy-2-methylpropyl pendant arms and therefore more energy is needed to desolvate THETAC than THMPTACD. THETAC should have a more favourable entropy term than THMPTACD. However, THMPTACD should benefit more from an enthalpy effect than THETAC because less heat of desolvation is used to desolvate the parent macrocyclic ring in THMPTACD than in THETAC. The difference in stability between THETAC and THMPTACD metal complexes is 2.31 log units.

4.3.3.2 Complexation with Zn(II)

The stability constant of Zn(II) with THMPTACD is 18.08 log units whereas the stability constant of the parent macrocyclic ligand, 12aneN_3, is 8.75 log units (Zompa, 1978). There is an increase of 9.33 log units in stability on addition of hydroxy-2-methylpropyl pendant arms to 12aneN_3. THMPTACD, like THPTACD, has three nitrogen donor atoms on the parent macrocyclic ring and three oxygen donor atoms on the pendant arms affording a hexadentate

ligand. The six donor atoms are expected to fold around the Zn(II) metal ion just like in the case of THPTACD thereby forming a caged metal complex structure with the Zn(II) metal ion sitting in between the oxygen and the nitrogen donor atom sets.

The stability constant of Zn(II) with THETAC is 12.07 log units (Sayer *et al.,* 1983) whereas the stability constant of the parent macrocyclic ligand, 9aneN_3, is 11.62 log units (Zompa, 1975). In this case, there is a small increase of 0.45 log units in stability on addition of hydroxyethyl pendant arms to 9aneN_3. This is in contrast with the large increase in stability constant on addition of hydroxyl-2-methylpropyl pendant arms to 12aneN_3. Hydroxyethyl pendant arms are less bulky and impose a weak steric hindrance to solvation. This means that THETAC is more solvated than its analogues with hydroxyl-2-methylpropyl pendant arms. More energy is, therefore, needed to remove the solvent molecules in THETAC than in corresponding macrocycles with hydroxyl-2-methylpropyl pendant arms. Unlike THMPTACD which has six-membered chelate rings, THETAC has three five-membered chelate rings which are known to favour large metal ions and therefore it is not surprising that THMPTACD forms more stable Zn(II) complexes than THETAC.

4.3.3.3 Complexation with Co(II)

The stability constant of Co(II) with THMPTACD is 14.63 log units. There is no data available for the stability constant of Co(II) with the parent macrocyclic ligand, 12aneN_3. THMPTACD is a hexadentate ligand with three nitrogen and three oxygen donor atoms and should form more stable Co(II) metal complexes than 12aneN_3, which is a tridentate ligand. Unlike with THPTACD and THBTACD, there is a swap in stability between Co(II) and Pb(II). The stability constants of these two metal ions are very close and are both larger than the stability constant of Cd(II). This may be due to favourable change in electronic environment of THMPTACD induced by the Co(II) metal ion. Co(II) may still be acting as a bigger metal ion as compared to Zn(II) just like in the case of THPTACD.

4.3.3.4 Complexation with Pb(II)

The stability constant of Pb(II) with THMPTACD is 14.36 log units. There is no data available for the stability constant of Pb(II) with the parent macrocyclic ligand, 12aneN_3, but one would expect THMPTACD to form more stable complexes than 12aneN_3. This should be

the case because THMPTACD has three extra five-membered chelate rings formed by the oxygen donor atoms of the pendant arms and the nitrogen donor atoms of the macrocyclic rings on which they are appended whereas 12aneN_3 has only six-membered chelate rings which favours small metal ions over large metal ions (Martell and Hancock, 1996).

The stability constant of Pb(II) with THETAC is 11.98 log units (Luckay *et al.,* 1996) whereas the stability constant of its parent macrocyclic ligand, 9aneN_3, is 11.10 log units (Zompa, 1978). There is a small increase of 0.88 log units in stability on addition of hydroxyethyl pendant arms to 9aneN_3. This is very strange considering that THETAC has six five-membered chelate rings (three between nitrogen donor atoms of the parent ring, 9aneN_3, and the rest between the oxygen donor atoms of the pendant arms and the nitrogen donor atom on which they are attached). The increase in stability constant for Cd(II) and Zn(II) with THETAC is 1.27 and 0.45 log units, respectively. The increase in stability constant for Pb(II) with THETAC is larger than that of Zn(II) but smaller than the Cd(II) which means that other factors other than chelate ring sizes play a major role in determining the stability of THETAC with Pb(II) metal ion.

It is important to note that the trend in stability constants between metal complexes of Zn(II), Pb(II), and Cd(II) with THETAC as reported by Luckay *et al.,* (1996) is exactly the same as the ones reported here for all three ligands namely: THPTACD, THBTACD and THMPTACD. The stability of these metal complexes with THETAC increases in the following order: Cd(II) < Pb(II) < Zn(II).

4.3.4 Comparative study of THPTACD, THBTACD and THMPTACD

The three macrocyclic ligands, THPTACD, THBTACD and THMPTACD have the same parent macrocyclic ring but different pendant arms. THPTACD and THBTACD have secondary alcohol pendant arms whereas THMPTACD has tertiary alcohol thereby making it more sterically encumbered than the first two. THPTACD is less sterically hindered by its tethered groups than THMPTACD, because it has one methyl group directly attached to the carbon holding the oxygen donor atom as opposed to two methyl groups in THMPTACD. However, THMPTACD benefits more from the positive inductive effect of the side chains than THPTACD. THBTACD falls between the two in terms of steric hindrance. Even though

THBTACD has one ethyl group attached to the carbon atom holding the oxygen donor atom as opposed to two methyl groups in THMPTACD, the neutralisation of the inductive effect by the steric effect should be more pronounced in THMPTACD. In situations where steric effects play a less pronounced role, THMPTACD should benefit more from the inductive effect of the alkyl groups because it has tertiary alcohol groups as opposed to THBTACD which has secondary alcohol groups.

Table 4.6: The stability constants of THPTACD, THBTACD and THMPTACD with Co(II), Zn(II), Cd(II) and Pb(II)

Metal ion	THPTACD	THBTACD	THMPTACD
Zn(II)	21.22	20.02	18.08
Pb(II)	16.11	15.01	14.36
Cd(II)	14.03	13.55	12.91
Co(II)	15.45	13.93	14.63

Data reported at 25 °C, in 0.1000 $NaNO_3$.

This is in line with the explanation given in **Section 3.3.4** of **Chapter 3** for high second protonation constants of THBTACD compared to both THPTACD and THMPTACD. In general, there is a decrease in metal complex stability with the increase in steric hindrance which means that steric effects play a central role in determining the stability of these metal complexes (**Table 4.6**). There is however a reverse in stability constant of THBTACD and THMPTACD with Co(II) with the latter forming more stable Co(II) metal complexes than the former. This anomaly cannot be easily explained and shows how a fine balance of the various factors is maintained.

In general, Zn(II) forms the most stable metal complexes (see **Fig. 4.1**) whereas the soft Cd(II) forms the least stable metal complex with all three ligands as mentioned before. The molecular structures of Zn(II), Co(II) and Cd(II) with THPTACD showed that Zn(II) is actually behaving like the smallest metal ion followed by Co(II) and Cd(II) (**Table 4.2**). The short Zn(II)-N bond lengths indicates that Zn(II) cation is very close to the macrocyclic hole compared to both Co(II) and Cd(II). This behaviour may be attributed to both the electronic

effects (for Co(II)) and the size of the metal cation (for Cd(II)). The solvation of the metal ions seems not to play a big role in determining the stability of metal complexes. Co(II), as a small metal ion, is the most solvated whereas Pb(II) is the least solvated of the metal ions used in this investigation (Song *et al.*, 1994).

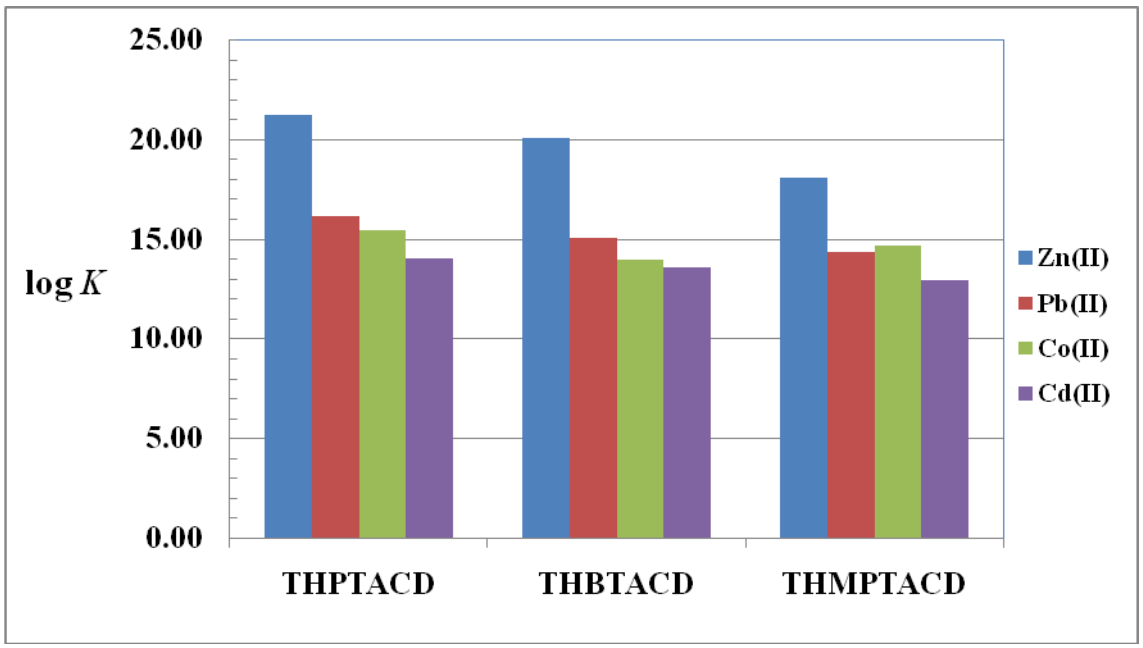

Fig. 4.1: The stability constants of THPTACD, THBTACD and THMPTACD with Zn(II), Pb(II), Co(II) and Cd(II) metal cations.

Fig. 4.1 clearly shows that the stability constants of Zn(II) complexes with THPTACD, THBTACD and THMPTACD is far greater than those of the Pb(II), Co(II) and Cd(II) metal complexes, which are very close to each other.

4.3.5 Selectivity of THPTACD, THMPTACD and THBTACD for Cd(II) and Zn(II)

The selectivity of ligand for one metal ion relative to that of another with the same ligand is normally given by log K_{sel} (Hancock and Martell, 1989). The selectivity of Zn(II) over Cd(II) will be written as Zn/Cd throughout this Chapter. To achieve synthesis of ligands tailored for a particular metal-ion binding application, the system needs to be designed such that it is able to read the information encoded in the metal ion of interest and differentiate it from that of other metals that might also be present (Lindoy, 1997). However, in general terms, recognition of a particular metal ion of interest will occur when the properties of the ligand

best match the steric and electronic nature of that metal ion relative to those of the other metal ions present. Particular attention has been given to mixed donor macrocyclic systems with emphasis on the recognition and/or discrimination of ions within the following industrially important groups: cobalt/nickel/copper; zinc/cadmium; and silver/lead (Adam *et al.*, 1981; Adam *et al.*, 1983; Adam *et al.*, 1988; Adam *et al.*, 1992; Adam *et al.*, 1993; Lindoy, 1997). In this thesis, particular attention will be given to the zinc/cadmium system.

Table 4.7: The selectivity of THPTACD, THBTACD and THMPTACD for Zn/Cd

Macrocyclic ligand	THPTACD	THBTACD	THMPTACD
Zn(II)	21.22	20.02	18.08
Cd(II)	14.03	13.55	12.91
log K_{sel}	**7.19**	**6.47**	**5.17**

Excellent selectivity for Zn/Cd were found for all the three ligands (**Table 4.7**). The selectivity for Zn/Cd refer to the stability constants for the following reactions (charges are omitted for clarity):

THPTACD-Cd(II) + Zn(II) ⇌ THPTACD-Zn(II) + Cd(II) log K_{sel} = 7.19 (**Equation 4.5**)

THBTACD-Cd(II) + Zn(II) ⇌ THBTACD-Zn(II) + Cd(II) log K_{sel} = 6.47 (**Equation 4.6**)

THMPTACD-Cd(II) + Zn(II) ⇌ THMPTACD-Zn(II) + Cd(II) log K_{sel} = 5.17 (**Equation 4.7**)

In theory, it should be possible to substitute Cd(II) with Zn(II) in a complex with relative ease since the forward reaction is thermodynamically favourable (log K is positive) as given by **Equations 4.5-4.7**. However, these reactions may not be as straightforward as it seems at the first glance due to the caged nature of the complexes which may slow down the kinetics of the reaction. The high selectivity of Zn/Cd by THPTACD over the other two ligands seems to

stem from the fact that Zn(II) is able to manipulate the THPTACD ligand in such a way that the metal ion comes very close to the macrocyclic hole as compared to Cd(II) hence the Zn(II) complexes have high thermodynamic stability. The results shown in **Table 4.7** indicate that THPTACD is able to form relatively more stable complexes with both Zn(II) and Cd(II) whereas THMPTACD forms the weakest complexes with the same metal ions. Consider the following reactions (charges are omitted):

THMPTACD-Zn(II) + THPTACD ⇌ THPTACD-Zn(II) + THMPTACD

log K = 3.14 (**Equation 4.8**)

THMPTACD-Cd(II) + THPTACD ⇌ THPTACD-Cd(II) + THMPTACD

log K = 1.12 (**Equation 4.9**)

THBTACD-Zn(II) + THPTACD ⇌ THPTACD-Zn(II) + THBTACD

log K = 1.20 (**Equation 4.10**)

THBTACD-Cd(II) + THPTACD ⇌ THPTACD-Cd(II) + THBTACD

log K = 0.48 (**Equation 4.11**)

From **Equations 4.8-4.11**, we can conclude that THPTACD has a good selectivity of Zn(II) over Cd(II) than both THBTACD and THMPTACD by preferentially increasing its binding affinity for Zn(II) as we move from THMPTACD to THBTACD to THPTACD while keeping its binding affinity for Cd(II) relatively low.

This seems to be in conflict with the fact that Cd(II) as a larger metal ion should adjust well to distortions brought about by changes in electronic and steric effects in the ligand than Zn(II). Normally, distortions of the M-N bonds for small metal ions are met by strong resistance from the much larger force constants; and the requirement of the metal ion to lie well above the plane of the nitrogen donors would cause more considerable steric strain in Zn(II) complexes than it would in Cd(II) complexes. Cd(II) metal ion is more polarisable than the Zn(II) metal ion. Since both Zn(II) and Cd(II) are d^{10} metal ions, they are not affected by tetragonal distortions in their octahedral geometry. The trigonal distortion in their

geometry is a result of steric effects and the difference should be directly related to the difference in their ionic radius hence their size. The M(II)-N bond lengths of the Cd(II) complexes with THPTACD has a difference of 0.015 Å between the shortest and the longest bond whereas Zn(II) complex has a difference of 0.052 Å (Table 4.2). However, Zn(II) complexes have greater stability than Cd(II) complexes because:

(i) the Zn(II)-N bond lengths are short and closer to the ideal bond length of 2.1 Å (Thöm *et al.*, 1985). The Zn(II) is closer to the parent macrocyclic ring which should result in a high enthalpy term and enhanced stability.

(ii) the distortions in the Zn(II)-N bond lengths are compensated by the N-Zn(II)-N bond angles (Hancock and McDougall 1980). The average N-Zn(II)-N bond angle is 100.1° whereas the average N-Cd(II)-N bond angle is 96.7° (**Table 4.2**).

Thus, the fact that coordination of THPTACD to the metal ion requires that the metal ion should sit above the plane of the three nitrogen donor atoms is of much benefit to Zn(II) than it is to Cd(II). This is in total agreement with **Equations 4.8-4.11**.

4.3.6 Comparative study of THTD, THTUD and THPTACD

The three macrocyclic ligands, THTD, THTUD and THPTACD have the same pendant arms but a different number of propylene bridges between the nitrogen donor atoms (**Chart 3.6** of **Section 3.3.5**, **Chapter 3**). The formation constants of Zn(II) with $10aneN_3$, $11aneN_3$ and $12aneN_3$ are 11.28, 10.41 and 8.75 log units, respectively (Zompa, 1978). The values of the stability constants of the Zn(II) complexes decrease as the number of five-membered chelate rings decreases within the macrocyclic ring. The stability constant of Cd(II) with $10aneN_3$, $11aneN_3$ and $12aneN_3$ are 9.25, 8.62 and 7.01, respectively (Zompa *et al.*, 1995), which shows the same trend. The increase in stability as the ring size decreases is attributed to differences in enthalpy of complexation since the solvation entropy is nearly the same for all reactions. The three ligands are all tridentate and therefore the solvation enthalpy should equally be similar because of the similar cyclic nature and charge localisation of the ligand (Zompa *et al.*, 1995; Zompa, 1978). If the entropy effect was then the driving force the reverse trend would have been observed because bigger rings are more flexible than smaller rings.

Table 4.8 shows the $\Delta\log K_{pe}$ for the three ligands. The $\Delta\log K_{pe}$ value for each metal ion is the difference in log K_1 for the complexes of the macrocyclic ligands with hydroxyalkyl pendant arms and the log K_1 for the corresponding parent macrocycles. $\Delta\log K_{pe}$ is, therefore, a measure of the influence of the pendant arms within each series hereby referred to as the *tris*-pendant effect. For tridentate macrocyclic ligands, the addition of the pendant arms with or without donor atoms of their own nearly always results in an increase in metal complex stability (Delgado *et al.,* 1993; Geraldes *et al.,* 1991; Luckay *et al.,* 1996; Bates and Parker, 1996; Barnard, 2008; Hama and Takamoto, 1975; Tei *et al.,* 2004; Cortes *et al.,* 1990; Sayer *et al.,* 1983; van der Merwe *et al.,* 1985; Bevilacqua *et al.,* 1987). This could be due to the fact that triazamacrocycles are very small and metal ions sit above the plane of the macrocyclic donor atoms. The pendant arms provide additional coordination sites thereby affording caged metal complexes. The *tris*-pendant effect is positive (**Table 4.8**) for all three ligands indicating that the hydroxypropyl pendant arms have a positive effect on THTD, THTUD and THPTACD.

Table 4.8: The *tris*-pendant effect ($\Delta\log K_{pe}$) of THTD, THTUD and THPTACD for Zn(II) and Cd(II) cations[e]

	Zn(II)	Cd(II)
THTD[a]	14.38	19.38
10aneN_3	11.28[b]	9.25[c]
Δlog K_{pe}	**3.10**	**10.13**
THTUD[a]	16.20	18.05
11aneN_3	10.41[b]	8.62[c]
Δlog K_{pe}	**5.79**	**9.43**
THPTACD[d]	21.22	14.03
12aneN_3	8.75[b]	7.01[c]
Δlog K_{pe}	**12.47**	**7.02**

[a] Data from Barnard, (2008). [b] Data from Zompa, (1978). [c] Data from Zompa *et al.,* (1995). [d] This work. [e] Zn(II) and Cd(II) were chosen because data for the parent macrocycle is available for all three parent macrocycles whereas for Co(II) and Pb(II), not all data is available. Data reported at 25 °C, in 0.1000 mol dm^{-3} $NaNO_3$.

Zn(II) is regarded as a small metal ion whereas Cd(II) is regarded as a medium to large metal ion which should give an idea about the ligand response to large and small metal ions as hydroxypropyl pendant arms are added. Comparing the effect of adding the hydroxypropyl pendant arms to the parent macrocyclic rings as the five-membered chelate rings are progressively replaced by six-membered chelate rings, two trends become clear (Table 4.8). The stability of the resultant Zn(II) complexes increases whereas the stability of Cd(II) complexes decreases. The values of the $\Delta\log K_{pe}$ follow the same trend. This is in agreement with the rule that replacement of five-membered chelate rings with six-membered chelate rings favours small metal ions over large metal ions (Hancock and Martell, 1989).

Table 4.9 shows that the increase in stability of Pb(II) as we successively replace the five-membered chelate rings with six-membered chelate rings is non-monotonic. This serves to further support the idea that Pb(II) may have a stereochemically active lone pair of electrons in these ligand-metal complexes. When Pb(II) acts like a large metal ion with ionic radius of 1.19 Å, it always shows a large drop in stability constants when five-membered chelate rings are converted to six-membered chelate rings (Martell and Hancock, 1996). However, the results for THTD, THTUD and THPTACD do not follow the same trend.

Table 4.9: The stability constant of THTD, THTUD and THPTACD with Co(II), Zn(II), Cd(II) and Pb(II)

Metal ion	Co(II)	Zn(II)	Cd(II)	Pb(II)
THTD[a]	22.22	14.38	19.38	15.47
THTUD[a]	17.52	16.20	18.05	14.63
THPTACD[b]	15.45	21.22	14.03	16.11

[a] Data from Barnard, (2008). [b] This work. Data reported at 25°C in 0.1 mol dm^{-3} $NaNO_3$.

The most intriguing question is why the stability of Co(II) metal complexes decrease with increasing six-membered chelate rings whereas the stability of Zn(II) increases with increasing six-membered chelate rings?

Molecular structure data analysis of the THPTACD complexes with Co(II) and Zn(II) in **Table 4.2** shows that Zn(II) acts like a small metal ion whereas Co(II) acts like a large metal ion. This means that for THPTACD, the stability results are consistent with available bond

distances data. It is interesting to note that Co(II) and Cd(II) follow the same trend which is opposite to the trend shown by Zn(II). **Table 4.10** gives crystal structure data for THTUD complexes with Co(II) and Zn(II). The M(II)-N bond lengths in the two crystals are not significantly different.

Table 4.10: The bond lengths and angles for $[Co(THTUD)]^{2+}$ and $[Zn(THTUD)]^{2+}$ crystal structures

THTUD	M-N	SMCR-N,N	FMCR-N,O	M-O	FMCR-N,N
Co(II)	2.183	104.1	77.5	2.099	96.5
Zn(II)	2.163	100.0	76.7	2.148	87.5

Data from Barnard, (2008). M(II)-N and M(II)-O are bond lengths in Å. FMCRA-N,N and FMCRA- N,O are bond angles (°) in five-membered chelate rings with nitrogen and oxygen donor atoms, respectively. SMCR-N,N are the bond angles for six-membered chelate rings with nitrogen donor atoms.

However, unlike in the case of Co(II) complexes with THPTACD (**Table 4.2**), the slight bond lengthening in the THTUD complex is more than compensated by the large six-membered chelate ring angles (Hancock and McDougall, 1980). This means that Co(II) fits the electronic environment of THTUD better than that of THPTACD and hence more favourable overlap between the orbitals of the nitrogen donor atoms and the orbitals of the Co(II) metal ion takes place giving Co(II) a stability edge over Zn(II).

The bond lengths of Co(II) complex with THTD are 2.170 and 2.112 Å for Co(II)-N and Co(II)-O, respectively (Al-Sagher *et al.,* 1993). No crystal data for the Zn(II) complex with THTD are available, however, comparison of molecular structures of THPTACD and THPTACN in **Tables 4.2** and **4.4** suggest that the same trend can be predicted.

4.4 Conclusions

During the early days of triazamacrocyclic ligands, many scientists believed that $9aneN_3$ and its derivatives were the most important azamacrocyclic ligands with three nitrogen donor atoms within the parent ring. This belief led to intense research on $9aneN_3$ and its derivatives while the larger triazamacrocycle, $12aneN_3$, received very little attention. The results reported in this thesis suggest that $12aneN_3$ with three hydroxyalkyl pendant arms is an equally good

complexing agent with transitional metal ions and might be useful in medical, biological and industrial applications.

The values of the stability constants found in this investigation together with bond lengths from X-ray crystal structure determination provide enough information to conclude that Zn(II) metal ion adjusts better than Co(II), Cd(II) and Pb(II) to changes in 12aneN_3 when *N*-functionalised with pendant arms carrying oxygen donor atoms. Zn(II) metal ion formed the most stable complexes with THPTACD, THBTACD and THMPTACD whereas Cd(II) metal ion formed the least stable metal complexes with the same ligands. THPTACD formed the most stable metal complexes with all four metal ions namely Co(II), Zn(II), Cd(II) and Pb(II) compared to corresponding metal complexes of THBTACD and THMPTACD.

The stability constants for the formation THPTACD, THBTACD and THMPTACD complexes do not conform to the well established ligand design rule as reported in the literature. The rule state that addition of pendant arms carrying neutral oxygen donor atoms increase the selectivity of the ligand for large metal ions relative to small metal ions, irrespective of whether the oxygen donor atoms are part of macrocyclic ring or not. This rule, however, is based on tetraazamacrocycles or ligands with more than four donor atoms within the macrocyclic ring and also to open chain ligands that have very different chemistry to triazamacrocyclic ligands. The ligands that have been studied by Hancock do not have severe steric strain as triazamacrocyclic ligands experience. THETAC reported by both Sayer and Luckay also breached this rule by forming more stable complexes with Zn(II) than Cd(II). THETAC has hydroxyethyl pendant arms appended to the nitrogen donor atoms of the ring. Triazamacrocyclic ligands are small and almost all transition metal ions cannot fit into their macrocyclic hole; as a result, the metal ions sit above the macrocyclic hole and responds to various modifications differently as they would have, had the metal and the macrocyclic hole an exact match. In general, *N*-functionalisation of 12aneN_3 with hydroxyalkyl pendant arms leads to an increase in stability of various metal complexes. The selectivity of Zn/Cd is enhanced as the hydroxyalkyl pendant arms tethered to 12aneN_3 are made less bulky by preferential adjustment of the ligand towards the Zn(II) metal ion while keeping the stability of Cd(II) complexes fairly low.

Chapter 5

The crystal and molecular structures of the macrocyclic ligands with divalent metal ions

5.1 Introduction

The formation of metal complexes of macrocyclic ligands is an important research field which is increasingly developing. The interest in this field also originates from the possibility of building supramolecular architectures tailored for specific needs. Crystal engineering is defined as the understanding of intermolecular and intramolecular interactions in the context of crystal packing and the utilisation of such understanding in the design of new molecules with desired physical and chemical properties (Desiraju, 1989). Systems that are self-assembled by weak interactions are important and essential in crystal engineering. In particular, molecular materials assembled by hydrogen bond formation are of considerable interest (Wang *et al.*, 2002). The goal to design new materials with a combination of desired properties, however, requires a quantitative understanding of the properties of the individual units, their response to chemical substitutions, as well as their interactions.

For synthetic chemists, it is a real challenge to find some keys to understanding the main factors that can determine the wide variety of supramolecular organisations. The study of single crystal structures of metal ion complexes greatly increases the level of understanding of the factors that control complex formation processes. This has led to improved abilities to design ligands with specified complexing properties. The cavities within the macrocycles are of prime interest in understanding their selectivity for metal ions. Usually, metal complexes show high stability when the metal ion exactly fits the macrocyclic hole (Martell and Hancock, 1996). In a classical study of the sizes of macrocyclic cavities done by Busch *et al.*, (1971), molecular mechanics (MM) was used to calculate the best-fit M-N bond lengths for coordinating to azamacrocycles in a fashion of minimum strain energy. In the calculations, the geometry of the central metal ion within the macrocyclic cavity was constrained to square

planar. However, the situation is more complex than suggested in these early studies. For example, the MM calculations of the macrocycles 12aneN_4 to 14aneN_4 showed that the metal ion is not always required to sit within the macrocyclic hole and that the geometry of the metal ion is not restricted to square planar (Hancock, 1989; Thöm *et al.*, 1984). When the metal ion is located outside the macrocyclic cavity, the factors that determine the selectivity of one metal ion over another are entirely different from those that determine the stability when the metal fits into the cavity. Crystal and molecular structure determination give account of those factors such as bond angle deformations and bond length distortions which can either be in a form of bond compression or elongation. In the present investigation, the procedure developed by Kong *et al.,* (2002) was employed in growing crystals. All crystal structures discussed in this thesis involve the interaction of divalent cations and selected macrocyclic ligands. M-N and M-O bond distances represent M(II)-N and M(II)-O bond separation, respectively and O-M-O, O-M-N and N-M-N bond angles represent O-M(II)-O, O-M(II)-N and N-M(II)-N angles, respectively.

The crystal structures were determined mainly to understand the solution chemistry of macrocyclic metal complexes. However, intramolecular interactions in a supramolecular context were also of interest and are pointed out where relevant.

5.2 Materials and methods

5.2.1 Chemicals and reagents

The ligands THPTACD, TMPTACD, THPETACD, THBTACD and THMPTACD were synthesised according to the procedures described in **Sections 2.6.1-2.6.5** of **Chapter 2**. $CrCl_3.6H_2O$ was purchased from NT laboratory supplies (PTY) LTD. $Cd(NO_3)_2.4H_2O$ and $Mn(NO_3)_2.4H_2O$ were obtained from Fluka and SAAR CHEM, respectively. $Zn(NO_3)_2.6H_2O$, $Hg(NO_3)_2.H_2O$, $Cu(NO_3)_2.3H_2O$, $Co(NO_3)_2.6H_2O$, $Fe(NO_3)_3.9H_2O$ and diethyl ether were purchased from Merck. $Pb(ClO_4)_2.xH_2O$, $Mn(C_2H_3O_2)_3.2H_2O$, $Ga(NO_3)_3.xH_2O$, $In(NO_3)_3.xH_2O$, $Y(NO_3)_3.4H_2O$, $Fe(ClO_4)_2.xH_2O$ and $Ni(NO_3)_2.6H_2O$ were purchased from Sigma-Aldrich.

Caution! *Although no problems were experienced during this work, metal perchlorate salts mixed with organic ligands and solvents are potentially explosive and should be prepared*

and handled only in small quantities and with great care. All reactions were carried out in a fumehood.

5.2.2 Instrumentation and determination of crystal structures

A suitable crystal was mounted on a thin glass fibre and coated with silicone-based oil to prevent decomposition. Data were collected on a Bruker SMART Apex CCD diffractometer with graphite monochromated Mo-Kα radiation (λ = 0.71073 Å) (Bruker, 2003). Data reduction was carried out using SAINT (Bruker, 2003). A Cryostat: Oxford Cryogenics (700 Series Cryostream Plus) was used to cool the crystal to 100 K. Empirical corrections were performed with SADABS (Bruker, 2002). The structure was solved by direct methods, while the remainder of the atomic positions were found using Difference Fourier methods. All non-hydrogen atoms were refined anisotropically (with appropriate restraints using SIMU and ISOR) by full-matrix least squares calculations on F^2 using SHELX-97 (Sheldrick, 1997) within the X-seed environment (Barbour, 2001; Atwood and Barbour, 2003). Hydrogen atoms were geometrically positioned and refined in the riding model approximation. ORTEP-III for Windows was used to generate figures at the 50% probability level.

5.2.3 Preparation of crystalline THPTACD metal complexes

$Cu(NO_3)_2.3H_2O$ (0.1737 g, 0.7189 mmol) was dissolved in EtOH (20.00 mL) at 60 ^oC with stirring. THPTACD (0.2484 g, 0.7189 mmol) was then added to the solution and stirred overnight at room temperature. The blue precipitate was filtered and dissolved in a small amount of dimethylformamide. Diethyl ether was slowly diffused into the metal solution in a sealed container from which blue crystals suitable for X-ray analysis were obtained. Anal. Calc. % for $C_{18}H_{41}CuN_4O_7$: C, 44.20; N, 11.46; H, 8.45. Found: C, 43.35; N, 11.23; H, 8.31.

The same procedure was used for the preparation of the crystals of the following systems: $Ni(NO_3)_2.6H_2O$ (0.2054 g, 0.7062 mmol), THPTACD (0.2440 g, 0.7062 mmol); Anal. Calc % for $C_{18}H_{41}NiN_4O_7$: C, 44.65; N, 11.57; H, 8.53. Found: C, 40.20; N, 10.41; H, 7.91.

$Co(NO_3)_2.6H_2O$ (0.2161 g, 0.7424 mmol), THPTACD (0.2565 g, 0.7424 mmol); Anal. Calc. % for $C_{18}H_{41}CoN_4O_7$: C, 44.63; N, 11.56; H, 8.53. Found: C, 40.39; N, 10.46; H, 7.90. $Zn(NO_3)_2.6H_2O$ (0.1749 g, 0.5881 mmol), THPTACD (0.2032 g, 0.5881 mmol); Anal. Calc. % for $C_{18}H_{41}ZnN_4O_7$: C, 44.04; N, 11.41; H, 8.42. Found: C, 40.01; N, 10.26; H, 7.81. $Cd(NO_3)_2.4H_2O$ (0.2285 g, 0.7406 mmol), THPTACD (0.2559 g, 0.7406 mmol); Anal. Calc. % for $C_{21}H_{46}CdN_6O_{10}$: C, 38.51; N, 12.83; H, 7.08. Found: C, 35.99; N, 11.97; H, 6.82. $Mn(NO_3)_2.4H_2O$ (0.1736 g, 0.6917 mmol), THPTACD (0.2390 g, 0.6917 mmol); Anal. Calc. % for $C_{18}H_{41}MnN_4O_7$: C, 50.00; N, 11.66; H, 8.43. Found: C, 47.09; N, 10.98; H, 8.29.

The following metal salts were also used and the complex solutions are still periodically checked for the formation of new suitable crystals: $Fe(NO_3)_3.9H_2O$, $Pb(ClO_4)_2.xH_2O$, $CrCl_3.6H_2O$, $Hg(NO_3)_2.H_2O$, $Ga(NO_3)_3.xH_2O$, $In(NO_3)_3.xH_2O$, $Y(NO_3)_3.4H_2O$, $Mn(C_2H_3O_2)_3.2H_2O$ and $Fe(ClO_4)_2.xH_2O$.

5.2.4 Preparation of crystalline THPETACD metal complexes

$Cu(NO_3)_2.3H_2O$ (0.0525 g, 0.2174 mmol) was dissolved in EtOH (20.00 mL) at 60 ^oC with stirring. THPETACD (0.1156 g, 0.2174 mmol) was added to the solution and stirred overnight at room temperature. The blue precipitate was filtered and dissolved in a small amount of dimethylformamide. Diethyl ether was slowly diffused into the metal solution in a sealed container from which blue crystals suitable for analysis were obtained. Anal. Calc. % for $C_{33}H_{4s}CuN_5O_9$; C, 55.10; N, 9.73; H, 6.31. Found: C, 51.34; N, 9.08; H, 6.11.

The following metal salts were also tried and the metal complex solutions are periodically checked for new crystals: $Ni(NO_3)_2.6H_2O$, $Co(NO_3)_2.6H_2O$, $Zn(NO_3)_2.6H_2O$, $Cd(NO_3)_2.4H_2O$ and $Mn(NO_3)_2.4H_2O$.

5.2.5 Preparation of crystalline THBTACD metal complexes

$Cu(NO_3)_2.3H_2O$ (0.1735 g, 0.7183 mmol) was dissolved in EtOH (20.00 mL) at 60 ^oC with stirring. THBTACD (0.2784 g, 0.7183 mmol) was added to the solution and stirred overnight

at room temperature. The blue precipitate was filtered and dissolved in a small amount of dimethylformamide. Diethyl ether was slowly diffused into the solution in a sealed container from which blue crystals suitable for X-ray analysis were obtained.

The following metal salts were also used and the metal complex solutions are still periodically checked for new suitable crystals: $Ni(NO_3)_2.6H_2O$, $Zn(NO_3)_2.6H_2O$, $Co(NO_3)_2.6H_2O$, $CrCl_3.6H_2O$, $Cd(NO_3)_2.4H_2O$, $Mn(NO_3)_2.4H_2O$, $Hg(NO_3)_2.H_2O$, $Fe(NO_3)_3.9H_2O$, $Pb(ClO_4)_2.xH_2O$, $Mn(C_2H_3O_2)_3.2H_2O$, $Ga(NO_3)_3.xH_2O$, $In(NO_3)_3.xH_2O$, $Y(NO_3)_3.4H_2O$ and $Fe(ClO_4)_2.xH_2O$.

5.2.6 Preparation of crystalline THMPTACD metal complexes

$Zn(NO_3)_2.6H_2O$ (0.1863 g, 0.6262 mmol) was dissolved in EtOH (20.00 mL) at 60 ^oC with stirring. THMPTACD (0.2427 g, 0.6262 mmol) was added to the solution and stirred overnight at room temperature. The white precipitate was filtered and dissolved in a small amount of dimethylformamide. Diethyl ether was slowly diffused into the metal solution in a sealed container from which white crystals suitable for X-ray analysis were obtained.

The following metal salts were also used and the metal complex solutions are regularly checked for the formation of new suitable crystals: $Cu(NO_3)_2.3H_2O$, $Cd(NO_3)_2.4H_2O$, $Mn(NO_3)_2.4H_2O$, $CrCl_3.6H_2O$, $Hg(NO_3)_2.H_2O$, $Co(NO_3)_2.6H_2O$, $Fe(NO_3)_3.9H_2O$, $Ni(NO_3)_2.6H_2O$, $Pb(ClO_4)_2.xH_2O$, $Mn(C_2H_3O_2)_3.2H_2O$, $Ga(NO_3)_3.xH_2O$, $In(NO_3)_3.xH_2O$, $Y(NO_3)_3.4H_2O$ and $Fe(ClO_4)_2.xH_2O$.

5.2.7 Preparation of crystalline TMPTACD metal complexes

$Zn(NO_3)_2.6H_2O$ (0.1216 g, 0.4089 mmol) was dissolved in EtOH (20.00 mL) at 60 ^oC with stirring. TMPTACD (0.1610 g, 0.4089 mmol) was added to the solution and stirred overnight at room temperature. The white precipitate was filtered and dissolved in a small amount of dimethylformamide. Diethyl ether was slowly diffused into the metal solution in a sealed container from which white crystals suitable for X-ray analysis were obtained.

The following metal salts were also used and the metal complex solutions are still periodically checked regularly for the formation of new suitable crystals: $CrCl_3.6H_2O$, $Cu(NO_3)_2.3H_2O$, $Cd(NO_3)_2.4H_2O$, $Fe(NO_3)_3.9H_2O$, $Mn(NO_3)_2.4H_2O$, $Hg(NO_3)_2.H_2O$, $Co(NO_3)_2.6H_2O$, $Pb(ClO_4)_2.xH_2O$, $Mn(C_2H_3O_2)_3.2H_2O$, $Fe(ClO_4)_2.xH_2O$, $Ga(NO_3)_3.xH_2O$, $In(NO_3)_3.xH_2O$, $Y(NO_3)_3.4H_2O$ and $Ni(NO_3)2.6H2O$

5.2.8 Preparation of crystalline $[Cd_2(C_9H_{21}N_3)_2(\mu\text{-}Cl)_2(NO_3)_2]$ binuclear complex and the protonated ligand, $[(C_{17}H_{38}N_3O_2)(NO_3)]H_2O$

$Cd(NO_3)_2.4H_2O$ (0.1965 g, 0.6370 mmol) was dissolved in EtOH (20.00 mL) at 60 ^oC with stirring. $12aneN_3$ (0.1091 g, 0.6370 mmol) was added to the solution and stirred overnight at room temperature. The white precipitate was filtered and dissolved in a small amount of dimethylformamide. Diethyl ether was slowly diffused into the metal solution in a sealed container from which white crystals suitable for X-ray analysis were obtained. Anal. Calc. % for $C_{18}H_{42}Cd_2N_8O_6Cl_2$; C, 28.36; N, 14.70; H, 5.55. Found: C, 28.20; N, 14.63; H, 5.42.

(*S*)-(-)-1,2-epoxybutane (0.1678 g, 0.002328 mol) was added to $12aneN_3$ (0.1329 g, 0.7759 mmol), which had shown 8 signals on a ^{13}C NMR spectrum, in EtOH (25.00 mL) at room temperature. After three days the solution was evaporated to dryness. DMF (0.50 mL) was then added and left to stand from which clear crystals suitable for X-ray analysis were obtained. MS (ESI): m/z 397 [M^+]. Anal. Calc % for $C_{17}H_{40}N_4O_6$; C, 51.49; N, 14.13; H, 10.17. Found: C, 51.30; N, 14.09; H, 10.11.

5.3 Results and discussion

Crystal and molecular structure results supply invaluable information about the interaction of metal ions with the macrocyclic ligands. In this investigation, crystals suitable for X-ray diffraction determination were grown by diffusion of diethyl ether vapour into a solution of the 1:1 metal-ligand complexes dissolved in DMF. Crystals of Zn(II), Co(II), Cd(II), Cu(II), Ni(II) and Mn(II) metal complexes with THPTACD, Cu(II) metal complexes with THPETACD, Cd(II) metal complexes with $12aneN_3$ and the protonated 1,5-*bis*[(2*S*)-2-hydroxybutyl]-1,5,9-triazacyclododecane were successfully determined. When no crystals were grown after a period of one month, the solutions were taken out of the ether containing container and left to evaporate slowly at room temperature. A crystal structure of a Pb(II)

complex obtained in this manner however, indicated that the acetate counter ions were attached to the metal ion and not the THPTACD ligand that was used in the preparation of the metal complex. Only elemental analysis results for the crystal structures which are discussed in this thesis are presented in corresponding sections.

In this thesis, we will use the notations λ‴ and δ‴ for the two enantiomeric forms of the chair conformation formed by the six-membered chelate rings of the parent macrocyclic ring (**Chart 5.1**). Schlager *et al.,* (1995) used the notations λ′/δ′ and λ″/δ″ for the boat and twist boat conformations, respectively.

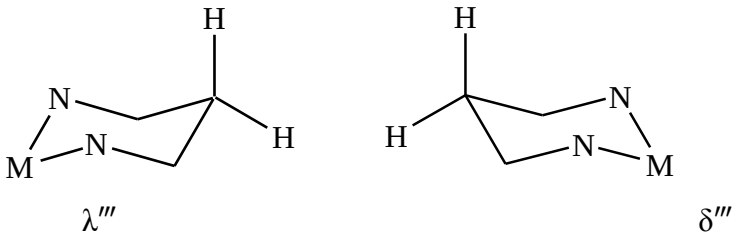

Chart 5.1: Schematic representation of the six-membered chelate ring in chair conformation.

5.3.1 The crystal and molecular structure of the $[Zn(C_{18}H_{39}N_3O_3)](NO_3)_2.H_2O$ complex

The unit cell contains $[Zn(C_{18}H_{39}N_3O_3)]^{2+}$ cationic complex, two nitrate counter ions and a water solvent molecule of crystallisation (**Fig. 5.1**). The compound crystallised in the orthorhombic crystal system, space group $P2_12_12_1$. The crystallographic data and structure refinement details are summarised and presented in **Table 5.20** (at the end of the discussion section).

The molecular structure of the $[Zn(C_{18}H_{39}N_3O_3)]^{2+}$ cationic complex with atom numbering scheme is shown in **Fig. 5.2**. The oxygen donor atoms of the pendant arms are *facially* coordinated to the central metal ion with nitrogen donor atoms on the other side giving rise to a caged-type structure. The Zn(II) metal ion is sitting above the plane defined by the nitrogen donor atoms of the macrocyclic ring.

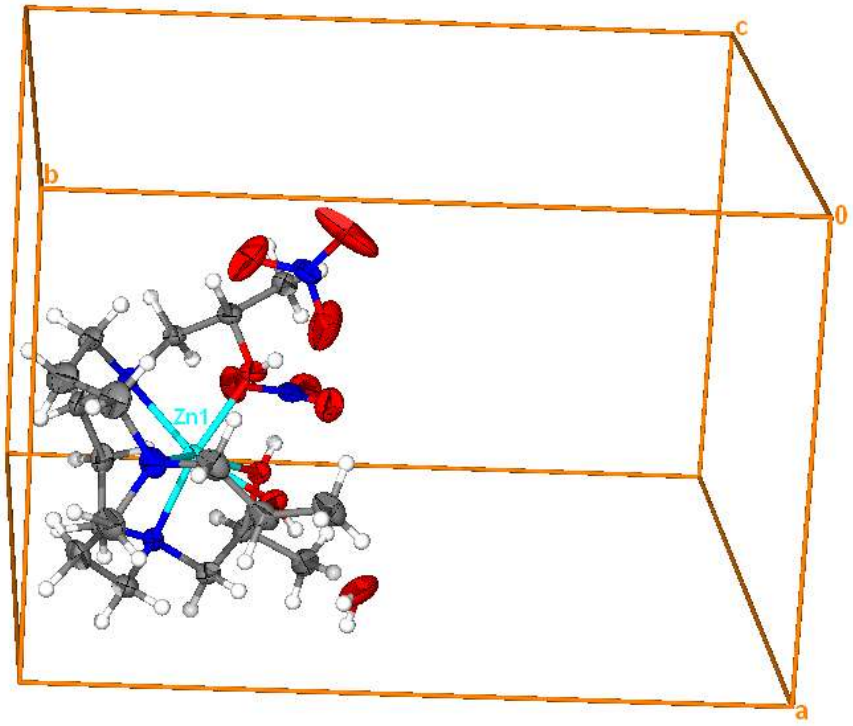

Fig. 5.1: Unit cell and contents of the asymmetric unit of the $[Zn(C_{18}H_{39}N_3O_3)](NO_3)_2.H_2O$ cationic complex (50% thermal ellipsoids).

The ligand imposes a trigonal distortion on the geometry of the complex because the propylene bridges are highly strained and the pendant arms are too short to allow the oxygen donor atoms, complexed to the metal ion, to span idealised 90° bond angles. The trigonal distortion is evident in the three independent intraligand O-Zn-O bond angles which are 84.27(11), 80.06(11) and 82.86(10)° for O1-Zn1-O2, O1-Zn1-O3 and O2-Zn1-O3, respectively. Selected bond lengths and angles are listed in **Table 5.1**. The bond distance of the Zn1-O3 is the longest presumably due to high steric interaction imposed by the crowding of the pendant arms.

The extent of tetragonal distortion can be quantified by the tetragonality parameter, T, which is defined as the average equatorial bond length divided by the average axial bond length (Hathway and Hodgson, 1973). A value of 1 indicates no tetragonal distortion whereas a value greater than 1 indicates an axial compression and less than 1 indicates an axial elongation. The tetragonality value of 1.00 (**Table 5.2**) indicates that Zn(II) metal ion does not undergo electronically induced distortions from an idealised octahedral coordination

environment. The absence of tetragonal distortion in Zn(II) complexes is consistent with the fact that Zn(II) is a d^{10} cation.

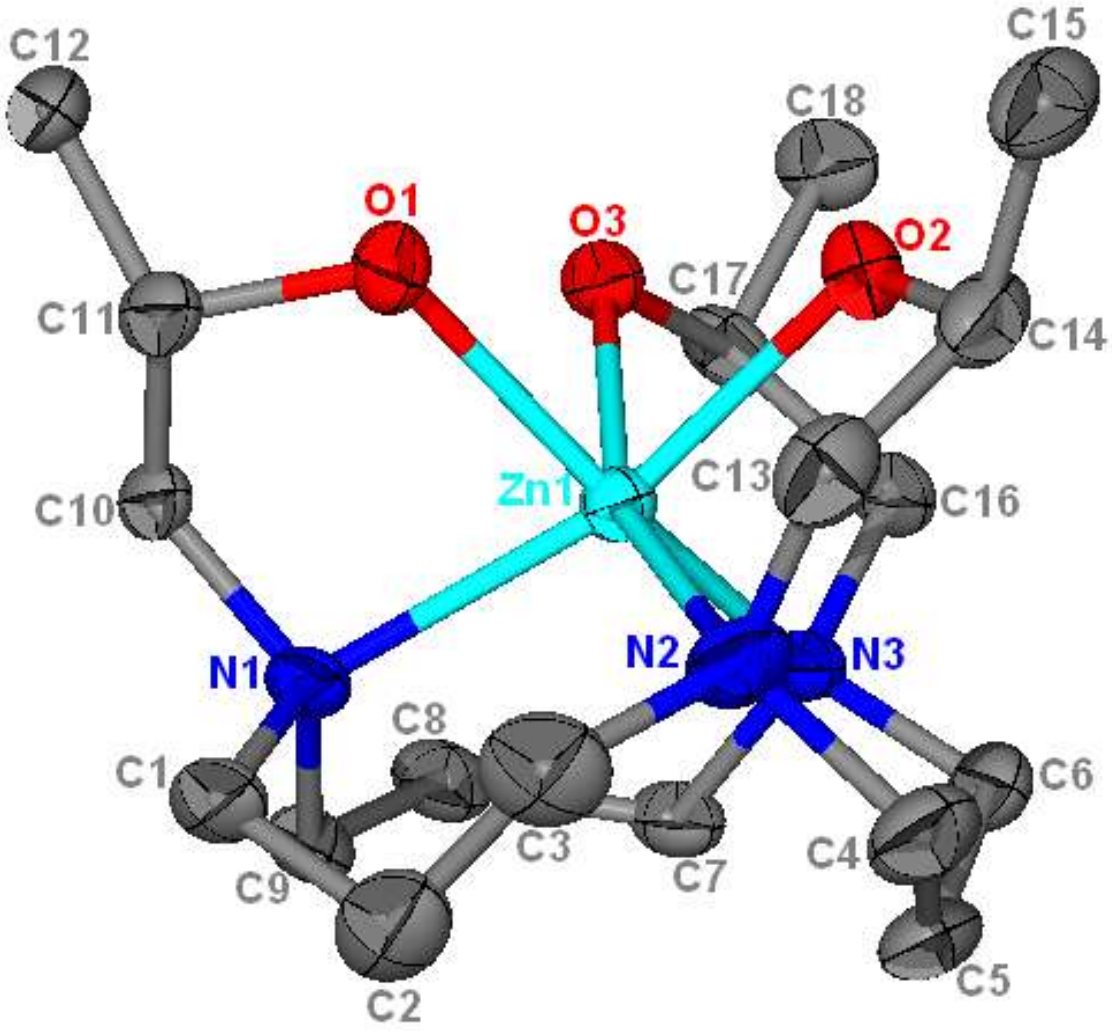

Fig. 5.2: ORTEP diagram of the $[Zn(C_{18}H_{39}N_3O_3)]^{2+}$ cationic complex (50% thermal ellipsoids) (H atoms, H_2O solvent molecule and NO_3^- counter ions are omitted for clarity).

Looking down the *pseudo* C_3 axis, the three oxygen donor atoms of the pendant arms are twisted in an anticlockwise direction with respect to the corresponding three nitrogen donor atoms (**Fig. 5.3**). The C_3 axis is described as *pseudo* or *quasi* because the bond lengths in the three nitrogen donor atoms (or the three oxygen donor atoms) are different such that if the molecule is rotated 120°, the bonds will superimpose but the position of the donor atoms will differ.

Table 5.1: Selected bond lengths and angles for the cationic $[Zn(C_{18}H_{39}N_3O_3)]^{2+}$ complex

Bond Lengths (Å)		**Bond Angles (°)**	
Zn1-O1	2.091(3)	N1-Zn1-O2	160.31(13)
Zn1-O2	2.137(3)	N2-Zn1-O3	160.29(13)
Zn1-O3	2.276(3)	N3-Zn1-O1	155.19(12)
Zn1-N1	2.181(3)	O2-Zn1-N3	98.67(12)
Zn1-N2	2.173(4)	O2-Zn1-O3	82.86(10)
Zn1-N3	2.129(3)	O2-Zn1-O1	84.27(11)

The three twist angles, φ [φ is defined as the angle of twist away from a staggered arrangement of the donor atoms as viewed down the *quasi* C_3 axis; thus φ is 0° for trigonal prismatic and 60° for octahedral geometry (Christiansen *et al.*, 1986)] are reported in **Table 5.3**. The three oxygen donor atoms belonging to the pendant arms are normally expected to be twisted by the same angle with respect to the three nitrogen donor atoms. The results show that this is not the case probably due to steric hindrance in the packing of the molecules. The average twist angle value of 44.1° indicates that the polyhedron can best be described as a distorted octahedron.

The absolute configuration of the complex is Λ-$[Zn(C_{18}H_{39}N_3O_3)](NO_3)_2.H_2O$. The convention adopted in this thesis assigns Δ or Λ to a structure where the trigonal oxygen donor atoms are twisted by an angle φ in the clockwise or anticlockwise direction, respectively, with reference to the trigonal nitrogen donor atoms of the parent ring when viewed down the *quasi* C_3 axis (Taylor *et al.*, 1983).

The three nitrogen donor atoms of the parent macrocyclic ring form six-membered chelate rings whereas oxygen donor atoms of the pendant arms and the corresponding nitrogen donor atoms of the parent ring, on which they are appended, form five-membered chelate rings (**Fig. 5.4**). The six-membered chelate ring adopts a *pseudo* chair conformation.

Table 5.2: The tetragonality parameter, T, of various hexadentate macrocyclic ligands in MO_3N_3 polyhedra discussed in this thesis

	M-D_{eq} (Å)	M-D_{ax} (Å)	T
$Cu(C_{18}H_{39}N_3O_3)^{2+}$	2.0508	2.3705	0.87
$Zn(C_{18}H_{39}N_3O_3)^{2+}$	2.1673	2.1590	1.00
$Cd(C_{18}H_{39}N_3O_3)^{2+,\,a}$	2.3098	2.3255	0.99
$Cd(C_{18}H_{39}N_3O_3)^{2+,\,b}$	2.3195	2.3195	1.00
$Mn(C_{18}H_{39}N_3O_3)^{2+}$	2.2148	2.2595	0.98
$Co(C_{18}H_{39}N_3O_3)^{2+}$	2.1333	2.1965	0.97
$Ni(C_{18}H_{39}N_3O_3)^{2+}$	2.0980	2.1525	0.97
$Cu(C_{33}H_{45}N_3O_3)^{2+}$	2.0663	2.5437	0.81

M-D_{eq} is the average equatorial bond length; M-D_{ax} is the average axial bond length; [a] Cd1- and [b] Cd2-half are the two halves of the hydrogen-bonded $[Cd_2(C_{18}H_{39}N_3O_3)_2]^{4+}$ cationic complex; The MO_3N_3 polyhedron is either an octahedron or trigonal prism and M is the central metal ion (Hathway and Hodgson, 1973).

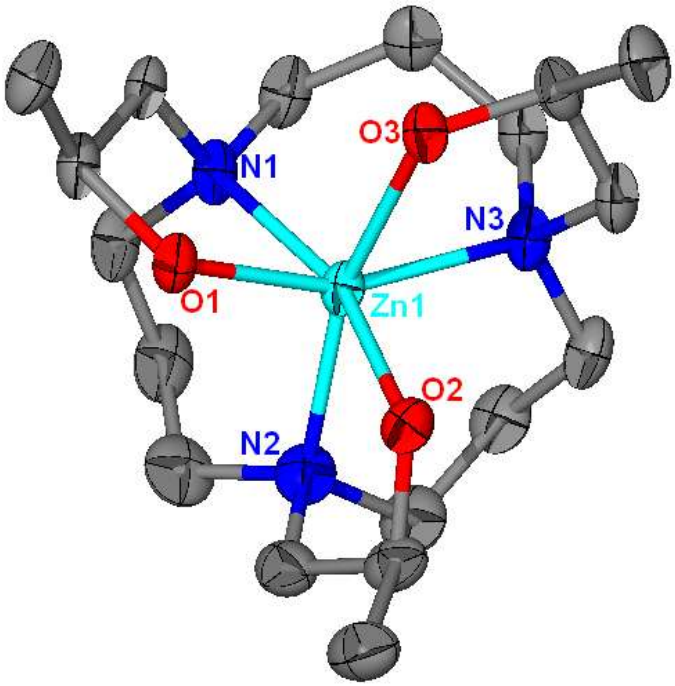

Fig. 5.3: ORTEP diagram of the $[Zn(C_{18}H_{39}N_3O_3)]^{2+}$ cationic complex (50% thermal ellipsoids) looking down the C_3 axis (H atoms, H_2O solvent molecule and NO_3^- counter ions are omitted for clarity).

Two of the endocyclic chelate rings (formed by the nitrogen donor atoms of the parent ring) are in the λ‴ conformation (C2 and C5 pointing away from the metal ion) whereas the third ring is in the δ‴ conformation (**Fig. 5.5**). The exocyclic chelate rings adopt the δ conformation with respect to the equatorial methyl group. The overall chirality description of the complex, using the nomenclature of Taylor *et al.*, (1983) is therefore [Λ((2λ‴)δ‴δ)].

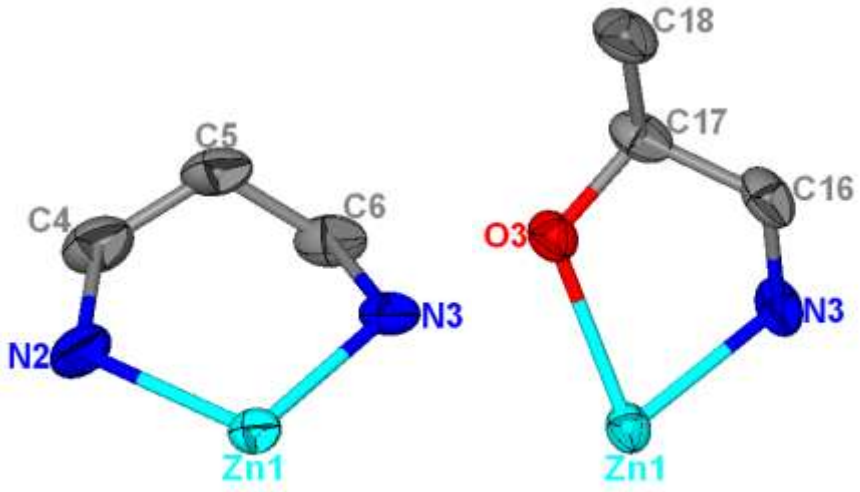

Fig. 5.4: ORTEP diagram of the six-membered chelate ring (left) and five-membered chelate ring (right) of the $[Zn(C_{18}H_{39}N_3O_3)]^{2+}$ cationic complex (50% thermal ellipsoids).

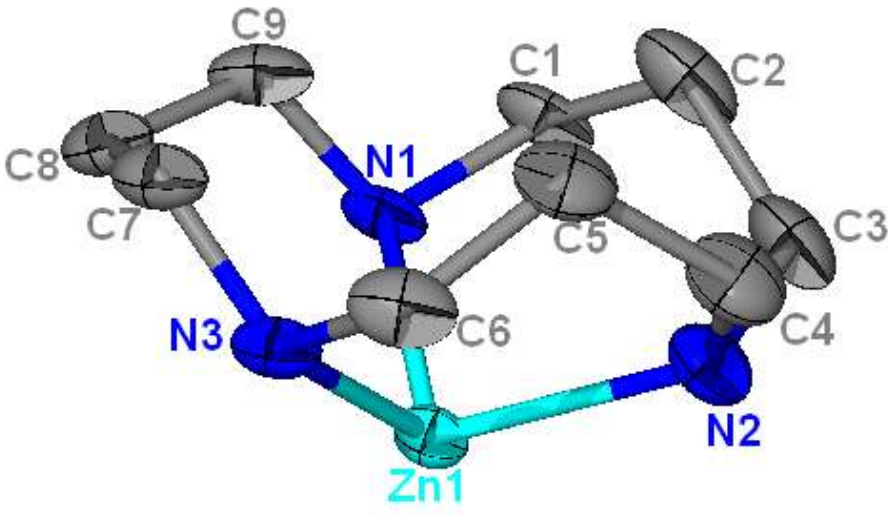

Fig. 5.5: ORTEP diagram of the parent macrocyclic ring of the $[Zn(C_{18}H_{39}N_3O_3)]^{2+}$ cationic complex (50% thermal ellipsoids) showing the six-membered chelate rings.

The bond angles of the six- and five-membered chelate rings are summarised in **Table 5.3**. The six-membered chelate rings form obtuse angles, whereas the five-membered chelate rings form three acute angles. The six-membered chelate ring angles are less than an ideal tetrahedral angle of 109.5° (Martell and Hancock, 1996). There is no reported standard angle value for five-membered chelate rings involving nitrogen and oxygen donor atoms. The bond angles are not symmetrical which can be attributed to steric strain.

Table 5.3: Six- and five-membered chelate ring angles and twist angles for the $[Zn(C_{18}H_{39}N_3O_3)]^{2+}$ cationic complex

6-MCR Bond Angles (°)		**5-MCR Bond Angles (°)**		**Twist Angles (°)**
N1-Zn1-N2	97.50(14)	N1-Zn1-O1	77.97(11)	49.96
N1-Zn1-N3	101.01(13)	N2-Zn1-O2	78.08(13)	49.66
N2-Zn1-N3	101.89(14)	N3-Zn1-O3	75.92(11)	32.58

MCR = Membered Chelate Ring

The crystal is held together by a network of hydrogen bonds involving the hydrogens of the hydroxyl group of the pendant arms and the nitrate counter ions. There is also intermolecular hydrogen bonding between the hydrogens of the hydroxyl group of the pendant arm with the oxygen of the water solvent molecules (**Fig. 5.6**).

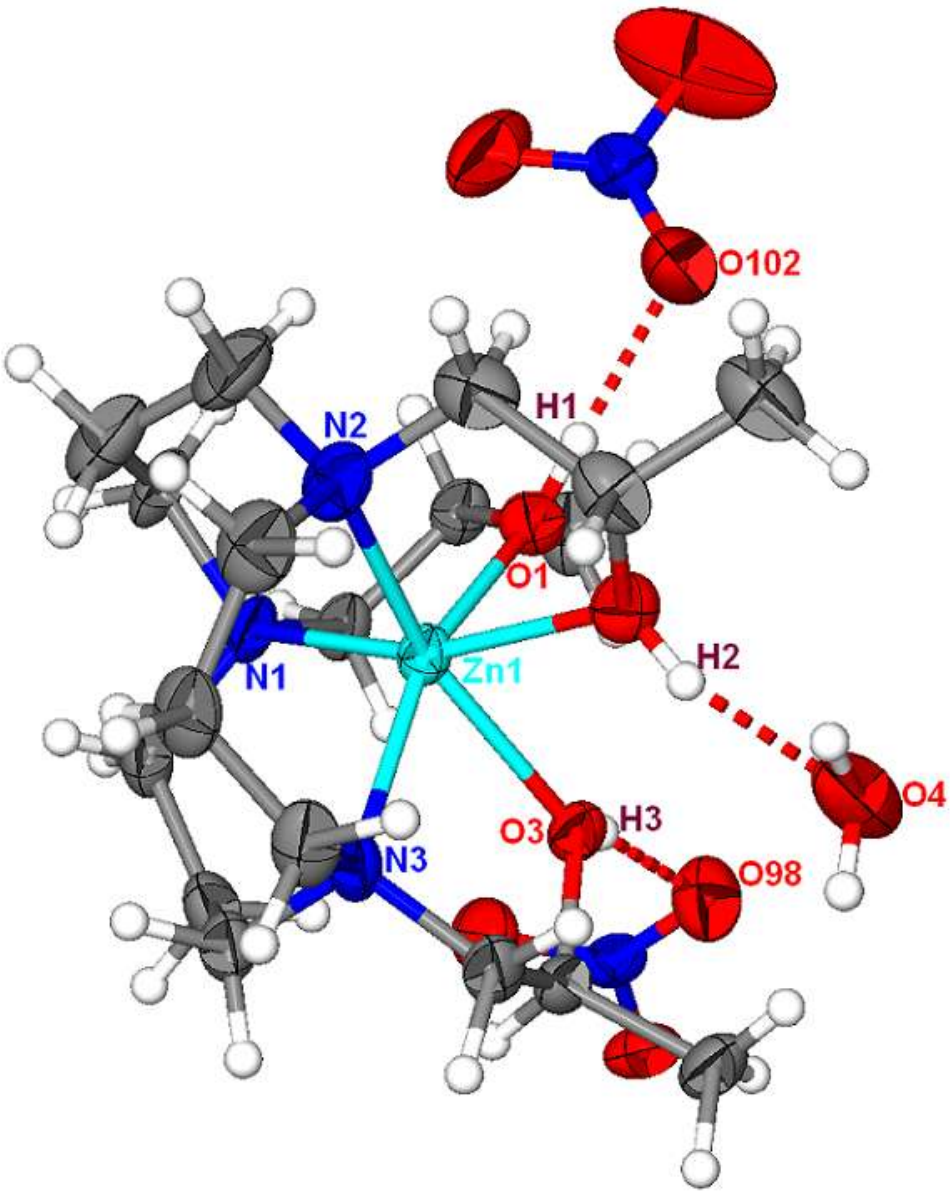

Fig. 5.6: ORTEP diagram of the $[Zn(C_{18}H_{39}N_3O_3)](NO_3)_2.H_2O$ complex (50% thermal ellipsoids) showing a network of hydrogen bonds.

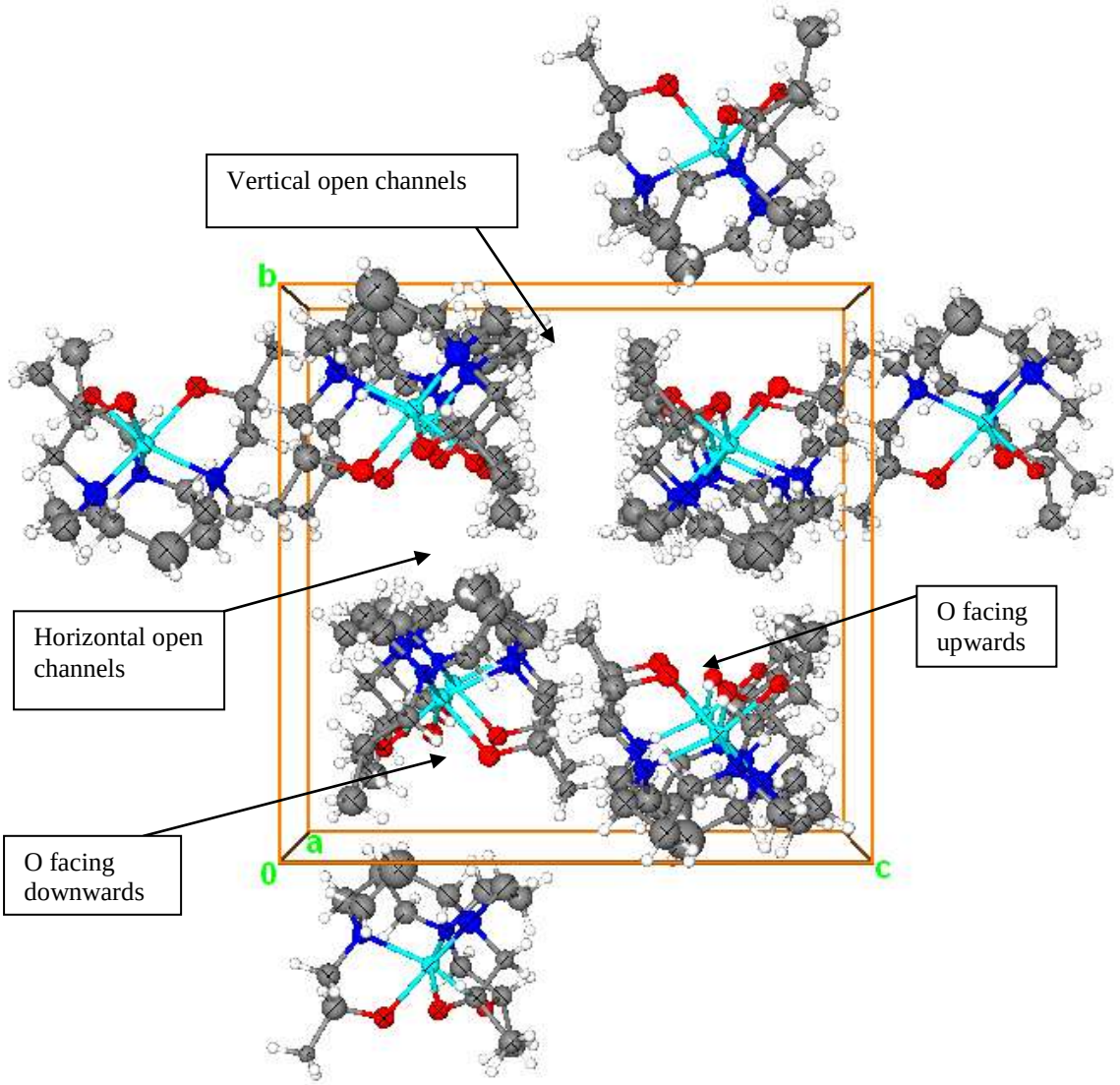

Fig. 5.7: The packing diagram of the $[Zn(C_{18}H_{39}N_3O_3)]^{2+}$ cationic complex (50% thermal ellipsoids) along the a-axis (H atoms, H_2O solvent molecule and NO_3^- counter ions are omitted for clarity).

The water solvent molecules of crystallisation occupy spaces between the metal complexes in horizontal channels, whereas the nitrate counter ions occupy spaces in vertical channels (**Fig. 5.8**).

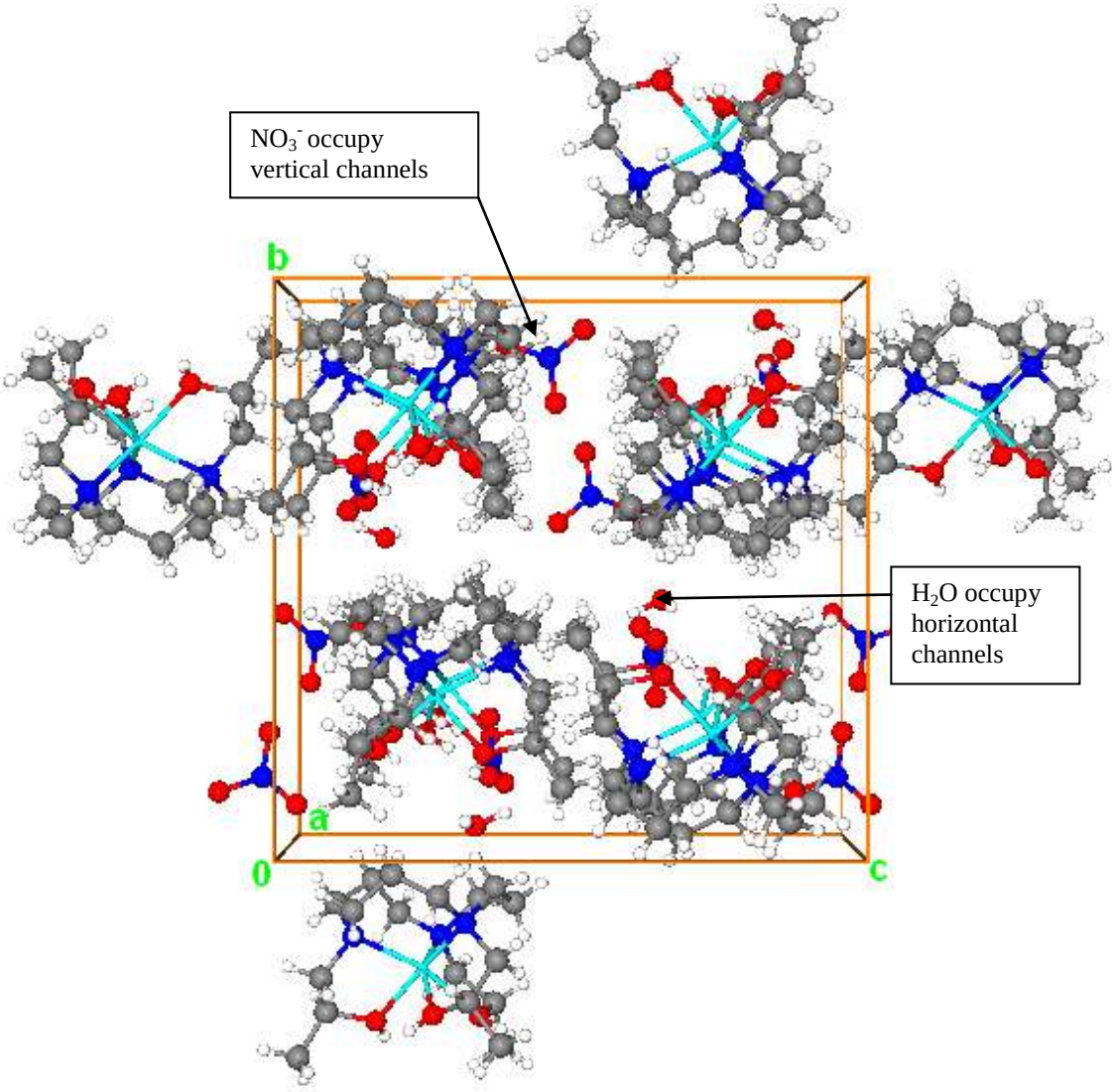

Fig. 5.8: Packing diagram of the $[Zn(C_{18}H_{39}N_3O_3)](NO_3)_2.H_2O$ complex (50% thermal ellipsoids) along the a-axis.

There are no open channels between the two adjacent cationic complexes and the packing along the a-axis can be regarded as a conglomerate of the two cationic complexes held together by the nitrate counter ions and the water solvent molecules (**Fig. 5.7**; **Fig. 5.8**; **Fig. 5.9**).

The average Zn(II)-N bond distance of the molecular structure reported here is 2.161 Å. The average Zn(II)-N bond separations reported in the literature for a THPTACN complexes are 2.143 (Feng *et al.,* 2007) and 2.157 Å (Weeks *et al.,* 2001) making an average difference of 0.011 Å. The average Zn(II)-N bond lengths reported in the literature for a 12aneN_3 complex

are 2.018 Å (Kimura *et al.,* 1990a) and 2.039 Å (Schaber *et al.,* 1988; Notni *et al.,* 2006) giving an average difference of 0.133 Å. The average Zn(II)-N bond length of the molecular structure described here is not significantly different from the literature for the molecular structures with similar pendant arms reported by Feng *et al.,* (2007) and Weeks *et al.,* (2001) but significantly longer than the average bond distance of the parent macrocycle. The bonds in azamacrocycles with pendant arms are elongated due to steric strain brought about by pendant arms. The average Zn(II)-N bond separation of 12aneN_3 with one hydroxyethyl pendant arm, 1-(2-hydroxyethyl)-1,5,9-triazacyclododecane, reported by Kimura *et al.,* (1994) is 2.124 Å, which falls in between that of the parent macrocycle, 12aneN_3 and THPTACD. The average Zn(II)-O bond lengths reported in the literature for a THPTACN ligand are 2.109 Å (Feng *et al.,* 2007) and 2.132 Å (Weeks *et al.,* 2001) and the average distance reported here is 2.168 Å. The average bond lengths are significantly different.

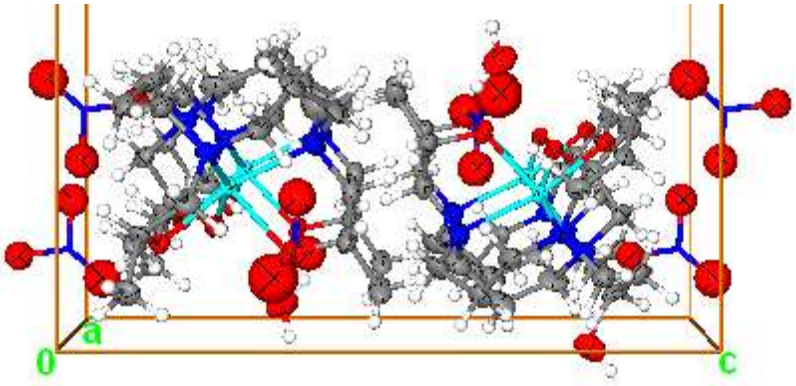

Fig. 5.9: One-half of the unit cell showing Cu(II) cationic conglomerate (50% thermal ellipsoids) along the a-axis.

The average N-Zn(II)-N bite angles reported in the literature for a similar ligand are 82.53° (Feng *et al.,* 2007) and 81.66° (Weeks *et al.,* 2001) and the average bite angle reported in this investigation is 100.1° which is significantly larger. The average N-Zn(II)-N bite angle reported here is for six-membered chelate rings which is normally larger than that of five-membered chelate rings (Martell and Hancock, 1996). The average N-Zn(II)-N bite angles for the parent macrocycle, 12aneN_3, are 105.5° (Kimura *et al.,* 1990) and 104.89° (Schaber *et al.,* 1988) which are larger than the average bite angle reported here probably due to steric strain in the pendant arms. The average O-Zn(II)-O bite angles reported in the literature for a

THPTACN complex are 90.64° (Feng *et al.*, 2007), 86.47° (Weeks *et al.*, 2001) and the average bite angle reported in this research is 82.4°.

5.3.2 The crystal and molecular structure of the $[Co(C_{18}H_{39}N_3O_3)](NO_3)_2.H_2O$ complex

The crystallographic data and structure refinement details of the compound are summarised in **Table 5.21**. The molecular structure of the $[Co(C_{18}H_{39}N_3O_3)]^{2+}$ cationic complex with its atom numbering scheme is shown in **Fig. 5.10**.

The crystal structures of $[Co(C_{18}H_{39}N_3O_3)](NO_3)_2.H_2O$, $[Mn(C_{18}H_{39}N_3O_3)](NO_3)_2.H_2O$, $[Ni(C_{18}H_{39}N_3O_3)](NO_3)_2.H_2O$ and $[Cu(C_{18}H_{39}N_3O_3)](NO_3)_2.H_2O$ are isomorphous with the $[Zn(C_{18}H_{39}N_3O_3)](NO_3)_2.H_2O$ crystal structure discussed in **Section 5.3.1** and only differences will be highlighted.

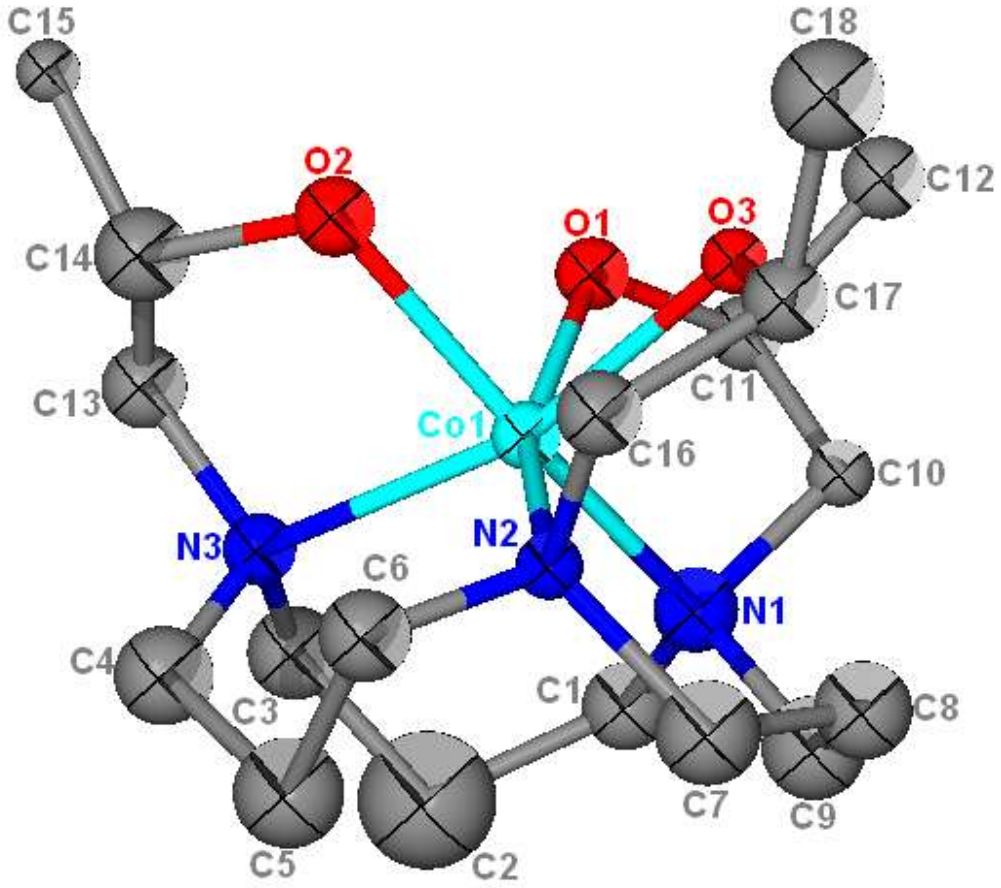

Fig. 5.10: ORTEP diagram of the $[Co(C_{18}H_{39}N_3O_3)]^{2+}$ cationic complex (50% thermal ellipsoids).

Selected bond lengths and angles are listed in **Table 5.4** and the values of the three twist angles are given in **Table 5.5**. The average twist angle value of 41.0° indicates that the geometry around the Co(II) metal ion is distorted octahedral.

Table 5.4: Selected bond lengths and angles for the $[Co(C_{18}H_{39}N_3O_3)]^{2+}$ cationic complex

Bond Lengths (Å)		**Bond Angles (°)**	
Co1-O1	2.078(3)	N1-Co1-O2	161.06(15)
Co1-O2	2.117(3)	N2-Co1-O1	158.89(15)
Co1-O3	2.198(3)	N3-Co1-O3	161.53(14)
Co1-N1	2.192(4)	O1-Co1-N3	101.66(14)
Co1-N2	2.146(4)	O1-Co1-O2	85.80(13)
Co1-N3	2.195(4)	O1-Co1-O3	83.64(13)

The tetragonality value of 0.97 (**Table 5.2**) indicates that Co(II) metal ion is slightly tetragonally elongated. Sakiyama *et al.,* (2004) reported a tetragonally elongated high-spin Co(II) complex and the elongation was attributed to distortion of the first transition band $^4T_1 \rightarrow {}^4T_2(^4F)$.

Table 5.5: Five- and six-membered chelate ring angles and twist angles for the $[Co(C_{18}H_{39}N_3O_3)]^{2+}$ cationic complex

6-MCR Bond Angles (°)		**5-MCR Bond Angles (°)**		**Twist Angles (°)**
N1-Co1-N2	100.34	N1-Co1-O1	77.32	41.34
N1-Co1-N3	96.26	N2-Co1-O3	76.31	42.14
N2-Co1-N3	99.45	N3-Cd1-O2	78.64	39.55

The average Co(II)-N and Co(II)-O bond lengths reported in the literature for a THPTACN complex are 2.117 and 2.087 Å (Feng *et al.,* 2007) and 2.170 and 2.112 Å (Al-Sagher *et al.,* 1993), respectively. The average Co(II)-N and Co(II)-O bond lengths described in this thesis are 2.178 and 2.131 Å, respectively. The average bond lengths reported here are generally significantly different from the literature value.

The average N-Co(II)-N and O-Co(II)-O bite angles reported in the literature for a THPTACN complex are 83.35° and 90.52° (Feng *et al.*, 2007) and 86.10° and 84.1° (Al-Sagher *et al.*, 1993) and the corresponding average bite angles reported here are 98.7° and 84.5°, respectively.

5.3.3 The crystal and molecular structure of the $[Mn(C_{18}H_{39}N_3O_3)](NO_3)_2.H_2O$ complex

The crystallographic data and structure refinement details are summarised in **Table 5.22**. The R-factor of this complex is too high and therefore, bond lengths and angles are not compared to other examples. The molecular structure of the $[Mn(C_{18}H_{39}N_3O_3)]^{2+}$ cationic complex with its atom numbering scheme is shown in **Fig. 5.11**.

Selected bond lengths and angles are listed in **Table 5.6**. The tetragonality value of 0.98 (**Table 5.2**) indicates that Mn(II) metal ion does not undergo electronically induced distortions from its octahedral coordination environment, which is consistent with d^5-systems.

Table 5.6: Selected bond lengths and angles for the $[Mn(C_{18}H_{39}N_3O_3)]^{2+}$ cationic complex

Bond Lengths (Å)		**Bond Angles (°)**	
Mn1-O1	2.178(6)	N1-Mn1-O2	160.5(3)
Mn1-O2	2.246(6)	N2-Mn1-O3	157.0(3)
Mn1-O3	2.155(6)	N3-Mn1-O1	159.5(3)
Mn1-N1	2.273(8)	O3-Mn1-N1	104.6(3)
Mn1-N2	2.261(6)	O3-Mn1-O2	84.9(2)
Mn1-N3	2.265(7)	O3-Mn1-O1	88.9(2)

The values of the three twist angles are shown in **Table 5.7**. The average twist angle value of 26.2° indicates that the geometry around Mn(II) is a distorted trigonal prism.

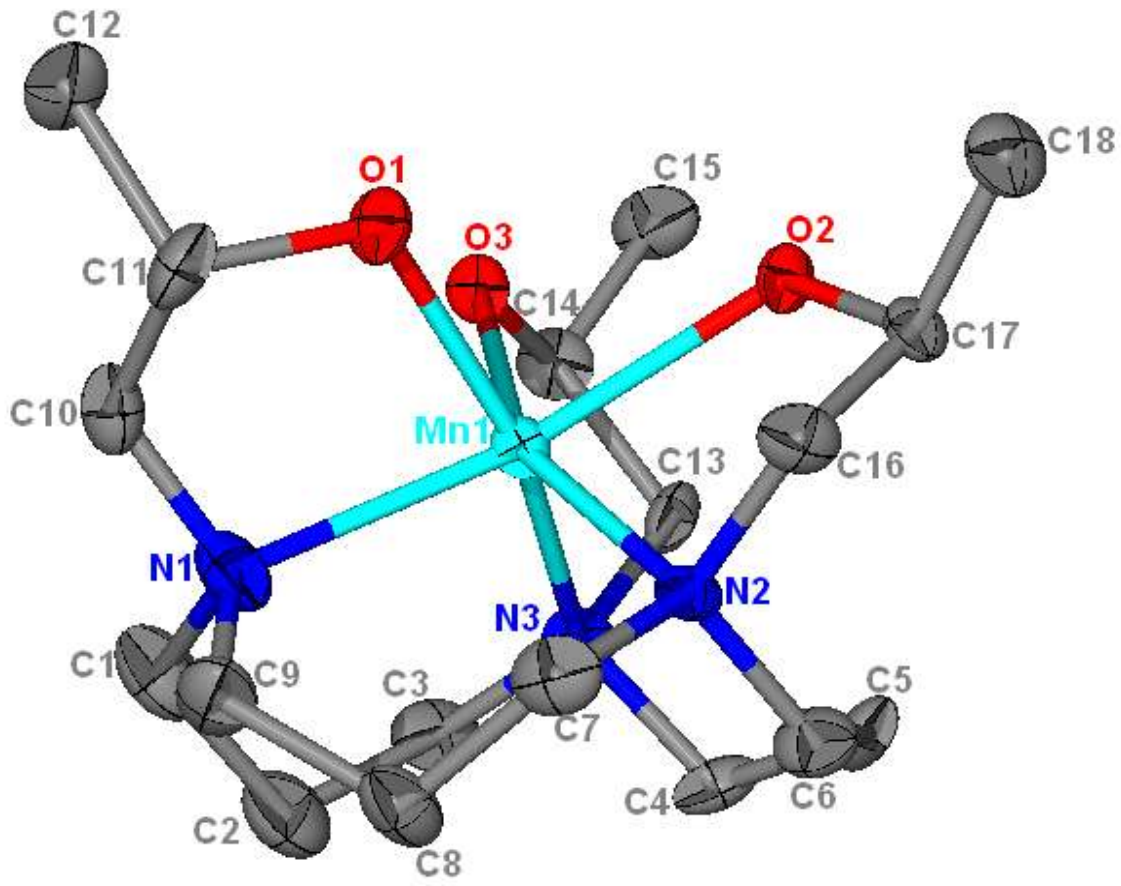

Fig. 5.11: ORTEP diagram of the $[Mn(C_{18}H_{39}N_3O_3)]^{2+}$ cationic complex (50% thermal ellipsoids) (H atoms, H_2O solvent molecule and NO_3^- counter ions are omitted for clarity).

Table 5.7: Six- and five-membered chelate ring angles for the $[Mn(C_{18}H_{39}N_3O_3)]^{2+}$ cationic complex

6-MCR Bond Angles (°)		**5-MCR Bond Angles (°)**		**Twist Angles (°)**
N1-Mn1-N2	97.9(3)	N1-Mn1-O1	76.5(3)	30.01
N1-Mn1-N3	94.3(3)	N2-Mn1-O2	75.1(2)	25.66
N2-Mn1-N3	98.3(3)	N3-Mn1-O3	75.6(2)	22.92

5.3.4 The crystal and molecular structure of the $[Ni(C_{18}H_{39}N_3O_3)](NO_3)_2.H_2O$ complex

The crystallographic data and structure refinement details are summarised in **Table 5.23** and the molecular structure of the $[Ni(C_{18}H_{39}N_3O_3)]^{2+}$ cationic complex with its atom numbering scheme is shown in **Fig. 5.12**.

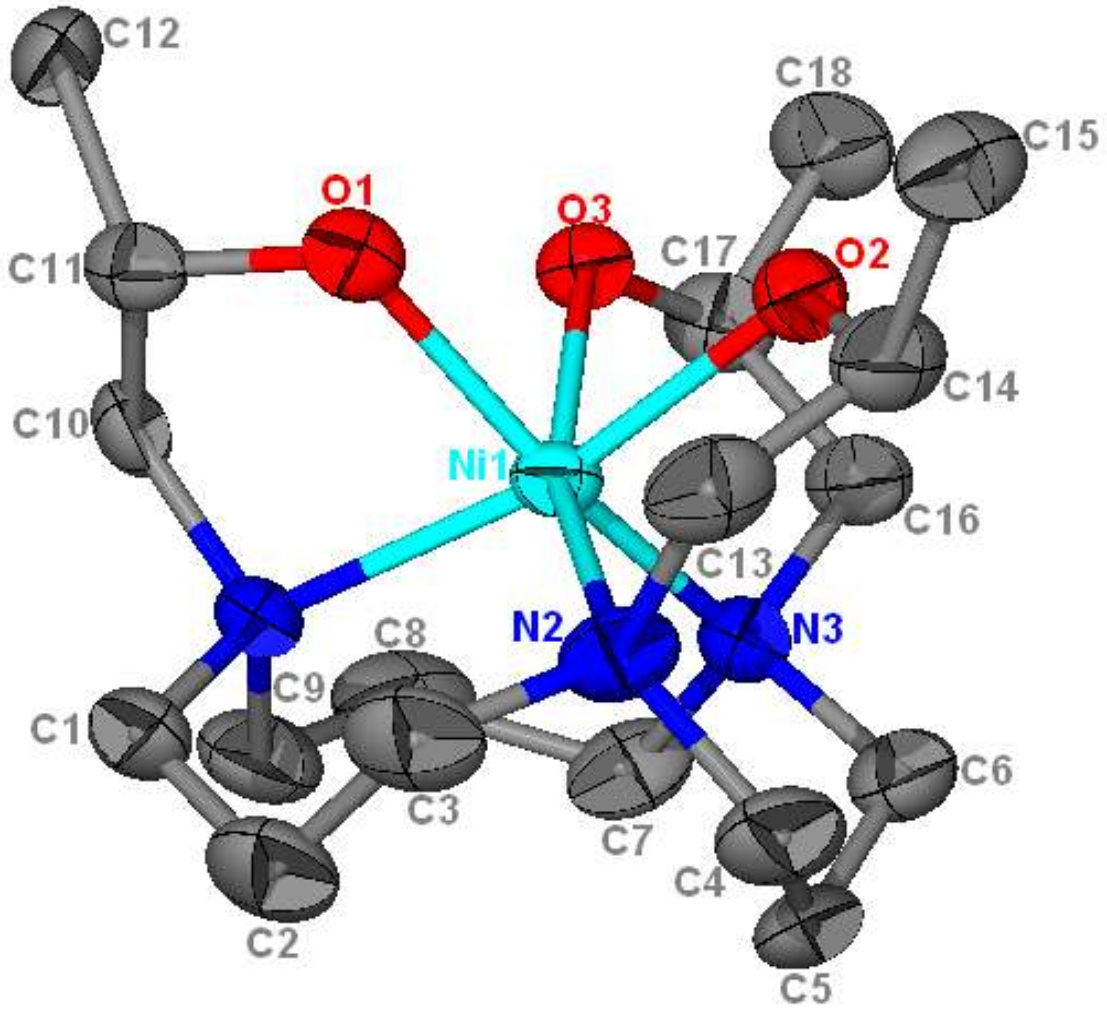

Fig. 5.12: ORTEP diagram of the $[Ni(C_{18}H_{39}N_3O_3)]^{2+}$ cationic complex (50% thermal ellipsoids) (H atoms, H_2O and NO_3^- are omitted for clarity).

Selected bond lengths and angles are listed in **Table 5.8**. The tetragonality parameter value of 0.97 (**Table 5.2**) indicates that the d^8 Ni(II) ion is only slightly tetragonally distorted like Co(II) ion in the $[Co[(C_{18}H_{39}N_3O_3)]^{2+}$ cationic complex. Pujari and Dash, (1976) reported several Ni(II) tetragonally distorted complexes. Weak tetragonal distortion was attributed to triplet $^3A_{2g}$ ground state whereas strong distortion was attributed to a singlet $^1E_g(D)$ ground

state in an octahedral geometry. Shin and Min, (2009) reported a Ni(II) complex with tetragonality value of 0.98.

Table 5.8: Selected bond lengths and angles for the $[Ni(C_{18}H_{39}N_3O_3)]^{2+}$ cationic complex

Bond Lengths (Å)		**Bond Angles (°)**	
Ni1-O1	2.053(4)	N1-Ni1-O2	162.97(19)
Ni1-O2	2.100(4)	N2-Ni1-O3	162.21(19)
Ni1-O3	2.159(4)	N3-Ni1-O1	160.55(18)
Ni1-N1	2.143(5)	O2-Ni1-N3	96.64(18)
Ni1-N2	2.146(5)	O2-Ni1-O3	83.46(15)
Ni1-N3	2.096(5)	O2-Ni1-O1	85.35(16)

The values of the three twist angles are given in **Table 5.9**. The average twist angle value of 26.6° indicates that Ni(II) is more twisted towards a trigonal prism which is nearly the same as the Mn(II) metal complex.

Table 5.9: Six- and five-membered chelate ring angles and twist angles for the $[Ni(C_{18}H_{39}N_3O_3)]^{2+}$ cationic complex

6-MCR Bond Angles (°)		**5-MCR Bond Angles (°)**		**Twist Angles (°)**
N1-Ni1-N2	96.5(2)	N1-Ni1-O1	79.01(17)	27.20
N1-Ni1-N3	100.4(2)	N2-Ni1-O2	79.2(2)	24.39
N2-Ni1-N3	100.4(2)	N3-Ni1-O3	77.67(18)	28.29

The average Ni(II)-N and Ni(II)-O bond separations reported by van der Merwe *et al.,* (1983) for a THPTACN complex are 1.925 and 1.912 Å whereas the corresponding average bond lengths of the complex described here are 2.128 and 2.104 Å, respectively.

The average N-Ni(II)-N and O-Ni(II)-O bite angles reported by van der Merwe *et al.,* (1983) are 89.33 and 91.33°, respectively. The average angles reported here are 99.1 and 84.1°, respectively.

5.3.5 The crystal and molecular structure of the $[Cu(C_{18}H_{39}N_3O_3)](NO_3)_2.H_2O$ complex

The crystallographic data and structure refinement details are summarised and presented in **Table 5.24**. The molecular structure of the $[Cu(C_{18}H_{39}N_3O_3)]^{2+}$ cationic complex with atom numbering scheme is shown in **Fig. 5.13**.

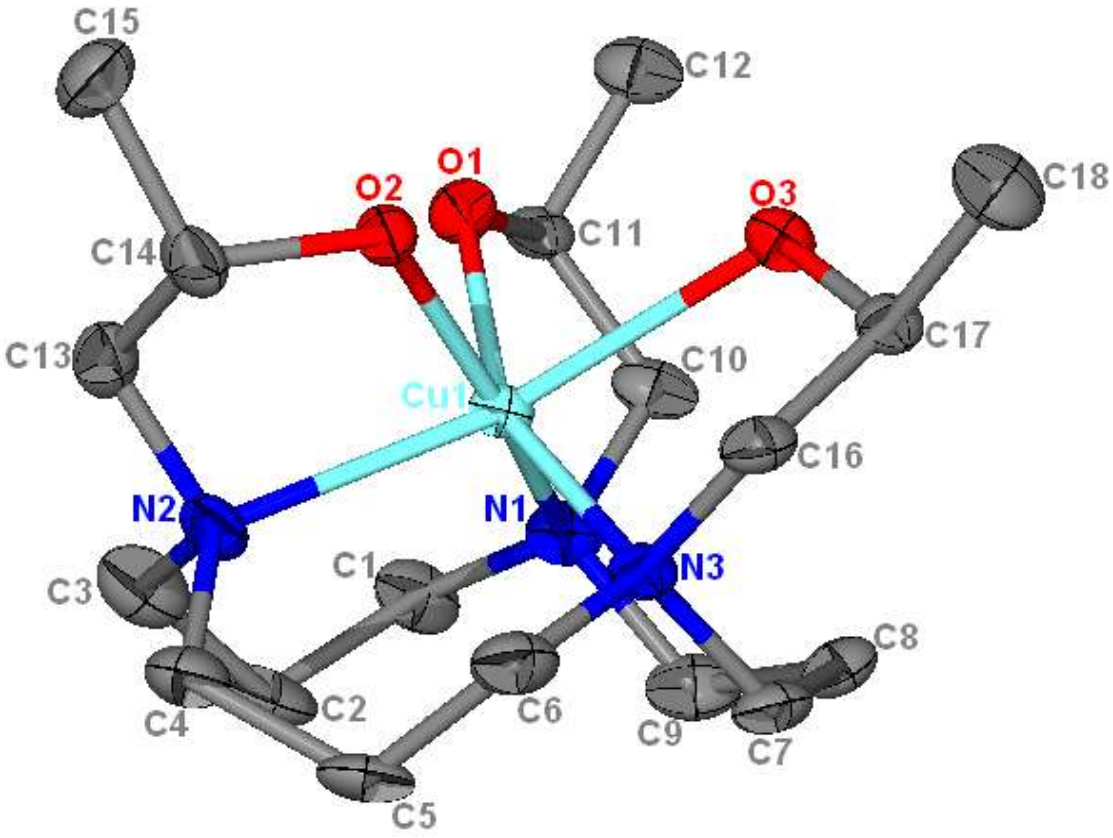

Fig. 5.13: ORTEP diagram of the $[Cu(C_{18}H_{39}N_3O_3)]^{2+}$ cationic complex (50% thermal ellipsoids) showing the Cu(II) cation between the two sets of donor atoms (H atoms, H_2O solvent molecule and NO_3^- counter ions are omitted for clarity).

The trigonal distortion is evident in the three intraligand O-Cu-O angles which are 84.69(14), 82.06(13) and 83.11(13)° for O1-Cu1-O2, O1-Cu1-O3 and O2-Cu1-O3, respectively. The two *trans*-oriented Cu-N and Cu-O axial bonds are significantly elongated relative to the equatorial bonds; the axial Cu-N2 and Cu-O3 bond lengths are 2.291(4) and 2.451(4) Å, respectively. Selected bond lengths and angles are listed in **Table 5.10**.

Table 5.10: Selected bond lengths and angles for the $[Cu(C_{18}H_{39}N_3O_3)]^{2+}$ cationic complex

Bond Lengths (Å)		**Bond Angles (°)**	
Cu1-O1	2.002(3)	N1-Cu1-O2	162.86(16)
Cu1-O2	2.069(3)	N2-Cu1-O3	159.50(14)
Cu1-O3	2.451(4)	N3-Cu1-O1	157.09(15)
Cu1-N1	2.053(4)	O2-Cu1-N1	162.87(16)
Cu1-N2	2.290(4)	O1-Cu1-O2	84.69(14)
Cu1-N3	2.079(4)	O3-Cu1-O1	82.06(15)

The small trigonal distortion does not resolve the e_g orbital degeneracy present in octahedral d^9 Cu(II) complexes and, therefore, the Cu(II) complexes exhibit further tetragonal distortions due to a first-order Jahn-Teller effect (Kavana *et al.,* 2000). The degeneracy is resolved by distortion along a vibrational mode which either compresses or elongates one axis and does the opposite to the other two axes. The $[Cu(C_{18}H_{39}N_3O_3)]^{2+}$ cationic complex has a tetragonality value of 0.87 indicating that the Cu(II) complex is tetragonally elongated (**Table 5.2**).

The three twist angles are reported in **Table 5.11**. The average value of the three twist angles reported here is 21.7° and, therefore, the $[Cu(C_{18}H_{39}N_3O_3)]^{2+}$ cationic complex can best be described as having a *pseudo* trigonal prism configuration. Simple ligand field stabilisation energy arguments (Zuckerman, 1965; Krishnamurthy and Schaap, 1969) show that for a d^9 electronic configuration, an octahedral geometry is favoured by only 0.5 Dq (with Dq the octahedral crystal field parameter) over a prismatic arrangement. The crystal field stabilisation energy (CFSE) provides very little preference for either of the two geometries and the observed geometry is dictated by the packing forces of the complex. This possibility is supported by the observation that the $[Cu(C_{33}H_{45}N_3O_3)](NO_3)_2$ crystal structure described in **Section 5.3.7** has an average twist angle value of 41.8°, which is close to octahedral geometry.

The average Cu(II)-N and Cu(II)-O bond lengths reported in the literature for a THPTACN complex are 2.087 and 2.129 Å (Feng *et al.,* 2007) and 2.101 and 2.132 Å (Han *et al.,* 2004), respectively. The corresponding average bond distances reported here are 2.174 and 2.314 Å,

which mean that the average bond lengths reported here are significantly different from the literature values.

Table 5.11: Six- and five-membered chelate ring angles and twist angles for the $[Cu(C_{18}H_{39}N_3O_3)]^{2+}$ cationic complex

6-MCR Bond Angles (°)		**5-MCR Bond Angles (°)**		**Twist Angles (°)**
N1-Cu1-N2	98.10	N1-Cu1-O1	80.08	29.47
N1-Cu1-N3	101.56	N2-Cu1-O2	77.64	16.32
N2-Cu1-N3	99.51	N3-Cu1-O3	75.25	19.32

The average N-Cu(II)-N and O-Cu(II)-O bite angles reported in the literature for a THPTACN complex are 85.13 and 88.29° (Feng *et al.,* 2007) and 84.80 and 88.73° (Han *et al.,* 2004), respectively. The corresponding average bite angles of the molecular structure reported here are 99.7 and 83.0°. The average corresponding bond angles reported here are significantly smaller than the literature values probably because of ring strain in a small macrocyclic ring, reported in the literature, which pushes the pendant arms away from the central metal. There is no report of the Cu(II) crystal of the parent macrocyclic ligand, $12aneN_3$.

5.3.6 The crystal and molecular structure of the hydrogen-bonded $[Cd_2(C_{18}H_{39}N_3O_3)_2](NO_3)_4.(C_3H_7NO)_2$ complex

The asymmetric unit contains two $[Cd(C_{18}H_{39}N_3O_3)]^{2+}$ cationic complexes, four nitrate counter ions and two DMF solvent molecules (**Fig. 5.14**). The complex crystallised in the monoclinic crystal system, space group $P2_1$. The two cadmium complexes present in the asymmetric unit are crystallographically independent. The crystallographic data and structure refinement details are summarised in **Table 5.25**.

The molecular structure of the $[Cd_2(C_{18}H_{39}N_3O_3)_2]^{4+}$ cationic complex with atom numbering scheme is shown in **Fig. 5.15**. Each Cd(II) cation is again *facially* coordinated to three oxygen donor atoms of the pendant arms and the three nitrogen donor atoms of the parent macrocyclic ring.

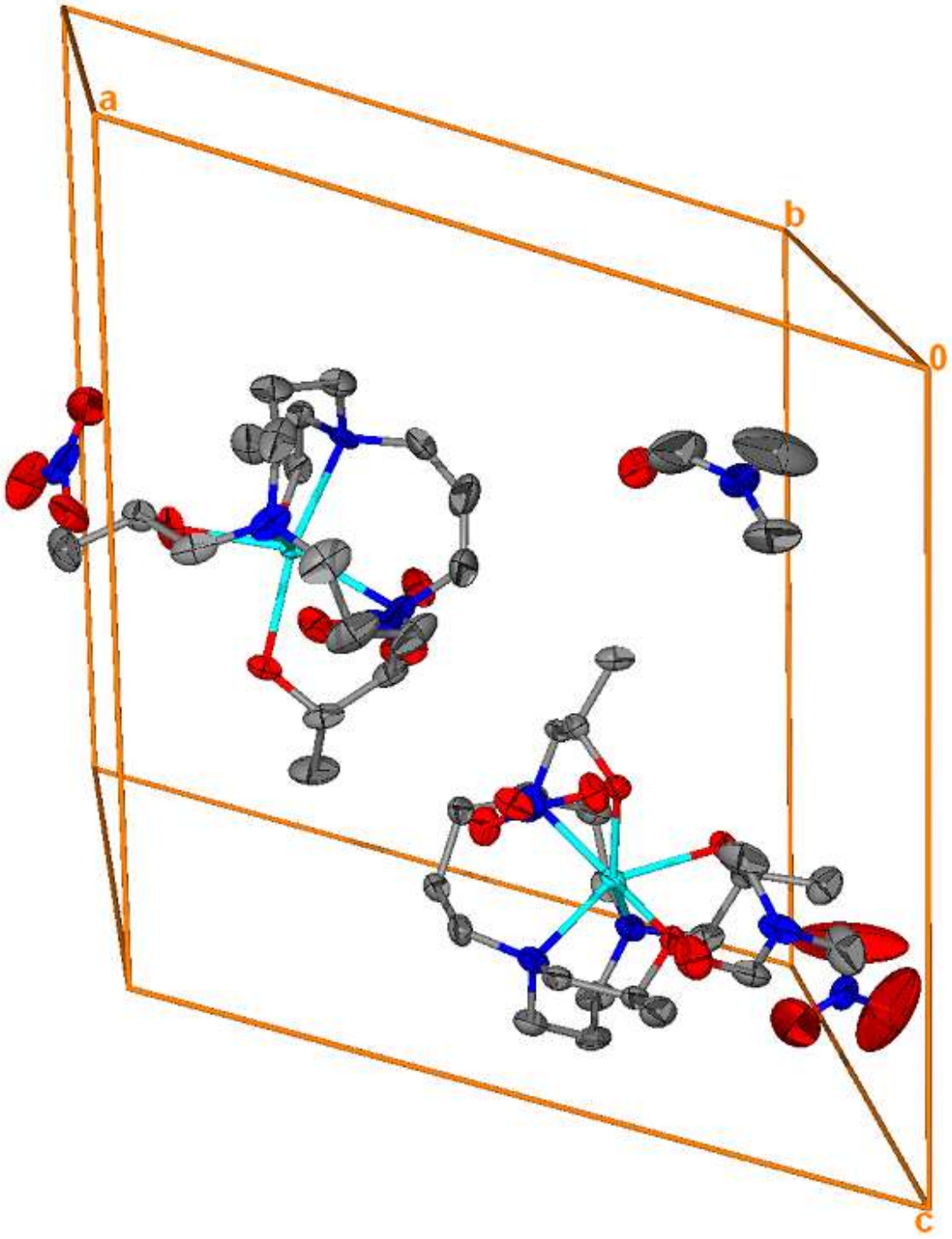

Fig. 5.14: The unit cell and contents of the asymmetric unit of the $Cd_2[(C_{18}H_{39}N_3O_3)_2](NO_3)_4.(C_3H_7NO)_2$ complex (50% thermal ellipsoids). The dimer is held together by a network of hydrogen bonds not shown in the figure.

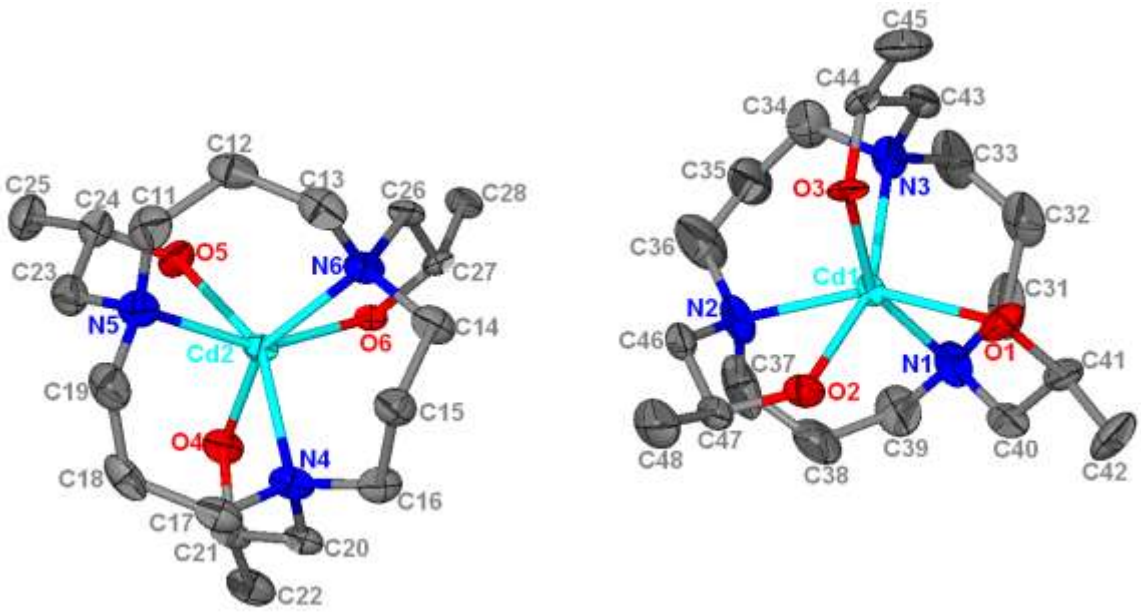

Fig. 5.15: ORTEP diagram of the hydrogen-bonded $[Cd_2(C_{18}H_{39}N_3O_3)_2]^{4+}$ cationic complex (50% thermal ellipsoids) (H atoms, NO_3^- counter ions and DMF solvent molecules are omitted for clarity).

The two independent Cd(II) complexes are designated as Cdl and Cd2 and in both cases the metal ion is positioned above the macrocyclic hole. The corresponding bond lengths and angles in the two complexes are significantly different. For example, the bond lengths for Cd1-O1 and Cd2-O5 are 2.279(4) and 2.316(4) Å, respectively. A search for missed symmetry elements with the program Platon did not detect any additional symmetry (Spek, 2003).

The two sets of the oxygen donor atoms of the pendant arms face in the opposite directions and the two nitrate counter ions occupy the space between the two Cd(II) complexes with the remaining two nitrate counter ions on each end of the two complexes in an asymmetric unit cell. The arrangement is similar to the packing arrangement of the Zn(II) cationic conglomerate but with nitrate counter ions between the two Cd(II) complexes (compare **Fig. 5.9** and **Fig. 5.16**).

The molecular structure of the Cd1 cationic complex with the donor atom numbering scheme is shown in **Fig. 5.17**. Selected bond lengths and angles are listed in **Table 5.12**. The absolute configuration of the Cd1-half of the dimeric complex is Λ-$[Cd(C_{18}H_{39}N_3O_3)](NO_3)_2.(C_3H_7NO)$. The three twist angle values are given in **Table 5.13**.

The average twist angle value of 31.3° indicates that the Cd1 polyhedron can best be described as mid-way between a trigonal prism and octahedron.

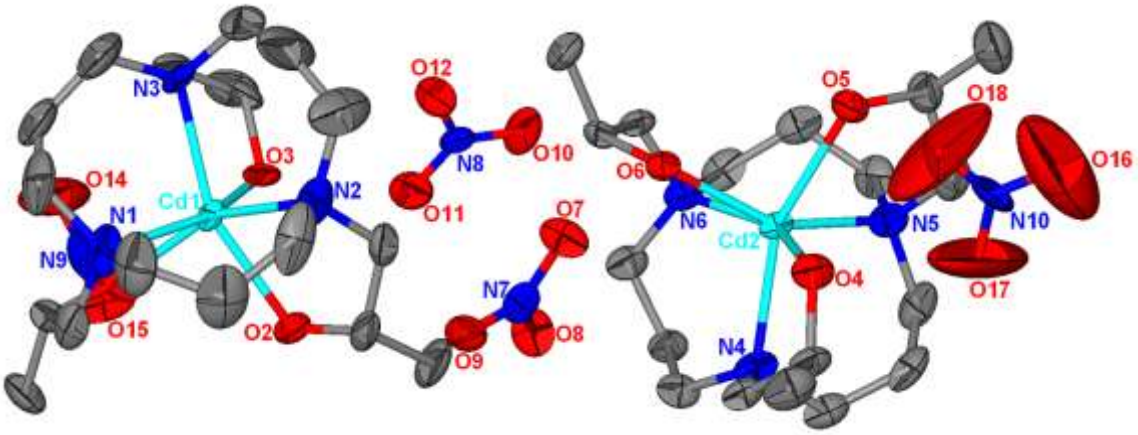

Fig. 5.16: ORTEP diagram of the $Cd_2[(C_{18}H_{39}N_3O_3)_2](NO_3)_4.(C_3H_7NO)_2$ complex (50% thermal ellipsoids) showing nitrate counter ions between the two $[Cd(C_{18}H_{39}N_3O_3)]^{2+}$ cationic complexes (H atoms and DMF solvent molecules are omitted for clarity).

The tetragonality value of 0.99 (**Table 5.2**) indicates that the Cd1 complex unit does not undergo any electronically induced distortions from the idealised octahedral-like coordination which is typical of d^{10} cations.

Table 5.12: Selected bond lengths and angles for the Cd1-half of the $[Cd_2(C_{18}H_{39}N_3O_3)_2]^{4+}$ cationic complex

Bond Lengths (Å)		**Bond Angles (°)**	
Cd1-O1	2.279(4)	N1-Cd1-O3	154.94(18)
Cd1-O2	2.317(4)	N3-Cd1-O2	155.07(17)
Cd1-O3	2.320(4)	N2-Cd1-O1	155.50(2)
Cd1-N1	2.331(5)	O3-Cd1-N2	107.71(19)
Cd1-N2	2.326(5)	O3-Cd1-O2	85.45(14)
Cd1-N3	2.317(5)	O3-Cd1-O1	85.90(14)

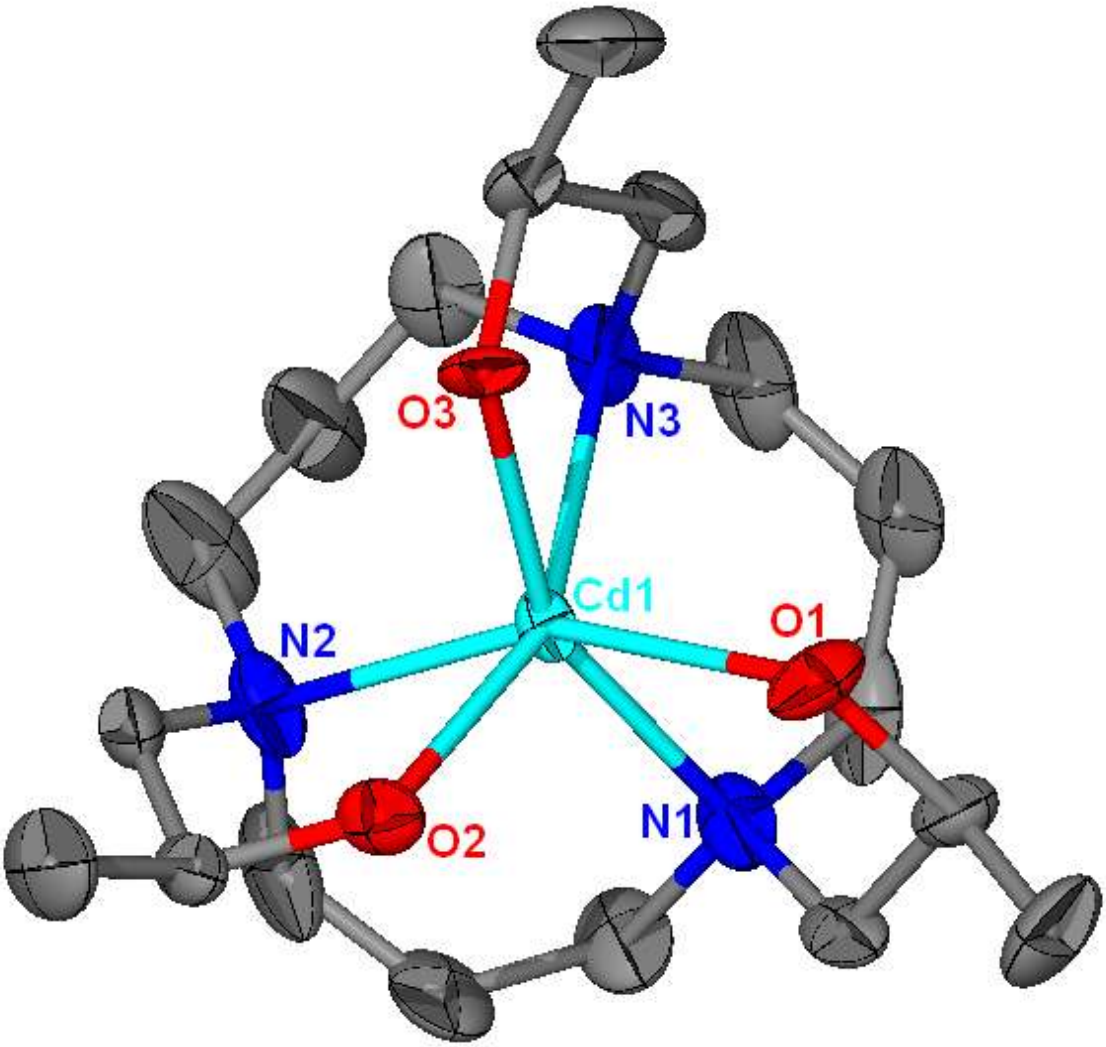

Fig. 5.17: ORTEP diagram for the Cd1-half of the $[Cd_2(C_{18}H_{39}N_3O_3)_2]^{4+}$ cationic complex (50% thermal ellipsoids) looking down the *quasi* C_3 axis.

Two of the endocyclic chelate rings (formed by the nitrogen donor atoms of the parent ring) are in the δ‴ conformation whereas the third ring is in the λ‴ (**Fig. 5.18**). The exocyclic chelate rings adopt the δ conformation. The overall chirality description of the complex is therefore [Λ(λ‴(2δ‴)δ)]. This is in contrast to the overall chirality of the Zn(II) complex which is [Λ(2λ‴)δ‴δ)].

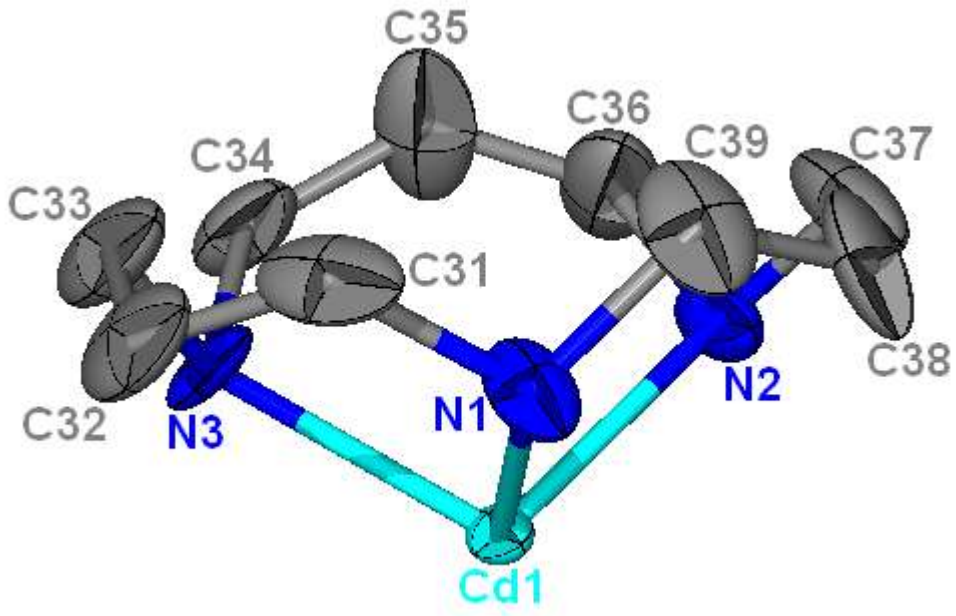

Fig. 5.18: ORTEP diagram of the three six-membered chelate rings of the parent macrocyclic ring of Cd1-half of the hydrogen-bonded $[Cd_2(C_{18}H_{39}N_3O_3)_2]^{4+}$ cationic complex (50% thermal ellipsoids).

The bond angles of the six- and five-membered chelate rings are summarised in **Table 5.13**.

Table 5.13: Six- and five-membered chelate ring angles and twist angles for the Cd1-half of the $[Cd_2(C_{18}H_{39}N_3O_3)_2]^{4+}$ cation complex

6-MCR Bond Angles (°)		**5-MCR Bond Angles (°)**		**Twist Angles (°)**
N1-Cd1-N2	96.6(2)	N1-Cd1-O1	73.71(18)	31.53
N1-Cd1-N3	96.6(2)	N2-Cd1-O2	74.24(18)	31.13
N2-Cd1-N3	96.8(2)	N3-Cd1-O3	75.06(17)	31.15

The molecular structure of the Cd2 cationic complex with the donor atom numbering scheme is shown in **Fig. 5.19**. Selected bond lengths and angles are listed in **Table 5.14**. The configuration of the Cd1- and Cd2-half of the complex is essentially the same (compare **Fig. 5.17** and **Fig. 5.18**) and the values of the three twist angles are listed in **Table 5.15**. The average twist angle value of 28.3° indicates that the Cd2-half of the complex is again half-way between a trigonal prism and octahedron.

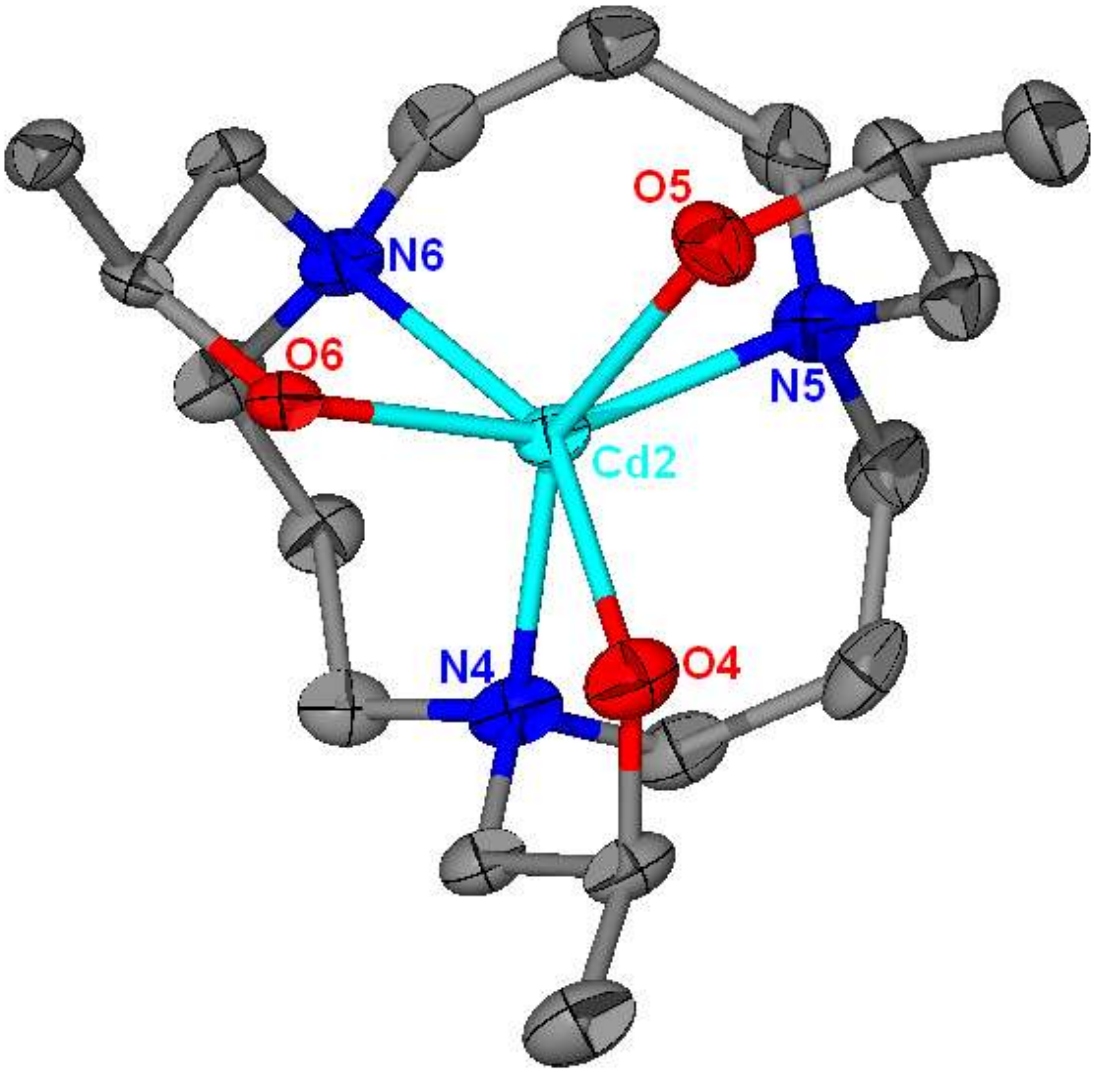

Fig. 5.19: ORTEP diagram for the Cd2-half of the $[Cd_2(C_{18}H_{39}N_3O_3)_2]^{4+}$ cationic (50% thermal ellipsoids) looking down the *pseudo* C_3 axis.

The tetragonality value of 1.00 (**Table 5.2**) indicates that the Cd2-half of the $[Cd_2(C_{18}H_{39}N_3O_3)_2]^{4+}$ cationic complex does not undergo electronically induced distortions.

The bonds angles of the five- and six-membered chelate rings are summarised in **Table 5.15**. The parent macrocyclic rings of the two Cd(II)-halves of the cationic compound have also the same conformation (compare **Fig. 5.18** and **Fig. 5.20**) and overall chirality.

Table 5.14: Selected bond angles and lengths for the Cd2-half of the $[Cd_2(C_{18}H_{39}N_3O_3)_2]^{4+}$ cationic complex

Bond Lengths (Å)		**Bond Angles (°)**	
Cd2-O4	2.317(5)	N4-Cd2-O5	151.87(17)
Cd2-O5	2.316(4)	N5-Cd2-O6	153.06(16)
Cd2-O6	2.307(4)	N6-Cd2-O4	152.90(17)
Cd2-N4	2.317(5)	O5-Cd2-N6	110.69(17)
Cd2-N5	2.332(5)	O5-Cd2-O4	83.09(15)
Cd2-N6	2.328(5)	O5-Cd2-O6	86.22(14)

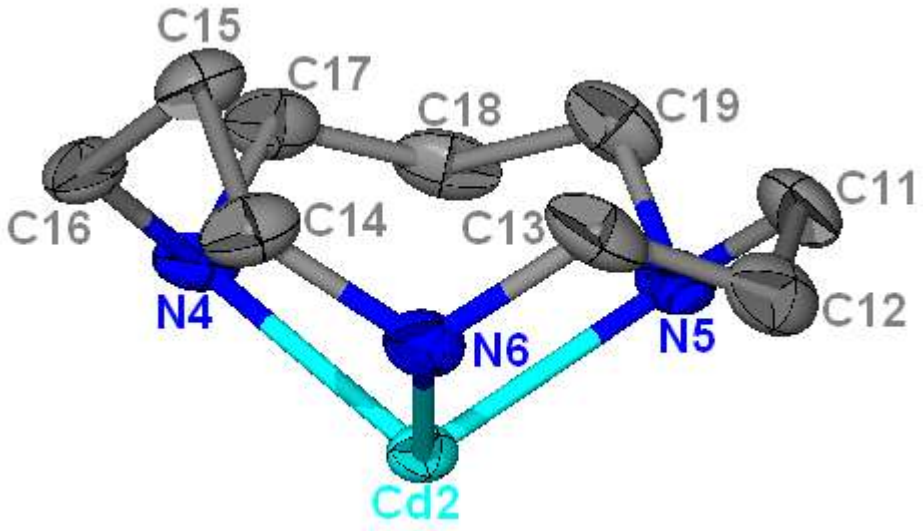

Fig. 5.20: ORTEP diagram of the three six-membered chelate rings of the parent macrocyclic ring of Cd2-half of the hydrogen-bonded $[Cd_2(C_{18}H_{39}N_3O_3)_2]^{4+}$ cationic complex (50% thermal ellipsoids).

Table 5.15: Six- and five-membered chelate ring angles and three twist angles for the Cd2-half of the $[Cd_2(C_{18}H_{39}N_3O_3)_2]^{4+}$ cationic complex

6-MCR Bond Angles (°)		**5-MCR Bond Angles (°)**		**Twist Angles (°)**
N6-Cd2-N5	94.47(18)	N6-Cd2-O6	74.71(15)	28.83
N5-Cd2-N4	98.67(18)	N4-Cd2-O4	74.19(15)	26.38
N4-Cd2-N6	96.89(17)	N5-Cd2-O5	74.46(17)	29.69

It is interesting to note that for Cd2, the three six-membered chelate ring angles are less symmetrical than the three five-membered chelate ring angles which is the opposite of Cd1-half of the cationic complex (**Table 5.13** and **Table 5.15**).

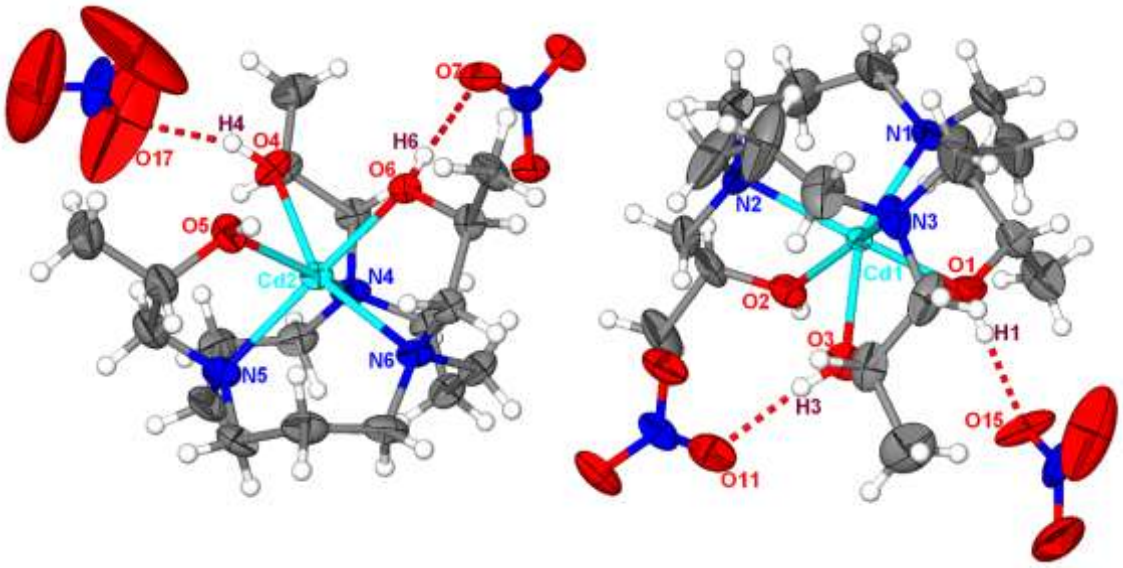

Fig. 5.21: ORTEP diagram of the $Cd_2[(C_{18}H_{39}N_3O_3)_2](NO_3)_4.(C_3H_7NO)_2$ cationic complex (50% thermal ellipsoids) showing hydrogen bonds (DMF omitted for clarity).

The molecular structure shows some steric crowding of the co-ordinated ligands, with short H·····H contacts between hydrogens on the adjacent pendant arms (**Fig. 5.22**). This acts to increase the van der Waals repulsions of the molecule.

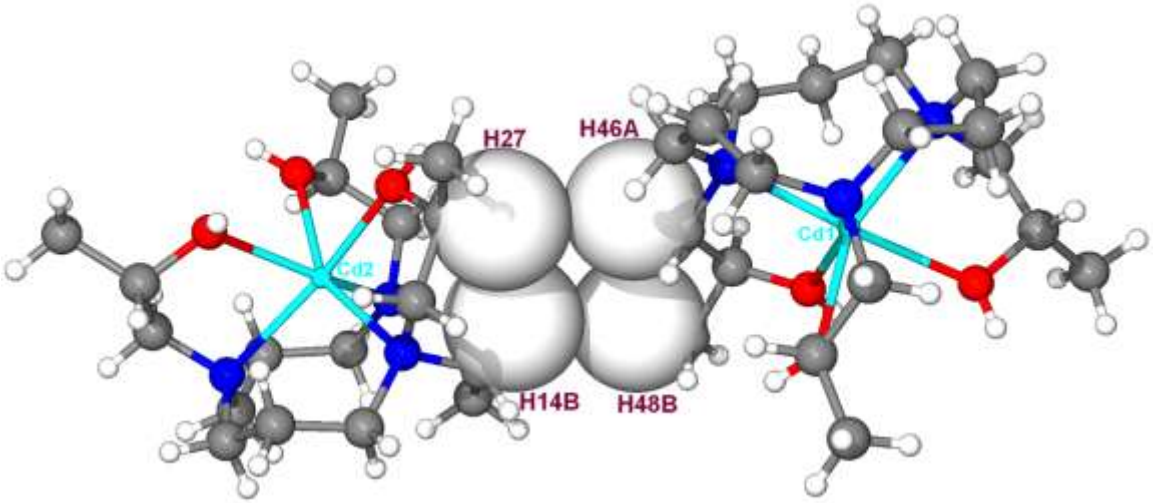

Fig. 5.22: Space filling diagram of the two pairs of hydrogen atoms in close proximity (50% thermal ellipsoids).

An extensive hydrogen bonding network involving hydrogen atoms of the hydroxyl group of the pendant arms with the oxygen atoms of the nitrate counter ions is present in the complex (**Fig. 5.21**).

The channels occupied by solvent molecules and counter ions are encroached by the methyl groups of the pendant arms (**Fig. 5.23**). This is in contrast to the crystal packing of Cu(II) and Zn(II) complexes, along the a-axis, which may be the cause of severe van der Waals repulsions and hence high steric strain in the $[Cd(C_{18}H_{39}N_3O_3)]^{2+}$ cationic complex.

The average Cd-N bond length reported in the literature for the Cd(II) molecular structure of $11aneN_3$ is 2.395 Å (Zompa 1995) and the average Cd-N of the $12aneN_3$ molecular structure reported in **Section 5.3.9** is 2.321 Å. The average Cd-N bond separations reported here are 2.325 and 2.326 Å for Cd1 and Cd2 halves of the complex, respectively. The average difference in Cd-N bond distances for the $12aneN_3$ and the ones reported here are not significantly different but differ significantly with the average literature value of the $11aneN_3$ complex. There is no report for a crystal structure of a Cd(II) complex with a macrocycle carrying oxygen donor atoms on the pendant arms.

The two halves of a hydrogen-bonded Co(II) complex reported by Belal *et al.*, (1989) with THPTACN have distorted octahedral geometry like the Cd-THPTACD complex reported here whereas the two halves of the corresponding Mn(II) cationic complex reported by the same authors have different geometries (Belal *et al.*, 1991). One half adopts nearly a perfect trigonal prism and the other half a *pseudo*-octahedral geometry. Luckay *et al.*, (1996) reported the same results for the $[Fe_2(THETAC)_2H_{-3}]^{3+}$ cationic complex.

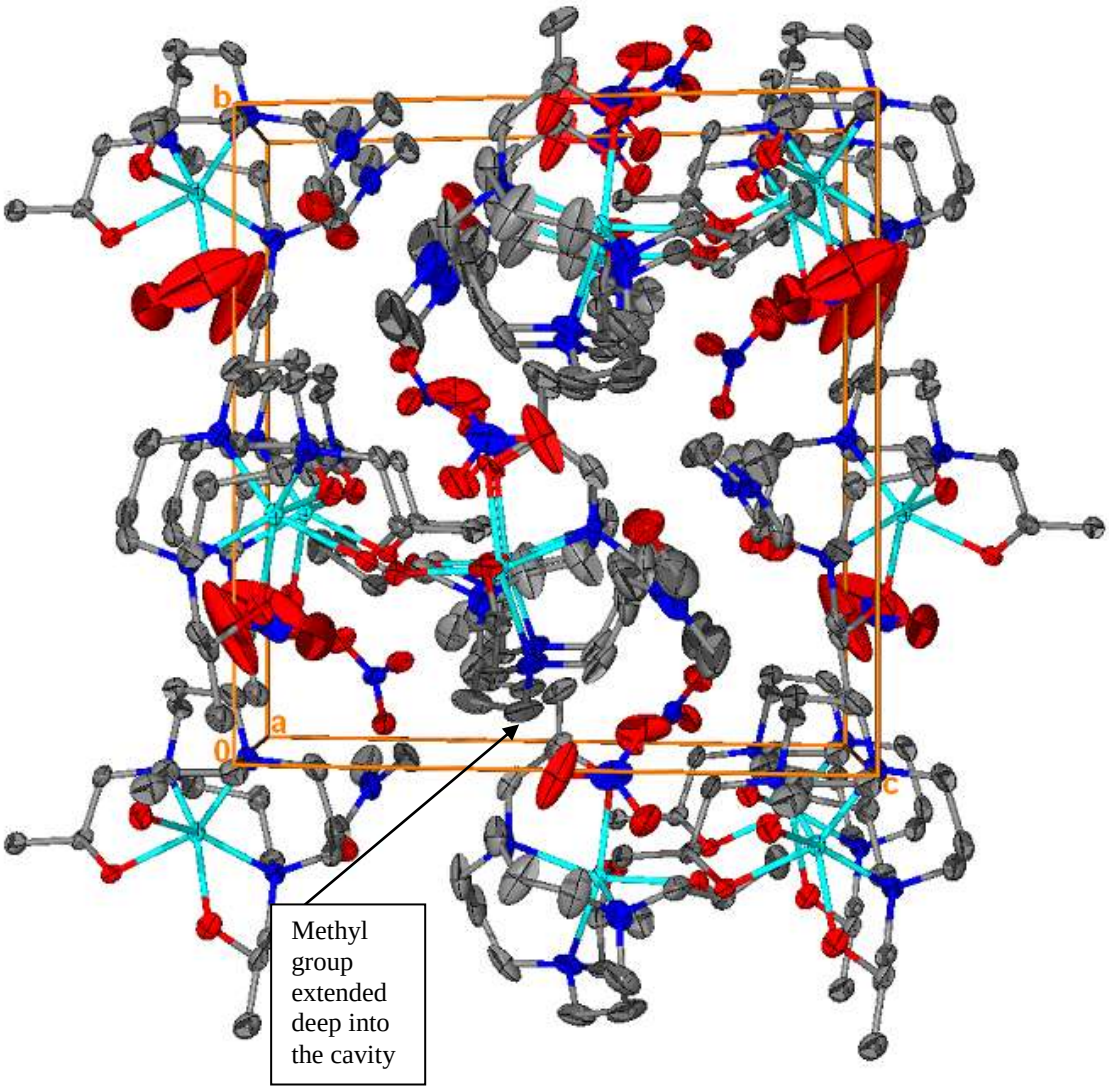

Fig. 5.23: Packing diagram of the $[Cd_2(C_{18}H_{39}N_3O_3)_2]^{4+}$ cationic complex (50% thermal ellipsoids) along the a-axis (H atoms omitted for clarity).

5.3.7 The crystal and molecular structure of the $Cu[(C_{33}H_{45}N_3O_3)](NO_3)_2$ complex

The unit cell contains $[Cu(C_{33}H_{45}N_3O_3)]^{2+}$ cationic complex and two nitrate counter ions (**Fig. 5.24**). The complex crystallised in the monoclinic crystal system, space group $P2_1$. The crystallographic data and structure refinement details are summarised in **Table 5.26**. The molecular structure of the $[Cu(C_{33}H_{45}N_3O_3)]^{2+}$ cationic complex with atom numbering scheme is shown in **Fig. 5.25**. The complex has similar donor atom set to the Cu(II) complex with THPTACD described in **Section 5.3.5** and are both *facially* coordinated to the central metal ion.

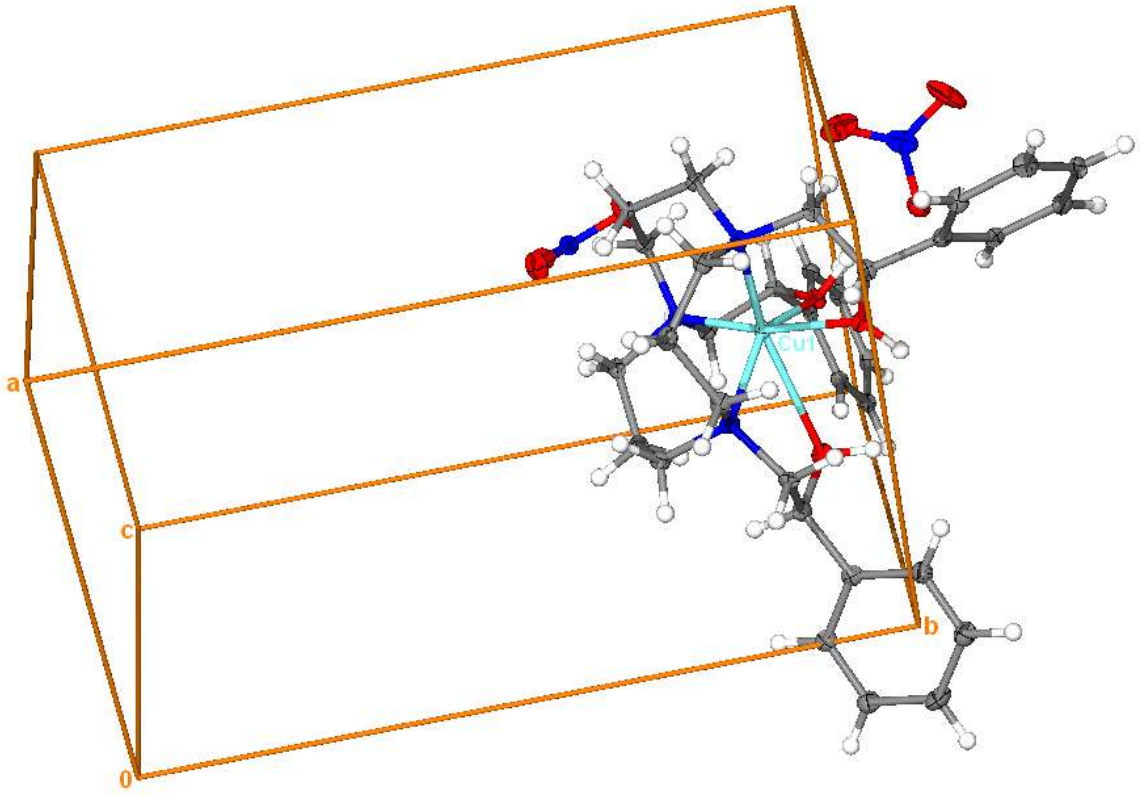

Fig. 5.24: The unit cell and contents of the asymmetric unit of the $[Cu(C_{33}H_{45}N_3O_3)](NO_3)_2$ complex (50% thermal ellipsoids).

Selected bond lengths and angles are listed in **Table 5.16**. The complex is also trigonally distorted because of the high strain due to overcrowding of the pendant arms. The three O-Cu-O bond angles: O24-Cu1-O15, O15-Cu1-O33 and O24-Cu1-O33 are 85.14(6), 84.85(5) and 72.25(5)°, respectively. The two *trans*-oriented Cu-N and Cu-O bonds are elongated relative to the equatorial bonds; the axial Cu-N1 and Cu-O33 are 2.2349(16) and 2.8525(16) Å, respectively. The fact that the Cu-O bond length to the axially co-ordinated oxygen donor atom differ significantly to the other two oxygen donor atoms, without significantly affecting the axial Cu-N bond length, indicates the weakness of the axial interaction. A search for X-ray crystal structures of Cu-O bond length greater than 2.7 Å on the Cambridge crystallographic database (Bruno *et al.*, 2002) gave 453 hits as of 9th February, 2010.

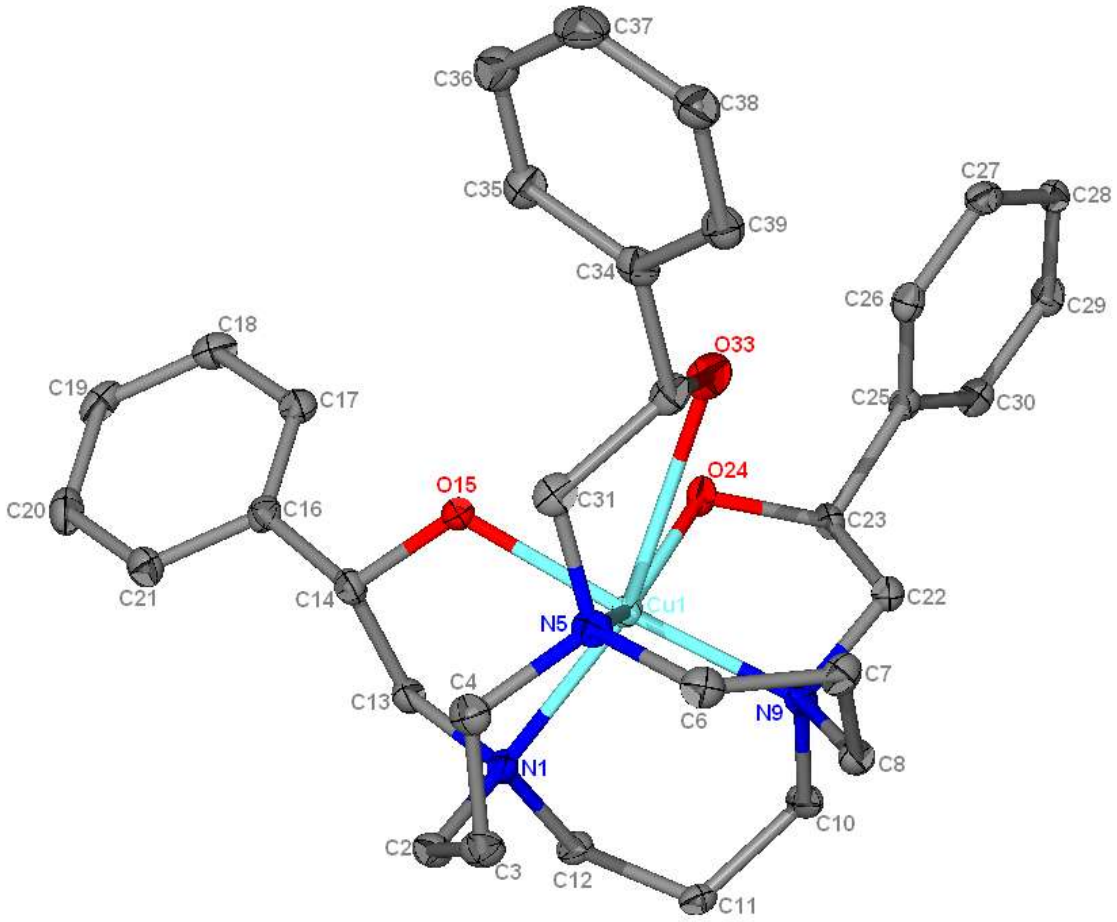

Fig. 5.25: ORTEP diagram of the $[Cu(C_{33}H_{45}N_3O_3)]^{2+}$ cationic complex (50% thermal ellipsoids) (H atoms and NO_3^- counter ions are omitted for clarity).

The tetragonality value of 0.81 (**Table 5.2**) indicates that the $[Cu(C_{33}H_{45}N_3O_3)]^{2+}$ cationic complex is tetragonally elongated, which is evident from the axial bond lengths. The values of the three twist angles are given in **Table 5.17**. The average value of the three twist angles is 41.8°, which means that $[Cu(C_{33}H_{45}N_3O_3)]^{2+}$ cationic complex can best be described as a *pseudo* octahedron. This in contrast to the geometry of $[Cu(C_{18}H_{39}N_3O_3)]^{2+}$ cationic complex described in **Section 5.3.5**, which is more twisted towards trigonal prismatic, with the average twist angle value of 21.7°. However, the two complexes have the same absolute configuration. The difference in geometry between the two Cu(II) complexes is due to differences in packing forces rather than the gain in crystal field stabilisation energy. The replacement of methyl groups of the pendant arms with the phenyl groups has a profound effect on the packing forces of the ligand. The observed structures for Cu(II) complexes can, therefore, be best described as a thermodynamic compromise between the crystal packing

forces and the Jahn-Teller distortion. The bond angles of the six- and five-membered chelate rings are summarised in **Table 5.17**.

Table 5.16: Selected bond lengths and angles for the $[Cu(C_{33}H_{45}N_3O_3)]^{2+}$ cationic complex

Bond Lengths (Å)		**Bond Angles (°)**	
Cu1-O15	2.0546(15)	N1-Cu1-O33	161.48(6)
Cu1-O24	2.0267(15)	N5-Cu1-O24	142.79(6)
Cu1-O33	2.8525(16)	N9-Cu1-O15	165.26(7)
Cu1-N1	2.2349(16)	O33-Cu1-N9	98.90(6)
Cu1-N5	2.1478(18)	O33-Cu1-O15	84.85(5)
Cu1-N9	2.0361(19)	O33-Cu1-O24	72.25(5)

The packing diagram along the a-axis shows that the phenyl groups occupy spaces that are taken by water solvent molecules and the nitrate counter ions in the $[Cu(C_{18}H_{39}N_3O_3)]^{2+}$ cationic complex as shown in **Fig. 5.8** ($[Cu(C_{18}H_{39}N_3O_3)]^{2+}$ and $[Zn(C_{18}H_{39}N_3O_3)]^{2+}$ cationic complexes have similar packing pattern). The parallel phenyl ring-stacking interaction of the phenyl groups of the pendant arms is responsible for the crystal packing (**Fig 5.26**). The Cu(II) metal centres are arranged in diamond pattern in $[Cu(C_{33}H_{45}N_3O_3)]^{2+}$ cationic complex whereas in $[Cu(C_{18}H_{39}N_3O_3)]^{2+}$ they are arranged in a square pattern along the a-axis. The two arrangements are depicted in **Chart 5.2**.

Table 5.17: Six- and five-membered chelate ring angles and twist angles for the $[Cu(C_{33}H_{45}N_3O_3)]^{2+}$ cationic complex

6-MCR Bond Angles (°)		**5-MCR Bond Angles (°)**		**Twist Angles (°)**
N1-Cu1-N5	101.36(6)	N1-Cu1-O15	78.97(7)	42.24
N1-Cu1-N9	99.02(7)	N5-Cu1-O33	70.62(6)	43.98
N5-Cu1-N9	100.82(7)	N9-Cu1-O24	82.48(7)	39.13

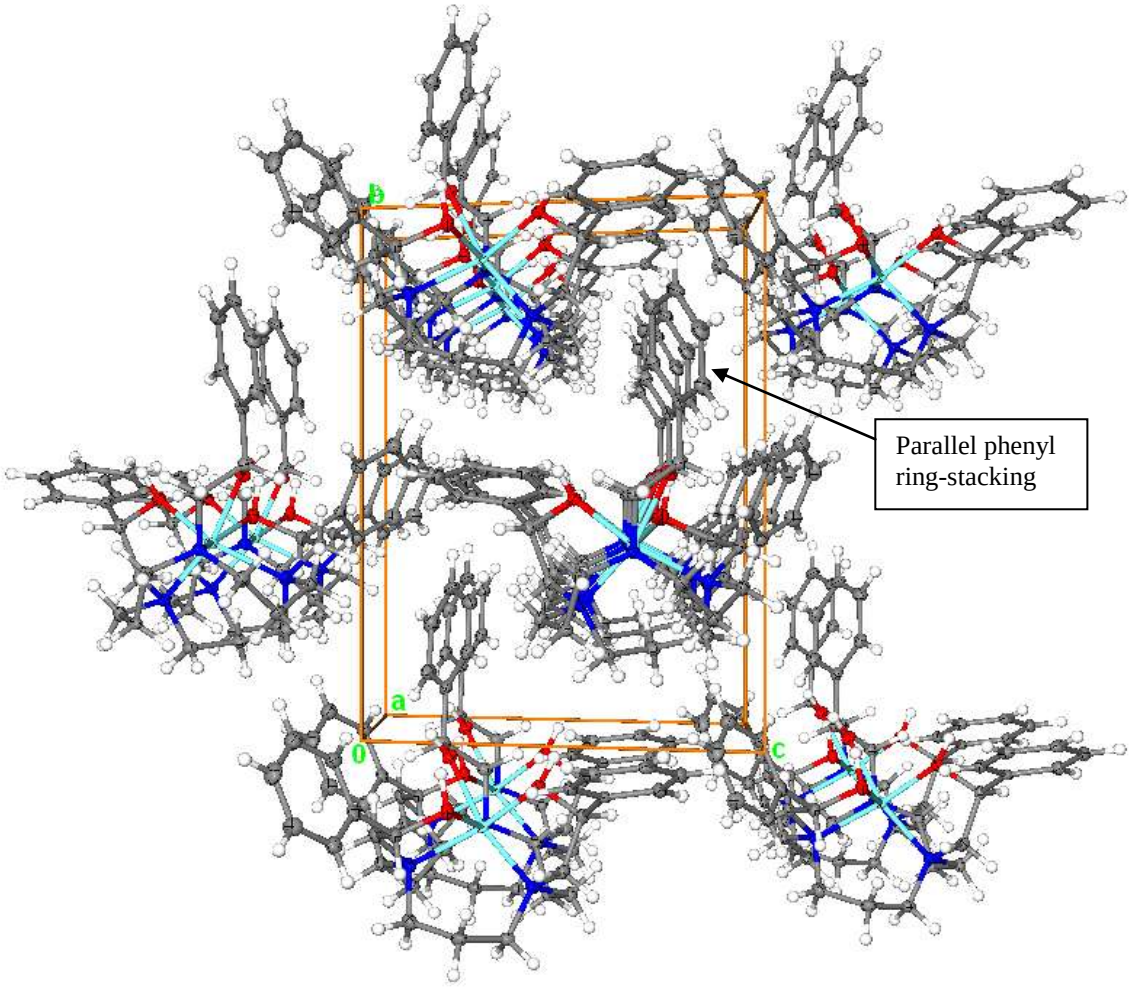

Fig. 5.26: Packing diagram of the $[Cu(C_{33}H_{45}N_3O_3)]^{2+}$ cationic complex (50% thermal ellipsoids) along the a-axis showing parallel phenyl ring-stacking.

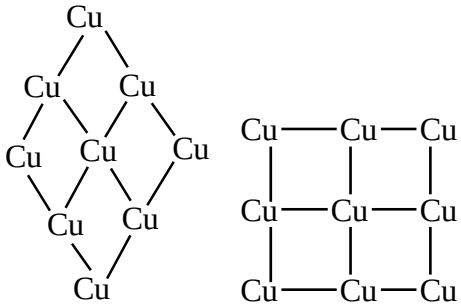

Chart 5.2: The pattern of the Cu(II) metal cation arrangement in the crystal packing of $[Cu(C_{33}H_{45}N_3O_3)(NO_3)_2]$ (left) and $[Cu(C_{18}H_{39}N_3O_3)(NO_3)_2](H_2O)$ (right) along the a-axis (The solid lines do not indicate bonds here).

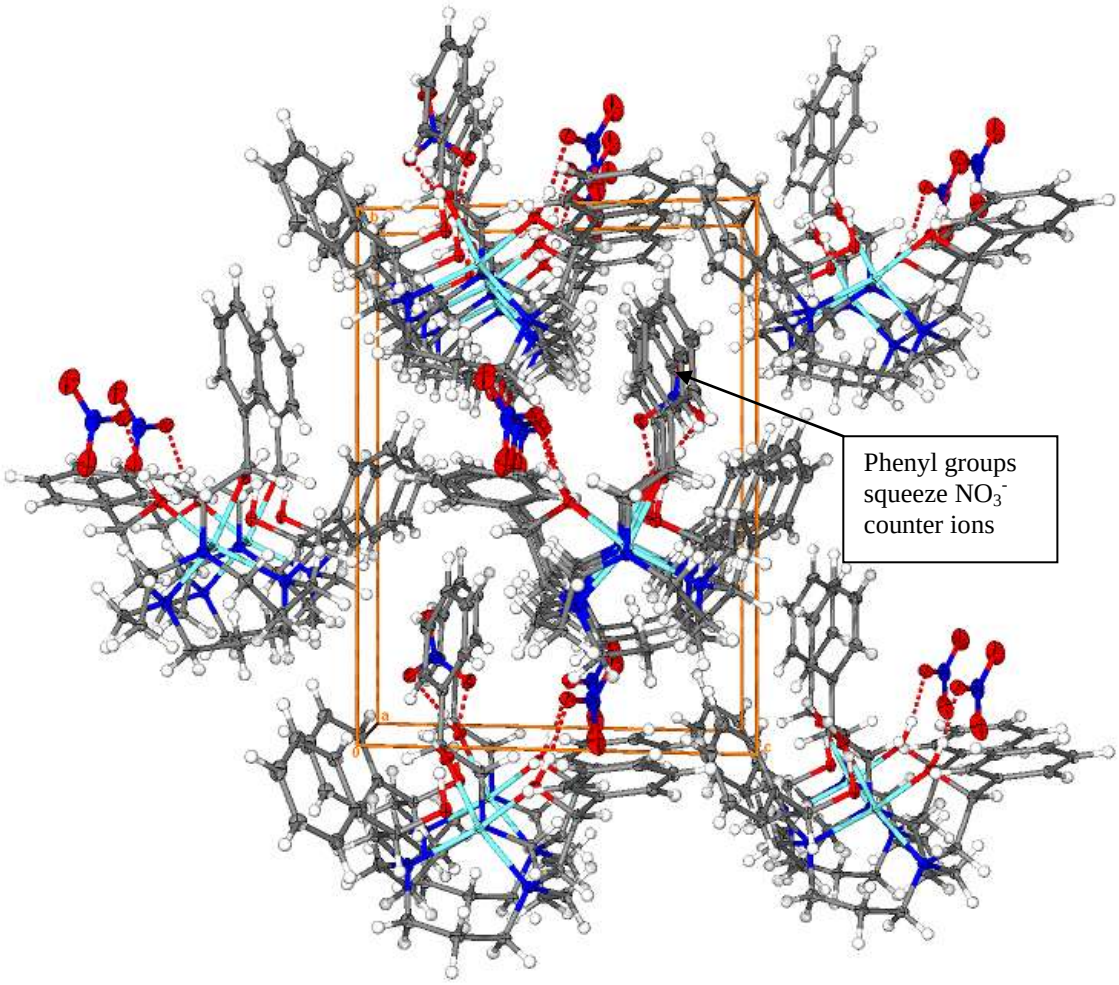

Fig. 5.27: Packing diagram of the $[Cu(C_{33}H_{45}N_3O_3)](NO_3)_2$ complex (50% thermal ellipsoids) along the a-axis.

The average Cu(II)-N bond distance reported by Feng *et al.*, (2007) for a THPTACN complex is 2.087 Å and the average Cu(II)-N bond length of the $[Cu(C_{18}H_{39}N_3O_3)]^{2+}$ cation complex is 2.139 Å. The average Cu(II)-N bond separation of the $[Cu(C_{33}H_{45}N_3O_3)]^{2+}$ cation complex is 2.140 Å. The bond length of the $[Cu(C_{33}H_{45}N_3O_3)]^{2+}$ cation complex is not significantly longer than the one reported in **Section 5.3.5**. The literature average Cu(II)-O bond length is 2.129 Å (Feng *et al.*, 2007) and the average bond length reported here is 2.140 Å. The average bond length reported here is significantly longer than the literature value because of high steric strain in the axial position due to bulky phenyl groups of the pendant arms.

The average N-Cu(II)-N bite angle reported here is 100.4° whereas the literature value is 85.13° (Feng *et al.*, 2007). The average O-Cu(II)-O bite angles reported in the literature for a

THPTACN are 88.29° (Feng *et al.*, 2007) and 88.73° (Han *et al.*, 2004) and the average bite angle reported here is 80.7°. There is no report for the Cu(II) crystal of the parent macrocyclic ligand, 12aneN_3.

5.3.8 The crystal and molecular structure of a protonated ligand $[(C_{17}H_{38}N_3O_2)](NO_3).H_2O$

The crystal structure consists of a $[C_{17}H_{38}N_3O_2]^+$ cation, a nitrate counter ion and a water solvent molecule in the asymmetric unit cell. The ligand crystallised in the tetragonal crystal system, space group $P4_1$. The crystallographic data and structure refinement details are summarised in **Table 5.27**. The molecular structure of the $[(C_{17}H_{38}N_3O_2)]^+$ cation with atom numbering scheme is shown in **Fig. 5.28**.

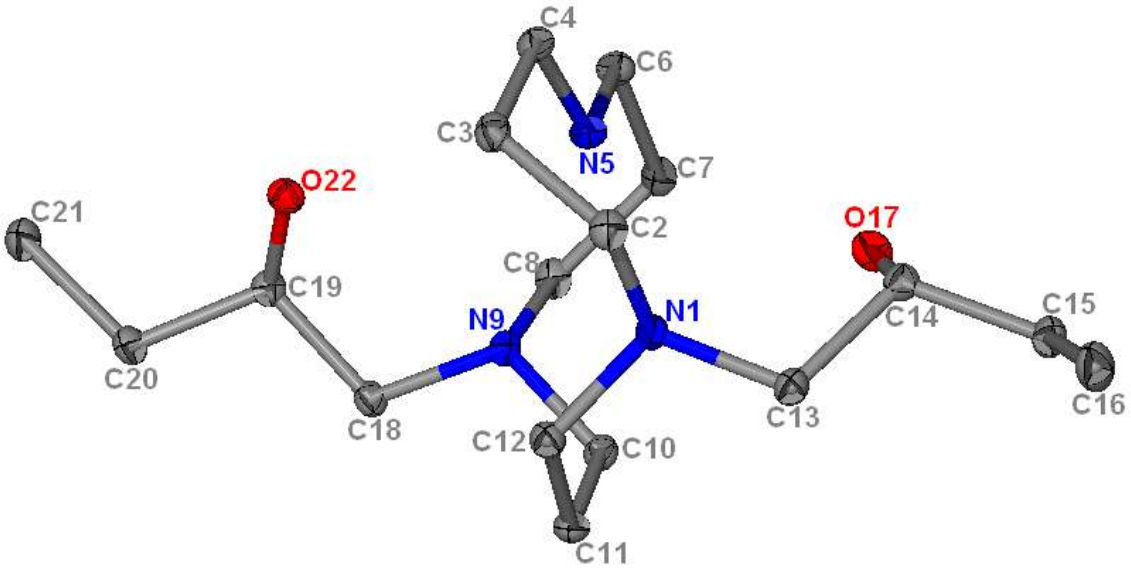

Fig. 5.28: ORTEP diagram of the $[(C_{17}H_{38}N_3O_2)]^+$ cation (50% thermal ellipsoids) (H atoms, H_2O solvent molecule, NO_3^- counter ions are omitted for clarity).

The proton seems to push the two unprotonated nitrogen donor atoms above and below the plane defined by N5, C2 and C10 to allow better intramolecular hydrogen bonding. The oxygen donor atoms of the pendant arms are pre-organised for *meridional* coordination. In the previous examples discussed above, all metal complexes are *facially* coordinated. The need to form efficient hydrogen bonds seems to be responsible for pushing the two arms in opposite directions (**Fig. 5.29**). The molecule is held together by a network of both intra- and intermolecular hydrogen bonding involving the hydrogen atoms on the protonated nitrogen

atom of the ring and oxygen donor atom of the pendant arms and water solvent molecule. Selected bond lengths and angles are listed in **Table 5.18**.

Table 5.18: Selected bond lengths and angles for the $[(C_{17}H_{38}N_3O_2)]^+$ cation

Bond Lengths (Å)		**Bond Angles (°)**	
O22-C19	1.4382(14)	C20-C19-O22	112.86(10)
O17-C14	1.4327(14)	C18-C19-O22	109.92(9)
N1-C13	1.4675(15)	C13-C14-O17	106.30(10)
N9-C18	1.4674(16)	C15-C14-O17	110.76(10)
N5-C4	1.4871(14)	C18-N9-C8	111.73(9)
N9-C8	1.4823(16)	C18-N9-C10	113.34(9)
N1-C2	1.4720(15)	C12-N1-C13	113.62(9)
C14-C15	1.5252(16)	C2-N1-C13	111.53(8)

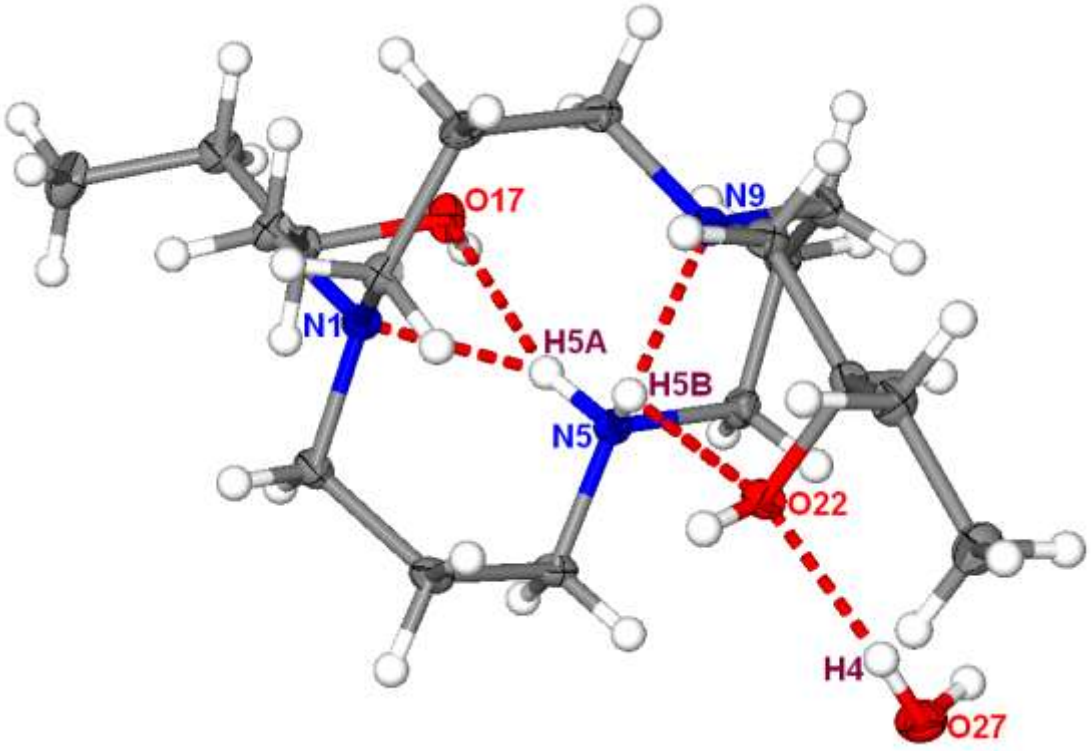

Fig. 5.29: ORTEP diagram of the $[(C_{17}H_{38}N_3O_2)](NO_3).H_2O$ molecular structure (50% thermal ellipsoids) showing a network of hydrogen bonds (NO_3^- counter ion is omitted).

The nitrate counter ion is very far away from the cationic complex in the unit such that it is not involved in intermolecular hydrogen bonding (**Fig. 5.30**).

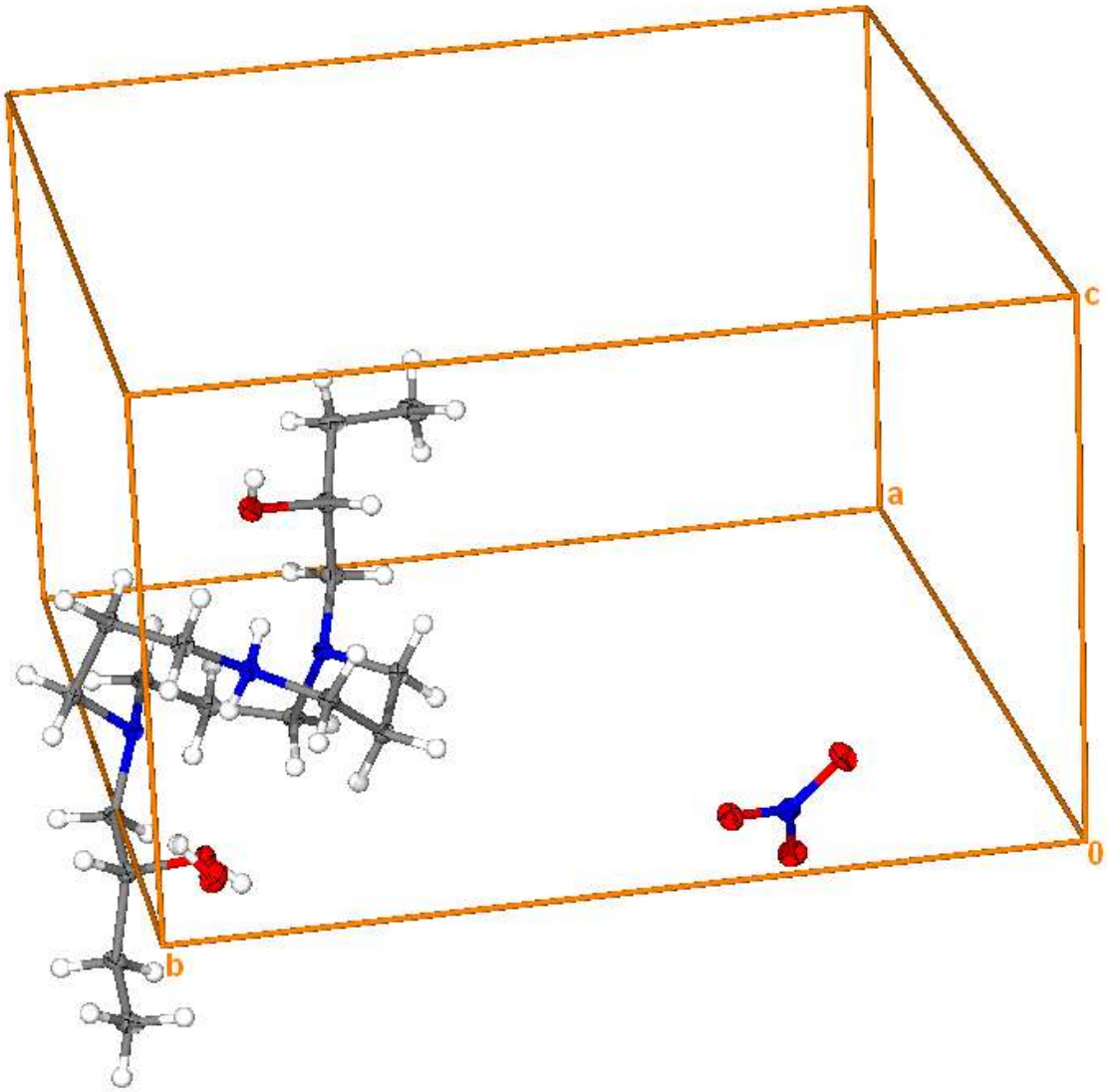

Fig. 5.30: The unit cell and contents of the asymmetric unit of the $[(C_{17}H_{38}N_3O_2)](NO_3).H_2O$ crystal structure (50% thermal ellipsoids).

The nitrogen atoms of the cationic ligand are stacked on top of each other forming layers along the c-axis (**Fig. 5.31**). The H_2O solvent molecules are located in the spaces between layers in the packing of the molecule along the c-axis whereas the nitrate counter ions are located nearly in the centre of the cationic ligand.

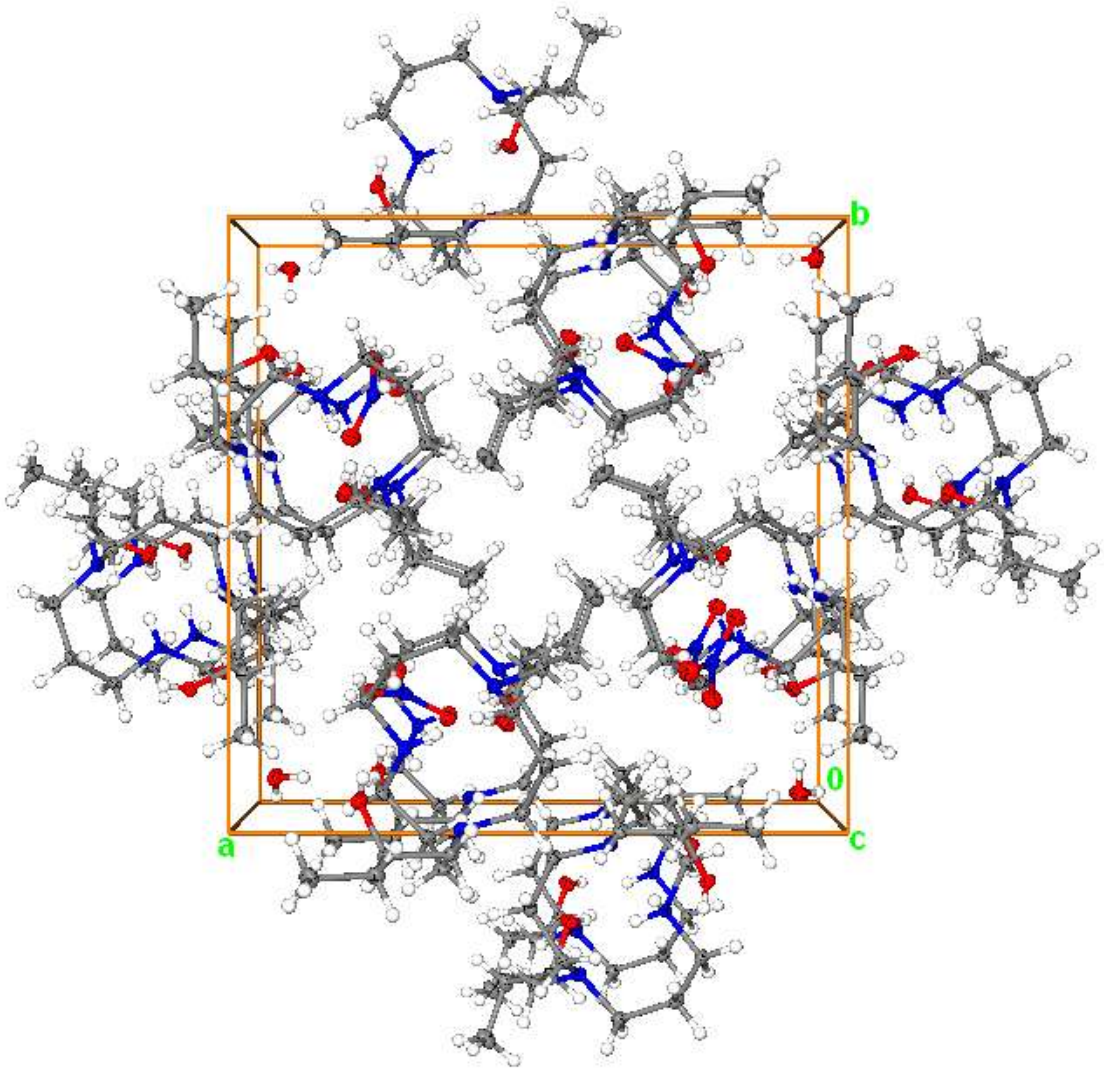

Fig.5.31: The packing diagram of the molecule $[(C_{17}H_{38}N_3O_2)](NO_3).H_2O$ crystal structure (50% thermal ellipsoids) along the c-axis.

5.3.9 The crystal and molecular structure of the $[Cd_2(C_9H_{21}N_3)_2(\mu\text{-}Cl)_2(NO_3)_2]$ binuclear complex

The crystal structure is a binuclear complex containing a di-μ-chloro bridge between Cd(II) metal ions. The asymmetric unit is one-half molecule such that each molecule contains an inversion centre coinciding with the crystallographic centre of symmetry. The four ions constituting the bridge are planar (**Fig 5.32**). The complex crystallised in the monoclinic crystal system, space group *C*2/c. The crystallographic data and structure refinement details are summarised in **Table 5.28**.

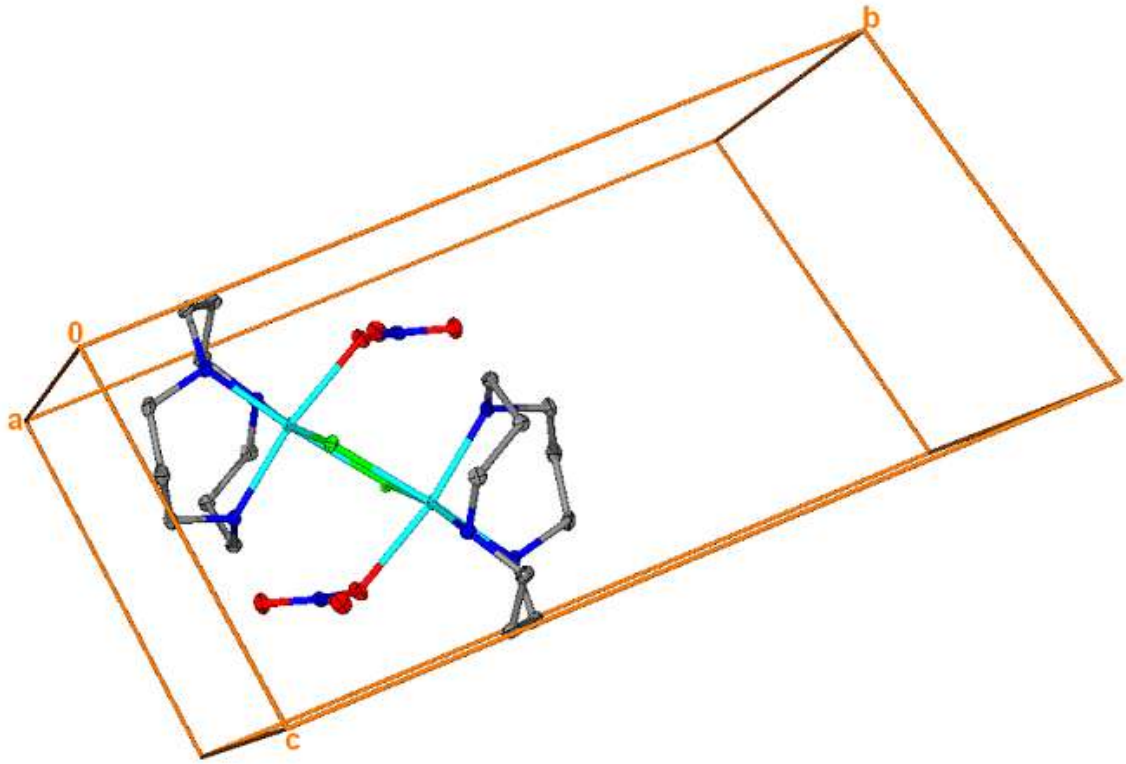

Fig. 5.32: Unit cell and contents of the asymmetric unit of the $[Cd_2(C_9H_{21}N_3)_2(\mu\text{-}Cl)_2(NO_3)_2]$ binuclear complex (50% thermal ellipsoids).

The molecular structure of the $[Cd_2(C_9H_{21}N_3)_2(\mu\text{-}Cl)_2(NO_3)_2]$ binuclear complex with its atom numbering scheme is shown in **Fig. 5.33**. Selected bond lengths and angles are listed in **Table 5.19**.

Table 5.19: Selected bond lengths and angles for the $[Cd_2(C_9H_{21}N_3)_2(\mu\text{-}Cl)_2(NO_3)_2]$ binuclear complex

Bond Lengths (Å)		**Bond Angles (°)**	
Cd1-N1	2.3116(9)	N1-Cd1-N5	91.00(3)
Cd1-N5	2.3104(9)	N5-Cd1-N9	89.70(3)
Cd1-N9	2.3400(9)	N1-Cd1-N9	94.25(3)
Cd1-Cl1	2.6144(2)	O1-Cd1-Cl1	86.29(2)
Cd1-Cl1A	2.6292(2)	O1-Cd1-Cl1A	80.94(2)
Cd1-O1	2.4224(2)	Cl1-Cd1-Cl1A	89.21(2)

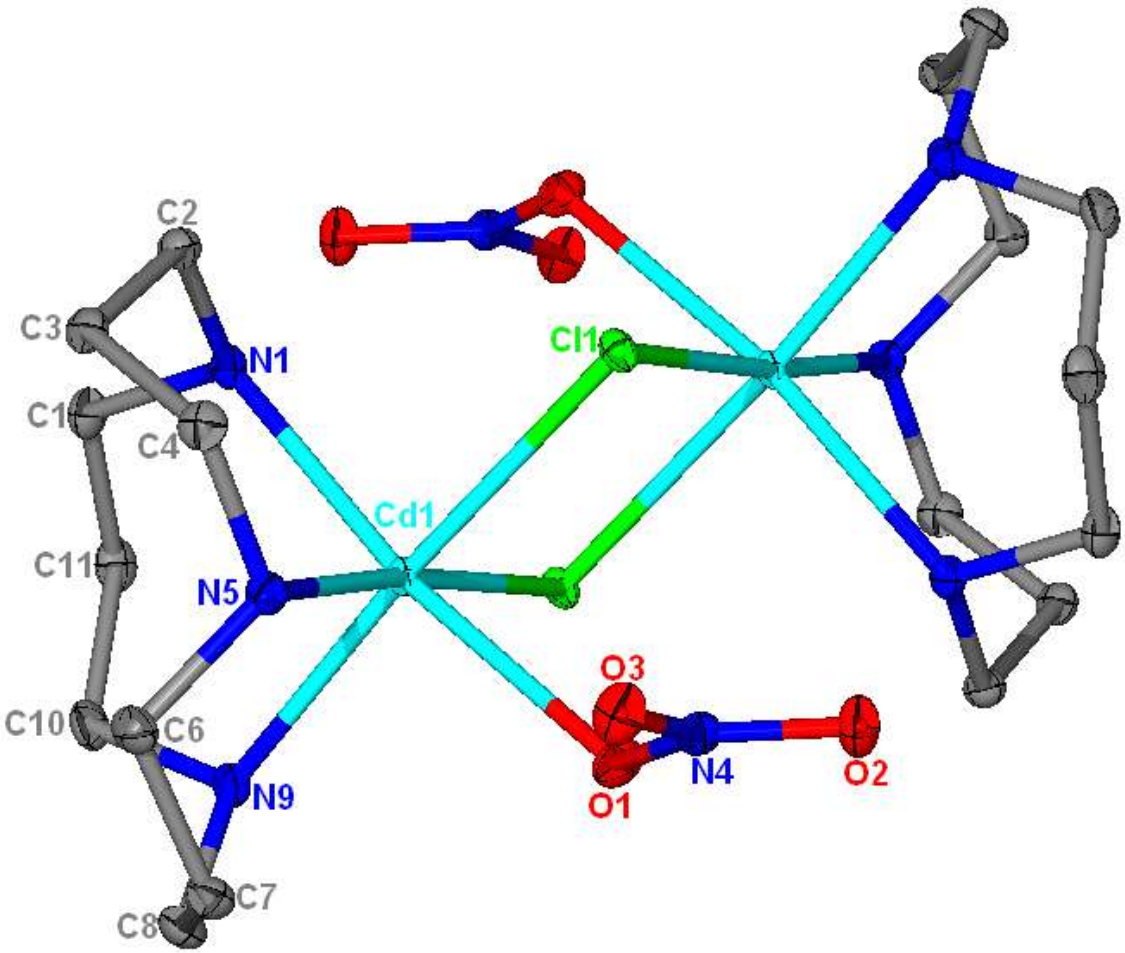

Fig. 5.33: ORTEP diagram of the $[Cd_2(C_9H_{21}N_3)_2(\mu\text{-}Cl)_2(NO_3)_2]$ binuclear complex (50% thermal ellipsoids).

Each cadmium cation is bonded to a nitrate ion and the two nitrate ions are in a *trans* position with respect to the plane formed by the di-µ-chloro bridge. The $12aneN_3$ functions as a tridentate ligand with nitrogen atoms occupying the remaining *facial* sites on the six-coordinate cadmiums.

The average Cd-N bond length of 2.321 Å is in the normal expected range for Cd-N(amine) bonds (Cannas *et al.*, 1980; Tan *et al.*, 1993). The bridged chloride and the two Cd(II) cations forms a rectangle with the dimensions of 2.629 Å long and 2.614 Å wide. The average Cd-Cl distance of 2.6218 Å is typical of µ-chloro bridged molecular structures (Zompa *et al.*, 1995).

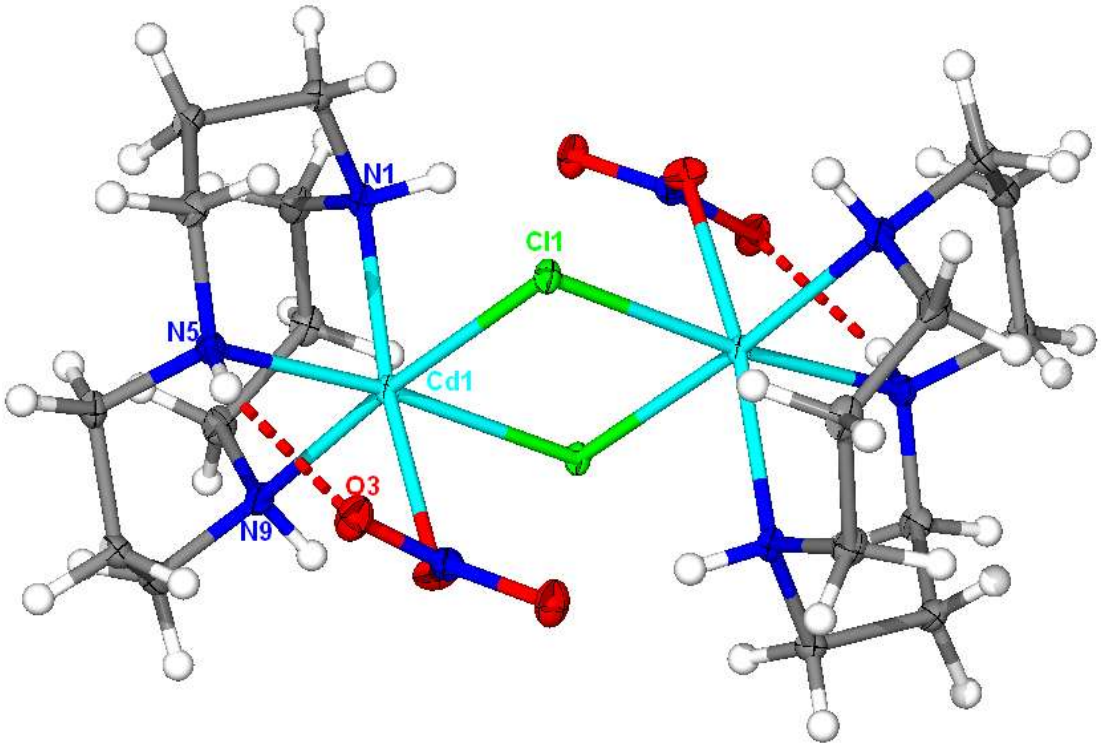

Fig. 5.34: ORTEP diagram of the $[Cd_2(C_9H_{21}N_3)_2(\mu\text{-}Cl)_2(NO_3)_2]$ binuclear complex (50% thermal ellipsoids) showing hydrogen bonding.

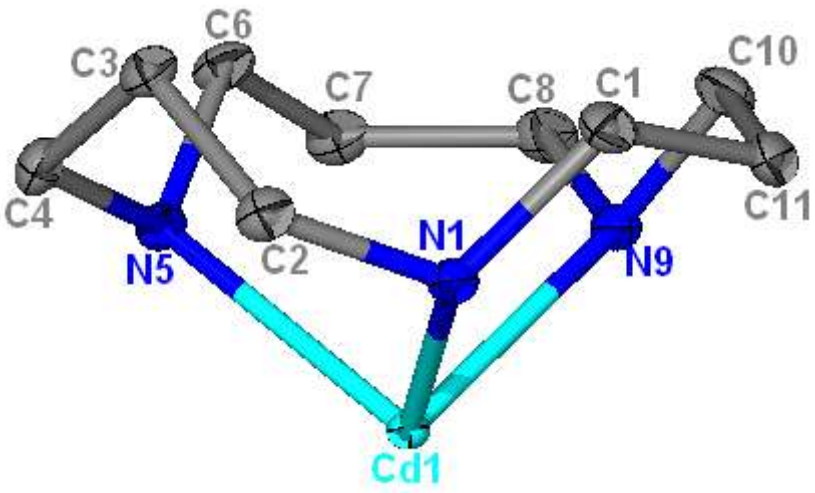

Fig. 5.35: ORTEP diagram of the parent macrocyclic ring of the $[Cd_2(C_9H_{21}N_3)_2(\mu\text{-}Cl)_2(NO_3)_2]$ binuclear complex (50% thermal ellipsoids) showing the conformation of the three six-membered chelate rings.

The non-bonded Cd----Cd and Cl----Cl distances of 3.733 and 3.682 Å, respectively, are typical for di-μ-chloro complexes (Zompa *et al.*, 1995). The Cd1-Cl1-Cd1A is nearly a perfect right angle at 90.79°. The conformations of the three six-membered chelate ring

angles are the same as those formed by the Cd(II) complex with THPTACD (compare **Fig. 5.18** and **Fig. 5.35**).

The packing diagram along the a-axis shows the nitrate ions forming a horizontal zigzag pattern. There are no open channels in the packing of the molecule (**Fig. 5.36**).

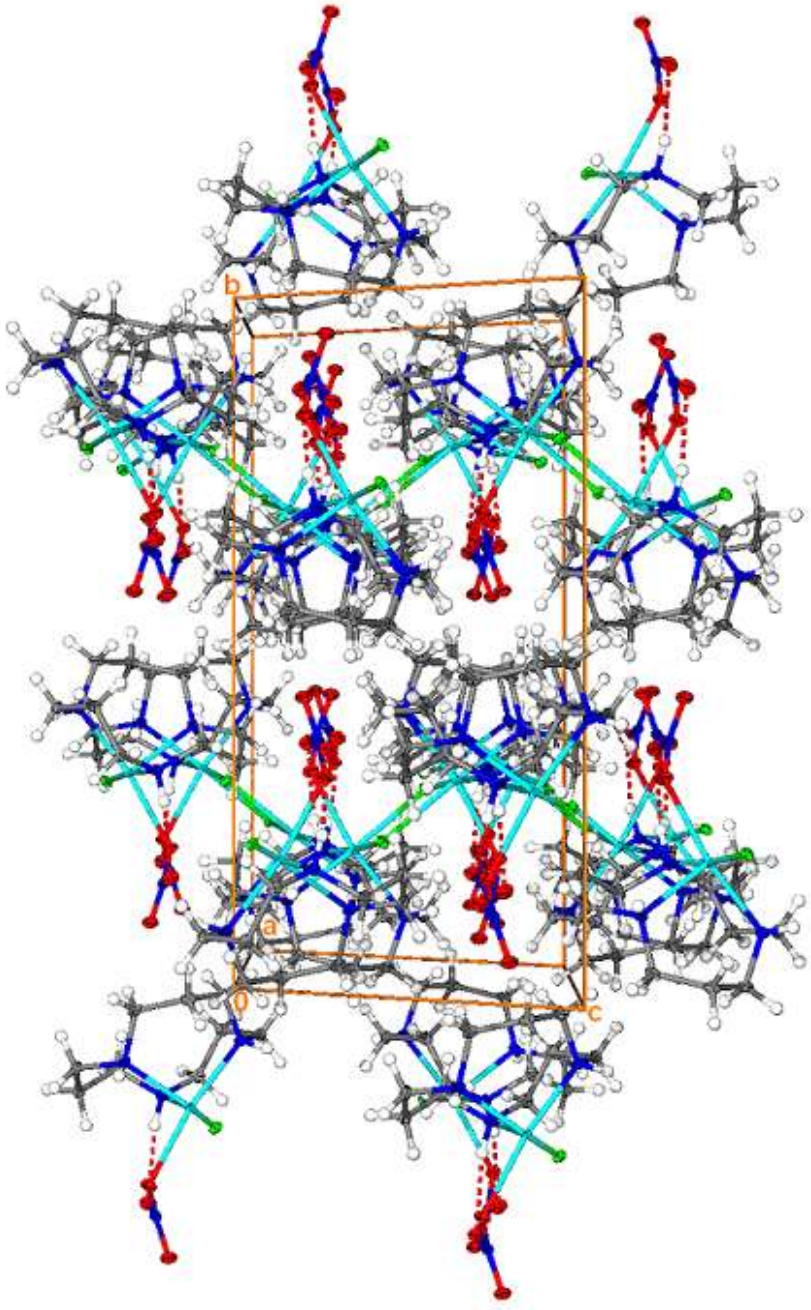

Fig. 5.36: The packing diagram of the $[Cd_2(C_9H_{21}N_3)_2(\mu\text{-}Cl)_2(NO_3)_2]$ binuclear complex (50% thermal ellipsoids) along the a-axis.

Table 5.20: Crystallographic data and structure refinement of the $[Zn(C_{18}H_{39}N_3O_3)]^{2+}$ cationic complex

Compound	$[Zn(C_{18}H_{39}N_3O_3)](NO_3)_2.H_2O$
Empirical formula	$C_{18}H_{41}ZnN_5O_{10}$
Mr	552.93
Crystal habit	Block
Crystal dimension (mm)	0.16x0.15x0.11
Crystal system	Orthorhombic
Space group	$P2_12_12_1$
a (Å)	10.1558(10)
b (Å)	15.4883(15)
c (Å)	15.7498(15)
α(º)	90.00
ß(º)	90.00
γ(º)	90.00
μ (Mo Kα) (mm^{-1})	1.052
V ($Å)^3$	2477.4(4)
Z, Dc (M, g m^{-3})	4, 1.482
Index ranges	$-12 \leq h \leq 10$, $-19 \leq k \leq 12$, $-18 \leq l \leq 19$
Reflections collected	14715
Independent reflections	5102
Absorption correction	Multi-scan
Max/min. transmission	0.890/0.850
Refinement method	Full matrix least squares on F^2
Data/restraints/parameters	4378/6/325
F(000)	1176
Final R indices [I >, 2∂(I)]	0.0479, 0.1085
R indices (all data) R1, wR2	0.0579, 0.1134
Goodness of fit on F^2	1.034

Table 5.21: Crystallographic data and structure refinement of the $[Co(C_{18}H_{39}N_3O_3)]^{2+}$ cationic complex

Compound	$[Co(C_{18}H_{39}N_3O_3)](NO_3)_2.H_2O$
Empirical formula	$C_{18}H_{41}CoN_5O_{10}$
Mr	546.49
Crystal habit	Prism
Crystal dimension (mm)	0.28x0.15x0.13
Crystal system	Orthorhombic
Space group	$P2_12_12_1$
a (Å)	10.1022(12)
b (Å)	15.4437(18)
c (Å)	15.834(2)
α(°)	90.00
ß(°)	90.00
γ(°)	90.00
μ (Mo Kα) (mm^{-1})	0.755
V ($Å)^3$	2470.3(5)
Z, Dc (M, g m^{-3})	4, 1.469
Index ranges	$-9 \leq h \leq 12$, $-18 \leq k \leq 19$, $-19 \leq l \leq 18$
Reflections collected	14664
Independent reflections	5062
Absorption correction	Multi-scan
Max/min. transmission	0.9088/0.7000
Refinement method	Full matrix least squares on F2
Data/restraints/parameters	4011/9/254
F(000)	1164
Final R indices [I >, 2∂(I)]	0.0628, 0.1488
R indices (all data) R1, wR2	0.0775, 0.1570
Goodness-of-fit on F2	1.051

Table 5.22: Crystallographic data and structure refinement of the $[Mn(C_{18}H_{39}N_3O_3)]^{2+}$ cationic complex

Compound	$[Mn(C_{18}H_{39}N_3O_3)](NO_3)_2.H_2O$
Empirical formula	$C_{18}H_{41}MnN_5O_{10}$
Mr	542.50
Crystal habit	Block
Crystal dimension (mm)	0.21x0.14x0.11
Crystal system	Orthorhombic
Space group	$P2_12_12_1$
a (Å)	10.170(2)
b (Å)	15.270(3)
c (Å)	16.029(3)
α(°)	90.00
ß(°)	90.00
γ(°)	90.00
μ (Mo Kα) (mm^{-1})	0.591
V ($Å)^3$	2489.3(9)
Z, Dc (M, g m^{-3})	4, 1.44(8)
Index ranges	$-12 \leq h \leq 11$, $-19 \leq k \leq 11$, $-20 \leq l \leq 18$
Reflections collected	14737
Independent reflections	5095
Absorption correction	Multi-scan
Max/min. transmission	0.9384/0.8865
Refinement method	Full matrix least squares on F^2
Data/restraints/parameters	4270/24/277
F(000)	1156
Final R indices [I >, 2∂(I)]	0.1094, 0.2831
R indices (all data) R1, wR2	0.1238, 0.3015
Goodness of fit on F^2	1.034

Table 5.23: Crystallographic data and structure refinement of the $[Ni(C_{18}H_{39}N_3O_3)]^{2+}$ complex cation

Compound	$[Ni(C_{18}H_{39}N_3O_3)](NO_3)_2.H_2O$
Empirical formula	$C_{18}H_{41}NiN_5O_{10}$
Mr	546.25
Crystal habit	Needle
Crystal dimension (mm)	0.41x0.27x0.16
Crystal system	Orthorhombic
Space group	$P2_12_12_1$
a (Å)	10.0341(13)
b (Å)	15.471(2)
c (Å)	15.769(3)
α(º)	90.00
ß(º)	90.00
γ(º)	90.00
μ (Mo Kα) (mm^{-1})	0.854
V $(Å)^3$	2447.9(5)
Z, Dc (M, g m^{-3})	4, 1.482
Index ranges	$-12 \leq h \leq 10$, $-14 \leq k \leq 19$, $-19 \leq l \leq 19$
Reflections collected	14414
Independent reflections	5012
Absorption correction	Multi-scan
Max/min. transmission	0.8806/0.6839
Refinement method	Full matrix least squares on F^2
Data/restraints/parameters	4346,9,254
F(000)	1168
Final R indices [I >, 2∂(I)]	0.0692, 0.1746
R indices (all data) R1, wR2	0.0780, 0.1841
Goodness of fit on F^2	1.075

Table 5.24: Crystallographic data and structure refinement of the $[Cu(C_{18}H_{39}N_3O_3)]^{2+}$ cationic complex

Compound	$[Cu(C_{18}H_{39}N_3O_3)](NO_3)_2.H_2O$
Empirical formula	$C_{18}H_{41}CuN_5O_{10}$
Mr	551.05
Crystal habit	Needle
Crystal dimension (mm)	0.24x0.11x0.08
Crystal system	Orthorhombic
Space group	$P2_12_12_1$
a (Å)	10.0599(16)
b (Å)	15.341(2)
c (Å)	15.796(3)
α(º)	90.00
ß(º)	90.00
γ(º)	90.00
μ (Mo Kα) (mm^{-1})	0.958
V $(Å)^3$	2437.8(7)
Z, Dc (M, g m^{-3})	4, 1.501
Index ranges	$-12 \leq h \leq 11$, $-19 \leq k \leq 17$, $-19 \leq l \leq 19$
Reflections collected	14341
Independent reflections	4990
Absorption correction	Multi-scan
Max/min. transmission	0.927/0.803
Refinement method	Full matrix least squares on F^2
Data/restraints/parameters	4116/9/255
F(000)	1172
Final R indices [I >, 2∂(I)]	0.0616, 0.1456
R indices (all data) R1, wR2	0.0737, 0.1515
Goodness of fit on F^2	1.052

Table 5.25: Crystallographic data and structure refinement of the $[Cd_2(C_{18}H_{39}N_3O_3)_2]^{4+}$ cationic complex

Compound	$[Cd_2(C_{18}H_{39}N_3O_3)_2](NO_3)_4.(C_3H_7NO)_2$
Empirical formula	$C_{42}H_{92}Cd_2N_{12}O_{20}$
Mr	1310.07
Crystal habit	Plate
Crystal dimension (mm)	0.41x0.29x0.03
Crystal system	Monoclinic
Space group	$P2_1$
a (Å)	14.2705(18)
b (Å)	14.4566(18)
c (Å)	14.60(77)
α(º)	90.00
ß(º)	109.206(2)
γ(º)	90.00
μ (Mo Kα) (mm^{-1})	0.828
V $(Å)^3$	2845.9(6)
Z, Dc (M, g m^{-3})	4, 1.529
Index ranges	$-17 \leq h \leq 17$, $-18 \leq k \leq 18$, $-14 \leq l \leq 18$
Reflections collected	16677
Independent reflections	10740
Absorption correction	Multi-scan
Max/min. transmission	0.974/0.767
Refinement method	Full matrix least squares on F^2
Data/restraints/parameters	9402/25/713
F(000)	1368
Final R indices [I >, 2∂(I)]	0.0448, 0.0984
R indices (all data) R1, wR2	0.0531, 0.1033
Goodness of fit on F^2	1.033

Table 5.26: Crystallographic data and structure refinement of the $[Cu(C_{33}H_{45}N_3O_3)]^{2+}$ cationic complex

Compound	$Cu[(C_{33}H_{45}N_3O_3)](NO_3)_2$
Empirical formula	$C_{33}H_{45}CuN_5O_9$
Mr	719.28
Crystal habit	Shard
Crystal dimension (mm)	0.27x0.21x0.13
Crystal system	Monoclinic
Space group	$P2_1$
a (Å)	10.0555
b (Å)	14.8041
c (Å)	11.5577
α(°)	90.00
ß(°)	109.145
γ(°)	90.00
μ (Mo Kα) (mm^{-1})	0.736
V $(Å)^3$	1625.4(3)
Z, Dc (M, g m^{-3})	2, 1.470
Index ranges	$-13 \leq h \leq 12$, $-19 \leq k \leq 12$, $-12 \leq l \leq 15$
Reflections collected	9778
Independent reflections	5793
Absorption correction	Multi-scan
Max/min. transmission	0.9072/0.8261
Refinement method	Full matrix least squares on F^2
Data/restraints/parameters	5448/1/436
F(000)	634
Final R indices [I >, 2∂(I)]	0.0269, 0.0595
R indices (all data) R1, wR2	0.0293, 0.0608
Goodness of fit on F^2	1.002

Table 5.27: Crystallographic data and structure refinement of the $[C_{17}H_{38}N_3O_2](NO_3).H_2O$ cation

Compound	$[C_{17}H_{38}N_3O_2]^+$
Empirical formula	$C_{17}H_{40}N_4O_6$
Mr	396.53
Crystal habit	Block
Crystal dimension (mm)	0.60x0.45x0.40
Crystal system	Tetragonal
Space group	$P4_1$
a (Å)	14.9880(3)
b (Å)	14.9880(3)
c (Å)	9.3539(2)
α(°)	90.00
ß(°)	90.00
γ(°)	90.00
μ (Mo Kα) (mm^{-1})	0.094
V (Å)3	2101.26(7)
Z, Dc (M, g m^{-3})	4, 1.253
Index ranges	$-19 \leq h \leq 15$, $-19 \leq k \leq 19$, $-12 \leq l \leq 12$
Reflections collected	10085
Independent reflections	4873
Absorption correction	Multi-scan
Max/min. transmission	0.963/0.912
Refinement method	Full matrix least squares on F^2
Data/restraints/parameters	4638/1/260
F(000)	872
Final R indices [I >, 2∂(I)]	0.0297, 0.0747
R indices (all data) R1, wR2	0.0319, 0.0766
Goodness of fit on F^2	1.051

Table 5.28: Crystallographic data and structure refinement of the $[Cd_2(C_9H_{21}N_3)_2(\mu\text{-}Cl)_2(NO_3)_2]$ binuclear complex

Compound	$[Cd_2(C_9H_{21}N_3)_2(\mu\text{-}Cl)_2(NO_3)_2]$
Empirical formula	$C_{18}H_{42}Cd_2Cl_2N_8O_6$
Mr	762.31
Crystal habit	Block
Crystal dimension (mm)	0.23x0.18x0.09
Crystal system	Monoclinic
Space group	*C*2/c
a (Å)	16.3655(3)
b (Å)	18.3789(4)
c (Å)	11.7074(2)
α(º)	90.00
ß(º)	129.3630(10)
γ(º)	90.00
μ (Mo Kα) (mm^{-1})	1.807
V (Å)3	2722.51(9)
Z, Dc (M, g m^{-3})	4, 1.860
Index ranges	$-24 \leq h \leq 27$, $-30 \leq k \leq 30$, $-19 \leq l \leq 19$
Reflections collected	19794
Independent reflections	6514
Absorption correction	Multi-scan
Max/min transmission	0.8542/0.6813
Refinement method	Full matrix least squares on F^2
Data/restraints/parameters	6061/0/164
F(000)	1536
Final R indices [I >, 2∂(I)]	0.0193, 0.0457
R indices (all data) R1, wR2	0.0217, 0.0457
Goodness-of-fit on F^2	1.061

5.4 Conclusion

The crystal and molecular structures of the divalent metal complexes with various macrocyclic ligands were successfully determined by X-ray crystallography. THPTACD formed crystals with Co(II), Mn(II), Ni(II), Cu(II), Zn(II) and Cd(II) with the ligand acting as a hexadentate chelator. The geometry of all six cation complex structures were distorted octahedral with Cu(II) being the most twisted towards trigonal prismatic geometry. The crystal structures of Zn(II), Co(II), Mn(II), Ni(II) and Cu(II) with THPTACD are isomorphous with all of them having the overall chirality of [Λ(2λ‴)δ‴δ)]. Two independent Cd(II) complexes with THPTACD crystallised in a unit cell with two DMF solvent molecules and four nitrate counter ions. The two halves are joined by a network of hydrogen bonds and have the overall chirality of [Λλ‴(2δ‴)δ)]. The other Cu(II) complex with THPETACD has the same chirality as the Cu(II) complex with THPTACD. Both Cu(II) complexes show strong Jahn-Teller tetragonal distortion, whereas Ni(II) and Co(II) complexes exhibit weak distortions. Both THPTACD and THPETACD formed both five- and six-membered chelate rings. The six-membered chelate rings adopted a *pseudo* chair conformation with the metal cation at the apex of the chelate ring.

The crystal structure of the protonated 1,5-*bis*[(2*S*)-2-hydroxybutyl]-1,5,9-triazacyclododecane, which has two pendant arms, shows strong hydrogen bonding and the pendant arms are on opposite sides of the ring.

Lastly, the parent macrocyclic ligand, 12aneN_3, crystallised as a binuclear Cd(II) complex with μ-dichloro bridging groups. The overall chirality of the Cd(II) complexes with both THPTACD and 12aneN_3 are the same.

Chapter 6

General conclusions

The five macrocyclic ligands, THPTACD, TMPTACD, THMPTACD, THBTACD and THPETACD were successfully synthesised by the addition of pendant arms to a preformed 1,5,9-triazacyclododecane ligand. The 12aneN_3 parent macrocycle was prepared from simple starting materials, 1,3-propanediol and *bis*(3-aminopropyl)-amine which were protected by toluene-4-sulfonyl chloride. The deprotection of the parent macrocycle was done using a mixture of 48% hydrobromic acid and glacial acetic acid. Preparation of macrocyclic ligands is difficult owing to several reaction pathways occurring simultaneously and which often lead to thermodynamically stable open chain compounds. To obtain cyclic products, reaction conditions must be strictly controlled. The open chain amine compounds are difficult to separate from the macrocyclic ligands. According to our protocol, preparation of sufficiently pure macrocyclic ligands with pendant arms was achieved.

In this work, the protonation constants of THPTACD, THBTACD and THMPTACD were successfully determined by means of potentiometric titrations, using a glass electrode under inert conditions. All the three ligands are less basic than the parent macrocyclic ligand, 12aneN_3, a result that can be rationalised in terms of less steric hindrance to solvation of the protonated species and formation of strong hydrogen bonds between the proton and unprotonated nitrogen donor atoms of the ring. On the other hand, THPTACD is more basic than both THBTACD and THMPTACD, a result that can be attributed to less steric hindrance to solvation of both protonated and unprotonated species. Solvation of the protonated species is important in dispersing the positive charge on the nitrogen atom carrying the proton whereas desolvation of the free ligand has an important effect on the entropy of the system. The mono-protonated THBTACD, in turn, is more basic than the protonated THPTACD and THMPTACD, which can be rationalised in terms of better correlation between the inductive and steric effects. In general, the first protonation is sterically driven, whereas the second protonation is mostly inductively driven. The third protonation constants for all three ligands were not determined because of the lack of sensitivity of the glass electrode in very acidic medium. It is important to realise that the relative significance of the factors involved in the protonation of the macrocyclic ligands is

very complicated and for a complete interpretation of the thermodynamics involved, one has to fully understand the different steps in a Born Haber-type cycle of the complete process. In the cycle, desolvation of the reactive species takes place from the aqueous phase and the bond formation then occurs in the gaseous phase, in line with quantum mechanical interpretation of bond formation. After the bond formation, the protonated species are resolvated in aqueous phase. The desolvation of the ligand is an endothermic process whereas both bond formation and resolvation of the protonated species are exothermic processes. The associated entropy changes are also not easily understood.

The same procedure used for the protonation titration was employed for the determination of the stability constants of the three ligands, THPTACD, THBTACD and THMPTACD with Co(II), Zn(II), Cd(II) and Pb(II). The stability constants of all three ligands peaked at Zn(II) which can be attributed to better dative interaction between the donor atoms and the central metal ion owing to ring size selectivity. The crystal structure of the Zn(II) complex with THPTACD showed that the metal ion is situated very close to the macrocyclic ring thereby leading to strong σ-donation for Zn(II)-N bond formation and should result in a highly negative enthalpy term. The Cd(II) formed least stable complexes with all three ligands which can be understood in terms of long Cd(II)-N bond lengths (weaker overlap) and the hardness of the oxygen donor atoms. THPTACD formed strong metal complexes with all metal ions owing to less steric hindrance imposed by the hydroxypropyl groups compared to hydroxybutyl and methyl-2-methylpropyl groups of the pendant arms in THBTACD and THMPTACD, respectively. The stability of Pb(II) and Co(II) metal complexes are between the two extremes. This is surprising considering that Co(II) and Pb(II) as the smallest and largest metal ions used in this investigation, respectively, are expected to form either the least or the most stable complexes depending on which one of the five- or six-membered chelate rings has the largest influence on the stability of the resultant metal complexes. The crystal structure determination of Co(II) associated with THPTACD showed that the metal ion sits far from the parent macrocyclic ring exhibiting long Co(II)-N and short Co(II)-O bond lengths indicating that the metal ion is placed closer to five-membered chelate rings as compared to Zn(II) which is closer to the six-membered chelate rings. Pb(II), on the other hand, is acting like a small metal which can be attributed to either high polarisability or the fact that the ion possesses a stereochemically active lone pair of electrons. The formation of the metal-ligand bonds is, just like in the protonation reactions, considered to take place in the gaseous phase but again the data for the different steps in the thermodynamic cycle are

not available. Some light can be shed upon the problem by consideration of the bond lengths determined from molecular mechanics studies or data generated from crystal and molecular structure determination. In this investigation, by careful consideration of crystal and molecular structure data, successful interpretation of the stability constants of THPTACD, THBTACD and THMPTACD with Co(II), Zn(II), Cd(II) and Pb(II) has been achieved.

Suitable crystals for single crystal X-ray diffraction were successfully grown from the DMF solution of the divalent metal complexes by slow diffusion of the diethyl ether. In the complexes of THPTACD with Zn(II), Co(II), Mn(II), Ni(II), Cu(II), and Cd(II), the nitrogen donor atoms of the parent macrocyclic ring define one plane below the metal ion and oxygen donor atoms of the pendant arms define another plane above the central metal ion. The crystal structures of Zn(II), Co(II), Mn(II), Ni(II) and Cu(II) are isomorphous. The geometry of all six cationic macrocyclic complex structures are *pseudo* octahedral with Cu(II) being the most distorted towards trigonal prismatic geometry. The Cu(II) complex shows strong Jahn-Teller tetragonal distortion whereas Ni(II) and Co(II) exhibits much weakened distortions. Two of the six-membered chelate rings for isomorphous structures adopt *pseudo* chair λ''' conformation and the third one adopt a δ''' conformation with the metal cation at the apex of the chelate ring whereas the five-membered chelate rings appear in δ conformation. The hydrogen-bonded Cd(II) complex of THPTACD contrasts with the di-μ-chloro-bridged dimeric Cd(II) complex of 12aneN$_3$. The crystal structure of the latter has a centre of inversion such that the asymmetric unit is one-half of a complex unit whereas the former has no centre of symmetry. The overall chirality description of the isomorphous structures as well as a Cu(II) complex of THPETACD is $[\Lambda((2\lambda''')\delta'''\delta)]$. On the other hand, two of the six-membered chelate rings of the two Cd(II) structures adopt δ''' conformation and the third one adopt a λ''' conformation with the metal cation at the apex of the chelate ring whereas the five-membered chelate rings appear in the same conformations as those of the Zn(II), Co(II), Mn(II), Ni(II) and Cu(II) complexes. The overall chirality of each half of the dimeric Cd(II) complex with THPTACD is $[\Lambda(\lambda'''(2\delta''')\delta)]$.

The number of pendant arms present in a ligand can dictate its geometrical preference in complexes. The protonated ligand 1,5-*bis*[(2*S*)-2-hydroxybutyl]-1,5,9-triazacyclododecane, that contains only two such arms and is stabilised by various hydrogen bonds in the crystal, has two oxygen donor atoms on the opposite face of the ring and is pre-organised for

meridional metal coordination in contrast to the *facial* arrangement of all the complexes studied in this investigation.

Pb(II) formed unusually strong metal complexes with all three ligands used in this investigation and in future, more effort should be made to obtain complete crystal data for a series of Pb(II) metal complexes with all three ligands. The axial Cu(II)-O bond length for the THPETACD metal complex is exceptionally long and solution-phase magnetic susceptibilities and UV-VIS studies are necessary to determine the spin states. The Ni(II)-N and Cu(II)-N bonds in THPTACD complexes are short suggesting that these metal ions form strong metal-ligand bonds and it would be interesting to determine their stability constants. Finally, studies of TMPTACD complexation under extreme inert conditions are necessary to minimise polymerisation.

References

Adam K.R., Antolovich M., Baldwin D.S., Brigden L.G., Duckworth P.A., Lindoy L.F., Bashall A., McPartlin M. and Tasker P.A., *J. Chem. Soc., Dalton Trans.*, **1992**, 1869.

Adam K.R., Antolovich M., Baldwin D.S., Duckworth P.A., Leong A.J., Lindoy L.F., McPartlin M. and Tasker P.A., *J. Chem. Soc., Dalton Trans.*, **1993**, 1013.

Adam K.R., Dancey K.P., Leong A.J., Lindoy L.F., McCool B.J., McPartlin M. and Tasker P.A., *J. Am. Chem. Soc.*, **1988**, 110, 8471.

Adam K.R., Leong A.H., Lindoy L.F., Lip H.C., Skelón B.W. and White A.H., *J. Am. Chem. Soc.*, **1983**, 105, 4645.

Adam K.R., Lindoy L.F., Lip H.C., Rea J.H., Skelton B.W. and White A.H., *J. Chem. Soc., Dalton Trans.*, **1981**, 74.

Adamson A.W., *J. Am. Chem. Soc.*, **1954**, 76, 1578-1579.

Addison A.W., Rao T.N., Reedijk J., van Rijn J. and Verschoor G.C., *J. Chem. Soc., Dalton Trans.*, **1984**, 1349-1356.

Ahrland S., Chatt J. and Davies N.R., *Q. Rev., Chem. Soc.*, **1958**, 12, 265.

Al-Juaid S.S., Buttrus N.H., Eaborn C., Hitchcock P.B., Roberts A.T.L., Smith J.D. and Sullivan A.C., *J. Chem. Soc., Chem. Commun.*, **1986**, 908.

Allen F.H. and Taylor R., *Chem. Soc. Rev.*, **2004**, 33, 463-475.

Al-Sagher H., Fallis I., Farrugia L.J. and Peeacock R.D., *J. Chem. Soc., Chem. Commun.*, **1993**, 1499-1500.

Amendola V., Fabbrizzi L., Mangano C., Pallavicini P., Perotti A. and Taglietti A., *J. Chem. Soc., Dalton Trans.*, **2000**, 185.

Anichini A., Fabbrizzi L. and Paoletti P., *Inorg. Chim. Acta*, **1977**, 22, L25.

Argouarch G., Gibson C.L., Stones G. and Sherrington D.C., *Tetrahedron Lett.*, **2002**, 43, 3795-3798.

Arnett J.L., Mitchell E., Murty T.S.S.R., Gorrie T.M. and Schleyer P.V.R., *J. Am. Chem. Soc.*, **1970**, 92, 2365.

Arranz P., Bazzicalupi C., Bencini A., Bianchi A., Ciattini S., Fornasari P., Giorgi C. and altancoli B., *Inorg. Chem.*, **2001**, 40, 6383-6389.

Ashton M. J., Bridge A.W., Bush R.C., Dron D.I., Harris N.V., Jones G.D., Lythgoe D.J., Ridell D. and Smith C., *Bioorg. Med. Chem. Lett.*, **1992**, 2, 375.

Atwood J. L. and Barbour L. J., *Cryst. Growth Des.*, **2003**, 3, 3.

Barbour L. J., *J. Supramol. Chem.*, **2001**, 1, 189.

Barker J.E. and Ren T., *Tetrahedron Lett.*, **2004**, 45, 4681.

Barker J.E. and Ren T., *Tetrahedron Lett.*, **2005**, 46, 6805.

Barnard B.F., MSc Thesis, University of Stellenbosch, Stellenbosch, South Africa, **2008**.

Barton D.H.R., Li W. and Smith J.A., *Tetrahedron Lett.*, **1998**, 39, 7055.

Bates G.B. and Parker D., *J. Chem. Soc., Perkin Trans.*, **1996**, 2, 1109-1115.

Bates R.G., Paabo M. and Robinson R.A., *J. Phys. Chem.*, **1963**, 67, 1833.

Batigalhia F., Zaldini-Hernandes M., Ferreira A.G., Malvestiti I. and Cass Q.B., *Tetrahedron lett.*, **2001**, 57, 9669.

Beissel T., Burger K.S., Voigt G., Wieghardt K., Butziaff C. and Trautwein A.X., *Inorg. Chem.*, **1993**, 32, 124.

Belal A.A., Chaudhuri P., Fallis I., Farrugia L.J., Hartung R., MacDonald N.M., Nuber B., Peacock R.D., Weiss J. and Weighardt K., *Inorg. Chem.*, **1991**, 30, 4397-4402.

Belal A.A., Farrugia L.J., Peacock R.D. and Robb J., *J. Chem. Soc., Dalton Trans.*, **1989**, 1931-1935.

Bernhardt P.V. and Lawrance G.A., *Coord. Chem. Rev.*, **1990**, 104, 297.

Bevilacqua A., Gelb R.T., Hobard W.B. and Zompa L.J., *Inorg. Chem.*, **1987**, 26, 2699.

Bosnich B., Mason R., Pauling P.J., Robertson G.B. and Tobe M.L., *J. Chem. Soc., Chem. Commun.*, **1965**, 97.

Bossek U., Hanke D. and Wieghardt K., *Polyhedron*, **1993**, 12, 1.

Boyce R., Li G., Nestler H.P., Suenega T. and Still W.C., *J. Am. Chem. Soc.*, **1994**, 116, 7955.

Bradshaw J.S., Krakowiak K.E. and Izatt R.M., *Aza-crown Macrocycles*, John Wiley & Sons: New York, **1993**, 45.

Briellmann M., Kaderli S., Meyer C.J. and Zuberbühler A.D., *Helv. Chim. Acta.*, **1987**, 70, 680-689.

Bruno I.J., Cole J.C., Edginton P.R., Kessler M., Macrae C.F., McCabe P., Perason J. and Taylor R., *Acta. Cryst.*, **2002**, B58, 389

Busch D.H., Farmery K., Goedken V., Katovic V., Melnyk A.C., Sperati C.R., and Tokel N., *Advan. Chem. Ser.*, **1971**, 100, 44-78.

Cabbiness D.K. and Margerum D.W., *J. Chem. Soc., Chem. Commun.*, **1969**, 91, 6540-6541.

Cannas M., Margoniu G. and Saba G., *J. Chem. Soc., Dalton Trans.*, **1980**, 2090.

Chamberlain B.M., Sun Y., Hagadorn J.R., Hemmesch E.W., Young V.G., Pink M., Hillmyer M.A., and Tolman W.B., *Macromolecules*, **1999**, 32, 2400-2402.

Chang C.A., Liu Y.L., Chen C.Y. and Chou X.M., *Inorg. Chem.*, **2001**, 40, 3448-3455.

Christiansen L., Hendrickson D.N., Toftlund H., Wilson S.R. and Xie C., *Inorg. Chem.*, **1986**, 25, 2813-2818.

Ciampolina M., Paoletti P. and Sacconi L., *J. Chem. Soc.*, **1960**, 4553.

Clague A.D.H., Govil G. and Bernstein H.S., *Can. J. Chem.*, **1969**, 47, 625.

Collins F.M., Lucy A.R. and Sharp C., *J. Mol. Catal. A: Chem.*, **1997**, 117, 397.

Collman J.P. and Schneider P.W., *Inorg. Chem.*, **1966**, 5, 1380.

Constable E.C., *Coordination Chemistry of Macrocyclic Compounds*, Oxford University Press, New York, **1999**, 1-40.

Cortes S., Brucher E.,Geraldes C.F.G.C. and Sherry A.D., *Inorg. Chem.*, **1990**, 29, 5-9.

Costamagna J., Ferraudi G., Matsuhiro B., Campos-Vallette M., Canales J., Villagran M., Vargas J. and Aguirre M.J., *Coord. Chem. Rev.*, **2000**, 196, 125.

Cox P.H. and Rillay M., *The Clinical Application of Spect.*, Kluwer, New York, **1995**, 29

Cram D.J., Kaneda T., Helgeson R.C., Brown S.B., Knobler C.B., Maverick E. and Trueblood K.N., *J. Am. Chem. Soc.*, **1985**, 107, 3645.

Curtis N.F., *Coord. Chem. Rev.*, **1968**, 3, 3.

Davies P.J., Taylor M.R., Wainwright K.P., Harriott P. and Duckworth P.A., *Inorg. Chim. Acta.*, **1996**, 246, 1-6.

Davies T., Singer S.S. and Staveley L.A.K., *J. Chem. Soc.*, **1954**, 2304.

De Lagrange S. and Nepveu F., *Tetrahedron Lett.*, **1999**, 40, 4989-4992.

De Sousa A.S., Hancock R.D. and Reibenspies J.H., *J. Chem. Soc., Dalton Trans.*, **1997**, 939-944.

De Vos D.E. and Bein T., *J. Organomet. Chem.*., **1996**, 520, 195-200.

Delgado R. and Frausto da Silva J.J.R., *Talanta*, **1982**, 29, 815.

Delgado R., Frausto da Silva J.J.R., Vaz M.C.T.A., Paoletti P. and Micheloni M., *J. Chem. Soc., Dalton Trans.*, **1989**, 133.

Delgado R., Sun Y., Motekaitis R.J. and Martell A.E., *Inorg. Chem.*, **1993**, 32, 3320-3326.

Desiraju G.R., *Design of Organic Solids, Materials Science Monogarphs 54*, Elsevier, Amsterdam, **1989**.

Dhillon R.S., Madbak S.E., Ciccone F.G., Buntine M.A., Lincoln S.F. and Wainwright K.P., *J. Am. Chem. Soc.*, **1997**, 119, 6126.

Dhillon R.S., Madbak S.E., Ciccone F.G., Buntine M.A., Lincoln S.F. and Wainwright K.P., *J. Am. Chem. Soc.*, **1998**, 120, 11, 212.

Donohue J., *Structural Chemistry and Molecular Biology*; Rich A. and Davidson N., Eds., W.H. Freeman, san Francisco, **1968**, 459-601.

Drumhiller J.A., Montavon F., Lehn J.M. and Taylor R.W., *Inorg. Chem.*, **1986**, 25, 3751-3757.

Eigen M., *Advances in the Chemistry of the Coordination Compounds*, ,The Macmillan Co., New York, **1961**, 373.

Fani M., Vranjes S., Archimandritis S.C., Potamianos S., Xanthopoulos S., Bouziotis P. and Varvarigou A.D., *Appl. Radiat. Isot.*, **2002**, 57, 665-674.

Farrell N., Kiley D.M., Schmidt W. and Hacker M.P., *Inorg. Chem.*, **1990**, 29, 397.

Farrugia L.J., Macdonald N.M., Peacock R.D. and Robb J., *Polyhedron*, **1995**, 14, 541.

Feng X., Wang Z., Bian N. and Wang Z., *Inorg. Chim. Acta.*, **2007**, 360, 4103-4110.

Ferro-Flores G., Hernández-Oviedo O., Arteaga de Murphy C., Tendilla J.I., Monroy-Guzmán F., Pedraza-López M. and Aldama-Alvarado K., *Appl. Radiat. Isot.*, **2004**, 61, 1227-1233.

Geraldes C.F.G.C., Alpoim M.C., Marques M.P.M., Sherry A.D. and Singh M., *Inorg. Chem.*, **1985**, 24, 3876.

Geraldes C.F.G.C., Sherry A.D., Marques M.P.M., Alpoim M.C. and Cortes S., *J. Chem. Soc., Perkin Trans.*, **1991**, 2, 137.

Gerasimchuk N.N., Gerges A., Clifford T., Danby A. and Bowman-James K., *Inorg. Chem.*, **1999**, 38, 5633.

Gibson G.T.T., Mohamed M.F., Neverov A.A., and Brown R.S., *Inorg. Chem.*, **2006**, 45, 7891-7902.

Gillespie R.J. and Nyholm R.S., *Q. Rev. Chem. Soc.*, **1957**, 11, 339.

Gladkikh O.P., Inwood H., Nicholls D. and Weatherburn D.C., *Inorg. Chim. Acta.*, **2002**, 331, 131-135.

Greene R.N., *Tetrahedron Lett.*, **1972**, 1793.

Grunwald E. and Berkowitz B.J., *J. Am. Chem. Soc.*, **1951**, 73, 4939.

Haidar R., Ipek M., DasGupta B., Yousaf M. and Zompa L.J., *Inorg. Chem.*, **1997**, 36, 3125-3132.

Haines R.I. and McAuley A., *Coord. Chem. Rev.*, **1981**, 37, 77.

Hama H. and Takamoto S., *Nippon Kagaku Kaishi*, **1975**, 1182.

Han W., Li L., Gu W., Liu Z, Yan S., Liao D., Jiang Z. and Cheng P., *J. Coord. Chem.*, **2004**, 57, 41-47.

Hancock R. D., *Acc. Chem. Res.*, **1990**, 23, 253.

Hancock R.D. and MacDougall G.J., *J. Am. Chem. Soc.*, **1980**, 102, 6553-6555.

Hancock R.D. and Marsicano F., *J. Chem.* Soc., *Dalton Trans.*, **1976**, 1096.

Hancock R.D. and Martell A.E., *Chem. Rev*., **1989**, 89, 1875-1914.

Hancock R.D. and Thöm V.J., *J. Am. Chem. Soc.*, **1982**, 104, 291-292.

Hancock R.D., *Prog. Inorg. Chem.***, 1989**, 37, 187.

Hancock R.D., *Pur. Appl. Chem.*, **1986**, 58, 1445.

Hancock R.D., Shaikjee M.S., Dobson S.M. and Boeyens C.A., *Inorg. Chim. Acta.*, **1988**, 154, 229-238.

Hathaway B.J. and Hodgson P.G., *J. Inorg. Nucl. Chem.*, **1973**, 35, 4071.

Haymore B.L., Lamb J.D., Izatt R.M. and Christensen J.J., *Inorg. Chem.*, **1982**, 21, 1598.

Hegg E.L., Mortimore S.H., Cheung C.L., Huyett J.E., Powell D.R. and Burstyn J.N., *Inorg. Chem.*, **1999**, 38, 2961-2968.

Helps I.M., Parker D., Jankowski K.J., Chapman J. and Nicholson P.E., *J. Chem. Soc. Perkin Trans.*, **1989**, I, 2079-2082.

Hinz F.P. and Margerum D.W., *J. Am. Chem. Soc.*, **1974**, 96, 4994.

Holmes F. and Williams D.R., *J. Chem. Soc. A.*, **1967**, 1702.

Hu F., Cutler C.S., Hoffman T., Sieckman G., Volkert W.A. and Jurisson S.S., *Nucl. Med. Biol.*, **2002**, 29, 423-430.

Huskens J. and Sherry A.D., *J. Chem. Soc.*, *Dalton Trans*., **1998**, 177–184.

Iorio E.J. and Still W.C., *Bioorg.Med. Chem. let*., **1996**, 6, 2673-2676.

Irving H. and Williams R.J.P., *J Chem. Soc.*, **1953**, 3192.

Izatt R. M., Pawlak K. and Bradshaw J.S., *Chem. ReV.*, **1991**, 91, 1721.

Izatt R.M., Bradshaw J.S., Nielsen S.A., Lamb J.D., Christensen J.J. and Sen D., *Chem. Rev*., **1985**, 85, 271.

Izatt R.M., Pawlak K., Bradshaw J.S. and Bruening R.L., *Chem. Rev.*, **1995**, 95, 2529-2586.

Jain V.K. and Jakkal V.S., *J. Organomet. Chem.*, **1996**, 515, 81.

Jung S.K., Kang S.G. and Suh M.P., *Bull. Kor. Chem. Soc.*, **1989**, 10, 362.

Kaden T.A., *Top. Curr. Chem.*, **1984**, 121, 157.

Kaden T.A., Tschudin D., Studer M. and Brunner U., *Pure Appl. Chem.*, **1989**, 61, 879.

Kallinen K.O., Pakkanen T.T. and Pakkanen T.A., *J. Organometallic Chem.*, **1997**, 547, 319-327.

Kavana M., Powell D.R. and Burstyn J.N., *Inorg. Chim. Acta.*, **2000**, 297, 351-361.

Kimura E., Kodake Y., Shionya M. and Shiro M., *Inorg. Chem.*, **1990**, 29, 4991.

Kimura E., Nakamura I., Koike T., Shionoya M., Kodama Y., Ikeda T. and Shiro M., *J. Am. Chem. Soc.*, **1994**, 116, 4764-4771.

Kimura E., *Prog. Inorg. Chem.*, **1994**, 41, 443.

Kimura E., Shiota T., Koike T., Shiro M. and Kodama M., *J. Am. Chem. Soc.*, **1990a**, 112, 5805.

Kodama M. and Kimura E., *J. Chem. Soc., Dalton Trans.*, **1976**, 166, 1720.

Koikawa M., Jensen K.B., Matsushima H., Tokii T. and Toftlund H., *J. Chem. Soc., Dalton Trans.*, **1998**, 1085.

Kollman P.A. and Allen L.C., *J. Am. Chem. Soc.*, **1971**, 93, 4991.

Kong D., Huang X. and Xie Y., *Inorg. Chim. Acta.*, **2002**, 340, 133-138.

Konstantinovskaya M.A., Yatsimirskii K.B., Shcherbakov B.K., Polikarpov Y.M., Mdved T.Y. and Kabachnik M.I., *Russ. J. Inorg. Chem.*, **1985**, 30, 1463.

Koyama H. and Yoshino T., *Bull. Chem. Soc, Jpn.*, **1972**, 45, 481-484.

Krakowiak K.E. and Bradshaw J.E., *Ind. Eng. Chem. Res.*, **2000**, 39, 3499-3507.

Krakowiak K.E., Bradshaw J.S., Dalley N.K., Jiang W. and Izatt, R.M., *Tetrahedron Lett*., **1989**, 30, 2897.

Krakowiak, K.E., Bradshaw J.S. and Izatt R.M., *Synlett.*, **1993**, 611.

Krishnamurthy R. and Schaap W.B., *Ibid.*, **1969**, 46, 799.

Larpent C., Laplace A. and Zemb T., *Angew. Chem., Int. Ed.*, **2004**, 43, 3163.

Lehn J.M., *Acc. Chem. Res.*, **1978**, 11, 49.

Leugger A.P., Hertli L. and Kaden, T.A. *Helv. Chim. Acta.*, **1978**, 61, 2296.

Lewin A., Hill J.P., Boetzel R., Georgiou T., James R., Kleanthous C. and Moore G.R., *Inorg. Chim. Acta.*, **2002**, 331, 123-130.

Li H., Guan Y., Szczepanska A., Moreno-Vargas A.J., Carmona A.T., Robina I., Lewis G.K. and Wang L., *Bioorg. Med. Chem.*, **2007**, 15, 4220-4228.

Li W.P., Smith C.J., Cutler C.S., Hoffman T.J., Ketring A.R. and Jurisson S.S., *Nucl. Med. Biol.*, **2003**, 30, 241-251.

Liang F., Wang P., Zhou X., Li T., Li Z., Lin H., Gao D., Zheng C. and Wu C., *Bioorg. Med. Chem. Lett.*, **2004**, 14, 1901-1904.

Liang F., Wu C., Lin H., Li T., Gao D., Li Z., Wei J., Zheng C. and Sun M., *Bioorg. Med. Chem. Lett.*, **2003**, 13, 2469-2472.

Lindoy L.F., *Pur. App. Chem.*, **1997**, 69, 2179-2186.

Lindoy L.F., *The Chemistry of Macrocyclic Ligand Complexes*, Cambridge University Press, Cambridge, **1989**, 1-47.

Liu R., Wu L., Zhang X., Li Yi. and Wang Z., *Inorg. Chim Acta.*, **2007**, 360, 6562.

Luckay R.C., Hancock R.D., Cukrowski I. and Reibenspies J. H., *Inorg. Chim. Acta.*, **1996**, 246, 159-169

Luckay R.C., PhD Thesis, University of Witwatersrand, Johannesburg, South Africa, **1997**.

Marques F., Guerra K.P., Gano L., Costa J., Campello M.P., Lima L.M.P., Delgado R. and Santos I., *J. Biol. Inorg. Chem.*, **2004**, 9, 859-872.

Martell A. E. and Hancock R. D., *Metal Complexes in Aqueous Solutions*, Plenum, New York, **1996**, 24-298.

Martell A.E. and Motekaitis R.J., *Determination and Use of Stability Constants*, VCH Publishers, New York, **1988**, 1-31.

Martell A.E. and Smith R.M., *Critical Stability Constants*, Vol. 1-6, Plenum Press, New York, **1974-1989.**

Martell, A.E. and Motekaitis, R.J., *Determination and Use of Stability Constants*, 2nd ed., VCH, New York, **1992**.

Matthews R.C., Parker D., Ferguson G., Kaitner B., Harrison A. and Royle L., *Polyhedron*, **1991**, 10, 1951.

May P.M., Murray K. and Williams D.R., *Talanta*, **1988**, 35, 825-830.

McCann N., Lawrance G.A., Neuhold Y.M. and Maeder M., *Inorg. Chem.*, **2007**, 46, 4002-4009.

McDougall G.J., Hancock R.D. and Boeyens J.C.A., *J. Chem. Soc., Dalton Trans.*, **1978**, 1438.

Meyerstein D., *Coord. Chem. Rev.*, **1999**, 185-186, 141.

Moore D.A., Fanwick P.E. and Welch M. J., *Inorg. Chem.*, **1990**, 29, 672.

Moore D.A., Fanwick P.E. and Welch M.J., *Inorg. Chem.*, **1989**, 28, 1504.

Morphy J. R., Parker D., Kataky R., Harrison A., Eaton M.A.W., Millican A., Phipps A. and Walker C., *J. Chem. Soc., Chem. Commun.*, **1989**, 792.

Mosmann T., *J. Immunol. Methods*, **1983**, 65, 55.

Nation D.A., Martell A.E., Carroll R.I. and Clearfield A., *Inorg. Chem.*, **1996**, 35, 7246.

Norante G.M., Di Vaira M., Mani F., Mazzi S. and Stoppioni P., *J. Chem. Soc., Dalton Trans.*, **1992**, 361-365.

Notni J., Görls H. and Anders E., *Eur. J. Inorg. Chem.*, **2006**, 1444-1455.

Parker L.L., Anderson F.M., O'Hare C.C., Lacy S.M., Bingham J.P., Robins D.J., and Hartley J.A., *Bioorg. Med. Chem.*, **2005**, 13, 2389.

Pauling L., *The nature of the chemical bond*, 2nd ed., Cornell University Press, Ithaca, N. Y. **1940**, pp 76.

Pearson R.G., *J. Am. Chem. Soc.*, **1963**, 85, 3533-3539.

Pedersen C.J., *J. Am. Chem. Soc.*, **1967**, 89, 7017.

Pedersen C.J. and Frensdorff H.K., *Angew. Chem., Int. Ed. Engl.*, **1972**, 11, 16.

Poulsen I. and Bjerrum J., *Acta. Chem. Scand.*, **1955**, 9, 1407.

Prata M.I.M., Santos A.C., Geraldes C.F.G.C. and de Lima J.J.P., *Nucl. Med. Biol.*, **1999**, 26, 707.

Prata M.I.M., Santos A.C., Geraldes C.F.G.C. and de Lima J.J.P., *J. Inorg. Biochem.*, **2000**, 79, 359-363.

Pujari P. and dash K.C., *J. Inorg. Nucl. Chem.*, 1976, 38, 1891-1896.

Raymond K.N. and McCormick J.M., *J. Coord. Chem.*, **1998**, 46, 51-57.

Ribeiro-Claro P.J.A., Amado A.M., Marques M.P.M. and Teixeira-Dias J.J.C., *J. Chem. Soc., Perkin Trans.*, **1996**, 2, 1161-1167.

Richman J.E. and Atkins T.J., *J. Am. Chem. Soc.*, **1974**, 96, 2268-2270.

Robb J. and Peacock R.D., *Inorg. Chim. Acta.*, **1986**, 121, L15-L17.

Roh K.R., Kim K.S. and Kim Y.H., *Tetrahedron Lett.*, 1991, 32, 793.

Rosen w. and Busch D.H., *J. Am. Chem. Soc.*, **1969**, 91, 4694-4697.

Rossiter C.S., Mathews R.A. and Morrow J.R., *Inorg. Chem.*, **2005**, 44, 9397-9404.

Sabatini L. and Fabbrizzi L., *Inorg. Chem.*, **1979**, 18, 439.

SADABS, Version 2.05, Bruker AXS Inc., Madison, WI, **2002**.

SAINT, Data Reduction Software, Version 6.45, Bruker AXS Inc., Madison, WI, **2003**.

Sakiyama H., Watanabe Y., Ito R. and Nishida Y., *Inorg. Chim. Acta.*, **2004**, 357, 4309-4312.

Sayer B.A., Michael J.P. and Hancock R.D., *Inorg.Chim. Acta.*, **1983**, 77, L63.

Schaber P.M., Fettinger J.C., Churchill M.R., Nalewajek D. and Fries K., *Inorg. Chem.*, **1988**, 27, 16441-1646.

Schwarzenbach G. and Flaschka H., *Complexometric Titrations*, Methuen, London, **1969**.

Schwarzenbach G., *Helv. Chim. Acta.*, **1952**, 35, 2344.

Sessler J.L., Hugdahl J., Kurosaki H. and Sasaki Y., *J. Coord. Chem.*, **1988**, 18, 93.

Shannon R.D., *Acta Cryst. Sect. B.*, **1976**, 32, 751.

Sheldrick G.M., *SHELX-97. Program for Crystal Structure Analysis*, University of Göttingen, Germany, **1997**.

Shin B.C., Park K.B., Jang B.S., Lim S.M. and Shim C.K., *Nucl. Med. Biol.*, **2001**, 28, 719-725.

Shin J.W. and Min K.S., *Acta. Cryst.*, **2009**, E65, m234.

Shinkai S., Koreishi H., Ueda K., Arimura T. and Manabe, O., *J. Am. Chem. Soc.*, **1987**, 109, 6371.

Sidgwick N.V. and Powell H.M., *Proc. R. Soc. London, Ser. A*, **1940**, 176, 153.

Skerlj R.T., Nan S., Zhou Y. and Bridger G.J., *Tetrahedron Lett.*, **2002**, 43, 7569-7571.

SMART Data Collection Software, Version 5.629, Bruker AXS Inc., Madison, WI, **2003**.

Smith J.R.L. and Shul'pin G.B., *Tetrahedron Lett.*, **1998**, 39, 4909-4912.

Smith R.M., Martell A.E. and Motekaites R.J., *NIST Critically Selected Stability Constants of Metal Complexes Database*, Version 8.0, **2004**.

Smith W.L., Ekstrand J.D. and Raymond K.N., *J. Am. Chem. Soc.*, **1978**, 100, 3539-3544.

Solladié G., Collobert F. and Sonny F., *Tetrahedron Lett.*, **1999**, 40, 1227.

Solladié G., *Synthesis*, **1981**, 185.

Song B., Holy A. and Sigel H., *Gazz. Chim. Ital.*, **1994**, 124, 387.

Spek A.L., *J. Appl. Cryst.*, **2003**, 36, 7-13.

Stetter H. and Mayer K.H., *Chem. Ber.*, **1961**, 94, 1410.

Stetter H. and Roos E.E., *Chem. Ber.*, **1954**, 87, 566.

Stockheim C., Hoster L., Weyhermuller T., Wieghardt K. and Nuber J., *J. Chem. Soc., Dalton Trans.*, **1996**, 4409.

Suh J., Son S.J. and Suh M.P., *Inorg. Chem.*, **1998**, 37, 4872-4877.

Sutor D.J., *J. Chem. Soc.*, **1963**, 1105-1110.

Tan L., Taylor M., Wainwright K. and Duckworth P., *J. Chem. Soc., Dalton Trans.*, **1993**, 2921.

Taylor R. and Kennard O., *J. Am. Chem. Soc.*, **1982**, 104, 5063-5070.

Taylor S.G., Snow M.R. and Hambley T.W., *Aust. J. Chem.*, **1983**, 36, 2359.

Tei L., Bencini A., Blake A.J., Lippolis V., Perra A., Valtancoli B., Wilson C. and Schröder M.J., *J. Am. Chem. Soc., Dalton Trans.*, **2004**, 19344-1944.

Thöm V.J., Fox C.C., Boeyens J.C.A. and Hancock R.D., *J. Am. Chem. Soc.*, **1984**, 106, 5947-5955.

Thöm V.J., Hosken G.D. and Hancock R.D., *Inorg. Chem.*, **1985**, 24, 3378-3381.

Thöm V.J., Shaikjee M.S. and Hancock R. D., *Inorg. Chem.*, **1986**, 25, 2992.

Travis K. and Busch D.H., *J. Inorg. Chem.*, **1974**, 13, 2591-2598.

Turonek M.L., Duckworth P.A., Laurence G.S., Lincoln S.F. and Wainwright K.P., *Inorg. Chim. Acta.*, **1995**, 230, 51-57.

Van der Merwe M.F., Boeyens J.C.A. and Hancock R.D., *Inorg. Chem.*, **1985**, 24, 1208.

Van der Merwe M.F., Boeyens J.C.A. and Hancock R.D., *Inorg. Chem.*, **1983**, 22, 3490.

Van Winkle J. L., McClure J. D. and Williams P. H., *J. Org. Chem.*, **1966**, 31, 3300 .

Wainwright K.P., *Adv. Inorg. Chem.*, **2001**, 52, 293.

Wainwright K.P., *Coord. Chem. Rev.*, **1997**, 166, 35.

Wang Q., Yan S., Liao D., Jiang Z., Cheng P., Leng X. and Wang H., *J. Mol. Struct.*, **2002**, 608, 49-53.

Weeks J.M., Buntine M.A., Lincoln S.F., Tiekink E.R.T. and Wainwright K.P., *J. Chem. Soc*., *Dalton Trans*., **2001**, 2157-2163.

Whitbread S.L., Valente P., Buntine M.A., Clements P., Lincoln S.F. and Wainwright K.P., *J. Am. Chem. Soc.*, **1998**, 120, 2862.

Wieghardt K., Schmidt E., Hermann W. and Küppers H.J., *Coord. Chem. Rev.*, **1990**, 104, 297.

Wieghardt K., Schmidt W., Hermann W. and Küppers H.J., *Inorg. Chem.*, **1983**, 22, 2953.

Wieghardt K., Scoeffmann E., Nuber B. and Weiss J., *Inorg. Chem.*, **1986**, 25, 4877.

Yang R. and Zompa L. J., *Inorg. Chem.*, **1976**, 15, 1499.

Zhang D. and Busch H., *Inorg. Chem.*, **1994**, 33, 5138-5143.

Zompa L. J., *Inorg. Chem.*, **1978**, 17, 2531.

Zompa L.J. and Margulis T.N., *Inorg. Chim. Acta.*, **1978**, 28, L157.

Zompa L.J., Diaz H. and Margulis T.N., *Inorg. Chim. Acta.*, **1995**, 232, 131-137.

Zuckerman J.J., *J. Chem. Educ.*, **1965**, 42, 315.

Proton spectrum of the tosylated 1,3-propanediol

Appendix 1a

Acquisition Time (sec)	3.9947	***Comment***	Imported from VNMR.			***Date***	Aug 13 2009	***Date Stamp***	Aug 13 2009
File Name	C:\Documents and Settings\winxp\Desktop\sumanmr\123H					***Frequency (MHz)***	599.98	***Nucleus***	1H
Number of Transients	16	***Original Points Count***	38397	***Points Count***	65536	***Pulse Sequence***	s2pul	***Receiver Gain***	42.00
Solvent	CHLOROFORM-d			***Spectrum Offset (Hz)***	3607.9338	***Sweep Width (Hz)***	9611.92	***Temperature (degree C)***	25.000

DC-CG 1H

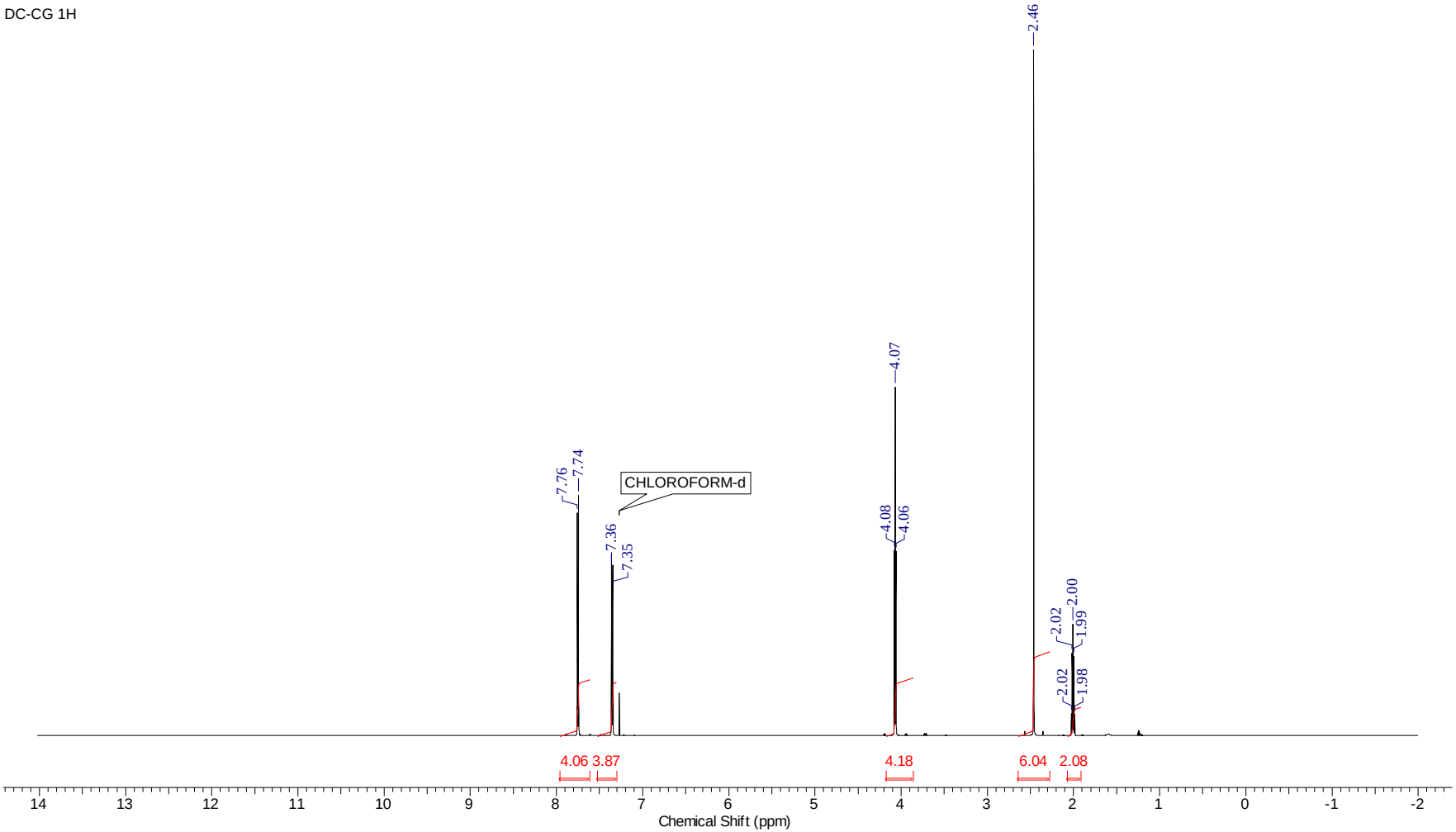

Carbon spectrum of the tosylated 1,3-propanediol

Appendix 1b

Acquisition Time (sec)	1.2984	***Comment***	Imported from VNMR.		***Date***	Aug 13 2009	***Date Stamp***	Aug 13 2009
File Name	C:\Documents and Settings\winxp\Desktop\sumanmr\123C			***Frequency (MHz)***	150.88	***Nucleus***	13C	***Number of Transients***	100000
Original Points Count	53933	***Points Count***	65536	***Pulse Sequence***	s2pul	***Receiver Gain***	60.00		
Solvent	CHLOROFORM-d			***Spectrum Offset (Hz)***	18481.9063	***Sweep Width (Hz)***	41536.86	***Temperature (degree C)***	25.000

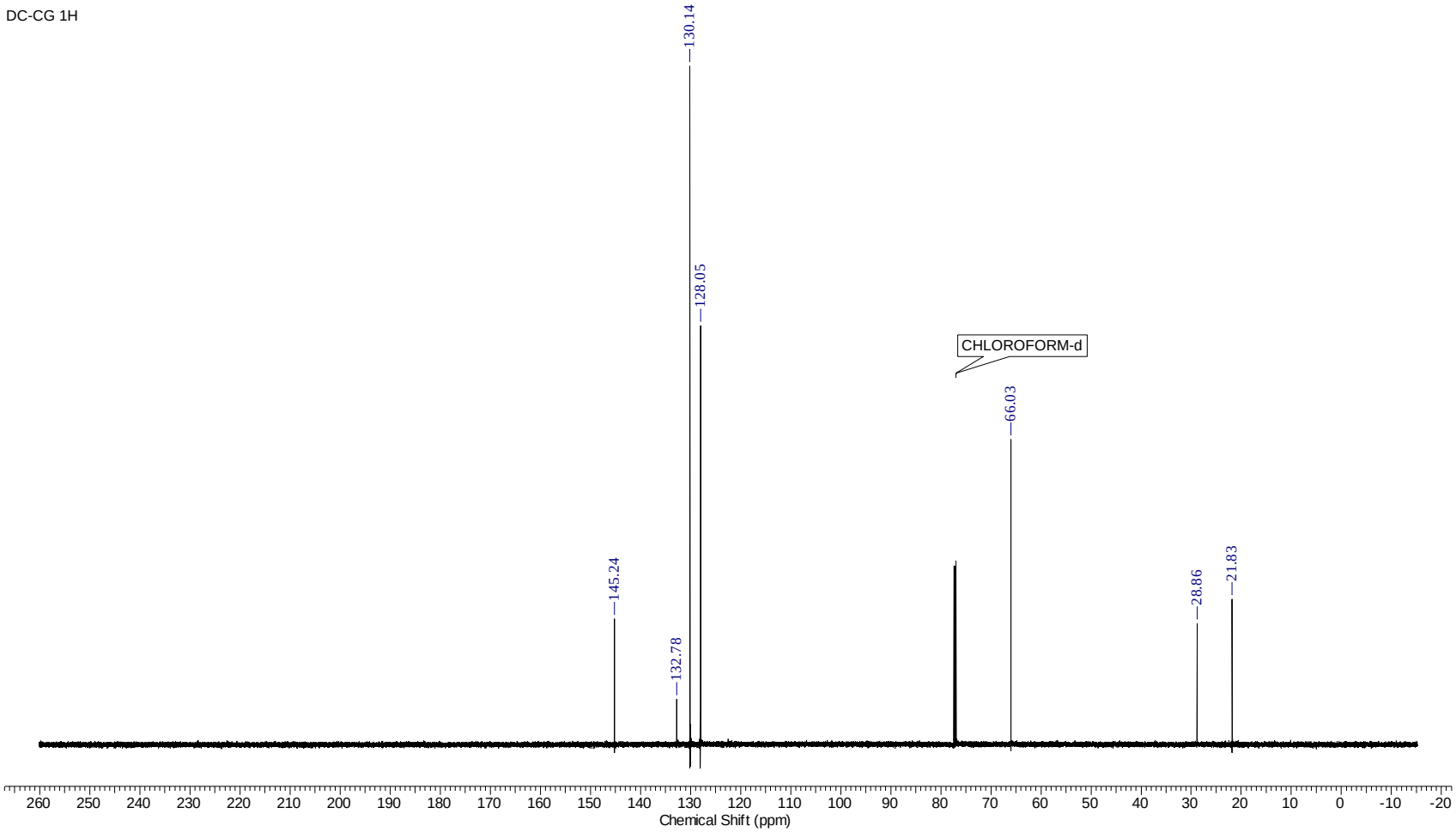

Proton spectrum of the tosylated bis(3-aminopropyl)-amine1,3-propanediol **Appendix 2a**

Acquisition Time (sec)	3.9947	***Comment***	Imported from VNMR.			***Date***	Aug 13 2009	***Date Stamp***	Aug 13 2009
File Name	C:\Documents and Settings\winxp\Desktop\sumanmr\122H					***Frequency (MHz)***	599.98	***Nucleus***	1H
Number of Transients	16	***Original Points Count***	38397	***Points Count***	65536	***Pulse Sequence***	s2pul	***Receiver Gain***	42.00
Solvent	CHLOROFORM-d			***Spectrum Offset (Hz)***	3607.9341	***Sweep Width (Hz)***	9611.92	***Temperature (degree C)***	25.000

DC-CG 1H

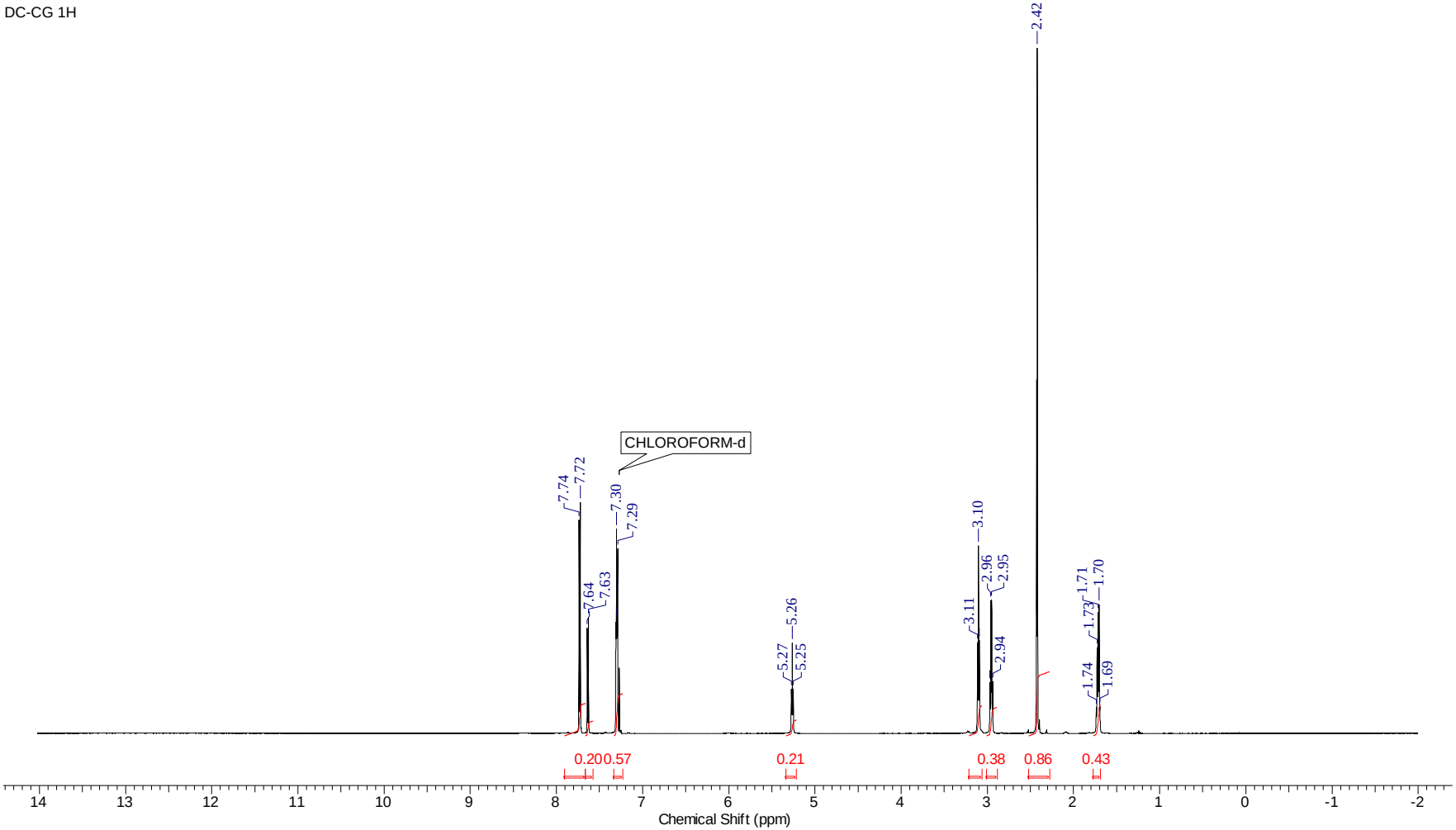

Carbon spectrum of the tosylated bis(3-aminopropyl)-amine1,3-propanediol

Appendix 2b

Acquisition Time (sec)	1.2996	***Comment***	Imported from VNMR.		***Date***	Aug 13 2009	***Date Stamp***	Aug 13 2009
File Name	C:\Documents and Settings\winxp\Desktop\sumanmr\122C			***Frequency (MHz)***	150.88	***Nucleus***	13C	***Number of Transients***	100000
Original Points Count	53982	***Points Count***	65536	***Pulse Sequence***	s2pul	***Receiver Gain***	60.00		
Solvent	CHLOROFORM-d			***Spectrum Offset (Hz)***	18483.1738	***Sweep Width (Hz)***	41536.86	***Temperature (degree C)***	25.000

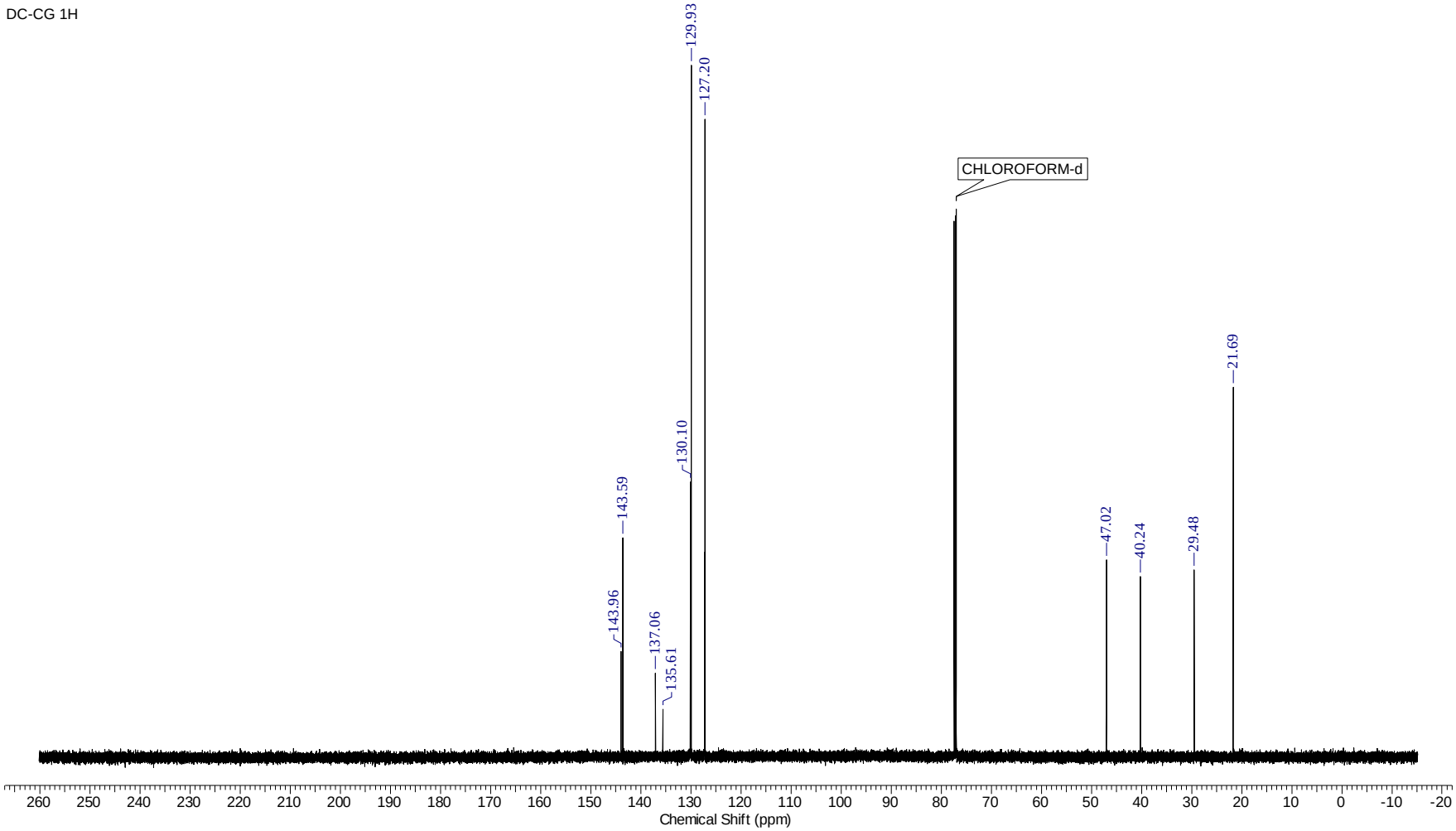

Proton spectrum of the tosylated 1,5,9-triazacyclododecane

Appendix 3a

Acquisition Time (sec)	4.0000	***Comment***	Imported from VNMR.			***Date***	Aug 27 2008	***Date Stamp***	Aug 27 2008
File Name	C:\Documents and Settings\winxp\Desktop\sumanmr\Ckept\Copy of 13					***Frequency (MHz)***	299.74	***Nucleus***	1H
Number of Transients	1	***Original Points Count***	19231	***Points Count***	32768	***Pulse Sequence***	s2pul	***Receiver Gain***	32.00
Solvent	CHLOROFORM-d			***Spectrum Offset (Hz)***	1794.7498	***Sweep Width (Hz)***	4807.69	***Temperature (degree C)***	25.000

DC-CG 1H

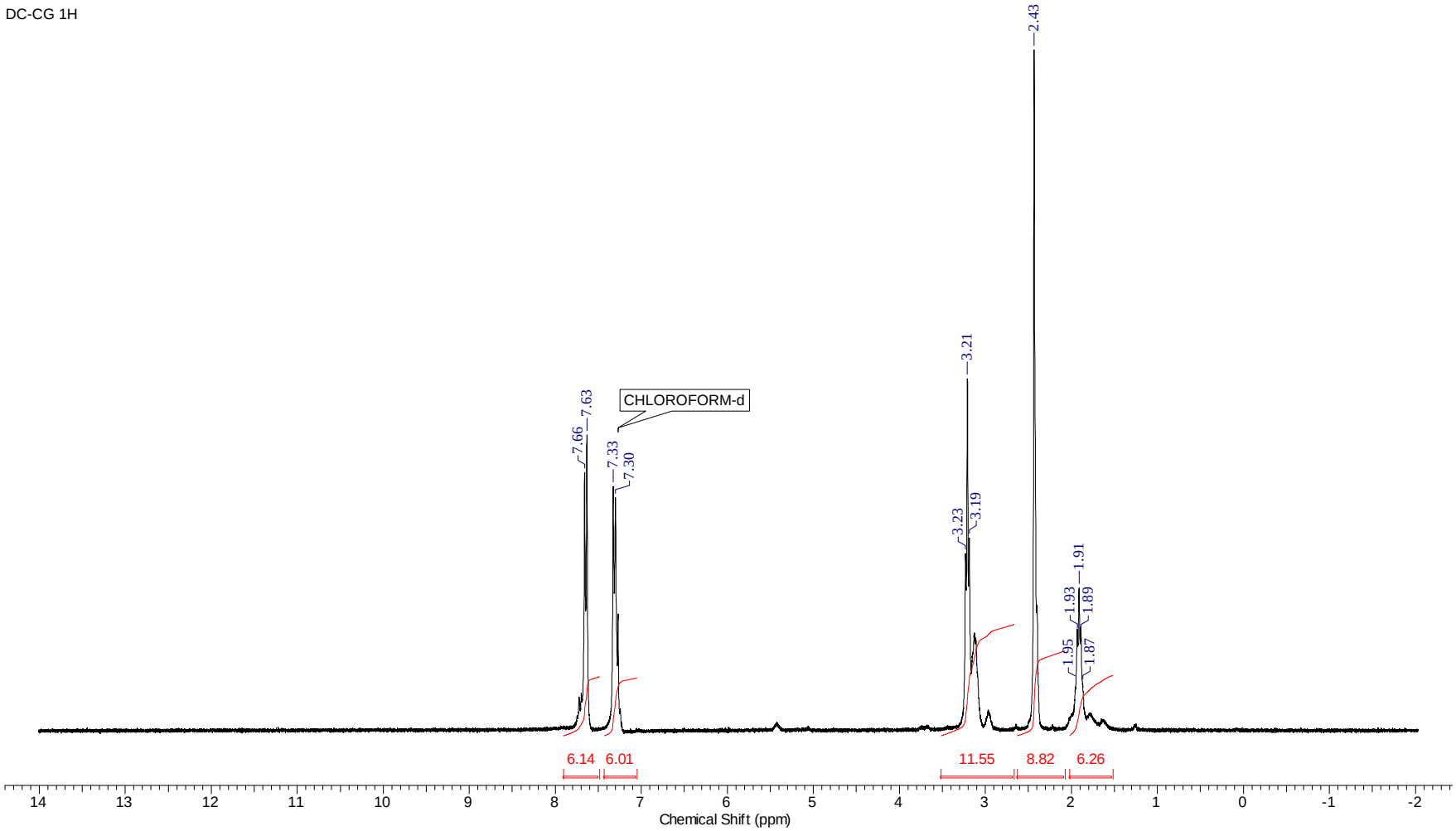

Carbon spectrum of the tosylated 1,5,9-triazacyclododecane

Appendix 3b

Acquisition Time (sec)	1.3046	***Comment***	Imported from VNMR.			***Date***	Aug 31 2009	***Date Stamp***	Aug 31 2009
File Name	C:\Documents and Settings\winxp\Desktop\sumanmr\132C			***Frequency (MHz)***	100.58	***Nucleus***	13C	***Number of Transients***	150000
Original Points Count	41219	***Points Count***	65536	***Pulse Sequence***	s2pul	***Receiver Gain***	30.00		
Solvent	CHLOROFORM-d			***Spectrum Offset (Hz)***	14316.1270	***Sweep Width (Hz)***	31595.58	***Temperature (degree C)***	25.000

DC-CG 1H

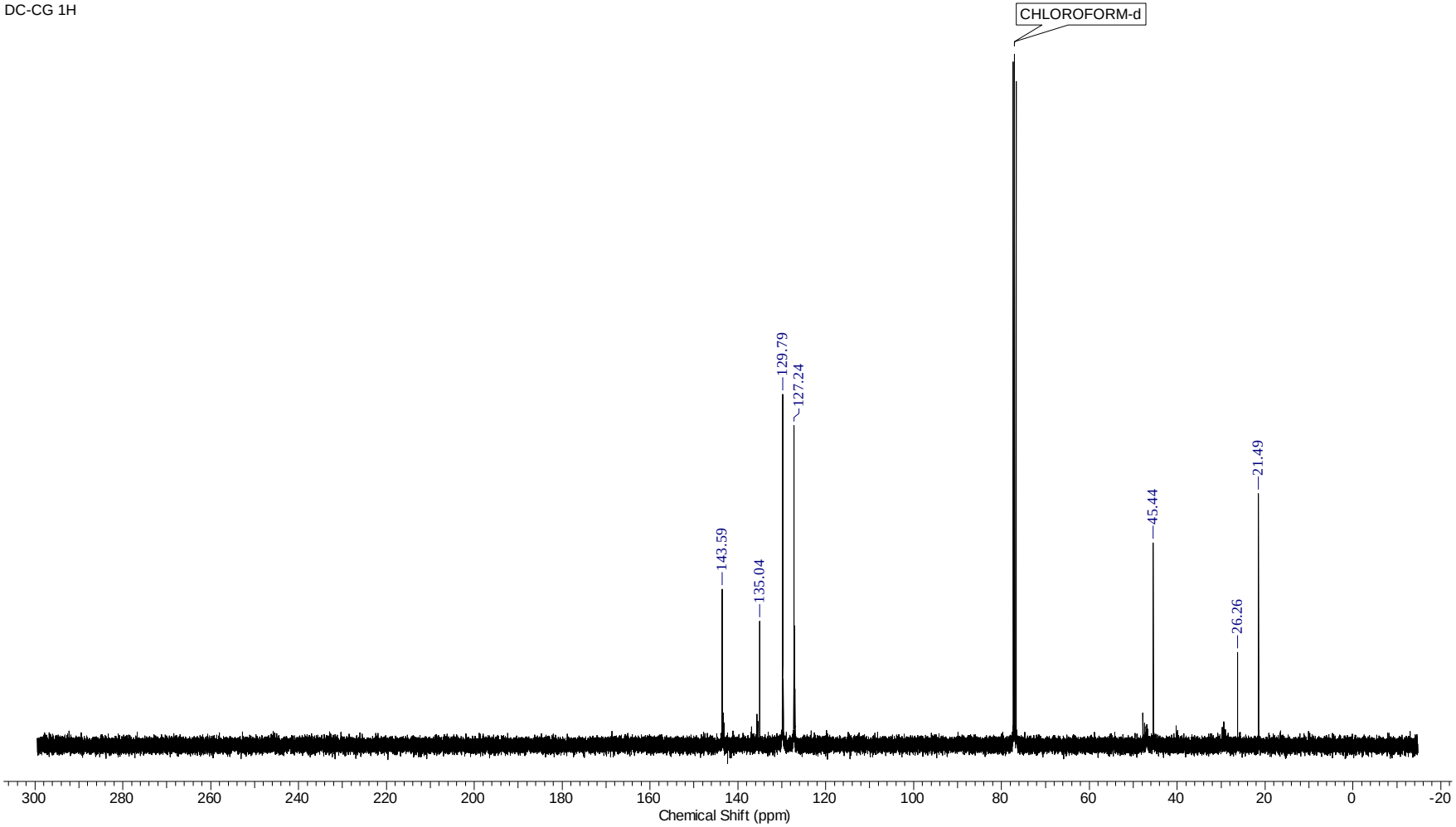

Proton spectrum of the 1,5,9-triazacyclododecane HBr Salt

Appendix 4a

Acquisition Time (sec)	4.0000	***Comment***	Imported from VNMR.			***Date***	Feb 24 2009	***Date Stamp***	Feb 24 2009
File Name	C:\Documents and Settings\winxp\Desktop\sumanmr\HKept\28					***Frequency (MHz)***	299.74	***Nucleus***	1H
Number of Transients	16	***Original Points Count***	19231	***Points Count***	32768	***Pulse Sequence***	s2pul	***Receiver Gain***	20.00
Solvent	DEUTERIUM OXIDE			***Spectrum Offset (Hz)***	1824.3860	***Sweep Width (Hz)***	4807.69	***Temperature (degree C)***	25.000

DC-CG 1H

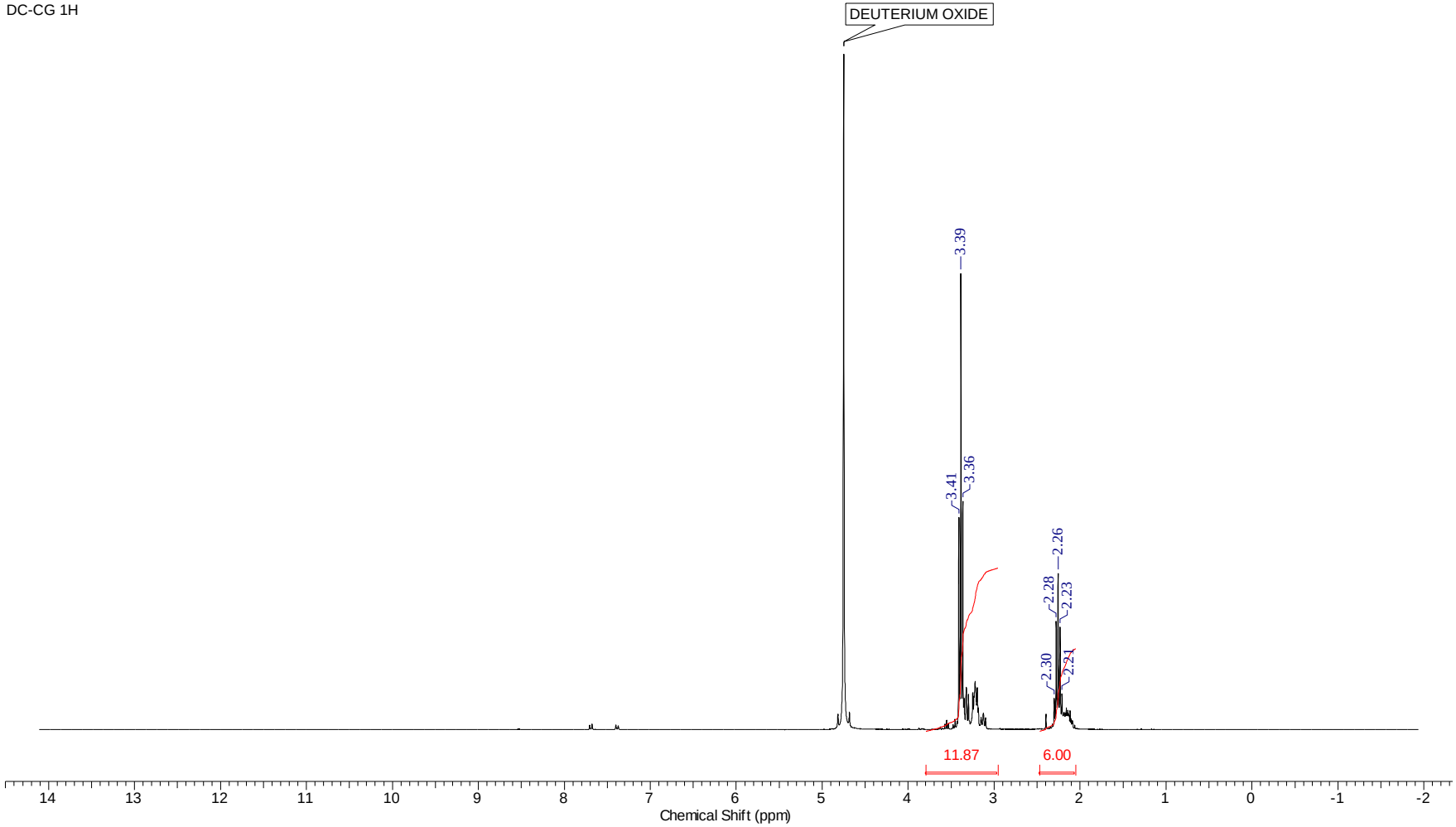

Carbon spectrum of the 1,5,9-triazacyclododecane HBr Salt

Appendix 4b

Acquisition Time (sec)	1.3020	***Comment***	Imported from VNMR.			***Date***	Jun 5 2008	***Date Stamp***	Jun 5 2008
File Name	C:\Documents and Settings\winxp\Desktop\nmr\39C			***Frequency (MHz)***	100.58	***Nucleus***	13C	***Number of Transients***	100000
Original Points Count	35942	***Points Count***	65536	***Pulse Sequence***	s2pul	***Receiver Gain***	30.00		
Solvent	DEUTERIUM OXIDE			***Spectrum Offset (Hz)***	12364.0420	***Sweep Width (Hz)***	27605.24	***Temperature (degree C)***	25.000

DC-CG 1H

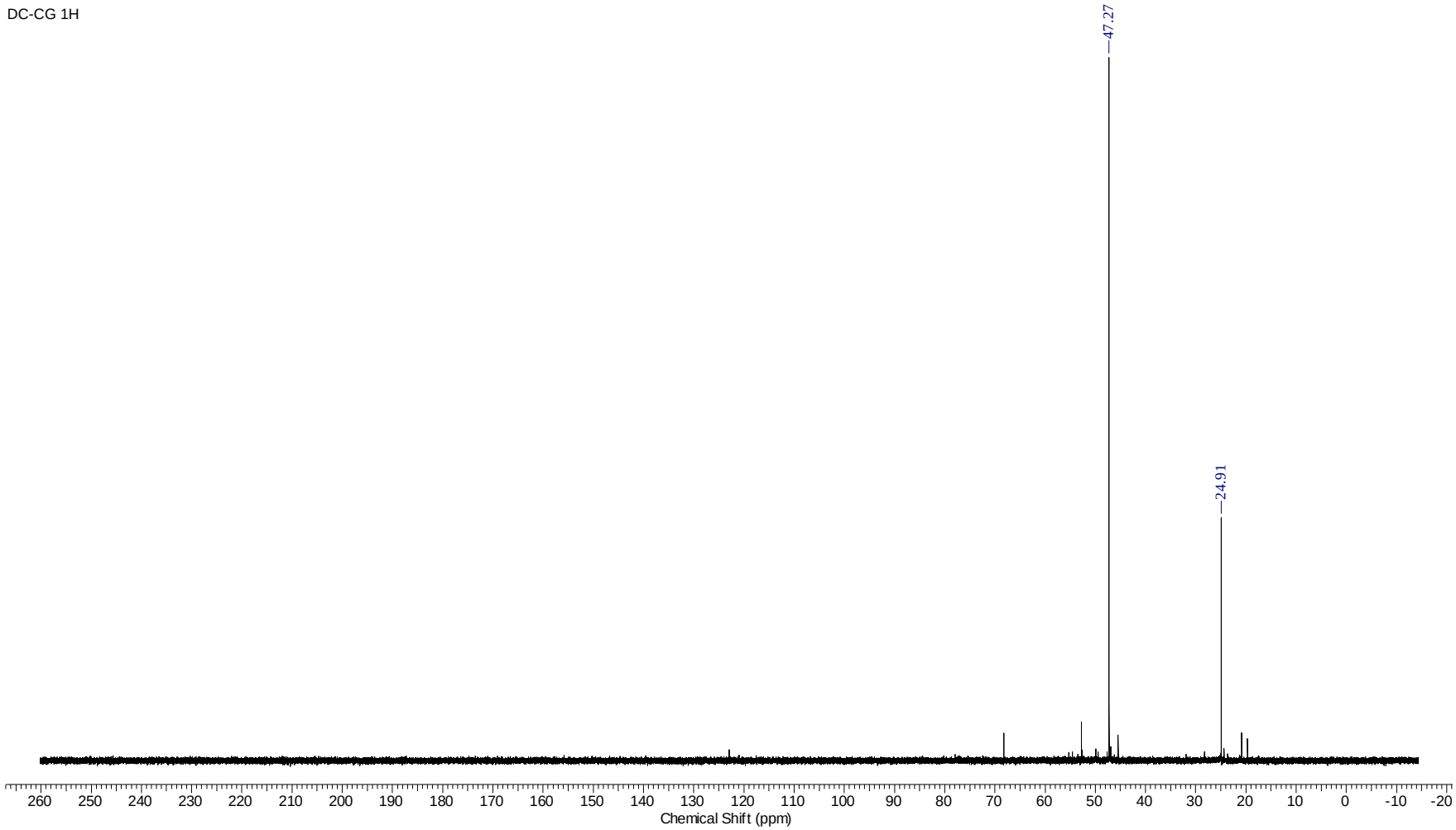

Proton spectrum of the 1,5,9-triazacyclododecane HCl salt

Appendix 5a

Acquisition Time (sec)	4.0000	***Comment***	Imported from VNMR.			***Date***	Mar 16 2009	***Date Stamp***	Mar 16 2009
File Name	C:\Documents and Settings\winxp\Desktop\sumanmr\HKept\37					***Frequency (MHz)***	299.74	***Nucleus***	1H
Number of Transients	16	***Original Points Count***	21645	***Points Count***	32768	***Pulse Sequence***	s2pul	***Receiver Gain***	28.00
Solvent	DEUTERIUM OXIDE			***Spectrum Offset (Hz)***	2119.9207	***Sweep Width (Hz)***	5411.26	***Temperature (degree C)***	25.000

DC-CG 1H

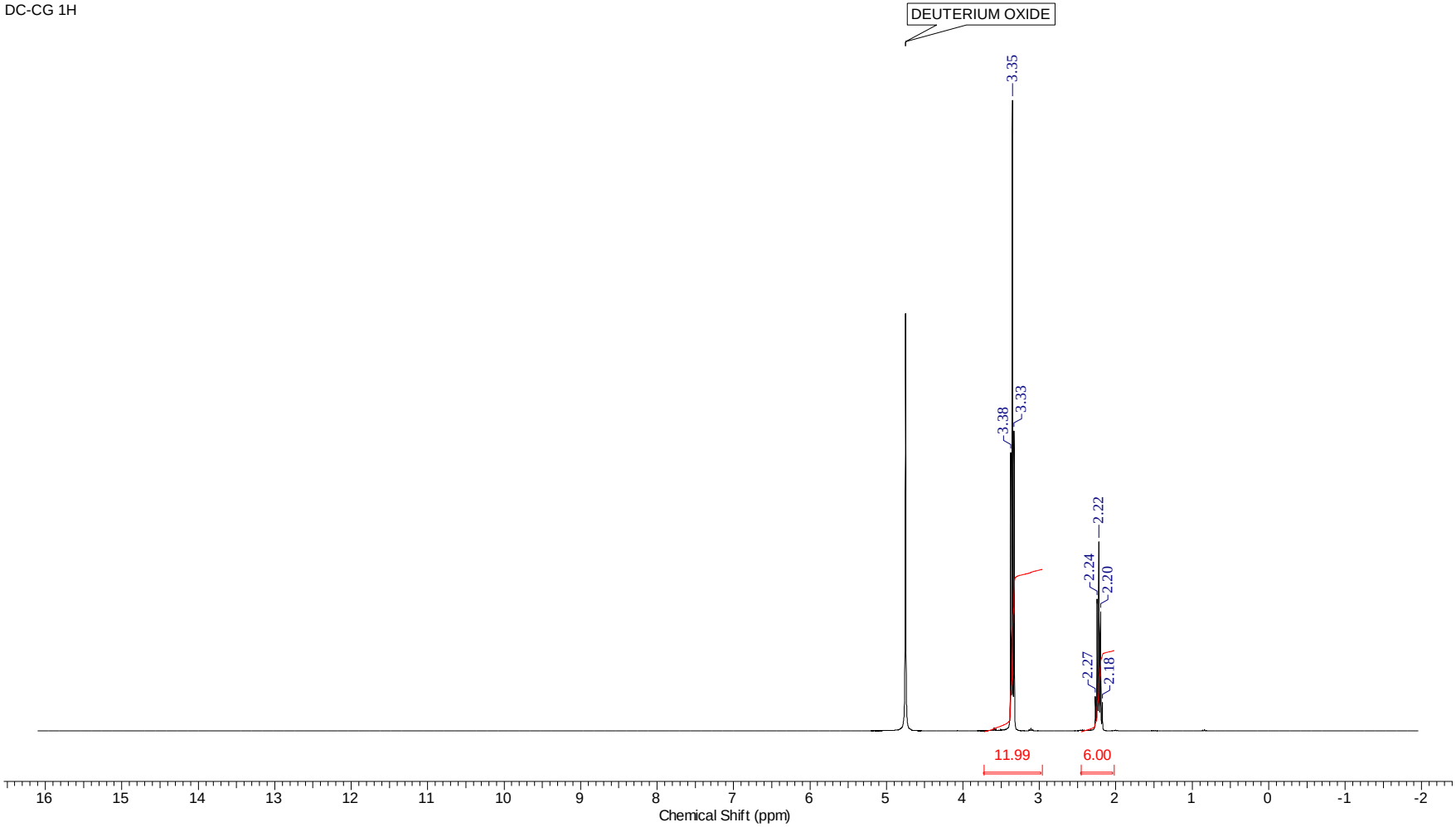

Carbon spectrum of the 1,5,9-triazacyclododecane HCl salt

Appendix 5b

Acquisition Time (sec)	1.3005	***Comment***	Imported from VNMR.			***Date***	Apr 20 2009
Date Stamp	Apr 20 2009	***File Name***	C:\Documents and Settings\winxp\Desktop\sumanmr\Ckept\Copy of 30				
Frequency (MHz)	75.38	***Nucleus***	13C	***Number of Transients***	150000	***Original Points Count***	27094
Points Count	32768	***Pulse Sequence***	s2pul	***Receiver Gain***	30.00	***Solvent***	DEUTERIUM OXIDE
Spectrum Offset (Hz)	9285.7461	***Sweep Width (Hz)***	20833.33	***Temperature (degree C)***	25.000		

DC-CG 1H

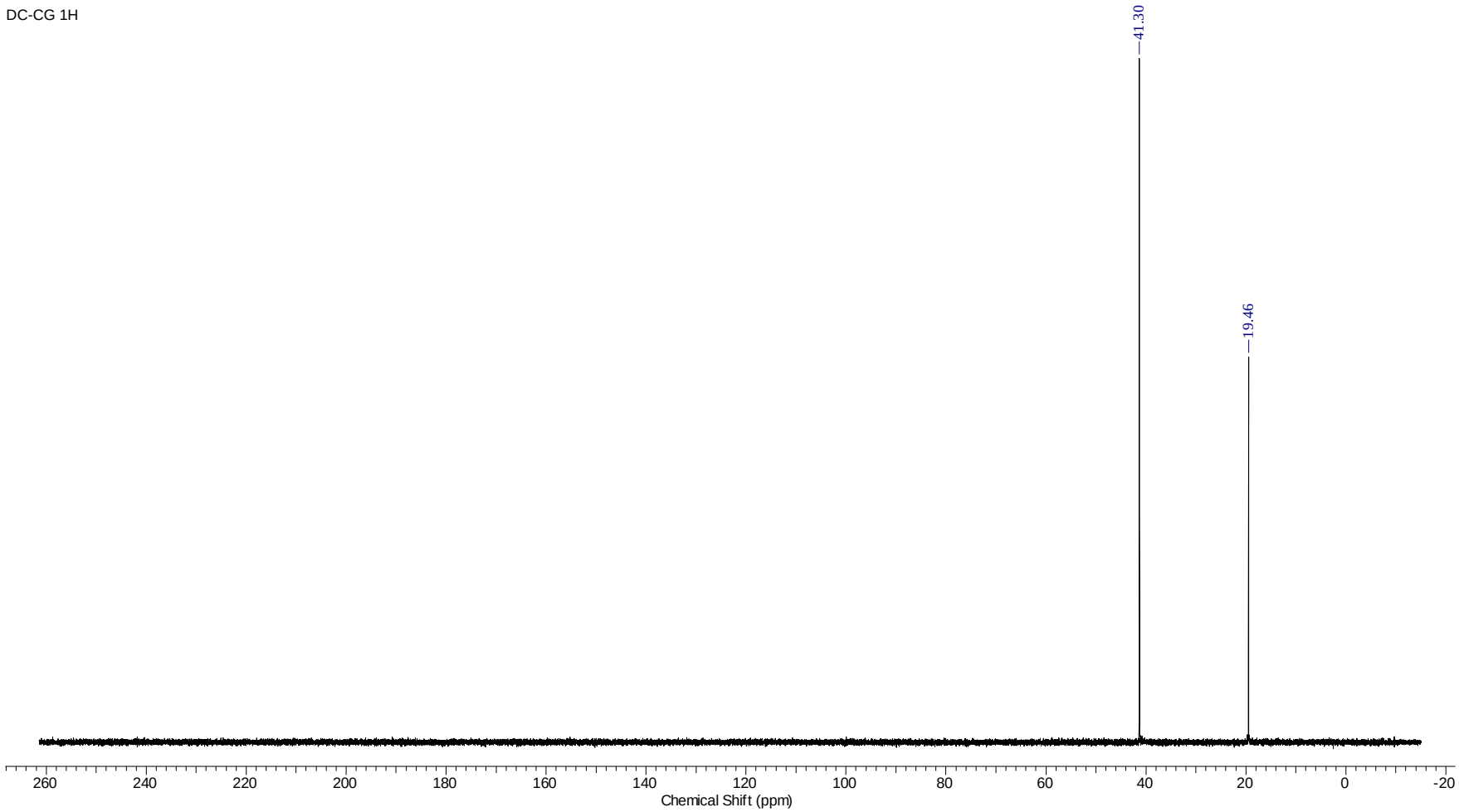

Proton spectrum of the deprotonated 1,5,9-triazacyclododecane ligand

Appendix 6a

Acquisition Time (sec)	4.0000	***Comment***	Imported from VNMR.			***Date***	Aug 26 2008	***Date Stamp***	Aug 26 2008
File Name	C:\Documents and Settings\winxp\Desktop\sumanmr\HKept\17					***Frequency (MHz)***	299.74	***Nucleus***	1H
Number of Transients	128	***Original Points Count***	19231	***Points Count***	32768	***Pulse Sequence***	s2pul	***Receiver Gain***	20.00
Solvent	CHLOROFORM-d			***Spectrum Offset (Hz)***	1807.5146	***Sweep Width (Hz)***	4807.69	***Temperature (degree C)***	25.000

DC-CG 1H

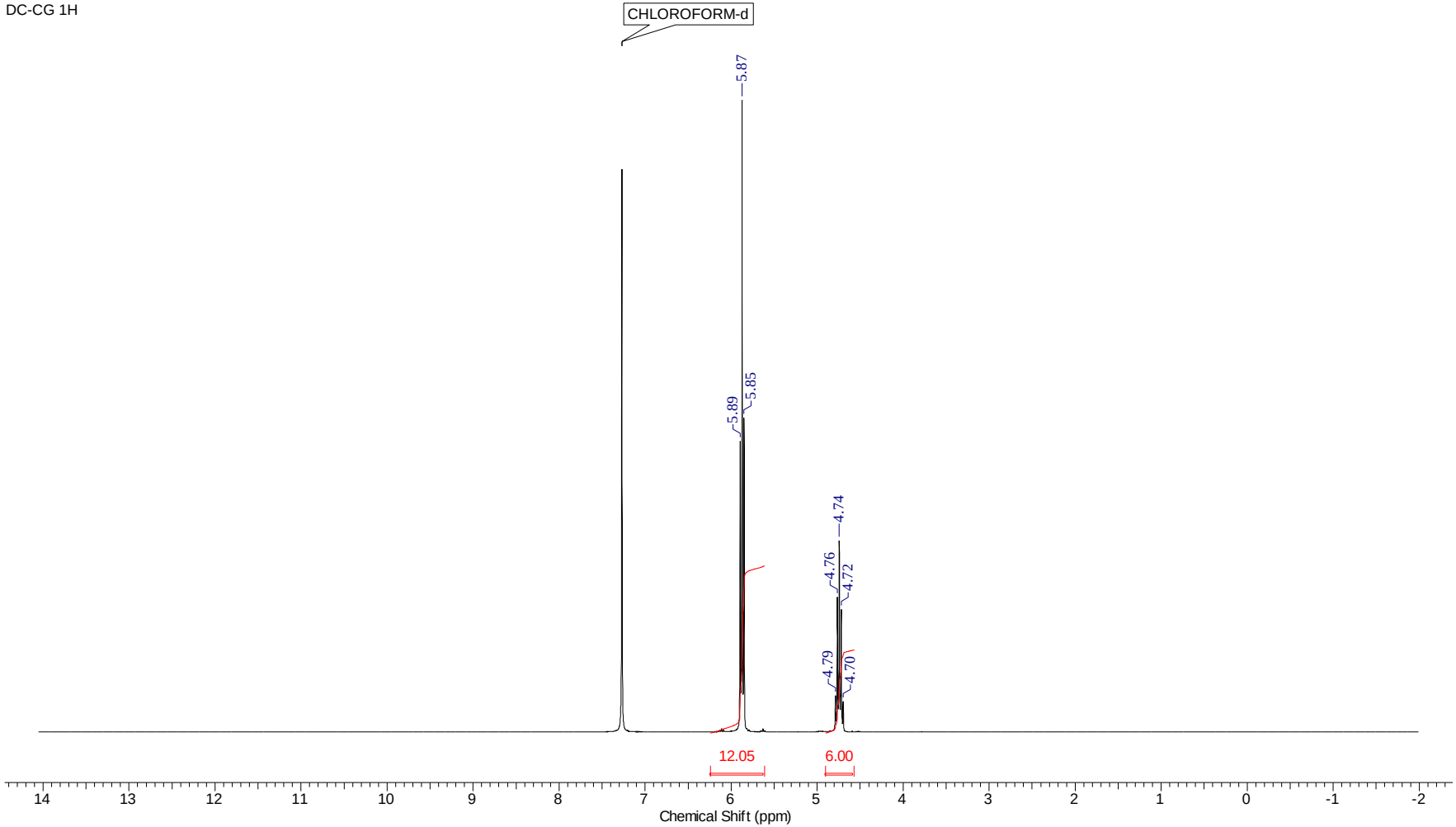

Carbon spectrum of the deprotonated 1,5,9-triazacyclododecane ligand

Appendix 6b

Acquisition Time (sec)	1.2984	***Comment***	Imported from VNMR.		***Date***	May 11 2009	***Date Stamp***	May 11 2009
File Name	C:\Documents and Settings\winxp\Desktop\sumanmr\102C		***Frequency (MHz)***	150.88	***Nucleus***	13C	***Number of Transients***	100000
Original Points Count	53933	***Points Count***	65536	***Pulse Sequence***	s2pul	***Receiver Gain***	60.00		
Solvent	CHLOROFORM-d			***Spectrum Offset (Hz)***	18405.8496	***Sweep Width (Hz)***	41536.86	***Temperature (degree C)***	25.000

DC-CG 1H

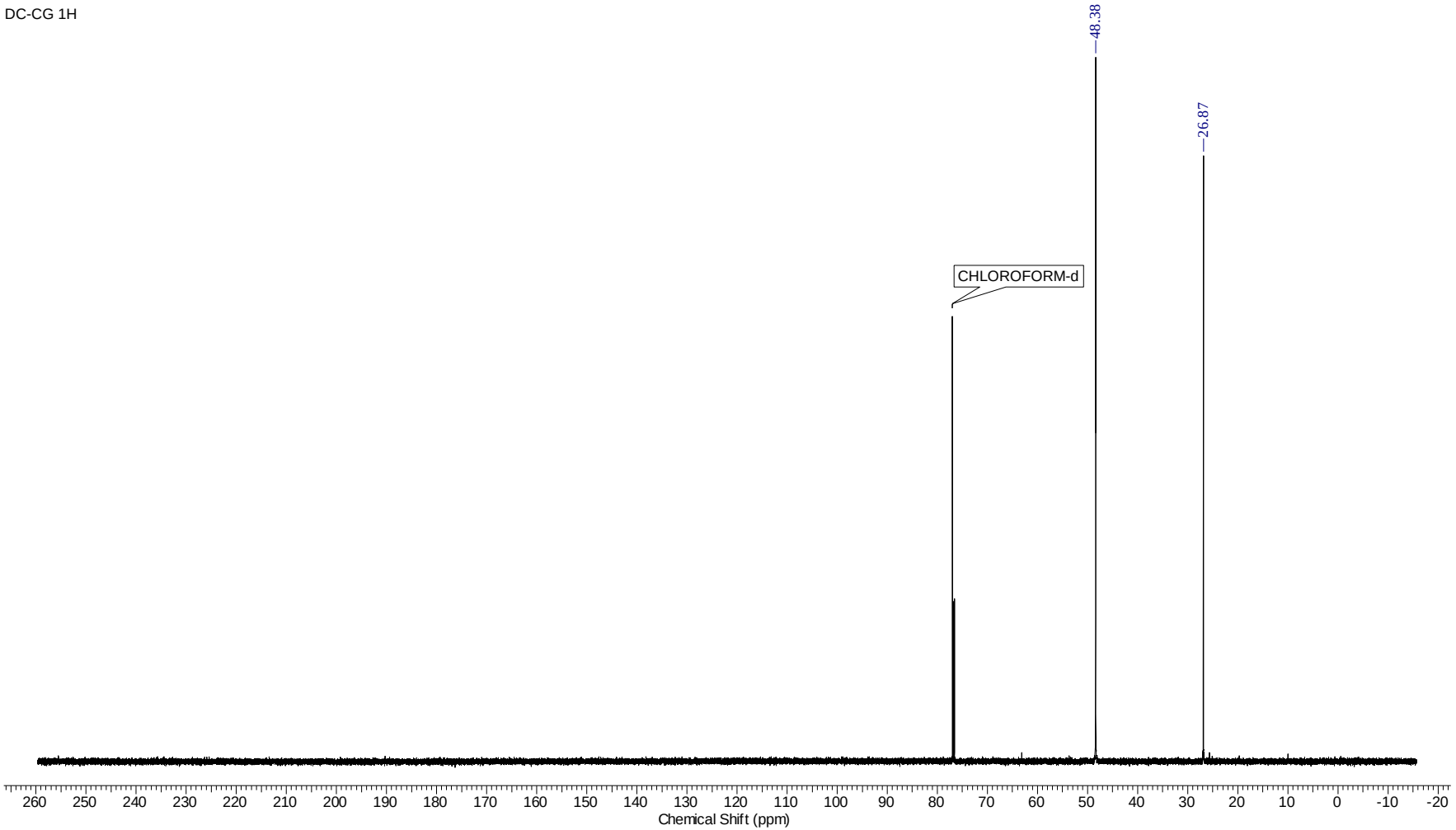

TGA graph of the 1,5,9-triazacyclododecane HCl salt **Appendix 7**

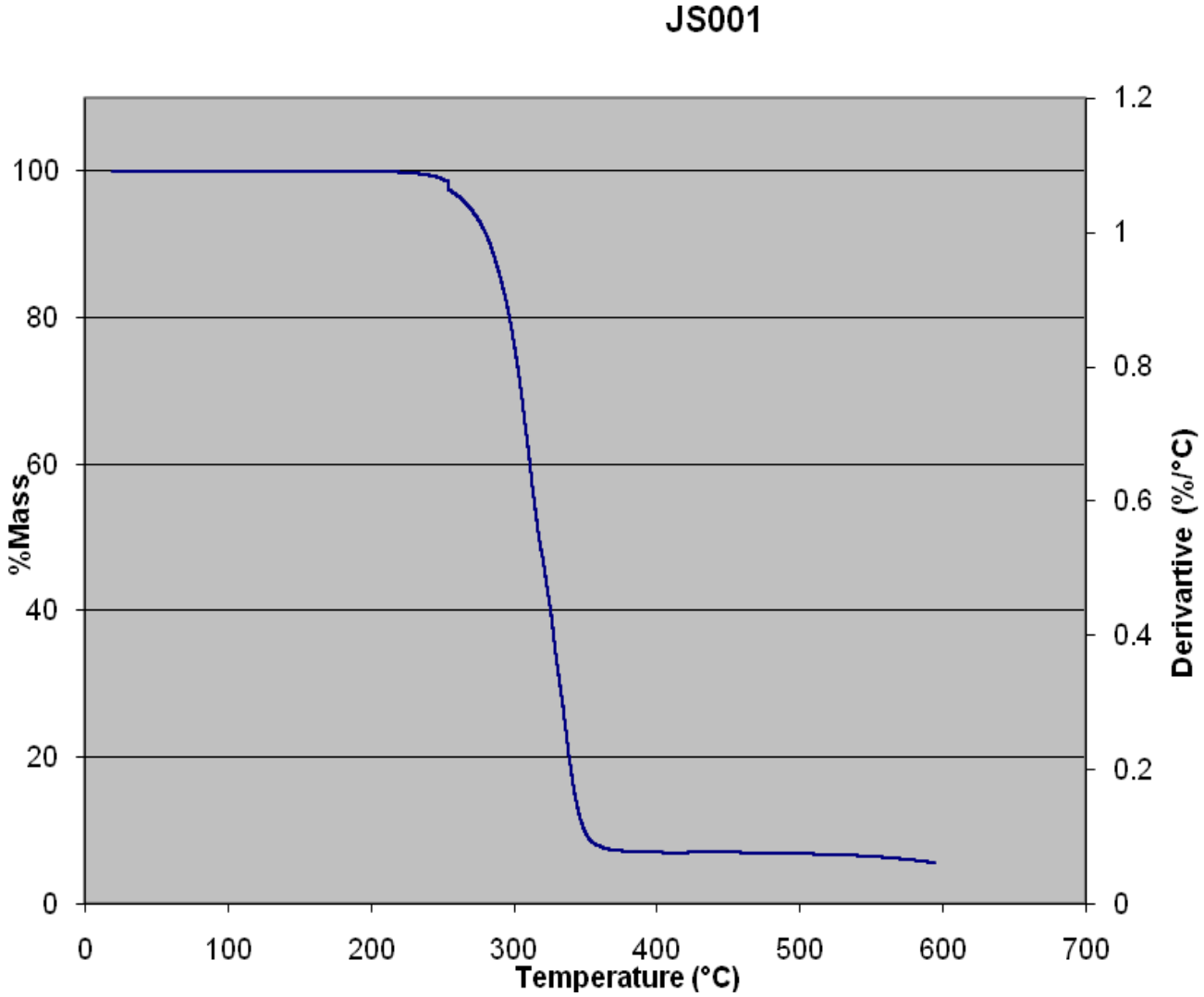

Proton spectrum of the THPTACD

Appendix 8a

Acquisition Time (sec)	4.0000	***Comment***	Imported from VNMR.			***Date***	Jun 18 2009	***Date Stamp***	Jun 18 2009
File Name	C:\Documents and Settings\winxp\Desktop\nmr\110H			***Frequency (MHz)***	299.74	***Nucleus***	1H	***Number of Transients***	16
Original Points Count	19231	***Points Count***	32768	***Pulse Sequence***	s2pul	***Receiver Gain***	18.00	***Solvent***	CHLOROFORM-d
Spectrum Offset (Hz)	1795.1899	***Sweep Width (Hz)***	4807.69	***Temperature (degree C)***	25.000				

DC-CG 1H

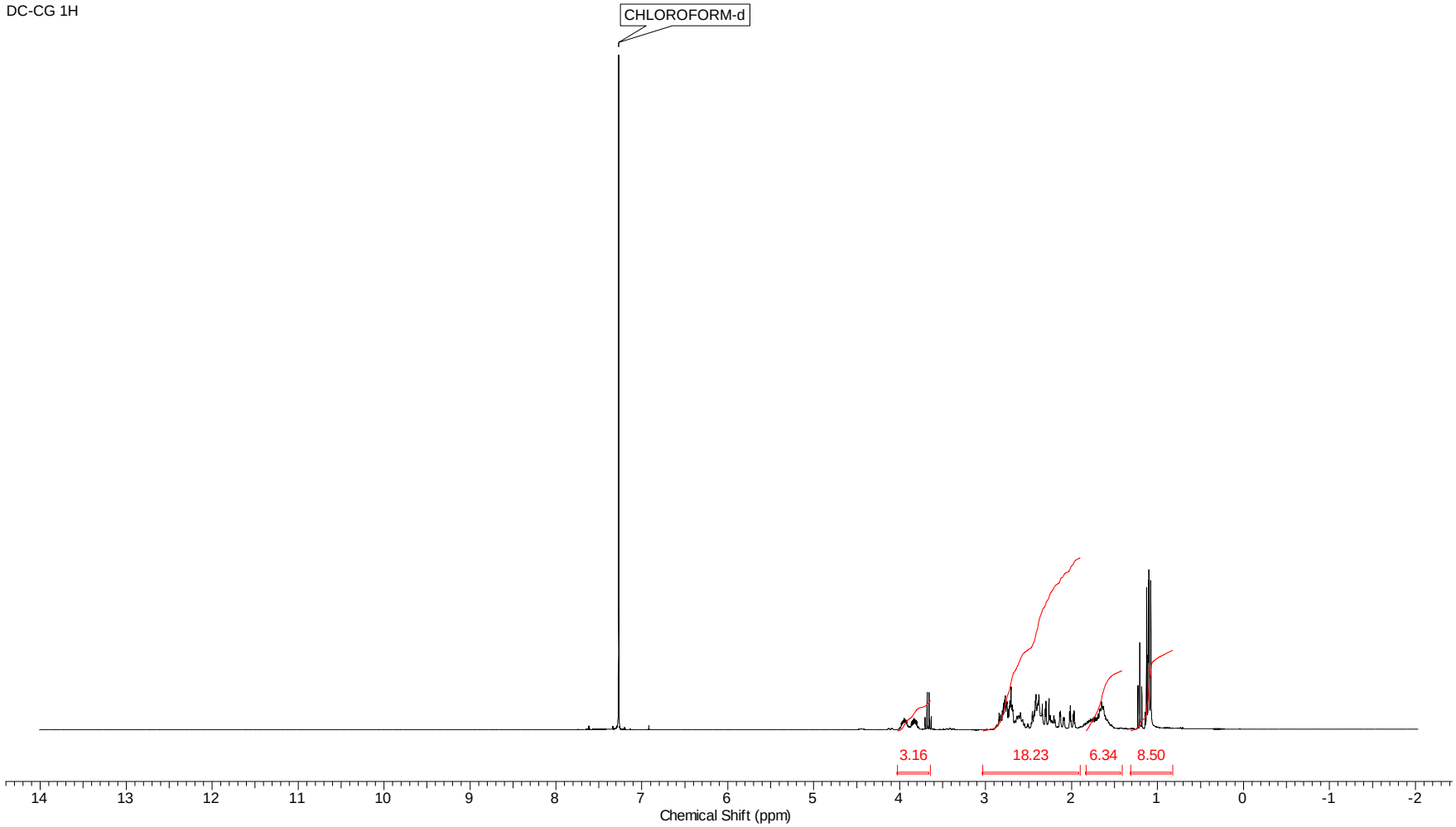

Carbon spectrum of the THPTACD

Appendix 8b

Acquisition Time (sec)	1.3005	***Comment***	Imported from VNMR.			***Date***	May 3 2009	***Date Stamp***	May 3 2009
File Name	C:\Documents and Settings\winxp\Desktop\sumanmr\97C			***Frequency (MHz)***	75.38	***Nucleus***	13C	***Number of Transients***	100000
Original Points Count	27094	***Points Count***	32768	***Pulse Sequence***	s2pul	***Receiver Gain***	30.00	***Solvent***	CHLOROFORM-d
Spectrum Offset (Hz)	9229.4795	***Sweep Width (Hz)***	20833.33	***Temperature (degree C)***	25.000				

DC-CG 1H

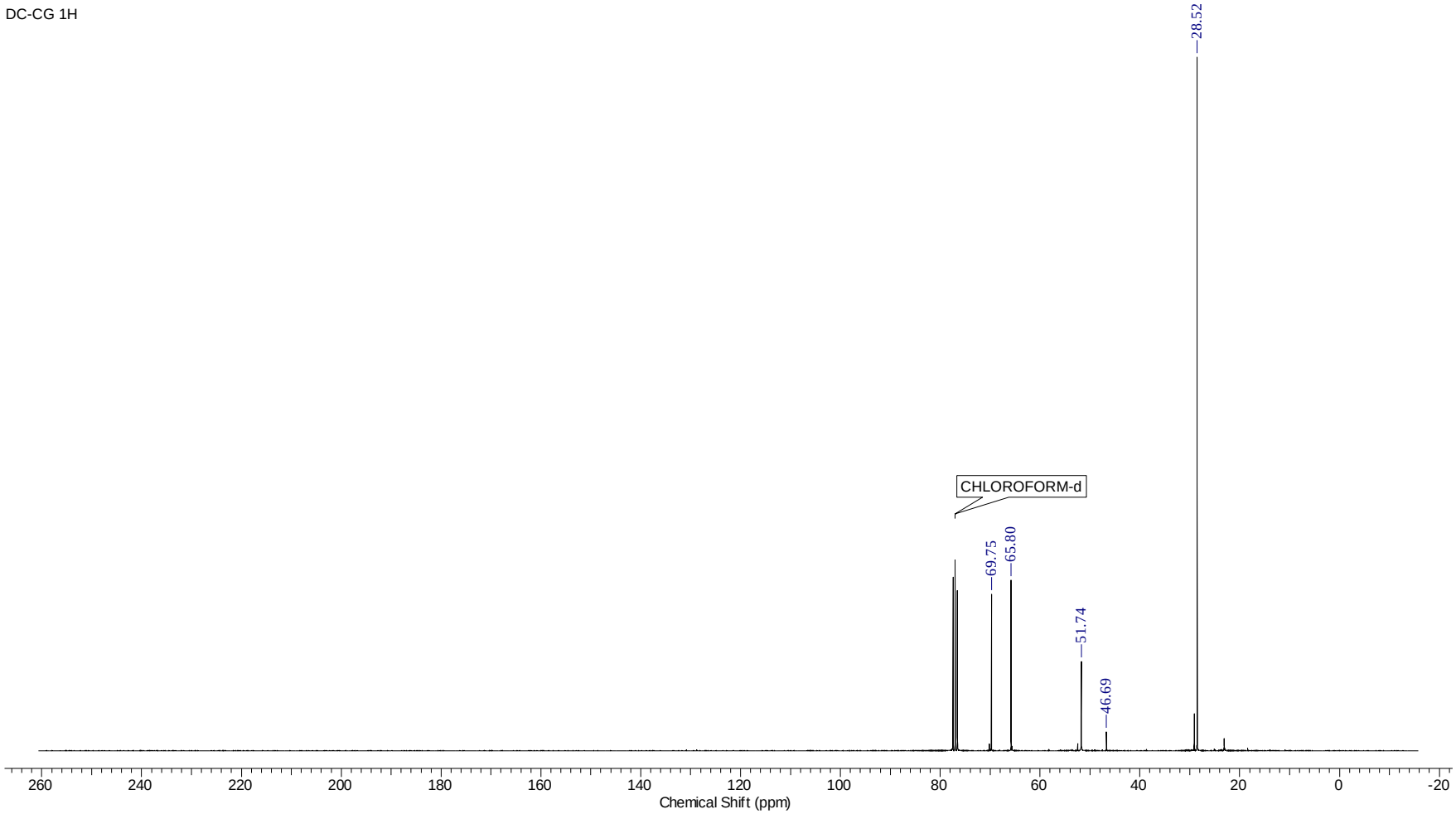

Mass spectrum of the THPTACD

Appendix 8c

Proton spectrum of the TMPTACD

Appendix 9a

Acquisition Time (sec)	4.0000	***Comment***	Imported from VNMR.			***Date***	Jun 12 2009	***Date Stamp***	Jun 12 2009
File Name	C:\Documents and Settings\winxp\Desktop\sumanmr\107H					***Frequency (MHz)***	299.74	***Nucleus***	1H
Number of Transients	32	***Original Points Count***	19231	***Points Count***	32768	***Pulse Sequence***	s2pul	***Receiver Gain***	20.00
Solvent	CHLOROFORM-d			***Spectrum Offset (Hz)***	1794.8964	***Sweep Width (Hz)***	4807.69	***Temperature (degree C)***	25.000

DC-CG 1H

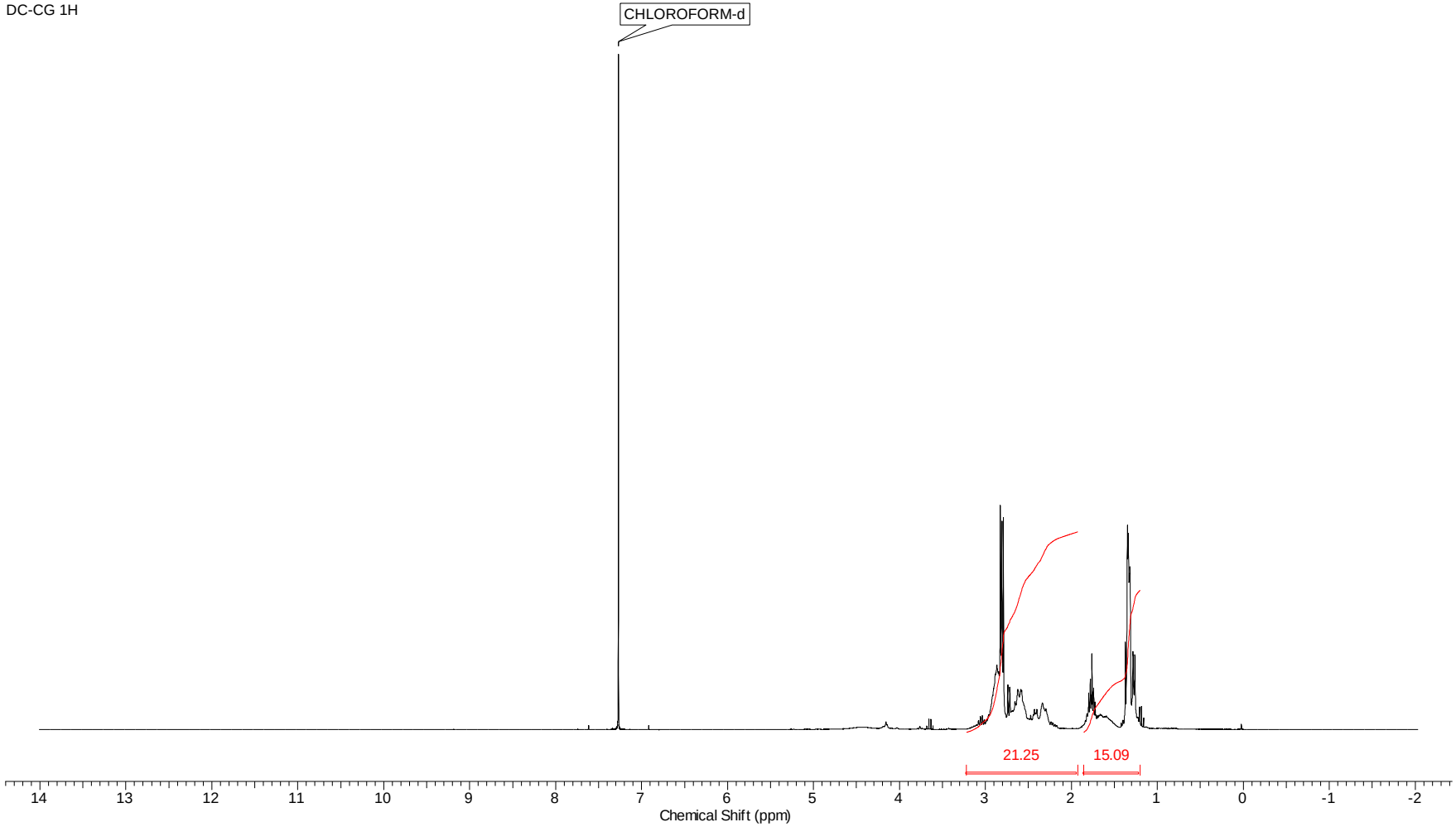

Carbon spectrum of the TMPTACD

Appendix 9b

Acquisition Time (sec)	1.3005	***Comment***	Imported from VNMR.			***Date***	Oct 10 2007	***Date Stamp***	Oct 10 2007
File Name	C:\Documents and Settings\winxp\Desktop\nmr\1nmr\FC			***Frequency (MHz)***	75.38	***Nucleus***	13C	***Number of Transients***	5000
Original Points Count	23560	***Points Count***	32768	***Pulse Sequence***	s2pul	***Receiver Gain***	30.00	***Solvent***	CHLOROFORM-d
Spectrum Offset (Hz)	7855.4175	***Sweep Width (Hz)***	18115.94	***Temperature (degree C)***	25.000				

DC-CG 1H

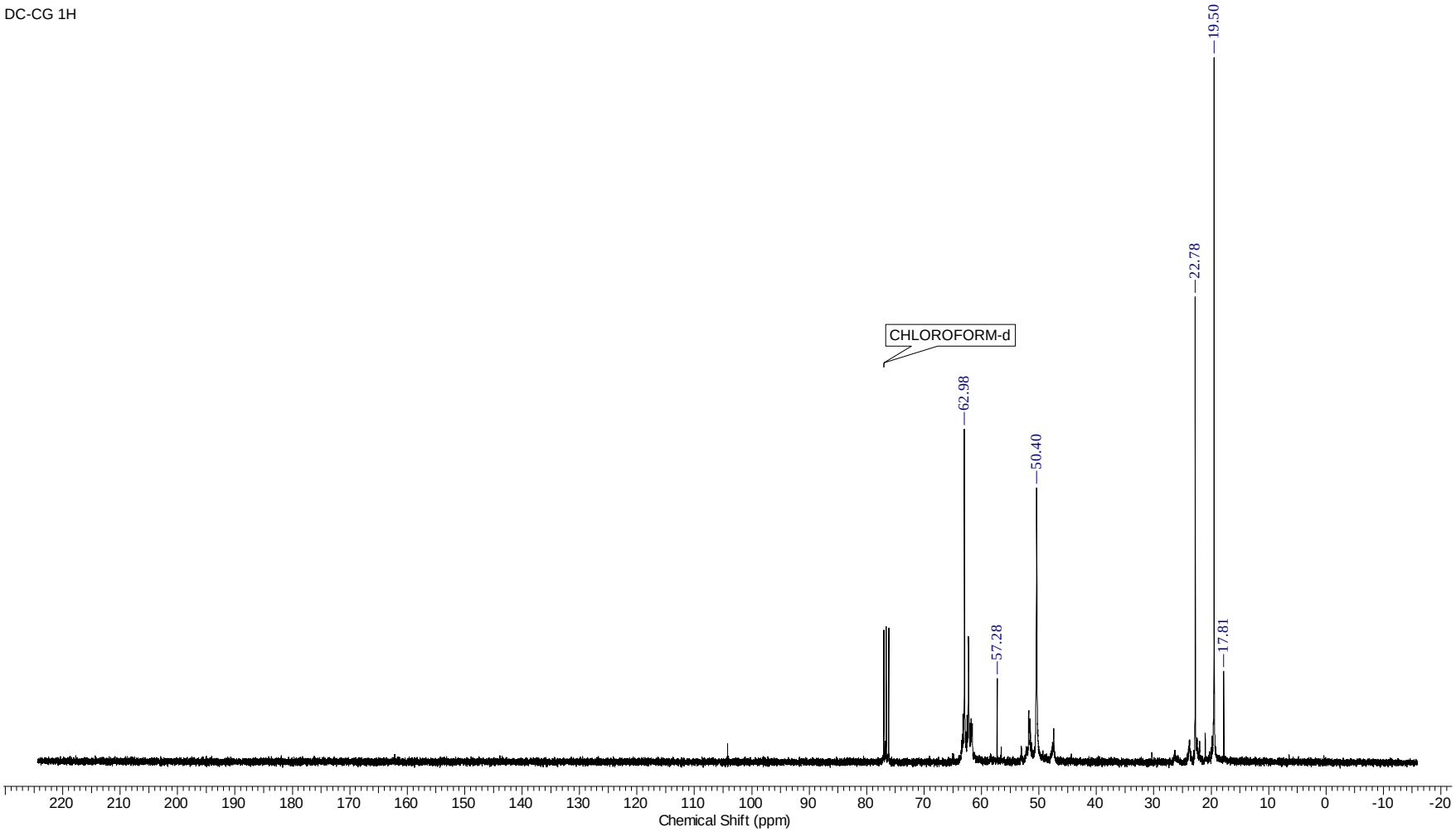

Mass spectrum of the TMPTACD

Appendix 9c

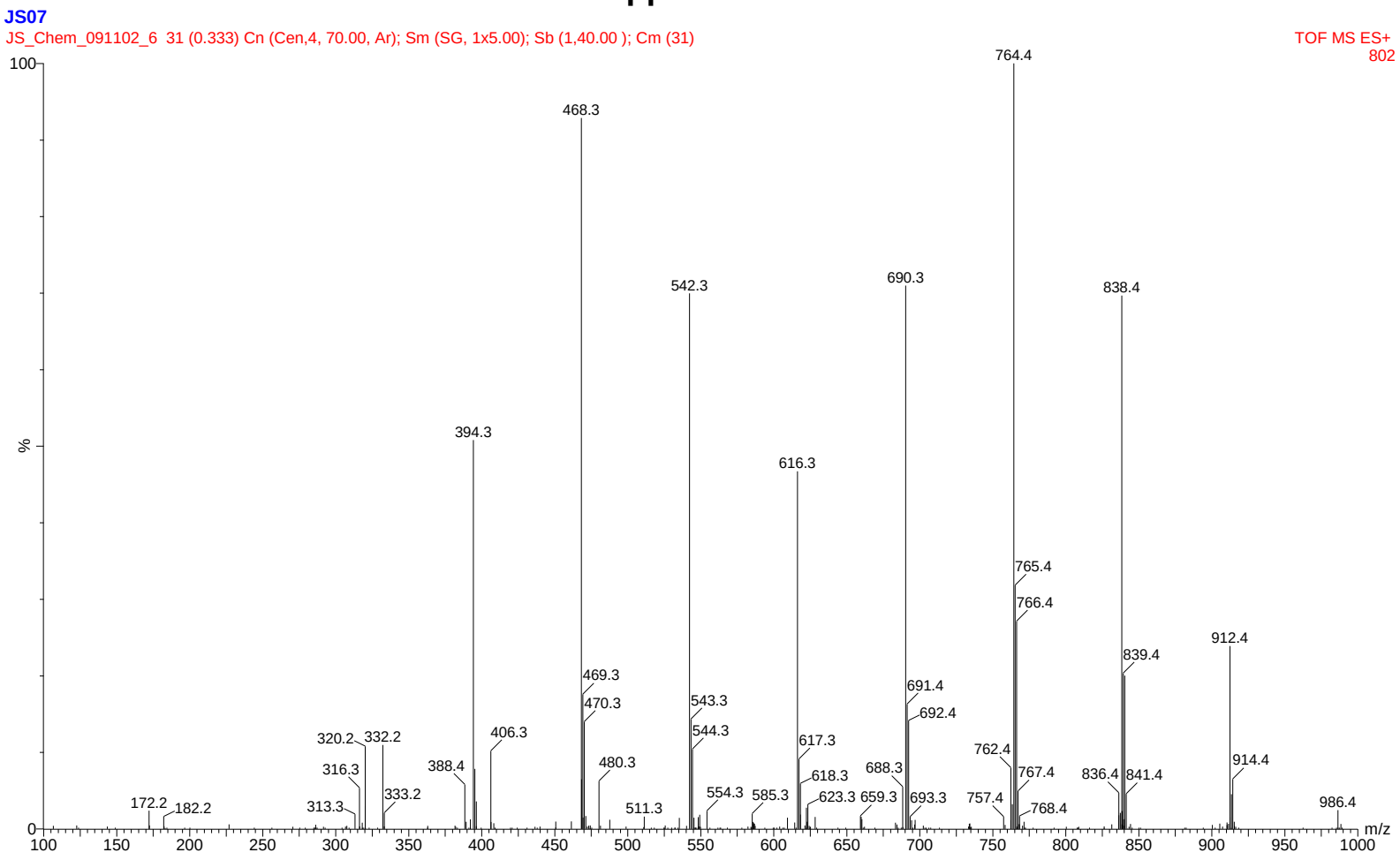

Proton spectrum of the THMPTACD

Appendix 10a

Acquisition Time (sec)	4.0211	***Comment***	Imported from VNMR.		***Date***	Oct 27 2009	***Date Stamp***	Oct 27 2009
File Name	C:\Documents and Settings\winxp\Desktop\nmr\1nmr\152H			***Frequency (MHz)***	399.94	***Nucleus***	1H	***Number of Transients***	32
Original Points Count	25686	***Points Count***	32768	***Pulse Sequence***	s2pul	***Receiver Gain***	42.00		
Solvent	DICHLOROMETHANE-d2			***Spectrum Offset (Hz)***	2390.7793	***Sweep Width (Hz)***	6387.74	***Temperature (degree C)***	25.000

DC-CG 1H

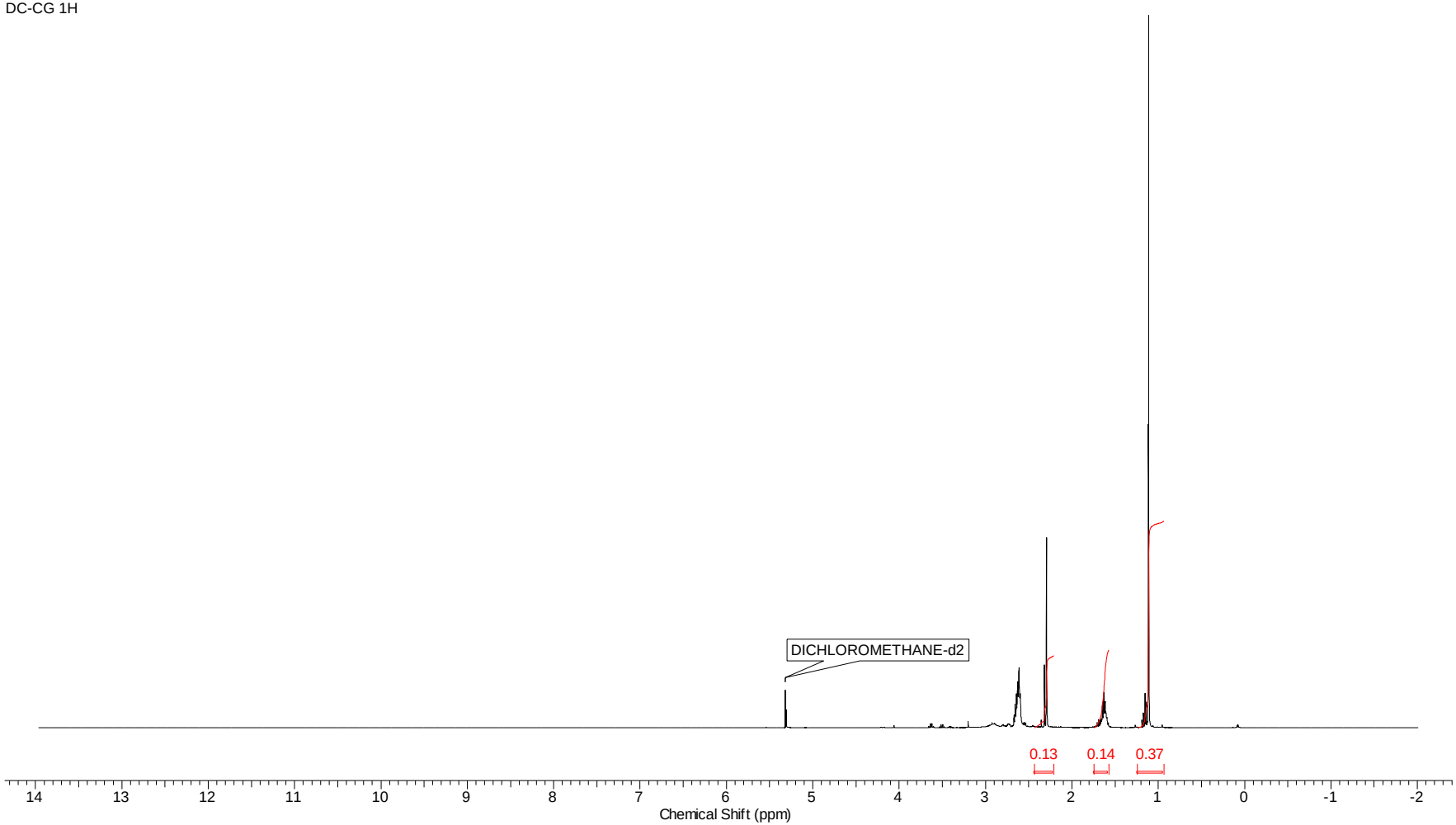

Carbon spectrum of the THMPTACD

Appendix 10b

Acquisition Time (sec)	1.3020	***Comment***	Imported from VNMR.		***Date***	Oct 27 2009	***Date Stamp***	Oct 27 2009
File Name	C:\Documents and Settings\winxp\Desktop\nmr\1nmr\151C			***Frequency (MHz)***	100.58	***Nucleus***	13C	***Number of Transients***	100000
Original Points Count	35942	***Points Count***	65536	***Pulse Sequence***	s2pul	***Receiver Gain***	30.00		
Solvent	DEUTERIUM OXIDE			***Spectrum Offset (Hz)***	14730.3604	***Sweep Width (Hz)***	27605.24	***Temperature (degree C)***	25.000

DC-CG 1H

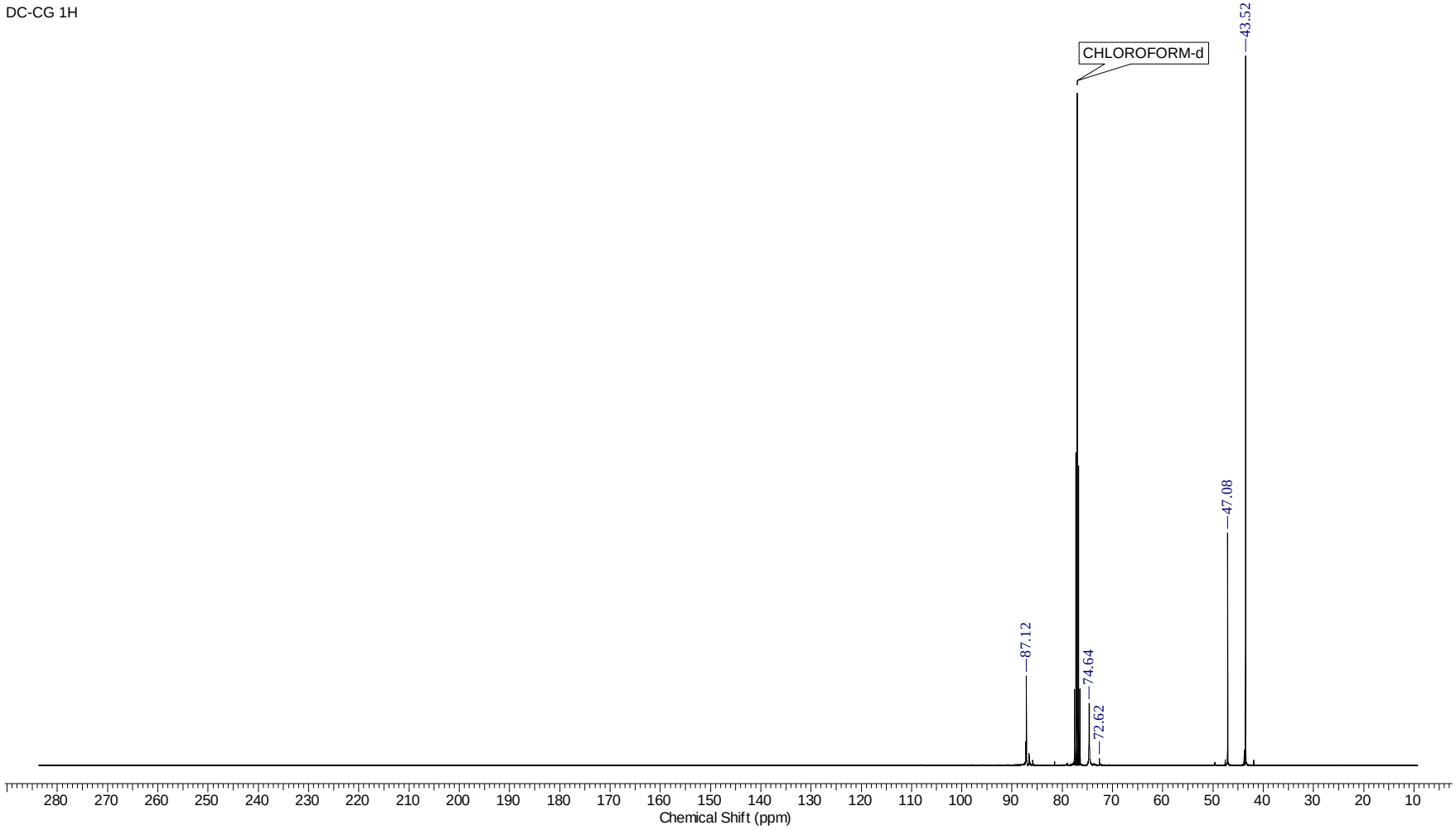

Mass spectrum of the THMPTACD

Appendix 10c

Proton spectrum of the THBTACD

Appendix 11a

Acquisition Time (sec)	4.0000	***Comment***	Imported from VNMR.			***Date***	Jun 18 2009	***Date Stamp***	Jun 18 2009
File Name	C:\Documents and Settings\winxp\Desktop\nmr\1nmr\109H					***Frequency (MHz)***	299.74	***Nucleus***	1H
Number of Transients	16	***Original Points Count***	19231	***Points Count***	32768	***Pulse Sequence***	s2pul	***Receiver Gain***	18.00
Solvent	CHLOROFORM-d			***Spectrum Offset (Hz)***	1795.1899	***Sweep Width (Hz)***	4807.69	***Temperature (degree C)***	25.000

DC-CG 1H

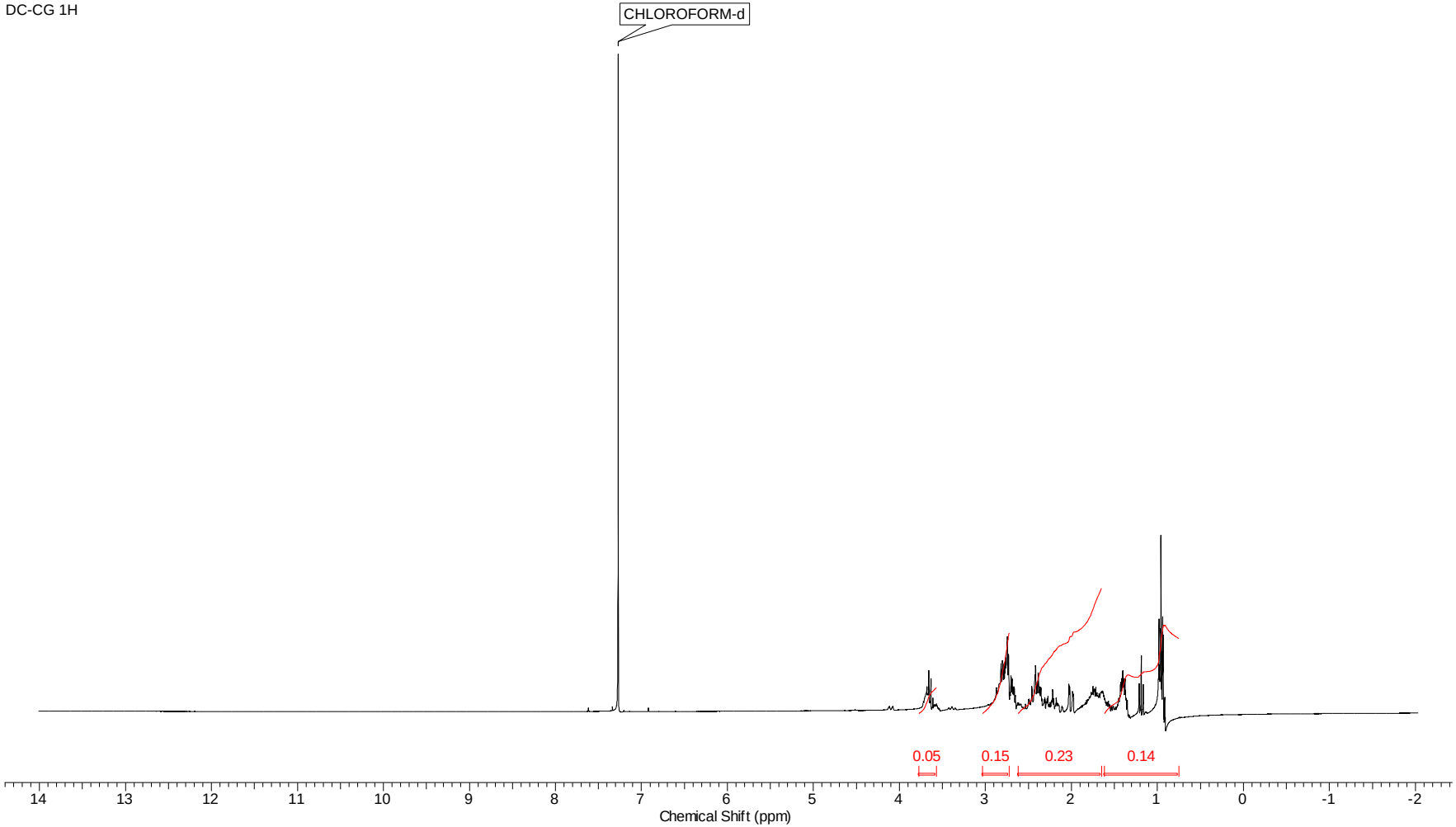

Carbon spectrum of the THBTACD

Appendix 11b

Acquisition Time (sec)	1.3020	***Comment***	Imported from VNMR.			***Date***	Oct 28 2009
Date Stamp	Oct 28 2009	***File Name***	C:\Documents and Settings\winxp\Desktop\sumanmr\153C			***Frequency (MHz)***	100.58
Nucleus	13C	***Number of Transients***	100000	***Original Points Count***	35942	***Points Count***	65536
Pulse Sequence	s2pul	***Receiver Gain***	30.00	***Solvent***	DICHLOROMETHANE-d2		
Spectrum Offset (Hz)	12351.3564	***Sweep Width (Hz)***	27605.24	***Temperature (degree C)***	25.000		

DC-CG 1H

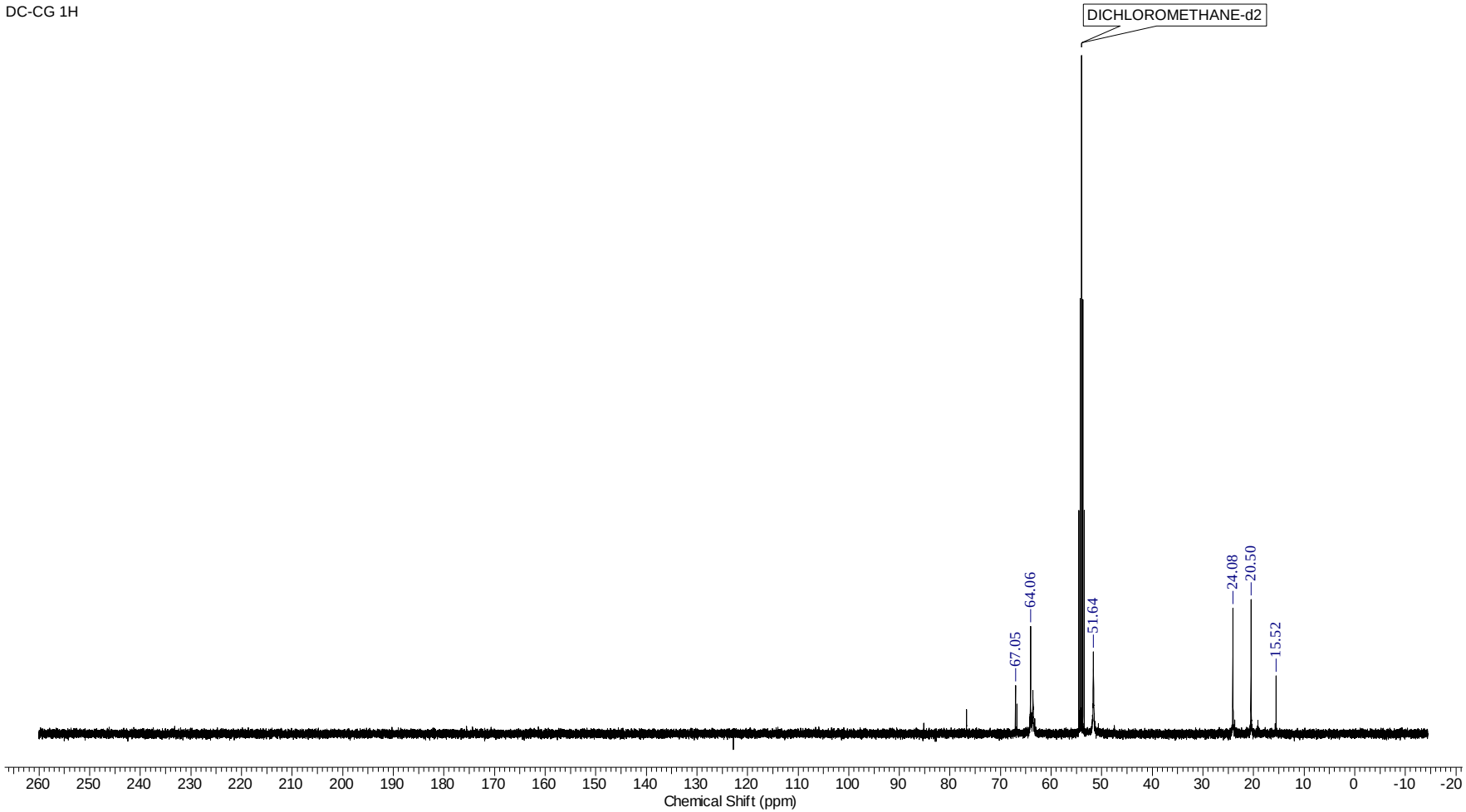

Mass spectrum of the THBTACD

Appendix 11c

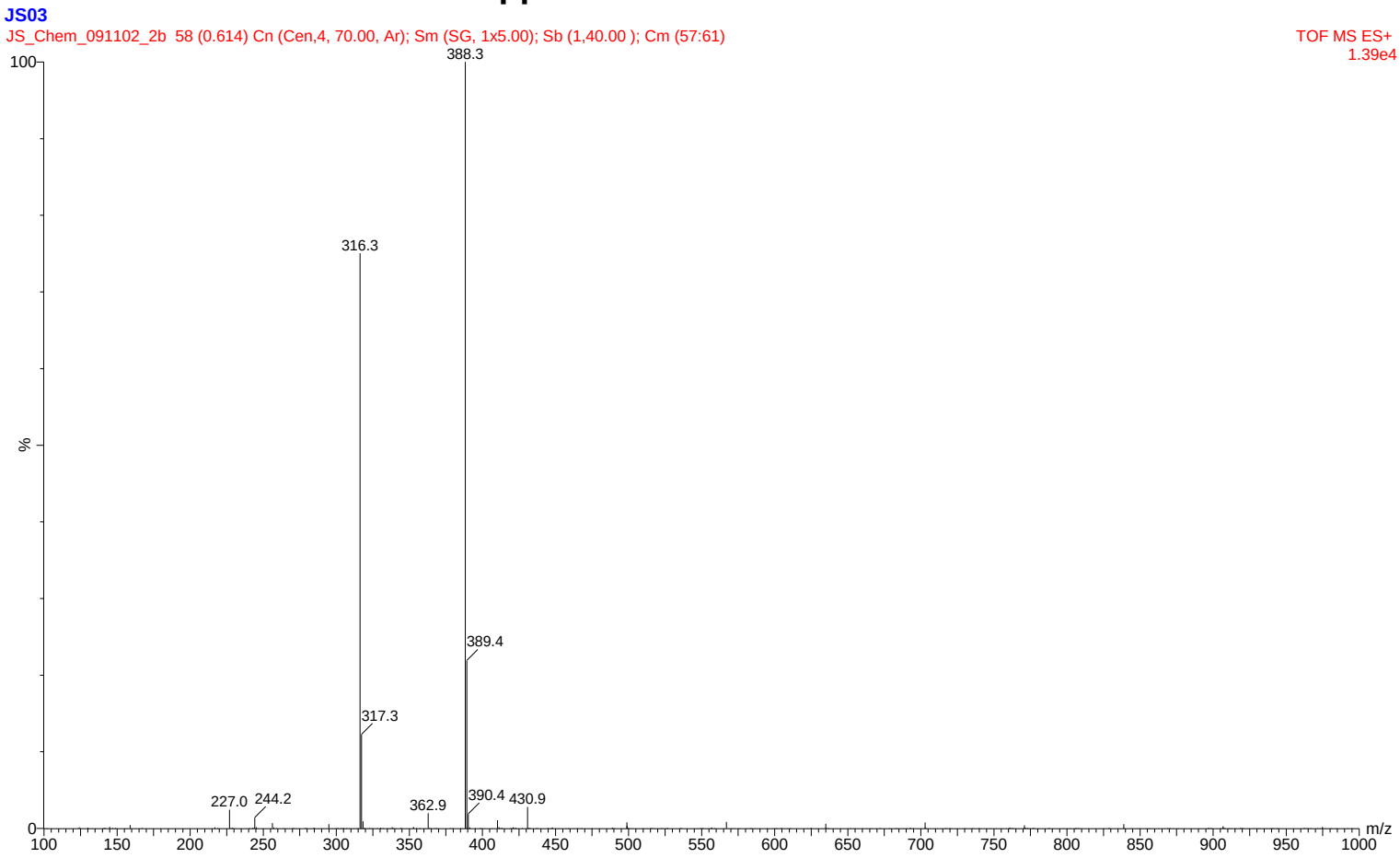

Proton spectrum of the THPETACD

Appendix 12a

Acquisition Time (sec)	4.0211	***Comment***	Imported from VNMR.			***Date***	Oct 5 2009	***Date Stamp***	Oct 5 2009
File Name	C:\Documents and Settings\winxp\Desktop\sumanmr\142H					***Frequency (MHz)***	399.94	***Nucleus***	1H
Number of Transients	64	***Original Points Count***	25686	***Points Count***	32768	***Pulse Sequence***	s2pul	***Receiver Gain***	38.00
Solvent	CHLOROFORM-d			***Spectrum Offset (Hz)***	2407.4583	***Sweep Width (Hz)***	6387.74	***Temperature (degree C)***	25.000

DC-CG 1H

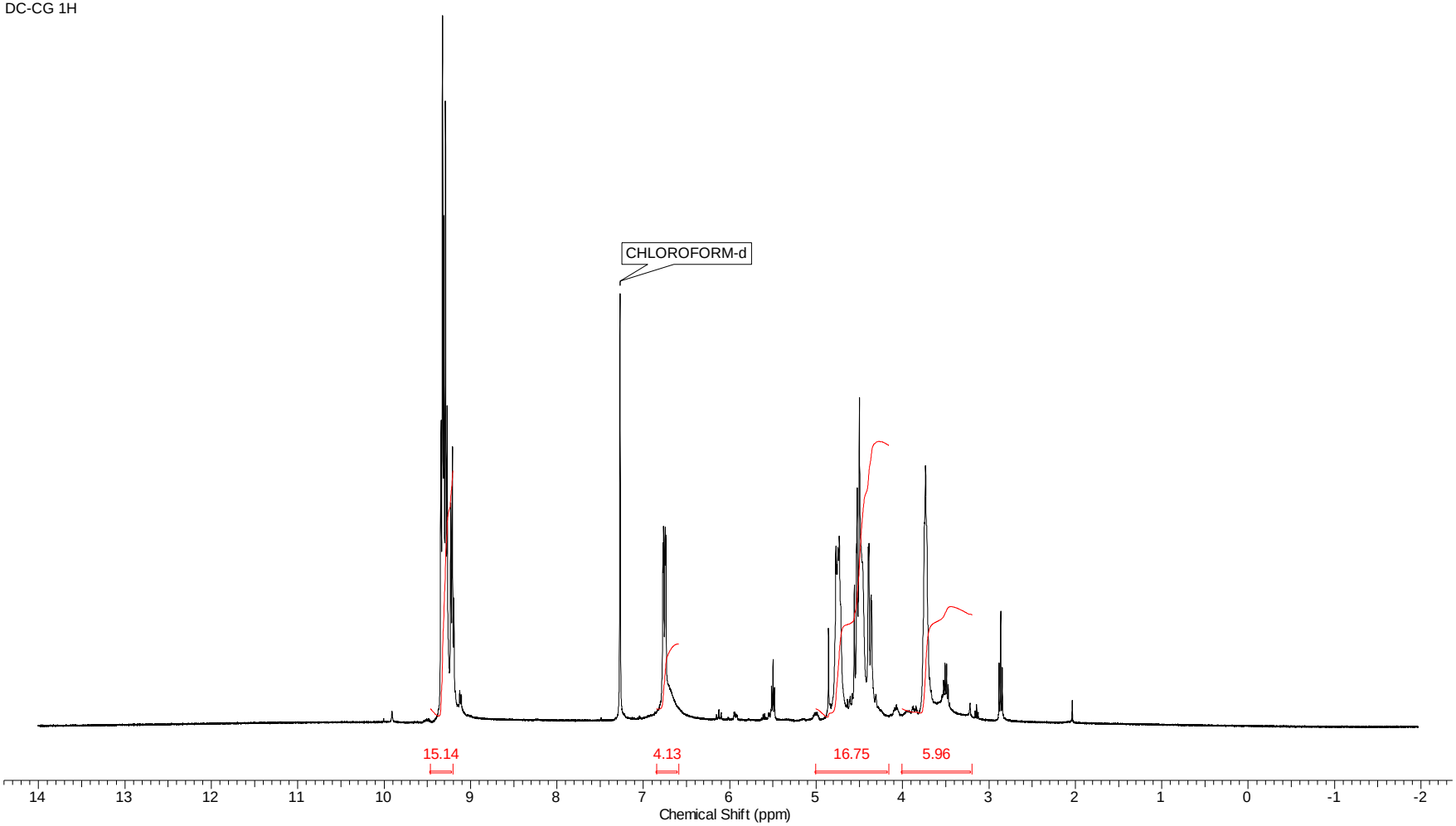

Carbon spectrum of the THPETACD

Appendix 12b

Acquisition Time (sec)	1.3011	***Comment***	Imported from VNMR.			***Date***	Oct 5 2009
Date Stamp	Oct 5 2009	***File Name***	C:\Documents and Settings\winxp\Desktop\sumanmr\142C			***Frequency (MHz)***	100.58
Nucleus	13C	***Number of Transients***	94000	***Original Points Count***	36624	***Points Count***	65536
Pulse Sequence	s2pul	***Receiver Gain***	30.00	***Solvent***	DICHLOROMETHANE-d2		
Spectrum Offset (Hz)	12089.5273	***Sweep Width (Hz)***	28149.19	***Temperature (degree C)***	25.000		

DC-CG 1H

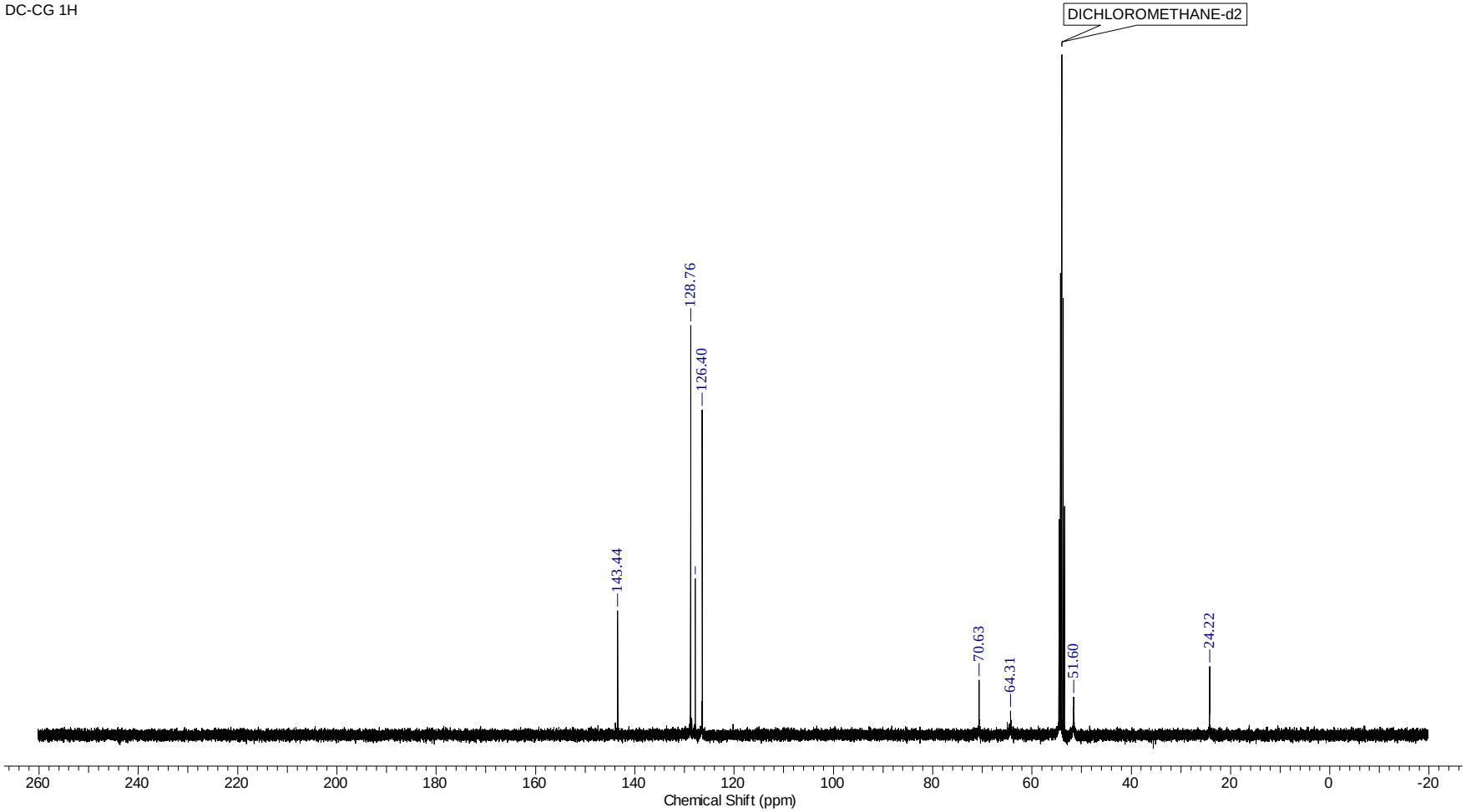

Mass spectrum of the THPETACD

Appendix 12c

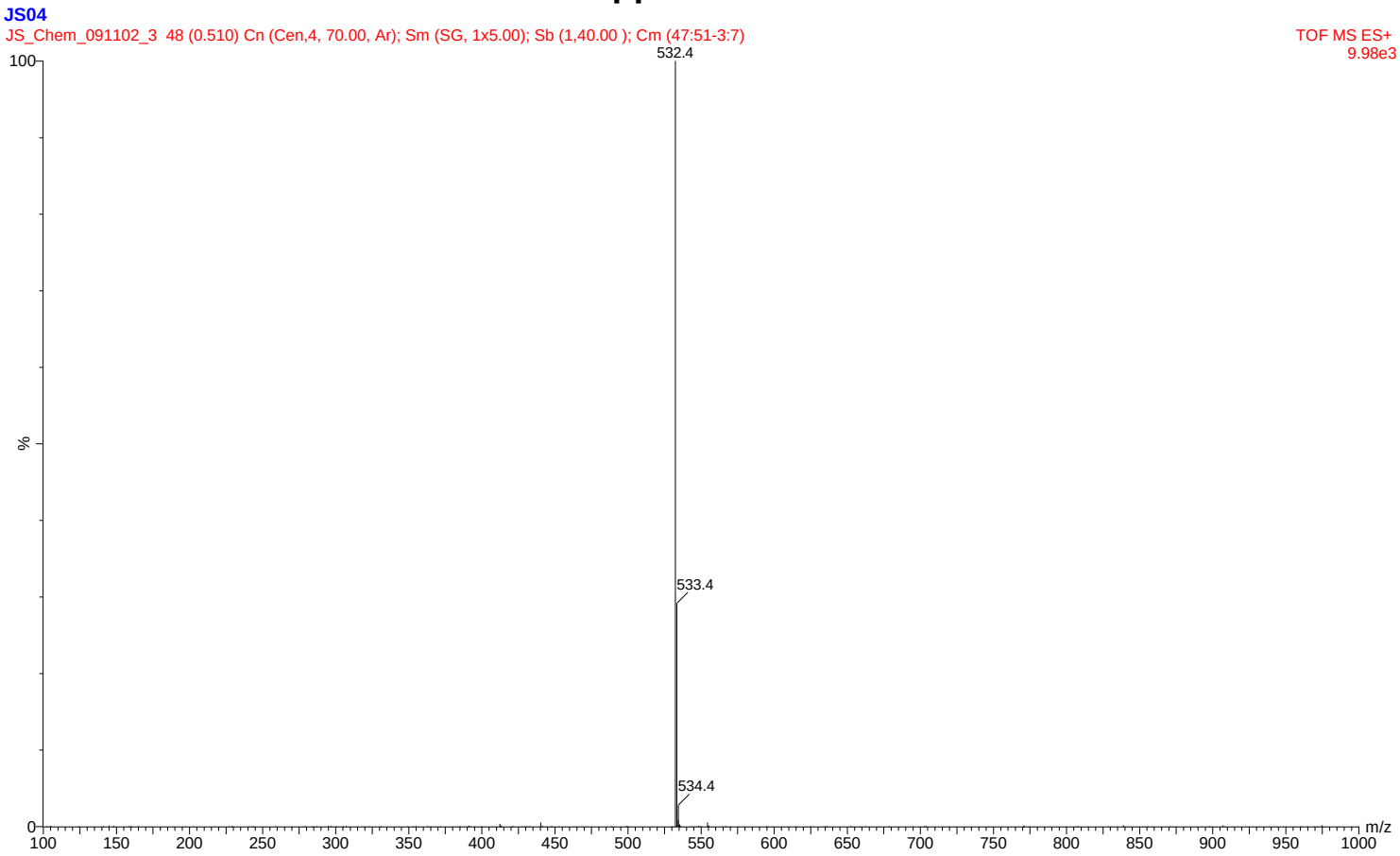

Appendix 13

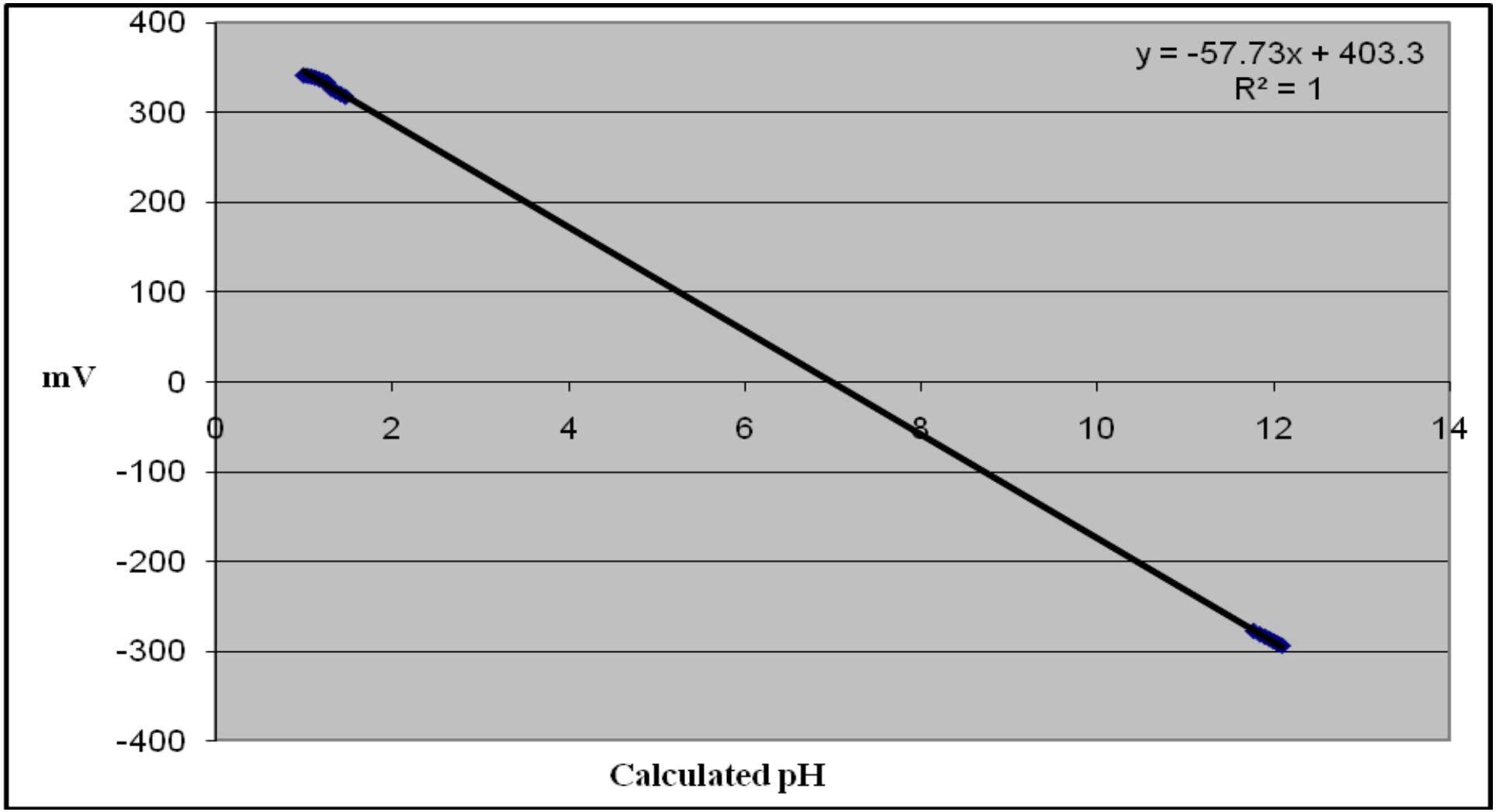

The graph of potential (mV) against the calculated pH values for the determination of E° and k values of THPTACD.

Appendix 14

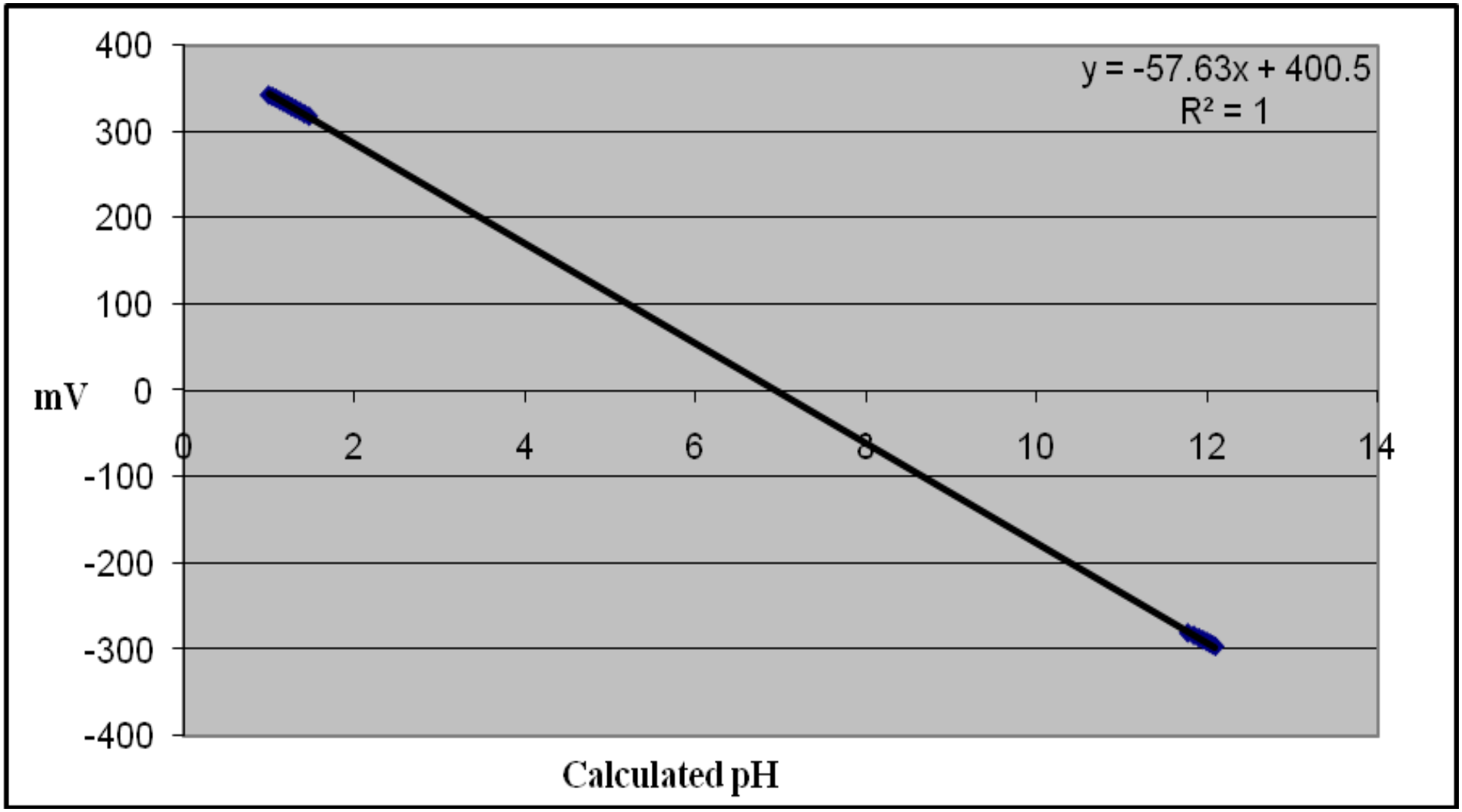

The graph of potential (mV) against the calculated pH values for the determination of E° and k values of THBTACD.

Appendix 15

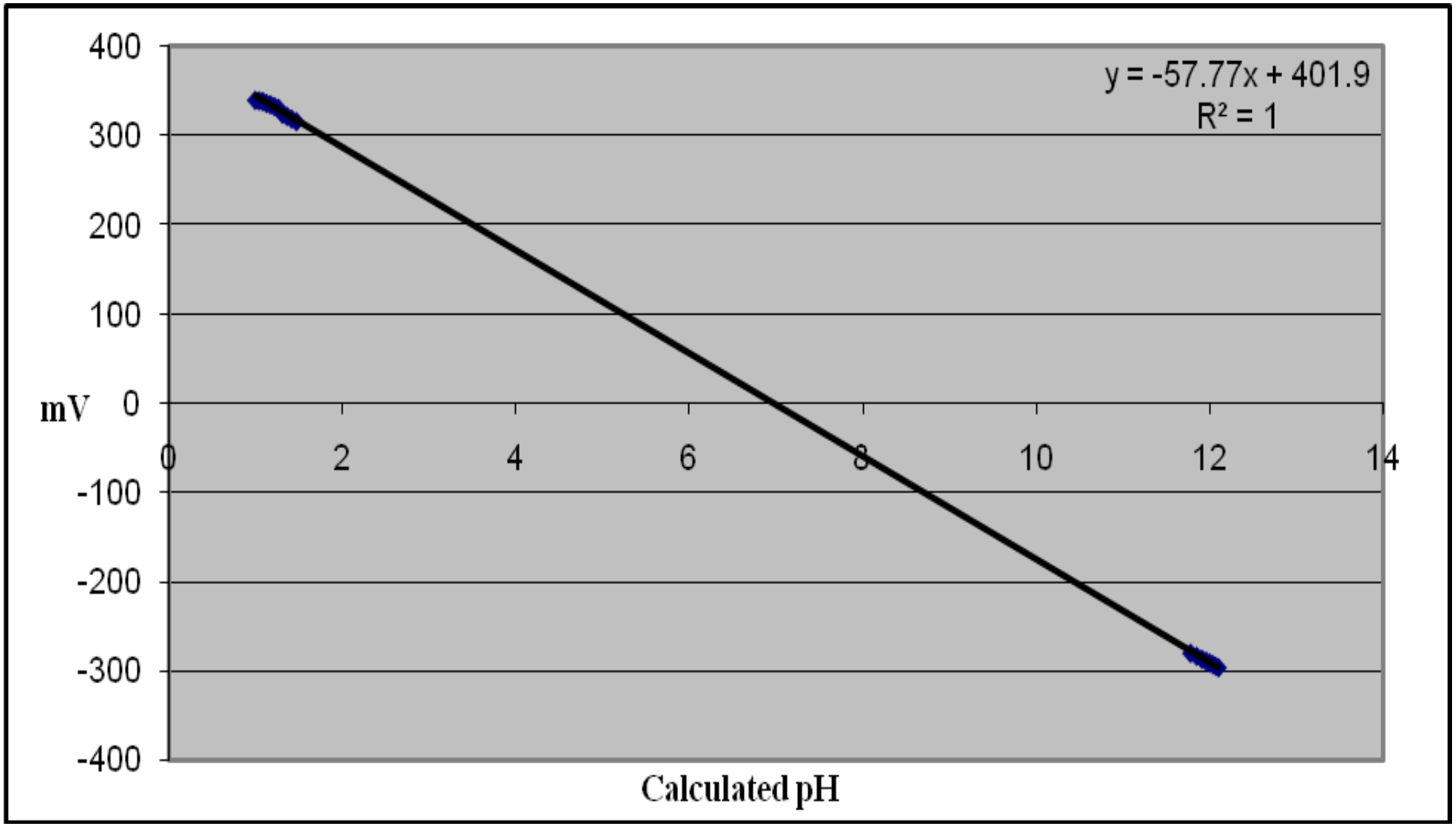

The graph of potential (mV) against the calculated pH values for the determination of E° and k value of THMPTACD